Design and Development of Vision Based Vibration Suppression Strategies for Industrial Robots in Assembly Operations with Gripper and Object Flexibilities

THESIS

Submitted in the partial fulfillment of the requirement for the degree of

DOCTOR OF PHILOSOPHY

by

CHETAN JALENDRA

Under the Supervision of

Prof. BIJAY KUMAR ROUT

&

Co-Supervision of

Dr. AMOL MARATHE

Department of Mechanical Engineering
Birla Institute of Technology & Science, Pilani – 333 031(Rajasthan)

BITS Pilani
Pilani | Dubai | Goa | Hyderabad

BIRLA INSTITUTE OF TECHNOLOGY & SCIENCE
PILANI – 333 031 (RAJASTHAN) INDIA

January 2024

Design and Development of Vision Based Vibration Suppression Strategies for Industrial Robots in Assembly Operations with Gripper and Object Flexibilities

THESIS

Submitted in the partial fulfillment of the requirement for the degree of

DOCTOR OF PHILOSOPHY

by

CHETAN JALENDRA
(2016PHXF0420P)

Under the Supervision of

Prof. BIJAY KUMAR ROUT

&

Co-Supervision of

Dr. AMOL MARATHE

Department of Mechanical Engineering
Birla Institute of Technology & Science, Pilani – 333 031(Rajasthan)

BITS Pilani
Pilani | Dubai | Goa | Hyderabad

BIRLA INSTITUTE OF TECHNOLOGY & SCIENCE
PILANI – 333 031 (RAJASTHAN) INDIA

January 2024

BIRLA INSTITUTE OF TECHNOLOGY & SCIENCE

PILANI - 333031 (RAJASTHAN) INDIA

C E R T I F I C A T E

This is to certify that the thesis entitled **"Design and Development of Vision Based Vibration Suppression Strategies for Industrial Robots in Assembly Operations with Gripper and Object Flexibilities"** submitted by **CHETAN JALENDRA,** ID. No: **2016PHXF0420** for award of Ph.D. of the institute embodies original work done by him under my supervision.

Signature of the Supervisor: _____

Name : **PROF. BIJAY KUMAR ROUT**

Designation : Professor
Department of Mechanical Engineering
Birla Institute of Technology & Science
PILANI (Rajasthan) - 333031

Signature of the Co-supervisor: _____

Name : **DR. AMOL M MARATHE**

Designation : Assistant professor
Department of Mechanical Engineering
Birla Institute of Technology & Science
PILANI (Rajasthan) - 333031

Date -

ACKNOWLEDGMENT

I would like to express my sincere appreciation to my esteemed supervisors, Prof. Bijay Kumar Rout and Dr. Amol Marutrao Marathe, for giving me the opportunity to participate in this exciting research and being the best supervisor. I would like to start by expressing my deepest gratitude to my advisors for all the assistance, encouragement, and direction they have given me since the beginning of my research. I owe a great debt of gratitude to them for inspiring me to strive for excellence, refine my research approach, and develop my sense of originality. I want to thank them for all the help, guidance, inspiration, and support they have given me over the years, without which this work would not exist.

I appreciate the encouragement and blessings of Prof. V. Ramgopal Rao (BITS-Pilani Vice Chancellor) and Prof. Sudhirkumar Barai (BITS-Pilani Pilani Campus Director). Prof. Shamik Chakraborty (Associate Dean, Academic Graduate Studies and Research Division) has also inspired me. I'm grateful for his unwavering belief in me and unending enthusiasm for my work. Prof. Srikanta Routroy, Head of the Department of Mechanical Engineering, has been a great help to me, and I am grateful to him. Thanks to Prof. P. Srinivasan (Head of the Work Integrated Learning Programme Division), Prof. Anshuman Dalvi (Associate Dean of the Faculty), Prof. Manishakar Das Gupta (Coordinator of the Institutional Quality Assurance Cell), and Dr. Prateek Kala for their support and insightful feedback. Prof. Karunesh K. Gupta and Dr. Arun Kumar Jalan, two DAC members, have my deepest gratitude for their insightful comments and for making the time to provide their expert departmental review of my thesis. In addition, I'd like to thank everyone who works in the Department of Mechanical Engineering, both academic and support staff, for their enthusiasm, positivity, and helpfulness throughout this project. Mr. Tulsi Ram Sharma of the BITS-CRIS team at the Pilani Campus has been an invaluable resource to me in developing the research apparatus used in this study. It is a pleasure to recognize the efforts of those who helped shape this piece into what it is today.

My colleagues Vivek Tiwari, Shailendra Pawanr, and Amresh Kumar are among the people I owe a heartfelt thanks to for their unwavering encouragement throughout my time as a research scholar there. Dr. Sangram Keshari Das deserves special recognition for his unwavering enthusiasm and dedication to propelling this work forward.

I would like to express my gratitude and appreciation to my wife, Mrs. Bharti, my loving sister, Ms. Mridula, and my brother, Mr. Harsh. Finally, I would like to thank my parents, Mr. Jagdish Prasad, and Mrs. Sunita Devi, who have always been there for me, both now and always. As a final act of gratitude, I pray that God continues to bless me with inner fortitude and patience.

CHETAN JALENDRA

ABSTRACT

Robotic assembly is one of the most important steps in automated manufacturing processes. Industrial robots perform benchmarked assembly operations like peg-in-hole or a horizontal beam-in-slot. Generally, it is assumed that a peg or beam is a rigid object grasped by a rigid robot gripper. The robot performs the assembly tasks through error compensation and impedance control. However, assembly becomes challenging when various flexibility comes into the picture. Flexibility may be present in the robot, robot gripper, and object. In addition, the transient disturbance may cause vibration during robotic manipulation and assembly when the robot gripper is rigid, and the object is flexible. Hence, quick suppression of undesirable vibrations during this automated process will reduce the cycle time and increase the efficiency of the assembly process.

In order to solve the above challenges, an extensive literature review on Peg-in-Hole, Beam-in-slot, assembly using robots was carried out, which addressed the key issue associated with the flexibility of objects and robot grippers. Most of these literature, emphasized the development of low-level control strategies to suppress vibrations of the objects. The low-level strategies require modification in the internal controller of the robot. In contrast, a high-level controller strategy does not need much modification and works along with the internal controller as a second-stage controller. It was observed that the use of external sensors like vision sensors for assembly operations has not been attempted for controller implementation to suppress vibration. Therefore, current work develops vision-based active vibration suppression strategies for industrial robots involved in assembly operations while accounting for the impact of the flexibility present in both the robot gripper and flexible objects.

To understand the challenges in peg-in-hole robotic assembly, an industrial robot with an underactuated non-deformable object (NDO) held by its gripper is considered. The high amplitude and low-frequency oscillation in NDO is observed due to high-speed manipulation motions of the robot arms. Most industrial robots are not endowed with the capability to control and suppress the induced vibration to improve productivity of automated assembly process. Therefore, a contactless vision-based approach for vibration suppression is proposed, which uses a Selective Predictive Vibrational Amplitude Error-Based (SPVAEB) second-stage controller. This controller used a real-time vibration

control strategy that comprised a physics-based model to determine errors for the estimation of controller output. The proposed second-stage controller used feedback from a vision sensor. To demonstrate the robustness of the proposed controller, experimental implementation is carried out on ABB make IRB 1410 model 6-DOF industrial robot with a low frame rate camera. The proposed controller suppresses vibration amplitude up to 96% in less than 3 s, and the time to achieve stability is reduced by 97.5% for a peg-in-hole assembly task. The comparative performance of the proposed controller against PID controller took 3 s compared to the 10 s as proposed controller takes into account system delay and designed control trajectory based on the maximum error in place of amplitude error at every time step.

The proposed second-stage controller dealt with the development of vision-based controller strategies for vibration suppression of a commercially available robot. However, vibration in the NDO may arise due to the presence of flexibility in the gripper. In this case, the flexible gripper object system is modeled as a pendulum with a torsion spring connected to moving support to represent the system. The torsion spring represents the flexibility of the flexible gripper. A contactless vision-based approach for vibration suppression is proposed, which uses a Predictive Vibrational Amplitude Error-Based (PVAEB) second-stage controller. An innovative approach for handling system delays is presented. Based on controller output and system delay, input trajectories are estimated for the internal controller of the robot. In this experiment, two objects have been considered that have a low (<2.38Hz) and high (>2.38Hz) natural frequency. The proposed controller suppressed 95% of vibration amplitude in less than 3 seconds and reduced the stability time by 90% for a peg-in-hole assembly task.

Further, a flexible object i.e., beam, is chosen that is grasped by a rigid robot gripper for assembly into a slot. In the pursuit of vibration suppression during assembly, an innovative robot-assisted camera calibration method is developed to determine the extrinsic camera parameters. This method identified the dimensions of the flexible object grasped and deflection using a virtual marker. In this case, the Finite Element Method (FEM) is used to model the dynamic behavior of the flexible beam. Here, Predictive Maximum Error Based (PMEB) second-stage controller is proposed that uses the maximum error to compute and send the control signal for vibration suppression. The proposed robot-vision method measures the dimension within an acceptable error limit, i.e., ±3%. The developed

controller used two types of robot motions as input for vibration suppression. The first is straight inline motion of end-effector through motion of arms and the second is angular motion to end-effector through wrist motion. It was observed that the controller that used the straight line motion can suppress vibration amplitude up to ~97% in an average time of 4.2 s and reduce the stability time to ~93%. Whereas the controller that used the wrist motion suppressed the vibration amplitude up to ~96% in 2 s and decreased the suppression time by ~97%. There are certain limitations of the proposed controllers due to factors like inaccuracies in the computation of Rayleigh damping coefficients, inaccurate model parameters, and initial conditions of the flexible beam related to tip deflection and velocity. These shortcomings can be eliminated by vision based system identification method was used. In this method the dynamic behaviour of the beam is considered, and the optimized performance based on mathematical model is developed. The data driven model can replace the FEM based model used earlier regardless of the material properties and the dimension of the flexible object. The performance of the data driven controller model is evaluated by comparing performance of straight line arm motion and wrist motion trajectory. Based on the performance of controller, natural frequency based selection of control trajectory is suggested for best performance. Finally, experimental results indicate that the proposed controller suppresses the vibration amplitude by 96% in an average time of 2.86 s and reduces the suppression time by 96%. In conclusion, limitations have been identified in the current vision-based vibration suppression, especially in sensor capabilities and addressed vibration modes. Nevertheless, the foundation has been laid for future exploration in 3D sensors, advanced AI, and enhanced robotic assembly vibration control.

Keywords: Industrial robot, Robotic assembly, Automated assembly, Peg-in-hole assembly, Flexible beam, Flexible gripper, Vibration suppression, Second-stage controller, Camera calibration, Robot-vision, Computer vision, System identification, Data-based optimization, Robust control, Finite element method, System delay.

TABLE OF CONTENTS

Contents Page No.

LIST OF TABLES

LIST OF FIGURES

LIST OF ABBREVIATIONS AND SYMBOLS

Abbreviations

1D	One dimensional
2D	Two dimensional
3D	Three dimensional
ABB	Asea Brown Boveri
AC	Alternative current
Al	Aluminum
ARX	Auto regressive exogenous
CCD	Charged coupled device
CCS	Camera coordinate system
COG	Center of gravity
CPU	Central processing unit
DSC	Dynamic surface control
EIH	Eye-in-hand
EOM	Equation of motion
ETH	Eye-to-hand
F/T	Force and torque
FEM	Finite element method
fps	Frame per second
GPS	Global positioning system
GRG	Generalized reduced gradient
HRI	Human robot interface
HSV	Hue saturation value
HTM	Homogenous transformation matrix
ICS	Image coordinate System
IDLE	Integrated development and learning environment
IMU	Inertial measurement unit
IRB	Industrial robot
IRC5	Industrial robot controller fifth generation
LSPB	Linear segment with a parabolic blend
LWR	Lightweight robot
NDO	Non-deformable object
openCV	open computer vision

PBVS	Position-based visual servoing
PC	Personal computer
PI	Proportional integral
PID	Proportional integral differential
PiH	Peg-in-hole
PMEB	Predictive maximum error based
PnP	Pick and place
PtP	Point-to-point
PVAEB	Predictive vibration amplitude error based
PVC	Polyvinyl chloride
RCS	Robot coordinate system
RGB	Red-green-blue
RoI	Region of interest
SCARA	Selective compliance assembly robot arm
SE	Special Euclidean group
SPVAEB	Selective predictive vibration amplitude error based
SS	Stainless Steel
SSE	Sum of squared errors
TCP	Tool coordinate point
TCP/IP	Transmission control protocol/internet protocol
TCS	Tool coordinate system
USB	Universal serial bus
WCS	World coordinate system

Symbols

K_P	Proportional gain parameter
K_I	Integral gain parameter
K_D	Derivative gain parameter
u	Controller output
Δt	Sampling period
e	Error
C	Coefficient of friction
θ	Swing angle of pendulum
q_T	Trajectory displacement
t_b	Trajectory blend time

t_g	Trajectory travel time
q_g	Total trajectory displacement
q_s	Trajectory starting point
$\ddot{q}^c$	Constant acceleration of trajectory
t_{gap}	Time gap between the zero position and extreme position
t_{rsd}	Robot system delay
t_{sd}	System delay
t_{rest}	Rest time
t_{ip}	Image processing time
t_{mc}	Model computation time
μ	Acceleration of the moving base of pendulum
l	Length
b	Width
h	Height
A	Cross-sectional area
m	Mass
I	Moment of inertia
T	Time period
u_0, v_0	Optical centre
f_x, f_y	Focal length
γ	Skew coefficient
p_w	Coordinate in WCS
p_r	Coordinate in RCS
p_i	Coordinate in CCS
K	Camera intrinsic parameter matrix
Π	Projection matrix
ρ	Density
E	Young's modulus
$w(x,t)$	Transverse displacement of finite element
$q(t)$	Nodal displacement
$\emptyset$	Shape function
M	Moment

F	Force
Δ_t	Column matrix containing velocity and deflection
θ_T	Trajectory angular displacement
θ_e	Maximum angular error
t_g	Trajectory travel time
t_c	Trajectory initiation time
t_e	Time at maximum deflection
B_p	Tip deflection at t_{sd}
a_0, a_1	Rayleigh damping coefficients
x	Amplitude of vibration
X	Maximum amplitude
ζ	Coefficient of damping
ω_n	Natural frequency
ω_d	Damping frequency
α	Phase angle

CHAPTER 1
INTRODUCTION

In modern manufacturing, robotic manipulators play a critical role in factory automation. The assembly process in manufacturing is carried out mainly at the intermediate or final stages. Most of the assembly processes require skill and human labor. However, with the advancement in robotics, manual assembly processes are shifting towards automated assembling processes that improve product quality and increase production output. In this regard, using robot manipulators is the perfect option for enhancing production. It complements human strengths in assembly and manufacturing by handling high repeatability, position precision, high payload, and fatigue (Ahmad and Plapper, 2016).

1.1 Motivation behind research

Assembly is a joining process of parts, usually interchangeable in manufacturing, to make a new composite part that can be used as a sub-assembly or a complete product. Some assembly processes are mating parts, inserting a peg into a hole, laying down actions, force fitting, and putting two parts together. These processes can be carried out temporarily and permanently. The temporary assembly or joining process uses a third part, i.e., a screw, nut-bolt, or rivet for fastening. Examples of permanent joining processes are welding and brazing. The final product obtained from the sequential assembly of components to the subassembly is complex and complicated. In many applications, it is performed manually and is very much labor-intensive. This step requires nearly 40-50% of human labor to get the intermediate or finished product.

The first industrial robot was deployed in 1961 in mass production systems where simple robotic arms were utilized to perform dedicated tasks. In the last few decades, the focus has shifted from mass production systems to flexible ones because of increased demand for product variety and customization. However, it is recently reported that humans still carry out 72% of manufacturing tasks and create almost three times more value than machines in the manufacturing industry (Zhang *et al.*, 2021). Assembly is considered as an important stage in the product lifecycle. Data show that the time spent on assembling takes 20%–50% of the total production time, and the cost for assembly counts about 20%–30% of the total cost of a particular product (Xu *et al.*, 2012). In this scenario, there is a growing need for automated assembly systems that can adapt to various products

assembled. Most products requiring assembly operations have low or medium production volumes, and substantial investments in specialized assembly equipment cannot be economically justified. A robot can be utilized in place of human workers or as a co-worker to perform assembly tasks intelligently, quickly, and continuously. The utilization of robots in industries leads to the term automation, which implies that the robot will be used for physical production processes and information processing. Some researchers show that many companies obtained an increase in productivity by 30%, a reduction of production cost by 50%, and an increase in utilization by more than 85% (Barosz *et al.*, 2020). However, the implementation of robotization requires high costs. Therefore, robotization will be profitable only in certain circumstances, including a high production volume and repetitive and precise tasks with harmful working conditions for people.

Robotic assembly is an essential step in the automated product manufacturing process. It is performed mainly by using an industrial robot (Saha, 2008). Among various assembly operations, the most common form of assembly is peg-in-hole (PiH) assembly. This assembly is considered as a benchmark for almost all assembly tasks that account for approximately 40% of the total assembly task (Jiang, Huang, *et al.*, 2020). In this task, the robot finds the hole location, manipulates it, and inserts a peg into it. There are some challenges during the PiH assembly process. These can be categorized as issues associated with robot interaction with the manufacturing environment. And some problems associated with the robot system and the object itself. Finding the hole location, avoiding collision during manipulation, and jamming the peg during the insertion task are related to the interaction of robot and object with the environment. Vibrations and deformation in the object are issues associated with object properties, gripper design, and robot systems. In literature, researchers have focused on the issues related to the interaction of the robot-object system with the environment. However, a few works address the issues associated with the robot, gripper, and object itself, which are also crucial for assembly tasks.

In robotic assembly, an industrial robot deals with grasping, manipulating, and inserting an object in a hole. The object can be categorized as rigid and flexible. Rigid objects are assumed to be non-deformable with negligible deflection in any dimension. In the peg-in-hole assembly task, the object is assumed to be rigid. The state-of-the-art works are reviewed comprehensively (Xu *et al.*, 2019). The review highlighted the methods to solve associated problems in a PiH assembly.

In most cases, manipulation does not affect the assembly operation if the object handled is rigid. However, the robot must handle impedance, positioning, and alignment errors for rigid object insertion tasks. Whereas for flexible objects such as beams, sheets, wires, and deformable linear objects (DLOs), the robot must handle additional problems such as temporary deformation, permanent deformation, and vibration due to the transient disturbance in the robot (Henrich *et al.*, 1999).

A robot needs to grasp the object with the help of the gripper attached at the tool coordinate point. There are two types of grippers: rigid and flexible or soft. Rigid grippers grasp the object without allowing motion relative to the gripper. In this case, the grasped object and gripper may be assumed as a single unit with no relative motion. Flexible grippers are used in many industrial applications to handle any misalignment during assembly (Bogue, 2016). However, flexibility causes relative motion between the object and the gripper. In this context, the object grasped may exhibit the behavior of a three-dimensional pendulum with a spring at its base. Manipulation of objects using a flexible gripper may result in undesirable oscillations.

In a standard robot assembly operation, an object held by a gripper of a robot is commanded to insert into a hole. This task is performed by the robot internal controller, which controls the movement of an industrial robot. However, the object vibrates after receiving such an input command due to high-speed manipulation. This vibration in the object consumes a good amount of productive time to become motionless before actual assembly. Even after the object becomes motionless, the object position is unknown due to the deflection caused by the flexibility of gripper and object. As a result, the unknown position of the object can cause the failure of assembly task and the object. Therefore, temporary deformation and vibration due to the flexible gripper and the object can be concluded as the dominant problems.

The same problems are associated with the design of the robot. The flexibility and compliance in the robot link and joints can cause vibrations even if the object and the gripper are rigid. However, the vibration related to the robot design can be considered a separate issue compared to the gripper and object. At present, most of the robots deployed are rigid link robots. Therefore, the robot can cause vibration due to its transient motion, not the flexibility of the robot. In the current work, the flexibility of the robot gripper and

object is considered as a cause of vibration. Thus, reducing suppression time improves the assembly process cycle time and reduces manufacturing costs.

Vibration suppression has been a well-known topic in the research community. Several methods have been proposed to suppress vibration as it has adhered to all mechanical systems. Nevertheless, in robotic assembly, where an industrial robot is used for assembly tasks, vibration suppression is still a challenge to make the robot a complete solution. The biggest challenge is applying the vibration suppression methods to the robot with its dynamical model to manipulate in the workspace. Most commercially available industrial robots use their internal controller to control the motion robot arm to execute a desired trajectory. The robot internal controller provides high-level communication to the user with limitations (Kapsalas *et al.*, 2018). Therefore, applying the method to these technologically inaccessible low-level robot internal controllers is extremely difficult.

The above issues can cause delays in assembly and even failure. The undesired vibrations in the object need to be eliminated before the assembly. Vibration suppression methods can be categorized as passive and active strategies. Passive vibration suppression strategies refer to techniques and methods used to reduce or eliminate unwanted vibrations in mechanical systems using passive, non-powered components. These strategies need dedicated design of robot grippers that use materials with high damping properties, such as viscoelastic polymers or metal alloys, to absorb vibrational energy. The gripper can also be designed with shape optimization to reduce vibration transmission, such as adding damping elements in strategic locations or using designs incorporating high rigidity and low mass. Some passive vibration control strategies were proposed for vibration suppression (Chen and Zheng, 1995). It increases the damping effect in the system, which helps quickly suppress vibration. Passive strategies needed a dedicated gripper design and required modification from case to case, making it costlier and time-consuming.

Active vibration suppression strategy is based on close loop control that uses anti-motion to suppress vibration using a feedback system. Most of the proposed force/torque sensor based active strategies are inspired by human skills (Ding *et al.*, 2011, 2012, 2014; Ding, Huang, *et al.*, 2019; Yue and Henrich, 2001, 2005, 2006). Active strategies can be used in two ways: control of vibration during manipulation and suppression of residual vibration after object manipulation. In the first method, vibration control during manipulation is known as vibration free manipulation of objects. The second method

controls vibrations after the manipulation task are completed. The controller provides the adjustment motion that leads to vibration suppression.

An important part of a robotic assembly system is a sensor which plays a key role and completes the control system cycle. A general active vibration control system can use acceleration, piezoelectric, force/torque, and vision sensor sensors. Acceleration and piezoelectric sensors are required to mount on the object to be assembled as feedback sensors for vibration suppression. However, in assembly operations, such a setup of sensors is not feasible and not practical for feedback. Therefore, researchers have widely used the force/torque sensor, which is generally mounted on a robot wrist with a gripper to manipulate the object and gain the ability like a human hand.

A vision sensor can also be used as a feedback sensor in robotic assembly. Vision sensors have many positives, as they can extract more object parameters such as length, shape, deformation profile, and low cost. It can play multiple roles in robotic assemblies, like robot hand-eye coordination, object identification, grasping, and inspection. Despite these qualities, the researchers do not give much attention to using vision sensors for feedback. Some of the main challenges in applying a vision sensor are that the frame rate and motion blur during vibration are much lower than other sensors.

1.2 Thesis aims

This thesis is focused on the design and development of active vibration suppression strategies for industrial robotic manipulators used for assembly operations with object and gripper flexibilities. Industrial robots with six degrees of freedom are mainly used for assembly tasks. These commercially developed robots have some limitations. One of the important limitations is the inaccessibility of the robot internal controller at a low level. These controllers provide only a high level of communication in the form of point-to-point (PtP) trajectory commands. Such a PtP trajectory allows the user to set some trajectory parameters, such as displacement, velocity, and acceleration. Even any change in these parameters during the trajectory execution is restricted to the user (Kapsalas *et al.*, 2018). Hence, the available low-level control strategies are no longer applicable in such a scenario. Therefore, a strategy is needed that works simultaneously with the available internal controller of the robot without disturbing the dynamic model of the robot and control strategy. Such a strategy can be implemented as a second-stage controller that communicates the control action to the internal controller of the robot at a high level. The

internal controller works as the first stage controller that contains the dynamic model of the robot-object system and executes the trajectories.

The strategy should design the control actions as trajectories that can be executed in the robot. The control trajectories are responsible for the suppression of undesired vibration of the object. These trajectories are generated in a separate personal computer (PC) system and communicated to the robot at a high level (Pires and Azar, 2018). In performing these activities, there is a time gap between the determination of the control trajectory parameters and the actual execution of the control trajectory by the robot. The time gap is considered as the delay in the whole robotic system. Therefore, the leading cause of the system delay is the computation time taken by the controller and depended on the hardware capabilities. Therefore, handling various delays is a significant challenge in developing the second-stage controller. Thus, the delays must be accounted for in the design and execution of control action for effective vibration suppression. One possible way to achieve it is if the dynamic behavior of the object is known in advance, the delays can be effectively addressed. The dynamic model can predict the future state space of the system and can plan accordingly. In this case, the performance relies on the accuracy of prediction based on the dynamic model. However, obtaining an exact dynamic model of a system is not easy. Most dynamic systems are nonlinear, whereas these have been approximated to be linear in control systems. The linear dynamic model will have some errors when non-linear dynamic behavior is linearized approximately. Though, it can be compensated using feedback on the state of the system. The feedback system requires a sensor that detects the state of the system. The state of the system is then sending the feedback to the model to reduce the error in prediction. A feedback sensor plays a significant role in successfully implementing vibration suppression strategies.

Vibration suppression strategies have been applied to a robotic system using potentiometers/inertial sensors or force/torque sensors for feedback. These are standard sensors and are mounted on the robot wrist easily. These sensors are helpful for the vibration suppression of objects only. In contrast, gripper flexibility cannot be accomplished with these sensors. It can provide only the vibrational response of the object at the base and fails to provide the object parameters like vibrational amplitude and vibration modes except for the frequency of the system. Therefore, these sensors are

limited to controlling vibration. Therefore, an alternative sensor is needed to make the system intelligent and suppress the vibration effectively.

A vision sensor can fulfill such requirements in the vibration control strategy of the object in robotic assembly. Vision sensors can play a role like the human eye, making the system intelligent and more practical. The use of vision as a percentage in assembly tasks (grasping, feeding, and insertion) is 30%, and automatic inspection is more than 50% (Noe, 1999). Only a single vision sensor can identify the object and its dimensions and measure the deflection, vibration amplitude in SI units, and frequency. It can be used in the assembly also. It does not need to be mounted on the robot or the object compared to the force/torque sensor and prevents unnecessary load on the robot. However, the vision sensor is not computationally cost-effective compared to other sensors. It contributes to the system delay.

Based on the above observations, this thesis aims to develop vision based active vibration suppression strategies. A vision-based vibration suppression method is proposed for a non-deformable object (NDO) that can oscillate about a hinge joint. The delays in the various system components, such as high-level communication, vision sensor, and image processing, are handled intelligently. Next, the gripper flexibility is considered as the cause of residual vibration in NDO grasped by it, and the strategy is developed to suppress vibration. After that, NDO is replaced by a flexible object grasped by a rigid gripper. A robot-assisted camera calibration method is proposed that eliminates the need for any physical reference like a checkerboard. The robot vision method is developed for object identification, dimension measurement, deflection, and vibration of the flexible object grasped by the robot. The flexible object is modeled using the finite element method (FEM), and the model is used in the vibration suppression method.

Subsequently, a vision-based system identification method is developed to reduce computational load and the time necessary to handle the FEM model. The methods should be capable of handling flexible objects regardless of material properties and dimensions. These vibration suppression methods even can handle the disturbance caused by collision or any other means during assembly. The thesis attempts to use low-cost, commercially available camera/vision sensors, as high-speed or stereo cameras are costly and computationally expensive. The vision sensor does not interfere with the robot workspace.

The vision system developed does not need a skilled user to calibrate and mount the vision system at any specific pose. A simple vision sensor like the used camera sensor can be used. The proposed method drastically reduced the suppression time and vibration deflection. The proposed controller used two types of robot gripper motion: (i) straight inline motion and (ii) wrist motion. The performance of controller using both types of motion is investigated to obtain the optimum performance for a particular case of flexible objects. All these advantages, such as the low-cost camera, delay not only assists the assembly task and makes the system intelligent but also save time and money.

1.3 Thesis structure

The research aims to develop active vibration control strategies for industrial robots used in the assembly operation of the object with gripper and object flexibility. These strategies are validated with a commercially available ABB make IRB 1410 industrial manipulator in simulation and experimental environments. There are three prominent cases of vibration: the vibration of a non-deformable object (NDO) with a single degree of freedom, the vibration of NDO due to gripper flexibility, and vibration in a flexible object like a metallic beam. The strategies for all the above cases are discussed. The robot vision method discussed here is used for feedback to the system and object identification, and dimension measurement. The following explains the important contents of each chapter and its contribution to the research topic.

Chapter 1 discusses the motivation of the research with a brief introduction to the importance of robotic assembly. The aim of the thesis is discussed by highlighting the various issues faced in applying control strategies to commercially available robots. It ends up with the structure of the thesis.

Chapter 2 provides background information on vibration control strategies developed for the industrial robot used in assembly operations and research gaps. The discussion is categorized based on the low-level and high-level control strategies, types of robots used, the sensors used, and physics-based and data-based modeling of the system, along with the robot vision strategies for object identification, vibration measurement, and camera calibration techniques.

Chapter 3 presents the active vibration suppression strategy proposed for the vibration suppression of an NDO with a single degree of freedom. A vision sensing strategy is

developed for the feedback to the robotic system. A square cross-section rigid wooden object is chosen that can oscillate about a hinge joint grasped by a rigid gripper. A physics-based model is used, and the control strategy is simulated. Simulation and experimental results validate the performance of the controller and are compared with a conventional PID controller.

Chapter 4 introduces a flexible robot gripper utilized to assemble an NDO. Although the flexibility of the gripper enables the NDO to move, it also causes unwanted vibration due to the high-speed motion of robot. A hollow square cross-section aluminum tube connected to a metal strip and a soft PVC tube is employed to address this issue. A physics-based model is developed to represent the gripper flexibility as a spring element located at the base of the NDO. A vision based vibration suppression strategy is developed for such scenarios and demonstrated through NDO assembly. The performance of controller is validated through simulation and experiments.

Chapter 5 presents the case of flexible objects assembled using an industrial robot. A robot-assisted camera calibration technique and robot vision method are discussed. The robot vision method is developed that identifies the object grasped by the robot gripper and measures its dimension along with the vibration. A flexible beam is considered as a flexible object that exhibits temporary deflection and vibration due to transient disturbances of the robot. The flexible beam model is obtained using the FEM. In this chapter, the vision-based vibration suppression strategy is developed that provides control action in the form of straight and angular motion of the robot gripper and wrist. The proposed controller used the FEM based computational model to predict upcoming errors in the deflection of the beam. Both the simulation and experimental results validate the performance of the controller tested on the three different metallic beams regardless of material properties and dimension. The developed strategy suppresses the vibration caused by high-speed motion of robot. It handles the disturbances to the object during the assembly task even after completion of the vibration suppression. The performance is also compared with the results available in the literature.

Chapter 6 presents the advancement of the proposed vibration suppression strategies. The vision-based system identification method is applied to develop the model of the vibration of the flexible objects using its vibrational response during the assembly task at high speed. The obtained model is used in the vibration suppression control strategies. The

controller design is based on the behavior of beams which will use either a straight line or angular motions of the robot to suppress vibration. The developed control strategies are implemented by conducting physical experiments. In these experiments, the vibration of three flexible beams is controlled with straight line motion using an arm or angular motion using the wrist.

Chapter 7 presents the thesis summary, its contributions, limitations, and the future directions of the work. The improvements in the performance of the proposed methods are presented in tabular form. Some important steps are discussed in various appendices, which provide detailed steps and necessary information to make the thesis more readable.

CHAPTER 2
LITERATURE REVIEW

In the previous chapter, the robotic assembly of flexible objects and the associated issues have been discussed with the aim of the present work. This chapter discusses the recent developments in the area of robotic assembly. The fundamental elements of the robotic assembly are the type of robot, type of gripper, properties of parts used for assembly, types of sensors used to sense the object in the environment, types of controllers, and the related technologies used for assembly. In this chapter, the latest state-of-the-art developments in these elements are discussed.

2.1 Robotic assembly

Product manufacturing industries are scurrying towards complete process automation with little human intervention. Robots are the perfect option for enhancing production automation and complementing human strengths in manufacturing processes, such as assembly, handling high repeatability, position precision, high payload, and fatigue. Automated assembly processes with state-of-the-art robot technologies will increase productivity in this case. A study compared the approximate efficiency of robotic applications versus manual applications. The efficiency of manual machine tending was about 40%–60%. For robotic machines, tending was about 90% (without set-up) (Barosz *et al.*, 2020). However, exact values are dependent on the characteristics of the real workstation. For successful assembly, an industrial robot requires comprehensive sensing ability, a priori knowledge of all parts to be assembled, and assembly environments. Therefore, industrial robots need an automatic intelligent solution to detect the frequently occurring risk of expected collisions and misalignment between the parts. It should also be able to quickly change the trajectory for collision prevention with other machinery, working parts, and humans.

The significance of the industrial robot is much dependent on the robot gripper. The gripper is also known as the end-effector device attached to the wrist of the robot responsible for performing assembly operations. Here the robot gripper can be used in assembly operations with abilities to handle objects of different types: parts, fasteners, and assembly tools. A multiple end-effector system will help the robotic assembly to manage all the cases.

The robotic assembly has the following advantages (Çil *et al.*, 2017):

1. Robots can perform repetitive tasks without interruption, leading to high throughput in traditionally dangerous, dirty, and difficult work areas.
2. Robotic assembly can be advantageous in terms of costs, stable quality, increased reliability, high payload, fatigue, and product yield for batch and mass production.
3. The involvement of robots makes the manufacturing process quite flexible for changeover among designs. It can be applied to other manufacturing processes for easy adaptation variation in production lines and variable production volume.
4. Robots can be very efficient in assembling long and flexible parts and small parts, for instance, micro-level parts.

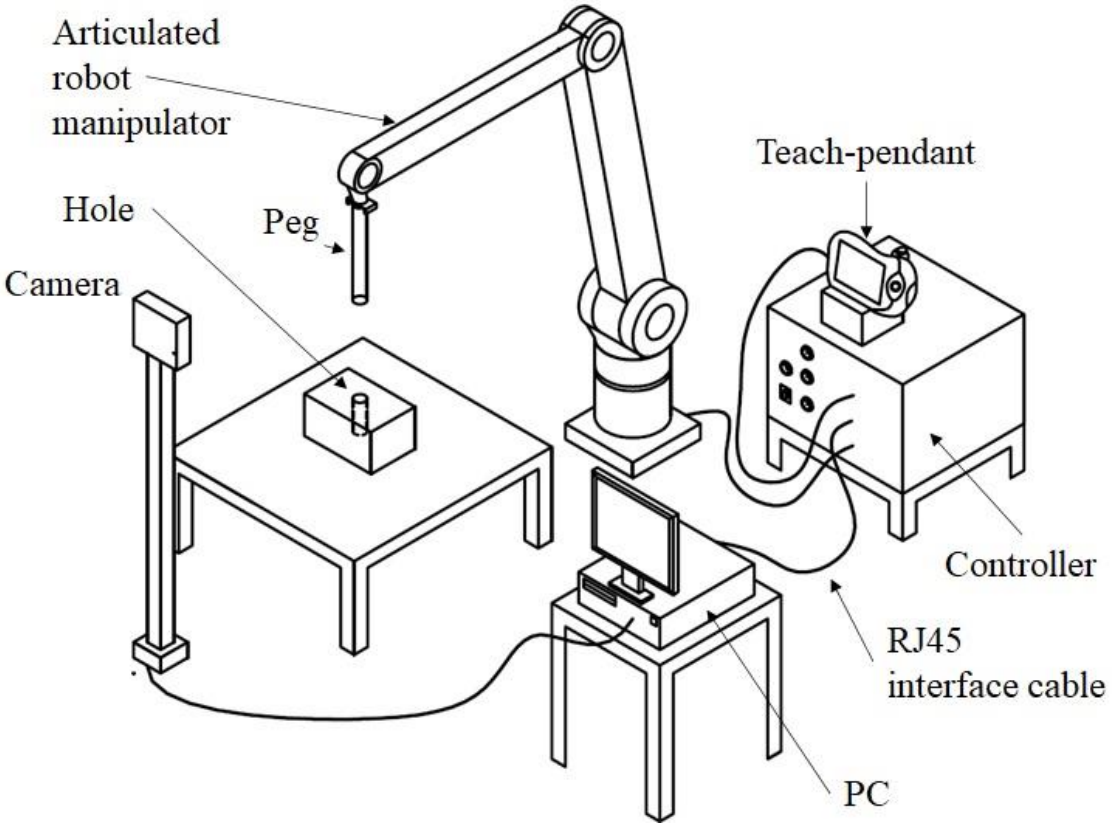

Figure 2.1 A robotic assembly of peg-in-hole with the vision sensor.

The most common assembly representation is a Peg in Hole (PiH) assembly. A cylindrical peg will be inserted into a hole, as shown in Figure 2.1. Here, PiH assembly is the most basic and benchmark problem in which a peg is inserted into a hole (Cienfuegos *et al.*, 2016), assuming a standard cross-section shape. The setup consists of an articulated robot manipulator, teach-pendant, controller, PC, camera, peg, and hole.

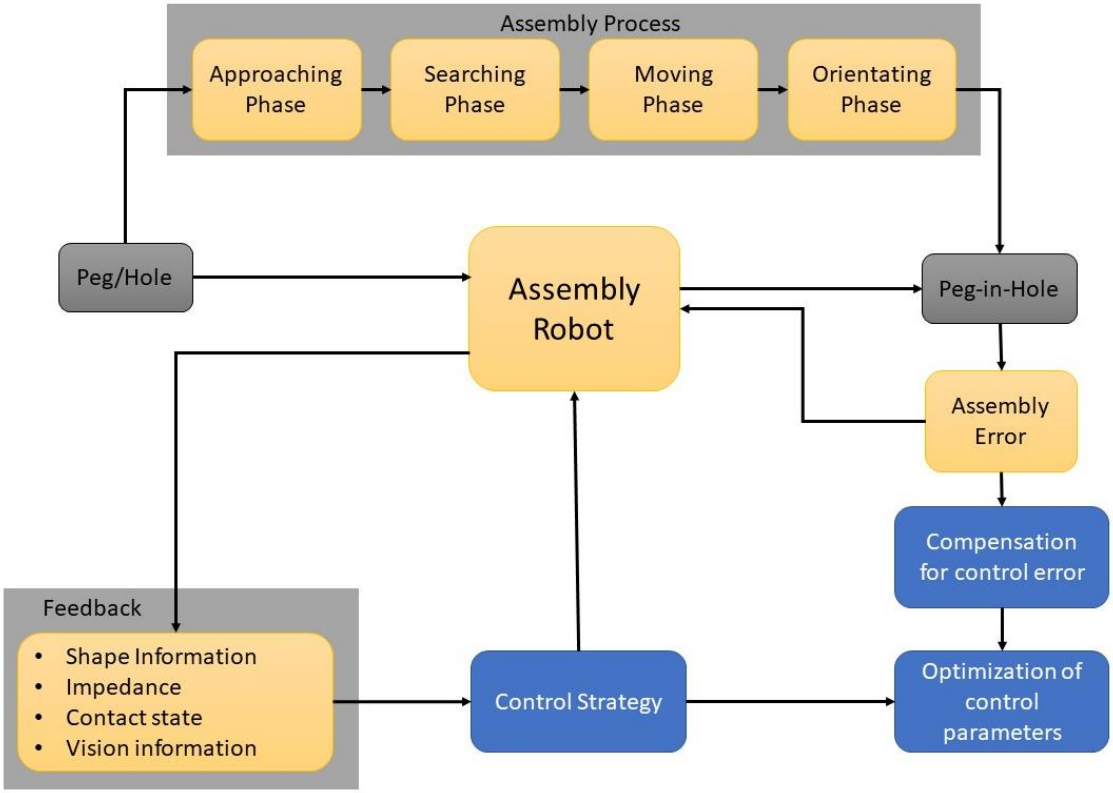

Figure 2.2 Robotic assembly process schematic diagram

It is an excellent example of the assembly process, which can be automated using robots to increase production. The robotic assembly process is shown in Figure 2.2. The robotic assembly has four phases: (i) Approaching phase, (ii) Searching phase, (iii) Moving phase, and (iv) Orientation phase (Jiang, Huang, *et al.*, 2020). The assembly robot performs based on the control schemes using the information provided by feedback sensor, i.e., force sensor, and vision sensor (Hayat *et al.*, 2022).

Intelligent robotic assembly has more aspects that justify using robots in assembly tasks. These aspects include (i) sensor-based part identification, grasping strategies, determination of hole location (Bhuyan, 2019), (ii) robot guidance with impedance control, obstacle avoidance, and (iii) error compensation and prevention of wedging and jamming during insertion task (Xu *et al.*, 2019). The researchers have been continuously working to solve the issues related to these aspects. State-of-the-art can be categorized based on significant elements involved in the robotic assembly. These are the objects to be assembled, sensors, robot configurations, tools, and technology.

2.2 Types of objects used in robotic assembly

Most assembly methods are based on the standard PiH assembly, which assumes cylindrical, rectangular, and complex shapes of a peg and a hole. It exhibits common issues such as alignment errors, wedging, and jamming. The material properties add more issues, such as temporary and permanent shape deformation and undesired motion. In industrial environments, the production parts have complex shapes and become more complicated with flexibility. The method developed can be categorized based on the shape, deformable and non-deformable object (NDO) in the following subsections.

2.2.1 Non-deformable object assembly

The NDO assembly assembles parts that do not substantially deform during assembly. It is a geometric problem; if parts are identical, perfectly made, and perfectly positioned, the assembly will always be successful and free of excessive mating force. The assembly of NDO can be divided into standard shapes and production part assembly.

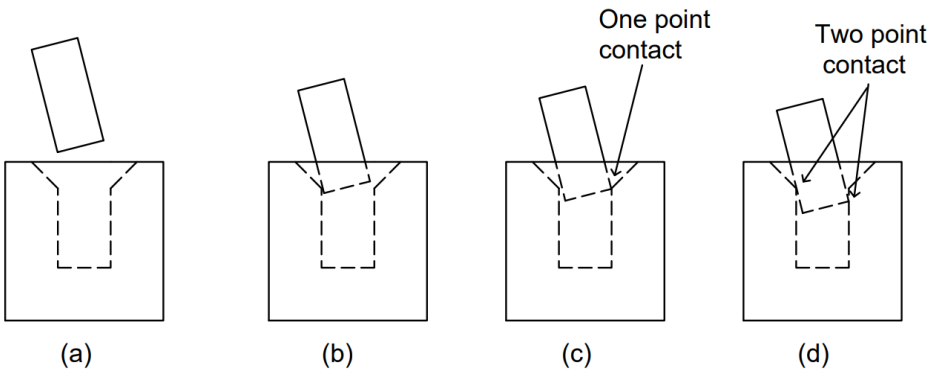

Figure 2.3 Four stages of assembly: (a) approach, (b) chamfer crossing, (c) one-point contact, (d) two-point contact

The popularity of the PiH insertion task is due to its complexity as a control problem that requires both position and force regulation. A human may achieve this task very quickly because a human can naturally perceive all the factors that this process involves. Nevertheless, for a robot, this task can be very complex. On the other hand, it will be a great benefit if robots can learn human skill and apply them autonomously. This way of functioning will improve productivity, reduce cost, and reduce repetitive manual tasks. There are four stages of PiH assembly: approach, chamfer crossing, one-point contact, and two-point contact (Whitney, 1982), shown in Figure 2.3. During contact between rigid assembling parts, it generally faces jamming issues that may lead to damaged parts and increased cycle time.

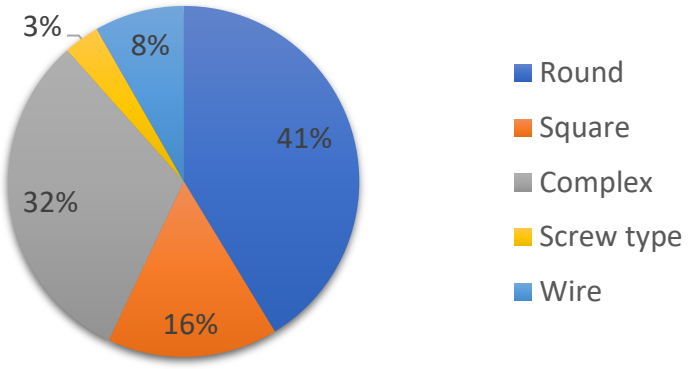

Figure 2.4 Types of shapes of objects used in robotic assembly.

Figure 2.4 represents the different types of shapes considered for robotic assembly in percentage. The researchers considered the circular cross-section object in most assembly cases. Then the square shape to demonstrate an assembly method. A round shape object represents an assembly scenario with jamming, wedging, alignment, and impedance issues. However, most production parts have complex shapes. An irregular shape with multiple edges and corners can represent a complex shape. The methods proposed based on complex shape objects can be applied to the assembly of production parts like a screw (Le *et al.*, 2016), micropart (Shen *et al.*, 2021), and spacecraft (Jiang, Cui, *et al.*, 2020).

Complex shape objects can replicate the behavior of most production parts. Nonetheless, researchers proposed methods considering a production part assembly such as strain gauge (Zheng *et al.*, 2013), screw fastening (Pitipong *et al.*, 2010), mobile phone (Feng *et al.*, 2017; Song *et al.*, 2020), chip-in-hole (Ho *et al.*, 2018), frame assembly (Fleischer *et al.*, 2014; Nottensteiner *et al.*, 2016; Qin *et al.*, 2016), golf club heads (Natsagdorj *et al.*, 2015), ball socket joint (Liu, Zhu, *et al.*, 2019), solid rocket motor assembly (Zhang, Pu, *et al.*, 2019), wheel hub (Cao *et al.*, 2019; Prabhu *et al.*, 2016), power connector (Kobari *et al.*, 2013), USB connectors (Nammoto *et al.*, 2013), electronic connector (Song *et al.*, 2017). These methods may apply to unique objects, thus limiting their usability.

2.2.2 Deformable objects assembly

Deformable objects, compared to NDOs, can be deformed by contact force during assembly (Kim *et al.*, 1998). Information about their deformation and possible misalignments between mating objects is essential for successful assembly. However, because of the nonlinear and complex relationship between object deformation and

reaction forces, it is difficult to acquire all the required information from them alone. Thus, deformable objects are more difficult to assemble due to their deformation during the assembly operation. Measuring object deformation and obtaining the relationship between object deformation and the forces acting on objects, such as reaction forces and their weight, constitute primary research goals.

Some recent developments in the last decade for standard flexible object assembly were proposed by (Jain *et al.*, 2011, 2015, 2018; Jain, Saha, *et al.*, 2013; Jiang *et al.*, 2012; Shi *et al.*, 2012; Wan *et al.*, 2017). The emphasis of this literature was on the assembly of flexible objects and less on rigid parts. The reason may be the uncertainty in the flexible object whose modeling is challenging and needs a state-of-the-art advanced sensor system. Nonetheless, some real flexible object assembly methods such as wire connectors (Yumbla *et al.*, 2020), sealing ring of battery lid (Gao *et al.*, 2017; Ma *et al.*, 2016), carburetor and gasket mating (Shoureshi *et al.*, 1989) were proposed. In the assembly process, it is considered that robots perform the assembly task. However, in all cases, it might not fulfill all the requirements. Therefore, the following section highlights the role of robots in design, dexterity, manipulation, and speed.

2.3 Need of sensors in robotic assembly

One of the main aspects of robotic assembly is intelligent interaction in an assembly environment full of uncertainty. Intelligent robotic assembly is expected to meet the challenge of dealing with the problem of uncertainty in the real world. Inevitably, there are variations in the shape and position of the parts. To achieve a task, programming a sequence of robot motions has to consider these uncertainties. One way to reduce uncertainty is to use sensors. Due to a lack of sensory capability, most robots cannot interact intelligently with their working environment. For instance, in a robotic assembly cell, the parts presented to a robot must be in predetermined precise locations and orientations. Therefore, including sensors make a robot intelligent and help in decision-making and performing tasks like a human.

Sensors used in the literature in the robotic assembly are listed below:

1. **Vision sensor:** A vision sensor deployment is an eye for the robot in a robotic assembly system. Vision sensors can provide live object position, orientation, dimensions (Centre of gravity, 2D, and 3D), shape (simple round, square and complex), and obstacle avoidance in static and dynamic robotic assembly. The

main types of vision sensors used in robotic assembly are single 2D cameras, stereo vision, and multiple cameras. These are configured as eye-in-hand and eye-to-hand. For flexible parts, e.g., wire, beam, sheet metal, and wire harness, a vision sensor can determine the elastic and plastic deformation and force acting on the part during the assembly process.

2. **Force/Torque (F/T):** F/T and load cell sensors measure force/torque acting on the parts during assembly, such as the nut-bolt assembly. F/T data are beneficial in finding a hole position, detecting contact, applying controlled force, avoiding collision, and preventing jamming. Generally, F/T sensors are mounted on the end-effectors of the robots.
3. **Laser sensor:** Laser sensors determine three-dimensional (3D) object depth information. The holes and edges can be easily identified and measured using this system. The system is also relatively high-cost, robust, and light enough to be directly mounted on an industrial robot.
4. **Load-cell sensors, Tactile, Piezoelectric, Strain gauge:** Tactile, piezoelectric, and strain gauge sensors are used to detect the presence and absence of contact between the sensor and object (Noe, 1999). Generally, these sensors are mounted in gripper fingers to detect the presence of objects in them. These can also be used for force, 3D shape recognition, and control of slippage in handling the components.
5. **Other sensors:** Sensors like the global positioning system (GPS) and Inertial measurement unit (IMU) are used to detect the position and speed of the robot or the parts.

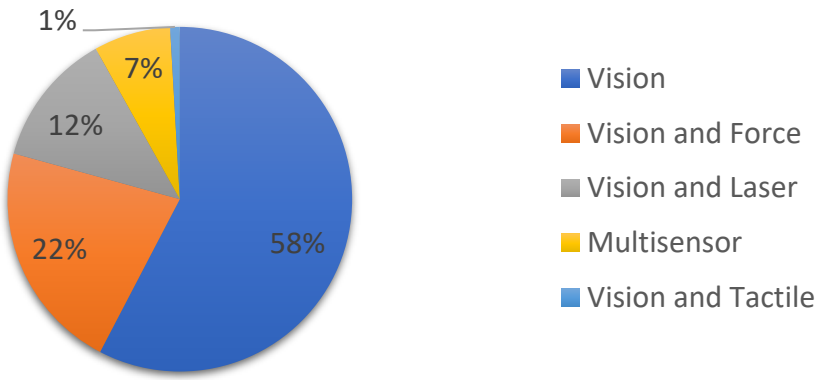

Figure 2.5 Percentage use of vision sensor with other sensors.

These sensors are used for local requirements such as orientation and position of the object, or only a part of the assembled component for the wrist or gripper fingers, and

verification of the presence of the objects and tools in the gripper are treated as local requirements (Noe, 1999). However, vision sensors can be used for global requirements like object recognition and location in the robot workspace. Multiple sensors are engaged to understand the environment with data fusion and deal with the uncertainty in the working environment intelligently. Thus, including a vision sensor with other sensors justifies the significance of it in robotics assembly for all aspects, as the researcher widely used other sensors with vision sensors in robotic assembly. Figure 2.5 presents the percentage use of vision sensors with other sensors based on the literature survey of vision-based robotic assembly.

2.3.1 Vision sensors in robotic assembly

Integrating vision sensor-based methods into the industrial robot is crucial, realizing a highly automatic assembly, improving product quality, and ensuring reliability. A typical industrial machine vision system includes a light source, an optical system, an image-capturing system, an image digitization module, a digital image processing module, and a control execution module. The system first uses a camera or other image-capturing devices to obtain an image of the target. The signals of the images are converted to digital type and sent to a dedicated image processing system to extract the characteristics of the target according to the pixel distribution, brightness, or color information. Further procedures can be done according to the recognition results.

Machine vision systems are used in assembly for three basic tasks: guidance, inspection, and process verification (Lazar *et al.*, 2003). In a guidance application, the vision system serves as the eyes for a production machine that must find a put and place it in a specific location. Examples are PnP operations, such as placing electronic components on printed circuit boards. Inspection operations typically occur at the end of an assembly process and use machine vision to scan for defects. Process verification involves ensuring that a step, such as the insertion of a component, has been performed before a product moves to the next manufacturing step.

The machine vision system does not rely on a single standard sensor. There are different types and configurations discussed in the following section.

2.3.1.1 Types of vision sensors

The vision sensors used for robot assembly are of various types and depend on the assembly task. Monochromatic cameras, RGB color cameras, stereo or 3D vision, and multiple-camera vision systems are commonly utilized. These vision systems have advantages, disadvantages, and limitations, as in Table 2.1.

Monochrome camera sensor provides image data in a single space or hue at different saturation levels, such as a greyscale camera. It divides the grey level between black to white colors using the 2^n formula. For an 8-bit camera sensor, there are 256 grey-levels in the image. This type of vision system has a long-range field of view and is cost-effective in image processing. In most cases, researchers used this camera (Ma *et al.*, 2020; Shao *et al.*, 2020; Song *et al.*, 2020; Yang *et al.*, 2019). It has some limitations, such as the depth of object being challenging to measure and detecting limited object features. The color camera is the extended version of the monochromatic camera that detects images in Red-Green-Blue (RGB) space. This vision-sensing system can detect more features than the monochromatic camera but increases the computation cost of image processing.

Table 2.1 Types of vision systems used in robotic assembly.

Type of vision sensing system	**Image data type**	**Depth**	**Occlusion avoidance**	**Computation Cost**	**Range**	**Cost**	**Limitation**
Monochromatic camera	Grayscale	No	No	Low	High	Low	Less features available
Color camera	RGB	No	No	Medium	High	Low	Sensitive to ambient light
Stereo camera	RGB	Yes	Yes	Medium	Low	Medium	Sensitive to ambient light
Multiple cameras	RGB	Yes	Yes	High	Low	High	Computationally more demanding

A stereo vision system is a smart configuration of two monocular cameras mounted at fixed, known positions. It uses the triangulation method to determine the depth of the scene. Therefore, it has been implemented by (Ding *et al.*, 2021; Gilli *et al.*, 2014; Schoettler *et al.*, 2020; Song *et al.*, 2021). However, the triangulation method limits the range of the camera drastically. Its manufacturing and image processing computation cost is much higher than the monocular camera-based sensing system. Multiple camera-based vision sensing system is a better option that uses multiple cameras. In the literature, two cameras system used by (Jain, Majumder, *et al.*, 2013; Jiang *et al.*, 2021; Le *et al.*, 2016),

three cameras system implemented by (Shen *et al.*, 2021; Weng and Chen, 2017), and six cameras by (Liu, Song, *et al.*, 2019) in robotic assembly. This vision-sensing system detects multiple views of the object simultaneously. Multiple cameras manage environmental uncertainty, occlusion, and obstacle avoidance. However, multiple vision sensor integration makes the vision sensing system costlier. It increases the image processing computation time and the system complexity.

2.3.1.2 Types of vision configurations

Vision is a non-contact sensor system. Even mounting the same on any element of robotic assembly is unnecessary. There are two types of robot-camera setups in robot vision: (i) eye-to-hand (ETH) and (ii) eye-in-hand (EIH). In the eye-to-hand configuration, cameras are mounted at a fixed position in the workspace. In the eye-in-hand configuration, cameras are mounted on the part of a robotic system, such as the robot end-effector, wrist, and upper arm. The former approach provides a larger workspace for assembly, which encourages the researcher to use this configuration (González *et al.*, 2016; Jain *et al.*, 2017; Nerakae *et al.*, 2016; Sato *et al.*, 2020; Xing, Xu, *et al.*, 2016; Zhang *et al.*, 2015; Zheng *et al.*, 2013). However, the increased distance between the cameras and the assembly parts, lower precision, and the possibility of occlusion arise. Nonetheless, ETH configuration can easily integrate multiple cameras to cover multiple views, which helps to avoid the occlusion of the peg and hole due to robot movement (Cienfuegos *et al.*, 2016). The latter approach EIH allows for increased task precision since the cameras are positioned closer to the assembly parts. Some recent development is presented in (Chang, 2018; Di *et al.*, 2009; Ding, Wang, *et al.*, 2019; Huang *et al.*, 2017; Schoettler *et al.*, 2019; Xing, Xu, *et al.*, 2016). However, as the camera and the object get too close, the binocular field of view effect is canceled, leaving two monocular fields of view instead, thus limiting the depth assessments. Therefore, using both setups is more practical than the single one proposed in (Liu, Li, *et al.*, 2020; Ma *et al.*, 2020; Weng and Chen, 2017). Multiple integrations of vision sensors increase the computing cost and complexity of the system.

2.3.1.3 Types of visual servoing

Vision sensors are widely used as feedback sensors in the robotic assembly process. It provides the capability of obtaining relative positional information between mating parts. Nevertheless, certain limitations are associated with it, including extended computation

time required for image processing and calibration and sensitivity to specific illumination conditions. Vision sensors are implemented for the visual servoing of an industrial robot. Visual servoing is defined as controlling the robotic manipulators using feedback from the vision sensors.

Depending on the control mechanism, visual servoing is classified into four groups (Malis, 2002):

1. **3D vision servoing** – This visual servoing is based on a geometric 3D model of the objects and is called position-based visual servoing (PBVS). The control law uses the positional error directly on the vision sensor.
2. **2D visual servoing** – The control error function is directly stated in the 2D image space and is known as Image-based visual servoing.
3. **2½ D visual servoing** – It is better than PBVS, which does not require a geometric 3D model of the object. It is based on partial vision sensor displacement estimation from the existing to the desired sensor poses at each iteration.
4. **Motion-based visual servoing** – Optical flow present in the image estimated using a reference frame.

Most vision systems are based on some fundamental, commonly used image transformations, which are the starting point for sophisticated digital image processing algorithms. The process of extracting data from an image can be divided into the following steps:

1. **Acquisition and storage of a vision signal** – an image is captured from an input device and possibly stored in memory.
2. **Image pre-processing techniques**– choosing RoI (Region of Interest), thresholding, filtration, and morphological operations conducted to eliminate noise (Chen *et al.*, 2015; Gao *et al.*, 2017; Ho *et al.*, 2018; Hu *et al.*, 2016).
3. **Image analysis** – there are three steps in image analysis. (a) Segmentation – Extraction of regions representing objects, (b) Extraction of object features – Estimating quantities of interest, e.g., shape coefficients, area, and color (Chang and Wu, 2012; Ha, 2013; Liu *et al.*, 2016) and (c) Object localization – Detecting features like the center of gravity (CoG) coordinates and orientation (Korta *et al.*, 2014).

4. **Image recognition** – Identification and classification of the objects found in an image in the preceding steps (Chang, 2018; Dharmara and Monfared, 2018; Ogun *et al.*, 2015; Wan *et al.*, 2017; Yumbla *et al.*, 2020). This information can be treated as an input for more advanced processing techniques (Korta *et al.*, 2014).

2.3.2 Vision-based robotic assembly

The vision sensor-guided assembly process begins with image collection of the assembling objects and their environment. It is used for robot camera calibration and acquiring position and orientation data. The insertion task employs a controller, such as a position error compensation method, to control the positional error between the object and the hole. Finally, the robot moves to perform the assembly task. These are common steps in vision-based robotic assembly.

The calibration of the vision system and the robot is essential to a successful assembly. Therefore, some recent camera calibration techniques for EIH and ETH configuration were presented by (Cui *et al.*, 2020; Jiang *et al.*, 2021; Jiang, Cui, *et al.*, 2020; Pitchandi and Subramanian, 2017; Shao *et al.*, 2020). Calibration provides the intrinsic and extrinsic parameters of a camera vision sensor which is required in the visual servoing. Before the visual servoing, the need for position and orientation information is essential to locate the object, hole, or slot. The researchers proposed methods to extract object and hole information like the CoG, position, and orientation of object and hole in the robot workspace (Ding *et al.*, 2021; Fang *et al.*, 2016; Nagarajan *et al.*, 2017). Some strategies were presented to extract the 3D information using stereo or 3D vision sensors (Cao *et al.*, 2019; Chang, 2018; Ma *et al.*, 2016). During the visual servoing of the objects, the robot might encounter an obstacle that needs appropriate techniques for seamless operation. These techniques were presented by (Ahmad and Plapper, 2016; Ge *et al.*, 2014; Jain, Majumder, *et al.*, 2013; Liu, Wu, *et al.*, 2019).

In the final step, the robot must insert the object in the hole using a controller such as an alignment error compensation. The control method uses the vision sensor as a feedback device. These strategies were proposed by (Feng *et al.*, 2017; Huang *et al.*, 2017; Natsagdorj *et al.*, 2015; Prabhu *et al.*, 2014; Yang *et al.*, 2018; Zhang, Pu, *et al.*, 2019). These methods are purely vision-based. However, the application of other sensors with vision sensors cannot be overlooked, such as laser and F/T. The review aims to highlight

the robotic assembly using a vision sensor. Thus, only the vision sensor-based strategies are reviewed. Nonetheless, the vision sensor has not been implemented as the only sensor in robotic assembly laser, F/T, and other sensors have been utilized along it.

The researchers used laser sensor in vision sensing system to acquire a CAD model of the objects (Dharmara and Monfared, 2018; Ogun *et al.*, 2015), compensate for alignment errors (Prabhu *et al.*, 2016; Qin *et al.*, 2016; Wang *et al.*, 2015; Zhu *et al.*, 2020), and visual servoing, for instance, super-twisting sliding mode control (Liu, Zhu, *et al.*, 2020). Laser sensors enhance the vision systems to measure depth, part deformation, and misalignment during assembly. The laser tracker is chosen where its relatively high cost can be justified by its performance characteristics. The F/T sensor with vision system is also used in recent techniques proposed by (Liu *et al.*, 2016; Liu, Li, *et al.*, 2020; Liu, Xing, *et al.*, 2019; Ma *et al.*, 2019; Sato *et al.*, 2020; Wang *et al.*, 2018; Xing, Liu, *et al.*, 2016; Zhao *et al.*, 2020). Mainly, F/T sensors were used along with the vision sensors to make the robot similar to human capabilities. A human uses vision and force sensing while inserting an object into a hole. Thus, researchers tried to give similar capacities to the robotic system. The primary use of the F/T sensor in assembly is impedance control, compliance control, collision detection, robust insertion control, and high precision. It is more important in the case of low-strength objects such as micro parts.

Multiple sensors are also used in some recently proposed methods to avoid uncertainties, avoid obstacles and occlusion, and improve precision (Mishra *et al.*, 2018; Ruth, 2019). An indoor GPS sensor and IMU are used with a vision sensor for trajectory estimation in a cylinder and block assembly operation (Schmitt and Cai, 2014). A laser-force guided robot system was developed for assembling earphone parts on factory automation (Zhang, Li, *et al.*, 2019). The most significant advantage of the system is that it performs well with irregular parts with small sizes and variety. They proposed an assembly strategy for assembling earphone parts with different poses to reduce position errors accidentally from the 3D sensor.

2.4 Challenges in robotic assembly

In literature, much effort has been incorporated into the development of robotic assembly by various researchers. Nonetheless, there are still many challenges in implementing the robotic assembly methods, as stated below.

- Due to the unstructured and dynamic environment of the assembly work, the assembly robot still needs many problems to be solved, such as: low sensing capability, high assembly environment requirements, poor assembly adaptability, low assembly efficiency, and inability to complete complicated assembly of complex environments (Jiang, Huang, *et al.*, 2020).
- From the literature review, DLO handling has been attempted rigorously. However, practical challenges in the robotic assembly of DLOs, such as temporary, permanent deformation and vibration, need more attention. Assembly on a moving workpiece called an assembly in motion demands that the assembly robot is synchronized in all DOF to the moving workpiece on which assembly parts are installed. Limited research has been conducted on producing larger parts, such as aircraft assembly, and assembly tasks requiring tighter tolerance fit, such as transition and interference.
- Vision-based assembly technologies using dual-arm robots are in their initial phase of development. Thus, it opens new opportunities to improve the dual-arm robot capabilities for more challenging assembly tasks by multiple sensor fusion. Integration of vision and force sensors may improve the contribution in accomplishing complicated assembly tasks involving small objects using the dual-arm robot. An intelligent control algorithm needed to be developed to improve the assembly efficiency for peg-in-hole assembly tasks using a dual-arm robot equipped with vision and force sensors. The information about the pose of small targets using vision has not been attempted yet. Here, the multi-link arm robot changes its pose according to the complex pose of targets in unstructured conditions. The application of coaxial vision measurement on large-scale stereo work pieces needed to be considered to achieve it. A more efficient way for robust recognition of the 3-D position and screw-type parts features detection algorithm is required.
- Multivariate calibration, calibration of diversified objects, and assembly of moving workpieces with partial information are some key issues in the application of robots in automatic assembly using vision. Therefore, a new auto-calibration algorithm is necessary, which determines the transformation matrices between coordinate systems of the camera, assembly parts, and robots automatically and more precisely without any standard physical reference.

- Uncertainty compensation, jamming avoidance, efficiency, and accuracy are some challenges in assembling production parts to apply the available methods.

2.5 Vibration suppression strategies

In robotic assembly, the parts grasped by the robot gripper are manipulated at high-speed. High-speed motion in robotic assembly is necessary for the automated manufacturing process in modern industry. A peg-in-hole assembly task represents a generic robot-assisted assembly process. Most researchers focus on developing peg-in-hole assemblies, where the peg is treated as a rigid object. However, a peg will be either a rigid or a flexible part, depending on a broader class of assembly process. Therefore, manipulation and assembly of flexible parts have additional challenges associated with the behavior, such as vibration in metallic flexible parts (beams, wires, sheets) and temporary deformation. These flexible parts can be treated as highly elastic deformable objects in robotic manipulation for assembly (Henrich *et al.*, 1999).

In most cases, the object to be inserted is held firmly and not allowed to move relative to the gripper. In such a case, the object may be assumed as a part of the tool, i.e., the gripper. Many researchers have considered the object rigid and assumed that the object has the same motion as the link of the robotic manipulator. However, in some scenarios, the object can swing freely like a chain held by a robot gripper. It can display three-dimensional (3-D) pendulum motion due to manipulation at high speed. These objects held by the gripper are considered under-actuated systems (Tanner and Kyriakopoulos, 2000), and manipulating these may give rise to undesirable oscillation. This type of undesirable dynamical behavior of objects cannot be neglected, especially when these are moved at high speed. The vibration in a flexible part delays the process and creates instability and safety issues during assembly.

Industrial robots manipulate flexible objects at high-speed using PtP motion trajectories before inserting these into the hole. However, the acceleration of the robotic arm during PtP motion excites vibration while manipulating flexible parts. The undesired residual vibrations in flexible objects consume extra time for naturally damping the vibration and completing the assembly process, which increases the cycle time of manufacturing processes. Therefore, it is essential to suppress the undesired vibration quickly to complete the PiH assembly task.

The undesired vibration in flexible objects can be suppressed using passive and active approaches. The passive approaches are based on vibration energy dissipation dependent on the design of the gripper. It needed a unique design of the gripper to absorb the vibration energy. In contrast, the active control strategies suppress the vibration through the anti-motion provided by a robot. The methods proposed by the researchers are discussed in the following section.

2.5.1 Active vibration suppression strategies

The investigation of residual vibration suppression during robotic assembly has been pursued by researchers for the last decade or so. Many researchers have considered the flexible object as a deformable linear object (DLO) and implemented vibration suppression strategies to suppress residual vibrations to solve the problem. Initially, feed-forward strategies have been developed to deal with such a problem. Starr proposed an open-loop feed-forward control algorithm to achieve swing-free transportation of suspended objects with a path-controlled robotic manipulator (Starr, 1985). Although the method is modest and applicable because of the open-loop control nature, its real-time implementation requires zero initial conditions. Chen and Zheng proposed a deformation transition graphs-based approach that guides a robotic manipulator for vibration-free manipulation of deformable beams (Chen and Zheng, 1995). It was an open-loop passive control approach. However, the application was limited due to the stable initial condition of the robot manipulator motion and a relatively simple trajectory of the previous motion. The latest development by the researchers can be categorized as low-level control and high-level control strategies.

2.5.1.1 Low-level control strategies

The low-level control strategies can be implemented in the internal controller of robot and sometimes require modifications in the dynamic model of internal controller. Such as Jain and Khorrami proposed a model of an articulated robot with a flexible payload, assuming a multi-link robot with a flexible link at the end with no actuation (Jain and Khorrami, 1995). An adaptive vibration suppression scheme accommodates the unknown or varying payloads using a force/torque sensor. Alici *et al.* presented a series of trajectories planned through a strict mathematical model to suppress the residual swing at the end of the transportation. They addressed the swing-free transport of suspended objects which robot

manipulators cannot grasp. Therefore, it must be carried by a hook or a similar device attached to the manipulator endpoint (Alici *et al.*, 1999). Jiang and Kohno proposed a linear control method based on force/torque feedback to suppress the vibration of flexible objects manipulated by a robot (Jiang and Kohno, 2002). The control scheme is divided into two parts. One control scheme assumed the robot links heavyweight compared to the flexible object and calibrated accordingly. These proposed strategies require precise knowledge of robot dynamics, which is unfortunately not the case for many industrial robots. Smith *et al.* used a dual-arm robot and presented a method for developing swing-free motion trajectories (Smith *et al.*, 2004). The method was designed only for base motion disturbance-free manufacturing environments. Chang and Shaw used adaptive sliding control and feedback active vibration control to deal with model uncertainty and the time-varying disturbance for a vision-based pan/tilt platform (Chang and Shaw, 2007). Although, its real-time implementation requires more study on the vision for complex and realistic backgrounds. Huang *et al.* developed a new approach to simulate the behavior of DLOs while manipulating them for robotic assembly (Huang *et al.*, 2008). The dynamic 2-D deformation of an inextensible linear object was formulated using the finite element method (FEM) and Lagrange motion equations for a single DLO. Ding *et al.* presented a skill-based position-control system for DLO manipulation based on a fuzzy controller appropriately switched to a PI-controller. The FEM and Lagrange motion equation is used for the dynamic model (Ding *et al.*, 2011). Its effectiveness is assessed via simulations and tested with an adaptive sliding mode control with input saturation (Ding *et al.*, 2012, 2014). Qiu *et al.* presented a vision sensor feedback-based active proportional plus derivative and finite-time control for residual vibration suppression of a piezoelectric flexible cantilever plate (Qiu *et al.*, 2016). Again Ding *et al.* applied a dynamic surface control (DSC) strategy for oscillation suppression at the end of a DLO throughout the manipulation of DLO (Ding, Huang, *et al.*, 2019). In the latest research, this problem is handled uniquely, where controlling force is applied externally, not by the robot. Yang *et al.* suppressed the bending vibration of a flexible long beam by optimizing the replacement of the distributed rotor module (Yang *et al.*, 2020). They applied a rotor on the flexible long beam for vibration suppression.

In most cases, the proposed vibration suppression strategies have considered the object a DLO and a flexible metallic beam. The modeling of these objects has been done based on the FEM and Lagrange equations. The controllers are based on conventional PID-type

controllers and advanced methods such as fuzzy logic, adaptive control, sliding mode, and dynamic surface control. These strategies successfully suppress vibrations or prevent their excitation of it. However, the successful implementation of low-level control strategies requires an exact dynamic model of the robot, which is difficult in most cases. These low-level control strategies require some form of modification in the commercially available industrial robot controller. Changing the dynamic control scheme of the robot only for vibration suppression may increase the cost of the robot or may limit it to a particular task. The low-level controller of the industrial manipulator is not accessible to users generally and does not allow speed or acceleration modifications to develop appropriate control schemes. These control schemes cannot directly apply to industrial manipulators with limited velocity and acceleration values. Therefore, the researchers proposed innovative high-level control schemes using less hardware to overcome the above limitations. These strategies are discussed in the following section.

2.5.1.2 High-level control strategies

The industrial robots deployed in the industries come with some limitations. Such as a user can set some trajectory parameters to provide automatic motion to the robot. These are PtP trajectories with parameters such as the displacement between two trajectory ends and velocity. Acceleration is not accessible to the user; however, change in acceleration is possible through percentage reduction, not the exact value. This limitation in acceleration is the foremost hurdle that prevents the implementation of dynamic control strategies in the robot controller. In any dynamic control scheme, the control output of a controller is in the form of acceleration to the system. Acceleration represents the input force that controls the dynamic system. Therefore, the control scheme developed for a commercially available robot should provide the control motion through PtP trajectories. It prevents the implementation of an available control scheme for the industrial robot controller. However, some control schemes have been proposed for vibration suppression of flexible objects in the literature.

Yue and Henrich presented a model-based acute vibration reduction method for DLOs using adjustment motions (Yue and Henrich, 2001). Since model-based vibration suppression strategies might work well for a given situation, their effectiveness and implementation are critical for real-time and other situations. Subsequently, they developed force/torque sensor-based skills for handling DLOs in a manner suitable to

reduce acute vibration. The skills are inspired by the simple human skill that consists of one or two adjustment motions (Yue and Henrich, 2005). The vibration was measured using a force/torque sensor equipped at the wrist of the robot. Later they addressed the problem of active damping skills for handling DLOs and proposed a strategy inspired by human manipulation skills (Yue and Henrich, 2006). August *et al.* designed and presented a transportation and stabilization system for suspended loads, consisting of an industrial robot manipulator, an optical sensor system, and a controller (August *et al.*, 2010). This work focused on only the transportation of pendulum-like suspended loads on construction sites. Boschetti *et al.* introduced an enhanced delayed reference control to control the swing of a robotic crane transporting a suspended load, significantly decreasing oscillations using stereo vision feedback (Boschetti *et al.*, 2014). Kapsalas *et al.* investigated an 'AutoRegressive with eXogenous' (ARX) based vibration control problem of flexible objects manipulated by industrial robots under normal production conditions (Kapsalas *et al.*, 2018). The applied convention PID-type controller for vibration suppression. Zurn *et al.* proposed a novel framework using a kinematic trajectory with a controller for manipulating DLO with constraint (Zurn *et al.*, 2021). Due to the high calculation effort for the simulation, increased dead time is observed.

In high-level control strategies, two control strategies work simultaneously to suppress the vibration. The vibration suppression strategies are active at high-level, providing the control input trajectory. These trajectories are communicated to the low-level controller of the robot. The main benefit of high-level control strategies is that the modification of the controller of the robot in any form is not required. These can be applied directly to any available industrial robot with some modifications. Nevertheless, the development of these control strategies is limited. The leading reason is that the most advanced control strategies, such as sliding mode control, dynamic surface control, H-infinity, linear quadratic control, and model predictive control, apply to the low-level system.

The successful implementation of control strategies comprises the use of sensors. The discussion is provided on the method proposed for vibration measurement and control in a robotic assembly in the following section.

2.5.2 Types of sensors in the controller for vibration suppression

A sensing system is the key component of any dynamic control strategy. The use of sensors can be avoided in feed-forward controllers where the control input is provided based on the knowledge of the dynamic model of the system. The successful implementation of a feed-forward controller requires an accurate dynamic model. Obtaining an accurate mathematical model of a real dynamic system is difficult. Dynamic systems are nonlinear in nature. The nonlinear dynamic model can be stated mathematically. However, the exact solution with many variables increases the computation cost. It can be solved by approximating the nonlinear system to a simple linear system. The linear system adheres to errors. The use of a sensor can compensate for the error. A sensor updates the state of the system and reduces model errors in real-time. The leading sensors used in the available development are the force/torque (F/T). Besides the F/T sensor, the vision sensor systems are also used for feedback to the system. The development of control strategies can be categorized based on the sensor implementation.

2.5.2.1 Force/torque sensor

In the literature, primarily, the F/T sensor was implemented for feedback. The robot held the flexible object by a gripper and manipulated it. It was mounted on the wrist of the robot, and the gripper was attached to it. This sensor configuration provides the force and torque data of the base of the flexible object. Some of the work can be found in (Chen *et al.*, 2007; Jiang and Kohno, 2002; Kapsalas *et al.*, 2018; Yue and Henrich, 2005, 2006). These control strategies used force/torque sensors for vibration suppression which are vulnerable to sensor noise (weak signal) for lightweight objects as well as small-amplitude vibrations. In addition, the force/torque sensors cannot measure the deflection of the beam and mode of vibration. Thus, these strategies are suitable only for limited vibration suppression applications. The above limitations with the force/torque sensor can be accomplished if a vision sensor is used, as discussed in the following sub-section.

2.5.2.2 Vision sensor

Vision systems in robotic assembly can play an important role in vibration suppression strategy as a feedback system and vision-based robot guidance to perform assembly tasks. The vision system can measure the beam deflection, vibration, mode of vibration, and

beam dimension. A low-level PID controller was proposed for vision-based vibration suppression of deformable linear objects (DLO) (Huang *et al.*, 2014). The DLO was a rubber strip, and vibration was detected through the background subtraction method. Qiu *et al.* used a CCD camera to detect the bending and torsional vibration of a cantilever plate by applying image filtering, image segmentation, and object recognition methods (Qiu *et al.*, 2016). Boschetti *et al.* used two camera-based vision systems to detect the swing of a suspended load by a robot in three-dimensional space (Boschetti *et al.*, 2014). A flexible rope crane system was studied using a vision system and machine learning method to obtain the rope curve model and measure the end-angle (Yang *et al.*, 2019).

Besides the advantages of vision sensing, it has some drawbacks, such as time for calibration and high computational costs that make it inconsequential. The measurement of an object dimension, vibration measurement, and deformation in 3D space using a 2D camera is a major problem for the vision-based measurement system. Although this type of requirement can be achieved using a 3D vision system, which further increases computational cost and requires high-capacity hardware for the processing increased cost. Some vision methods have been proposed to solve this problem using a physical reference (marker) on the object itself identified by the camera (Ji, 2010; Ji and Chang, 2008; Liu, Wu, *et al.*, 2019; Mu *et al.*, 2017; Ri, 2020). These methods were based on predefined physical references such as planner pattern, grater pattern, pre-known object, and structural lights on the object to track displacement and deformation measurement using a single 2D camera (Enebuse *et al.*, 2021). Some methods for 3D measurement based on digital image correlation were proposed (Bhowmick *et al.*, 2020; Helfrick *et al.*, 2011; Pankow *et al.*, 2010; Quan *et al.*, 2008; Réthoré *et al.*, 2014; Wang *et al.*, 2020). These methods can measure out-of-plane deflection or deformation without physical reference to the object. The digital image correlation method-based technique matches the pattern of the image at a sub-pixel level, however, for only small deflection and is not appropriate for larger deflection or deformation. Another drawback is the increase in computation cost, which delays decision-making and is not recommended for real-time vibration control. A 3D vision-based vibration measurement technique(Yu *et al.*, 2022) and calibration methods using a reference in the workspace and checkerboard were proposed (Deniz and Cakir, 2018; Ji and Chang, 2006; Pai *et al.*, 2013; Zhang *et al.*, 2017). This proposed vibration suppression and sensing system methods have shortcomings, which are concluded in the next section.

2.6 Gaps in research

Some attempts have been made for vision-based vibration suppression of flexible objects in robotic assembly at both low-level and high-level. Though, its application to the industrial robot is still difficult due to methods developed for particular cases. The comprehensive literature review on robotic assembly concludes that:

- The impact of robot gripper flexibility on both deformable and non-deformable object robotic assembly has not been thoroughly investigated in previous studies.
- Prior research has not extensively explored the use of mathematical models of objects in developing and implementing vibration suppression strategies on real-world robotic systems.
- The effect of changes in object dynamic behavior, which can be influenced by the object's size, shape, and material properties, on the performance of controllers used for vibration suppression has not been adequately studied.
- There is a lack of research on the impact of various delays within robotic systems, vision systems, and other integrated hardware on high-level control strategies, which is crucial for developing effective vibration suppression techniques.
- The potential of wrist motion in industrial robots for suppressing vibrations in flexible objects has not been thoroughly investigated in prior studies.
- Although some literature exists on using vision sensors for tasks such as object identification, dimension measurement, system identification, and vibration suppression, only a few studies have addressed these topics.

2.7 Objectives of the proposed research

Based on the identified gaps in the areas of robot assembly operation, the following objectives are enumerated below for further investigation.

1. Design and development of vision-based active control strategies for vibration suppression of non-deformable objects in assembly operations using industrial robots.
2. Design and development of vision-based control strategies for vibration suppression of objects with gripper flexibility.
3. Design and development of vision-based control strategies for vibration suppression of flexible objects using arm and wrist motion of the industrial robot.

4. Design and development of vision based data-driven system identification method for vibration suppression of flexible objects.

The thesis attempts to address the above objectives in various chapters. Chapter 3 discusses a vision sensor-based active vibration suppression strategy of a non-deformable object held by a robot gripper in assembly operation. Chapter 4 presents a vision-based vibration suppression strategy for the vibration of NDO with gripper flexibility. Chapter 5 proposed a camera calibration technique and object identification methods using robot pose information and vibration measurement of the flexible object and a second stage controller for vibration suppression of flexible objects. Chapter 6 presents an online system identification method with the help of the vibration response of the flexible object obtained by the vision-based vibration measurement.

CHAPTER 3
VISION SENSOR BASED RESIDUAL VIBRATION SUPPRESSION STRATEGY OF NON-DEFORMABLE OBJECT FOR ROBOT ASSISTED ASSEMBLY OPERATION

3.1 Introduction

In this chapter, an innovative active *Selective Predictive Vibration Amplitude Error Based* (SPVAEB) second stage controller has been proposed that uses feedback from vision sensor for residual vibration suppression and works along with the standard controller of industrial robot, which is an integral part. The proposed SPVAEB controller has an edge over traditional control strategies and works as an outer control loop with the standard controller of industrial robot. The developed control strategy is easy to implement. It does not interfere with the working of this controller or disturb the default settings of robot parameters. The present work uses a contactless sensing device such as a camera and a vision-based algorithm to process real-time images to provide feedback to the control system. The external hardware for the proposed second-stage control loop is a vision sensor for feedback and an external personal computer (PC) for image processing. This approach is cost-effective compared to an expensive force/torque sensor or any other active sensing strategy.

The chapter is organized in the following ways: section 3.2 discusses the proposed approach, section 3.3 presents the system on which the vibration suppression strategies have been investigated, and the mathematical model used for developing the second-stage controller. Subsequently, the steps used to develop the second stage controller and its simulation process are elaborated in section 3.3. The experimental results of the implementations are presented, and results are analyzed in section 3.4, and concluding remarks are presented in section 3.5.

3.2 Problem formulation

In robotic assembly operations, peg-in-hole is a common task performed by industrial robots. The peg-in-hole task contains two major activities: manipulation and insertion of the peg in the hole. Most industrial robots are designed to execute PtP trajectories with constant speed. The high-speed manipulation of objects such as flexible beams, ropes,

wires, and sheets may induce vibration. The present work is focused on designing a second-stage controller to attenuate residual vibration in the NDO.

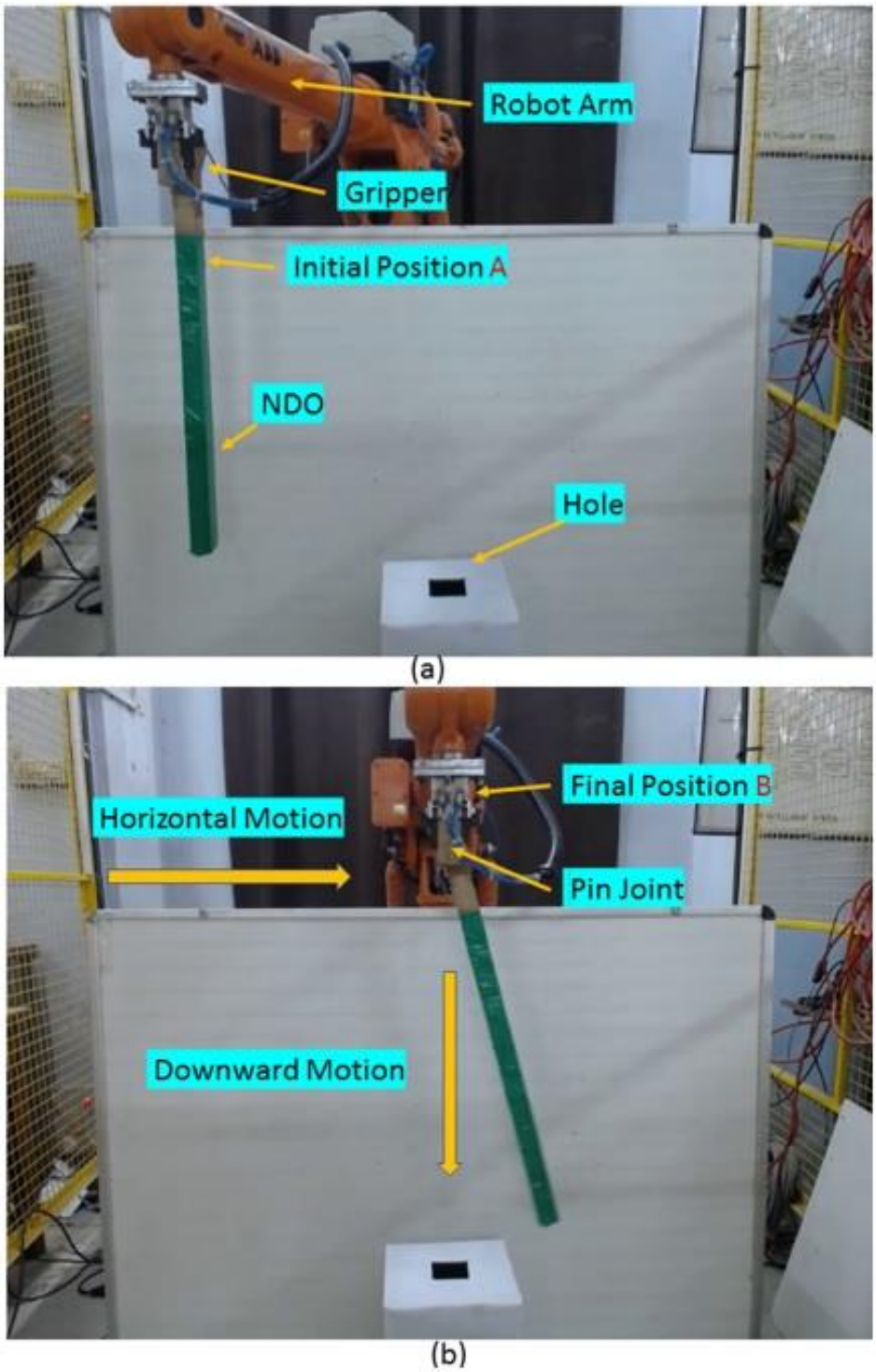

Figure 3.1 Front view of the set up for peg in hole assembly problem, (a) robot with NDO at initial position A and (b) robot moved to final position B.

In most cases, the internal controller of the robotic manipulator is not accessible to the user except for inputting the information for PtP motion, trajectory, and velocity with the

help of a teach pendant or any other human-robot interface. More specifically, Figure 3.1 presents the front view of the problem. For the current investigation, a square cross-section rigid NDO is held by the gripper of a robotic manipulator. The same object is held with a pin joint in the gripper to introduce oscillation during motion. For a peg-in-hole assembly, this NDO is moved at high-speed in the horizontal direction from initial position A (Figure 3.1(a)) to final position B (Figure 3.1 (b)) to reach right above the hole. After that, it is expected that the NDO will be inserted into the hole precisely. However, acceleration during high-speed manipulation along the horizontal direction results in residual oscillation of the hinged object that prevents the completion of the insertion task quickly. Thus, a controller is needed to suppress the residual vibration to complete the task quickly.

A generic approach for the vision-based residual vibration control method is proposed for the problem at hand. Initially, instructions are sent to the internal controller to execute the PtP horizontal trajectory to bring the object above the hole. This movement causes residual vibrations in the object, whose vibration is captured with the help of a vision sensor. Subsequently, the proposed second-stage controller comes into the picture when there is residual vibration. Else the controller does not get activated. The second stage controller supplies the required control signals to the robot internal control until the vibration amplitude reduces within a user-specified limit. For the design of the second stage controller, the essential steps depend on vision sensor-based feedback, and the details of the design phases are described in the next section.

3.3 Computer vision based residual vibration control method

To design the second stage controller, a computer vision based residual vibration control method has been proposed, and the essential steps are:

1. Estimation of residual vibration amplitude of the NDO using a vision sensor through an image processing technique
2. Physics-based mathematical modeling of the NDO for simulation and control
3. Design of SPVAEB second stage controller for an industrial robotic manipulator

Once the proposed second-stage controller is designed and its performance during simulation is investigated for different working conditions, the same approach can be implemented on the industrial robotic manipulator to demonstrate its efficacy.

3.3.1 Residual vibration amplitude estimation using vision sensor

A vision sensor has been used to estimate the residual vibration amplitude of the NDO. The vision sensor is mounted right in front of the robot at the appropriate height to adequately capture images of manipulation and assembly tasks. The same vision sensor is calibrated using the standard checkerboard method with the help of the MATLAB function. Through this method the intrinsic parameters of the camera are obtained, and the values are provided in Table C.5.1 of Appendix C. In this case, the MATLAB function is used to determine the intrinsic parameters of the camera which do not change with the position of the camera in the workspace. All the other computational tasks are performed using the Python programming language (Van Rossum and Drake Jr, 1995). The captured image is processed using the openCV3 package (Bradski, 2000) and Python program for vibration amplitude. The openCV3 is an open-source computer vision package available online and used along with a Python program for second-stage controller design. The basic idea behind the estimation process is color-based recognition, finding contours, estimating the area, and fitting a minimum area rectangle.

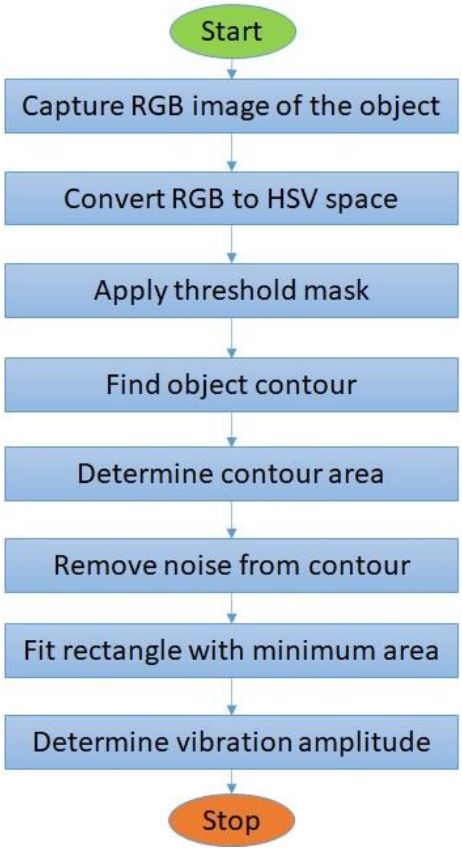

Figure 3.2 Steps for estimation of vibration amplitude of NDO using the image processing technique.

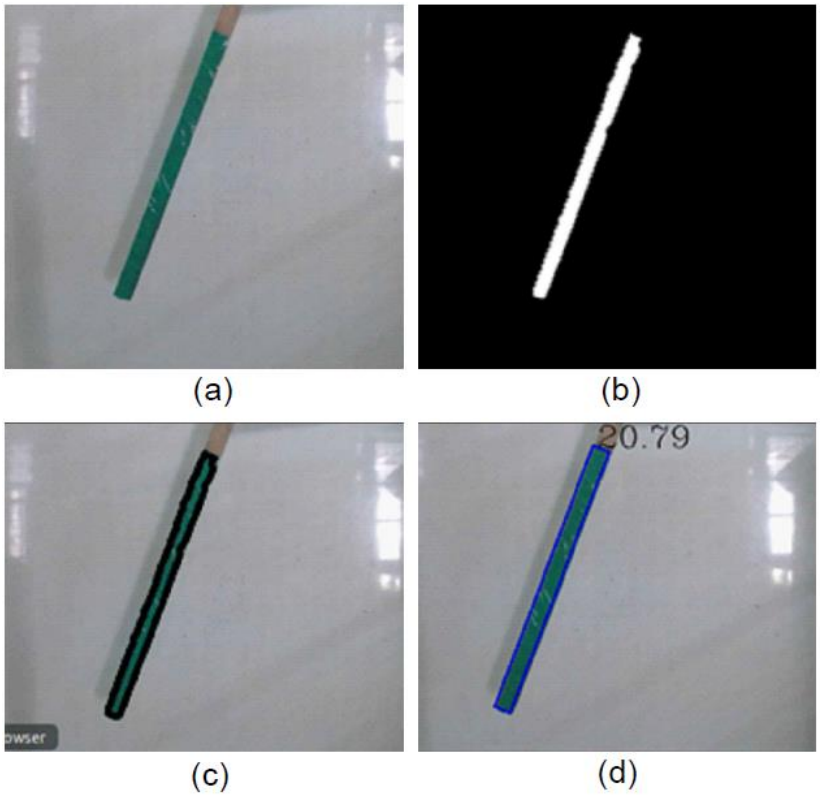

Figure 3.3 Steps for the image processing (a) Red-Green-Blue image, (b) grayscale image, (c) contour detection, and (d) Fitting rotated rectangle contour for vibration amplitude.

The steps used for image processing are shown in Figure 3.2. Initially, the vision sensor captures a Red-Green-Blue (RGB) image, as shown in Figure 3.3(a). The captured image is converted from RGB to Hue-Saturation-Value (HSV) space. In this case, object detection is based on the color detection technique. A threshold mask is created by setting a range of HSV values in which only desired object pixel value can easily fit. Image pixel values in the threshold mask range are converted to (0, 0, 100), which is a white color in HSV image space that indicates the object, and the rest of the image pixel values are converted to (0, 0, 0) i.e., black color in HSV Image space, and black color is indicated as background. Figure 3.3(b) shows the grayscale image after implementing the threshold mask with an object and background. The noise in the image is eliminated using an erode operator for further processing. The contour of NDO is detected using the 'findContour' method available in openCV3 and shown in Figure 3.3(c). Areas of the detected contours are measured using the ‘contourArea' method. The threshold mask also detects other objects that lie in the threshold mask, which is considered as noise in the image. A specific area limit was set based on the area of the desired object, which eliminates the noise present in the image.

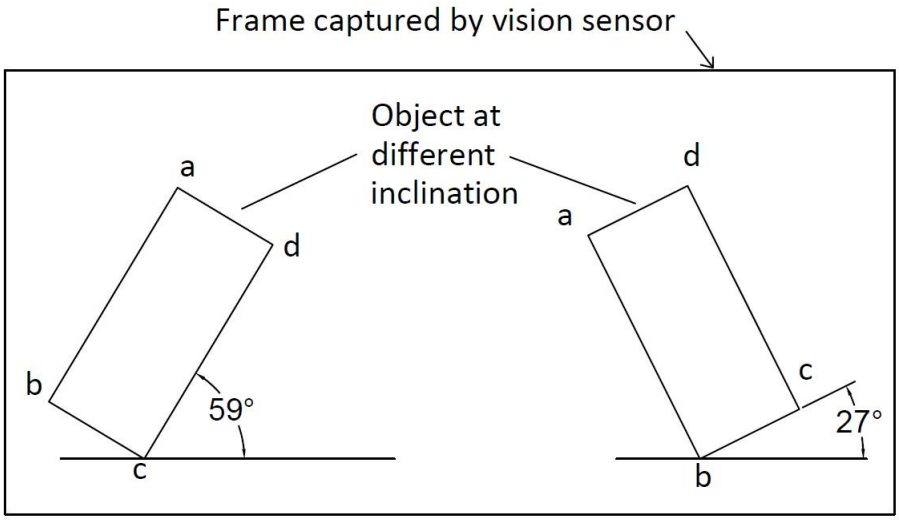

Figure 3.4 Vibration amplitude inclination measured using openCV3.

Contours are the boundaries of a shape with the same color and intensity. The contour detection method stores all the pixel coordinates of the boundaries. The boundary points stored in this method do not require all the points. Therefore, a contour approximation method called the Douglas-Peucker algorithm (Visvalingam and Whyatt, 1990) is implemented to approximate the boundary of the object. A rectangle is used to bound the contour by implementing the minimum area rectangle 'minAreaRect' method. The object used here had a rectangular shape in the front view. Therefore, this minimum area rectangle becomes congruent to the object, as shown in Figure 3.3(d). This method provides the angle of rotation of the rectangle. The angle formed by the horizontal axis of the view frame and the edge of the rectangle is converted to angular amplitude of object. Figure 3.4 shows inclination of the minimum area rectangle about the horizontal axis of the view frame of the camera at different orientations.

Two positions of the same object are considered to exhibit how the openCV3 inbuilt 'minAreaRect' method measures the angle of the rectangle. Here angle is measured between the horizontal axis and edge inclined in a counterclockwise direction irrespective of true inclination of the object. Thus, a computer program is developed to determine the actual inclination of the rectangle with the vertical axis.

3.3.2 Mathematical modeling of the non-deformable object

The NDO under consideration has been treated as a simple pendulum with moving support in the horizontal direction, as shown in Figure 3.5. The object is free to rotate around a

pivot fixed to the end-effector during actuation. The objective of the experiment is to suppress the residual vibration of the object in less time, as the increase in stabilization time increases the manufacturing cycle time. Therefore, an active second-stage control strategy is designed for the current work to stabilize the NDO by providing control movements to the first three joints of the robotic manipulator.

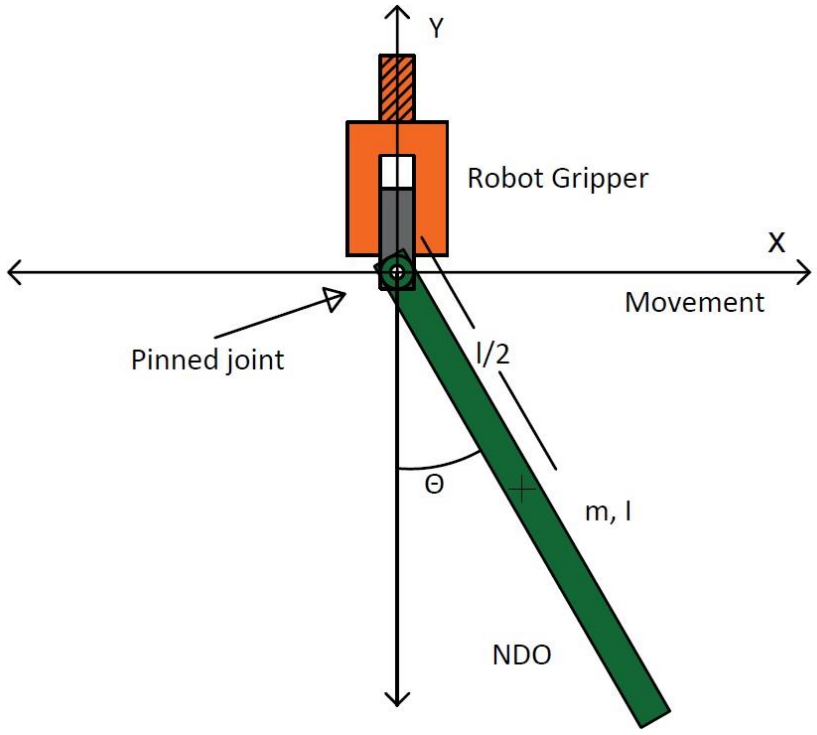

Figure 3.5 The model for oscillation of NDO

The equation of motion for the NDO with respect to the pivot point is presented in equation (3.1). This equation is derived using torque balance method:

$$I\ddot{\theta} + \frac{mgl}{2} sin\,\theta + \frac{ml\mu}{2} cos\,\theta + C\dot{\theta} = 0 \tag{3.1}$$

$$\frac{ml^2}{3}\ddot{\theta} + \frac{mgl}{2} sin\,\theta + \frac{ml\mu}{2} cos\,\theta + C\dot{\theta} = 0 \tag{3.2}$$

where C is the coefficient of friction present in the bearings of the object being held by end-effector. I is the moment of inertia, μ – acceleration of the moving base, θ –swing angle, m – mass, and l– length of the NDO. It is assumed that the gripper is stiff. Therefore, motion of the NDO does not affect position of the end-effector x and its derivatives. After rearrangements, the nonlinear equation is converted into a linear equation using the following small oscillation assumption: *i.e.,* $\sin\theta \approx \theta$ & $\cos\theta \approx 1$ when θ is small.

For the NDO, the equation of motion without damping and without external force is:

$$\ddot{\theta} = -\frac{3g}{2l}\theta - \frac{3\mu}{2l} - \frac{3C}{ml^2}\dot{\theta} \tag{3.3}$$

$$\ddot{\theta} = -\frac{3g}{2l}\theta \tag{3.4}$$

$$\ddot{\theta} + \frac{3g}{2l}\theta = 0 \tag{3.5}$$

This is a simple harmonic equation in the form:

From comparison of the square of the frequency

$$\ddot{\theta} + \omega^2\theta = 0 \tag{3.6}$$

$$\omega^2 = \frac{3g}{2l} \tag{3.7}$$

Thus, the natural frequency ω_n is:

The equation (3.3) in state-space form is:

$$\omega_n = \sqrt{\frac{3g}{2l}} \tag{3.8}$$

$$\begin{bmatrix}\dot{x}_1(t)\\ \dot{x}_2(t)\end{bmatrix} = \begin{bmatrix}0 & 1\\ -\left(\frac{3g}{2l}\right) & -\left(\frac{3C}{ml^2}\right)\end{bmatrix}\begin{bmatrix}x_1(t)\\ x_2(t)\end{bmatrix} + \begin{bmatrix}0\\ -\frac{3}{2l}\end{bmatrix}\mu(t) \tag{3.9}$$

Where

- $x_1(t)$ represents the angular position of the NDO.
- $x_2(t) = \dot{x}_1(t)$ is the angular velocity of the NDO.
- $\dot{x}_2(t) = \ddot{x}_1(t)$ is the angular acceleration of the NDO.

The state space form is used further for numerical integration to obtain velocity and displacement which will be used in the proposed controller for the prediction of the maximum error. A Python code is written and 'odeint' library function is called to numerically integrate the equation (3.9).

3.3.3 Selective predictive vibration amplitude error based second stage vibration controller design

The purpose of developing a control strategy for the industrial robot is to suppress the vibration during assembly tasks and improve the productivity of manufacturing. This work uses commercially available ABB make an industrial robot to demonstrate the

implementation. This robot has a robot controller, which allows planning in terms of displacement and velocity with a trapezoidal velocity profile. However, the said controller has limited control over the acceleration. Therefore, using continuous input control signals to suppress vibration during assembly is an impractical solution. To alleviate this problem, a selective predictive vibration amplitude error based second stage vibration controller is presented, which overcomes the need to continuously monitor amplitude error for control input. This control system attenuates the amplitude of the NDO measured with a vision sensor and suppresses the oscillation of pendulum-like objects. The controller is activated only when the robot has completed the desired PtP motion, and the gripper is right above the hole. The controller monitors the oscillation of the object, and the control action is inputted to the teach pendant of the robot as per the predictive error estimated at the specified point. The predictive error is the deflection of the NDO from its equilibrium position, i.e., the object is vertically downward.

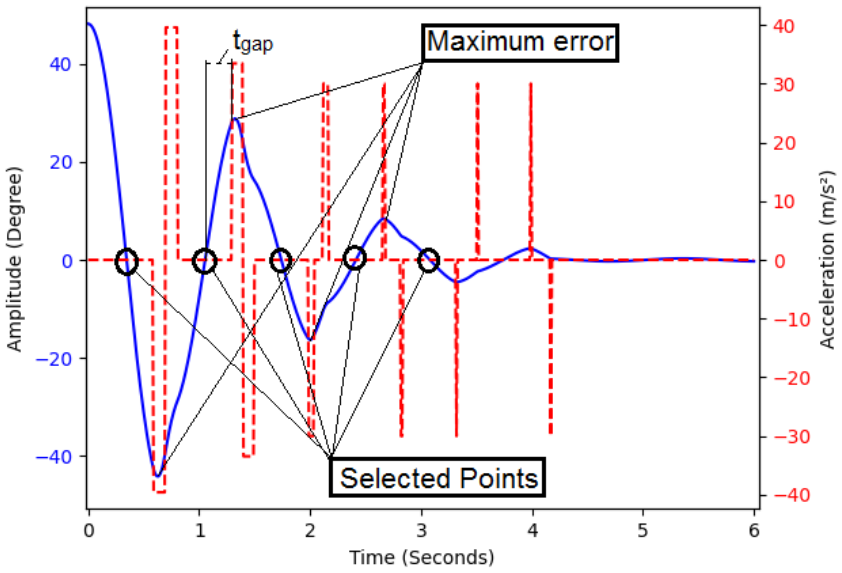

Figure 3.6 Illustrative example of selective predictive error based second stage vibration controller.

The simulated response of amplitude after implementations of the SPVAEB second-stage controller, including the acceleration profile of the robot gripper, is presented in Figure 3.6. The NDO has been released with initial conditions (amplitude is equal to 48.22° and zero angular velocity), exhibiting an oscillation of response that needs to be suppressed. Then the SPVAEB second stage controller is activated when the amplitude of the object changes its sign or crosses the equilibrium position. These selective amplitudes at two consecutive time points are used to estimate the maximum predictive error. The

maximum error is computed using the vibration amplitude at the extreme positions with respect to the stable position of NDO. For the selected points, initial conditions in terms of amplitude and angular velocity are inputted in the mathematical model of NDO. The amplitude at the next extreme position as well as the time to reach the extreme position from initial conditions, are estimated. The predictive deflection at the extreme position of NDO is used to compute actual error, which becomes the basis for subsequent control action. Based on this predictive error, the controller estimates a trajectory in the direction of X-axis, which uses trapezoidal velocity profile. The estimated control input is fed to the robot system, and the input trajectory suppresses the amplitude of the system significantly.

The proposed strategy for controller consists of a conventional error-based controller. Among available controller strategies, a typical discrete PID Controller was selected initially for this case as it is widely accepted in industries. Discrete PID controller is implemented as second stage controller for industrial robot system. The control law in standard form (Nagrath and Gopal, 2021; Visioli, 2006) is provided in equation (3.10):

$$u(t) = K_P e(t) + K_I \sum_{i=1}^{n_t} e_i\,(t)\Delta t + K_D \frac{e(t)}{\Delta t} \tag{3.10}$$

where K_P, K_I, and K_D are the corresponding gains of the proportional, integral, and derivative parts of the second-stage controller. Where $e(t)$ is the error amplitude of the pendulum, which is the difference between the reference point and current angle, Δt is the sampling period, and $u(t)$ is control output. The integral and derivative control laws are observed to be insignificant and thus eliminated from the control strategy. Therefore, a proportional control law is adopted as base controller for proposed controller, and equation (3.11) is changed to equation (3.12).

$$u(t) = K_P e(t) \tag{3.11}$$

$$e(t) = l \sin\theta \tag{3.12}$$

$$u(t) = K_P l sin\theta \tag{3.13}$$

The predictive amplitude error is converted into displacement of the control trajectory. The displacement of the trajectory is directly dependent on the amplitude error. Therefore, the length of the NDO is projected on the x-axis at extreme positions using the equation (3.12), where l is the NDO length, and θ is the predictive deflection (amplitude). The

control output is expressed as equation (3.13) using equations (3.11) - (3.12). The control output is considered as displacement to be covered by the end-effector in the corresponding direction that suppresses the amplitude. Based on this displacement in x-axis direction, a trapezoidal velocity profile (linear interpolation with parabolic blends) is generated, assuming constant acceleration (Mittal and Nagrath, 2015). The blend time t_b, displacement $q_T(t)$, velocity $\dot{q}_T(t)$ and acceleration $\ddot{q}_T(t)$ of the trapezoidal profile is calculated using the following equations.

$$t_b = \frac{t_g}{2} - \frac{1}{2}\sqrt{\frac{t_g^2\ddot{q}^c - 4(q^g - q^s)}{\ddot{q}^c}} \tag{3.14}$$

The constraint on the choice of acceleration during the blend is

$$|\ddot{q}^c| \geq \frac{4|q^g - q^s|}{t_g^2} \quad and \quad \ddot{q}^c \neq 0 \tag{3.15}$$

$$q_T(t) = \begin{cases} q^s + \frac{1}{2}\ddot{q}^c t^2, & 0 \leq t \leq t_b \\ q^s - \frac{1}{2}\ddot{q}^c t_b^2 + \ddot{q}^c t_b t\,, & t_b < t \leq t_g - t_b \\ q^g - \frac{1}{2}\ddot{q}^c (t_g - t)^2\,, & t_g - t_b < t \leq t_g \end{cases} \tag{3.16}$$

$$\dot{q}_T(t) = \begin{cases} \ddot{q}^c t, & 0 \leq t \leq t_b \\ \ddot{q}^c t_b, & t_b < t \leq t_g - t_b \\ \ddot{q}^c (t_g - t), & t_g - t_b < t \leq t_g \end{cases} \tag{3.17}$$

$$\ddot{q}_T(t) = \begin{cases} \ddot{q}^c, & 0 \leq t \leq t_b \\ 0, & t_b < t \leq t_g - t_b \\ -\ddot{q}^c\,, & t_g - t_b < t \leq t_g \end{cases} \tag{3.18}$$

where t_b - blend time, t_g - travel time, q_g - total trajectory displacement, q_s - start position, $\ddot{q}^c$ - constant acceleration. In a conventional PID type dynamical vibration control system, the error monitoring and control action are performed simultaneously to suppress the undesirable vibration. In this case, implementing a controller for control action to attenuate vibration with limited control input is arduous. In addition, delay caused due to image processing and execution of control trajectory is a major challenge in implementing the conventional PID controller for real-time vibration control.

The proposed SPVAEB controller overcomes the problem as it does not act continuously on the vibration error. Instead, it acts when the amplitude crosses the equilibrium or zero positions. The obtained positive and negative errors are treated in the same way. The time gap (t_{gap}) between the zero position and extreme position is treated as a delay in the control action execution. Therefore, the controller will wait for t_{gap} period and the control trajectory will be executed after the extreme position of NDO. This delay is utilized as an advantage rather than a drawback, unlike in conventional PID controllers.

The above approach will be less prone to amplitude measurement error using the vision sensors. The measurement error range for this sensor is found to be ± 0.53°. The rationale behind such an approach is that the NDO has zero angular velocity at the extreme position and maximum angular velocity at the zero-reference position. The rate of change of error is greater near the extreme position or exactly at extreme position than at an equilibrium position. Thus, computation of angular velocity close to equilibrium position can provide accurate feedback using vision sensor, and error measurement may disturb the control signal more at an extreme position compared to zero reference position.

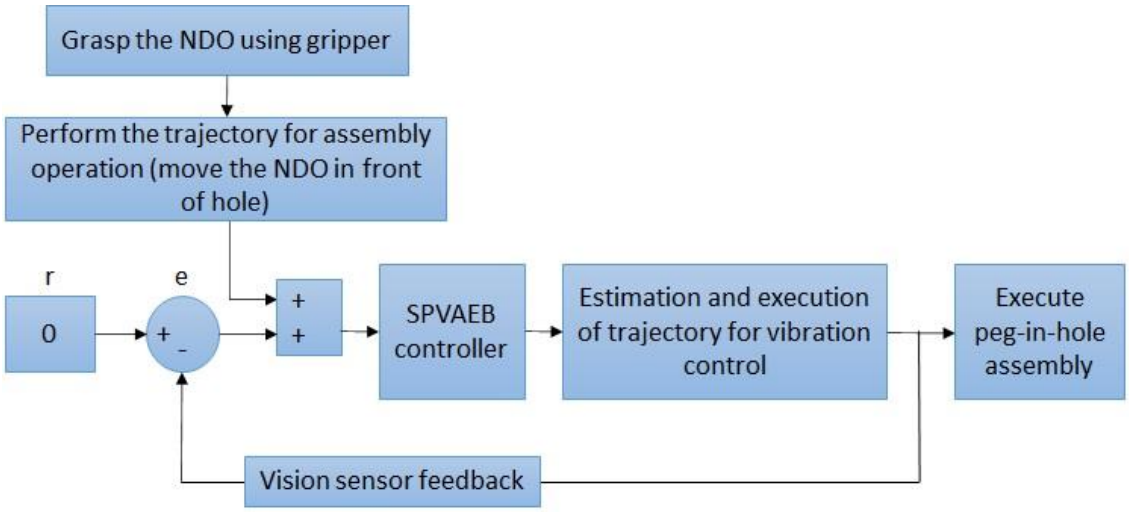

Figure 3.7 Schematic diagram of SPVAEB second stage controller design

The overall working principle of the proposed SPVAEB second-stage controller is represented in Figure 3.7. Initially, the industrial robot performs a manipulation task, such as moving the NDO held by the gripper. For position control, the robot is commanded to move the NDO from an initial position 'A' to the goal position 'B', using PtP trajectory. The robot internal controller executes this trajectory to perform the assembly task. Due to this motion, the NDO held by gripper oscillates and the oscillation is measured using

images captured by the camera. The physics-based model estimates the error at the next extreme point. The SPVAEB controller considers this predictive error and estimates the input trajectory, reducing the oscillation amplitude. The subsequent section provides information related to the experimental implementation and results.

3.4 Experimental implementation and analysis of results

A typical robotic assembly setup is shown in Figure 3.8(a). The setup consists of an articulated robotic arm, robot controller, camera, PC, and a gripper attached to the wrist of the manipulator, which is supposed to insert a peg in the hole. The robotic arm and teach-pendant are interfaced with the robot controller. Teach-pendant is an interfacing device that allows users to program the robot online. The assembly task is to insert the NDO in the square hole of a box placed within the workspace. To simulate the vibration in the object due to its motion, the NDO is attached to a hinge joint grasped by the gripper of the robot. This hinge joint allows the NDO to oscillate in the vertical plane. The camera is mounted on a tripod at a suitable height in front of the robot shown in Figure 3.8(b), to capture the oscillation of the object.

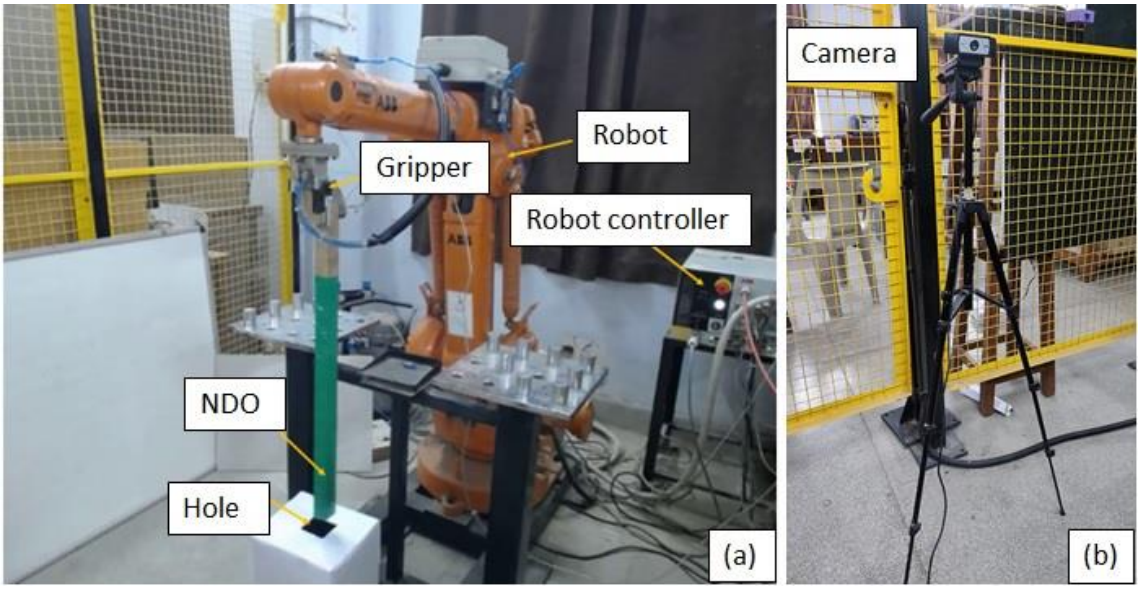

Figure 3.8 (a) Robotic peg in hole assembly environment and (b) Camera used in assembly operation.

3.4.1 Experimental details for validation

The articulated six degree of freedom (DOF), ABB 1410 industrial robot is provided with high-speed motion from a home position to the target location so that the NDO held by this robot is right above the hole before assembling it. The technical specification of

ABB 1410 is provided in Appendix A. The IRC5 robot controller has been used to execute and control the straight horizontal motion of the gripper that holds the NDO. A universal serial bus (USB) supported Logitech make C930e ultra-wide-angle web-camera with 1080 X 1920 pixels resolution has been used as a feedback sensor to measure the amplitude of the vibration with 30 frames per second (fps). This feedback sensor has been placed at a suitable height in front of the manipulator. The image processing algorithm has been implemented using openCV3 software, an open-source computer vision programming package developed in python 2.7 interactive development and learning environment (IDLE). The NDO has a dimension of 650 mm × 33 mm × 33 mm. A green color tape is pasted on the object to distinguish the object from the background, which would be detected easily in an assembly scenario through image processing. The end of NDO has been clamped in a two-finger gripper of the robot with a pin joint that permits free oscillation in vertical plane. In this experiment, an Xsens make inertial measurement unit (IMU) sensor has been mounted on the top end of NDO to record the angular amplitude and acceleration of the robot end-effector. The rationale behind the use of IMU sensor is to record response of the NDO for validation purposes and not to use this as a feedback sensor. For computation purpose, Intel® Core™ i5-3470 PC with central processing unit (CPU) @ 3.20GHz, 4 Core(s), has been used. Four logical processors are used for image processing as well as controller programming. Both the camera and IMU sensor are interfaced through USB to the PC. The IRC5 controller of the robot has been interfaced with the PC by RJ45 socket connection. All the control programming scripts have been written in python. For execution of the control input in the IRC5 controller, the rapid programming language has been used on RobotStudio software platform. The proposed controller has the capability to estimate and execute various trajectories. It is to be noted that the robot controller neither can handle mathematical model for vibration estimation nor can handle vision sensors for passive feedback using rapid programming language.

In this case, a python program has been developed to communicate with the IRC5 robot controller through socket programming. The communication strategy has been based on a client-server model (Pires and Azar, 2018). The block diagram is shown in Figure 3.9. The robot controller created the server and logger (client), the two independent tasks. The server task is used to move the manipulator, and the logger is used to communicate with client devices such as a computer or other robots available on the network. For the current setup, client-server transmission control protocol/internet protocol (TCP/IP) has been

employed over an ethernet network. The ethernet network with TCP/IP data protocol allows basic high-level communication and data sharing.

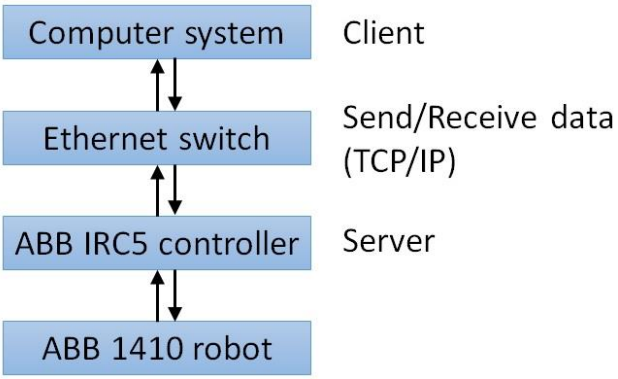

Figure 3.9 Communication architecture for computer system and the robot controller

In this experiment, the manipulator with NDO is moved from starting position 'A' to a target position 'B', which is at a displacement of 300 mm using a horizontally straight-line path at 2 m/s velocity. The target position 'B' is right above the hole where the NDO will be inserted. However, the NDO oscillates due to high-speed motion, and the oscillation must die before the assembly process resumes. It causes a delay in the insertion of the peg-in-hole assembly task. If this activity does not use any controller, the NDO takes 120 s to achieve a stable position when the initial amplitude is 90°. For reduction in residual vibration of the NDO, the SPVAEB controller is activated. This controller remains activated until the amplitude of NDO reduces to a specified limit i.e., ±2°. To investigate the performance of the controller, multiple experiments are performed with different initial amplitude of the NDO and introducing different types of disturbance. The results of these experiments are reported in the next section to indicate the validity of the controller and its robustness.

3.4.2 Tuning of control gain for second stage controller

The stabilization of the object can be achieved by designing and implementing the SPVAEB controller. It works as a second-stage controller over the existing internal industrial manipulator controller. The vision sensor detects the amplitude of the NDO. The amplitude between the two consecutive time points is used to detect the angular velocity of the NDO. The amplitude and the angular velocity are initial conditions for the NDO model to detect the predictive maximum amplitude error (the extreme position). Then the predictive error, along with a condition if the initial condition is considered only when the

amplitude changes its sign between the two consecutive time points, are plugged into the SPVAEB controller. The output of the controller is converted into the displacement trajectory the robot must execute. The actuators (AC servo motors in ABB 1410) of the robot exhibit saturation as they are limited by the IRC5 controller to maintain maximum velocity i.e., 2 m/s of end-effector with the maximum bounded acceleration (Approx. 33 m/s^2). The actuator saturation is desirable in dynamic model of the manipulator, which is one of the reasons why the robot weight to payload ratio is 45:1. The actuator saturation decreases the stress and undesirable vibration due to inertia produced by the own weight of manipulator. Thus, the control input for trajectory displacement was limited to ± 100 mm for the robot workspace.

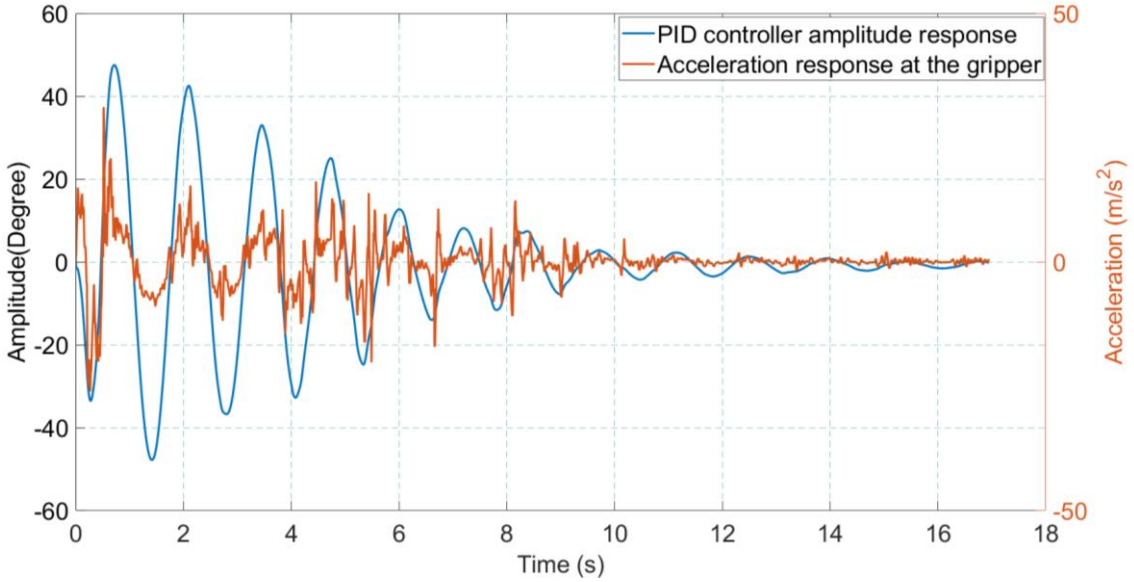

Figure 3.10 Conventional PID controller response

Before the implementation of SPVAEB controller, a discrete PID controller is used on the same setup to suppress residual vibrations of the NDO. The performance of PID controller is presented in Figure 3.10, including the amplitude and acceleration response at the robot gripper.

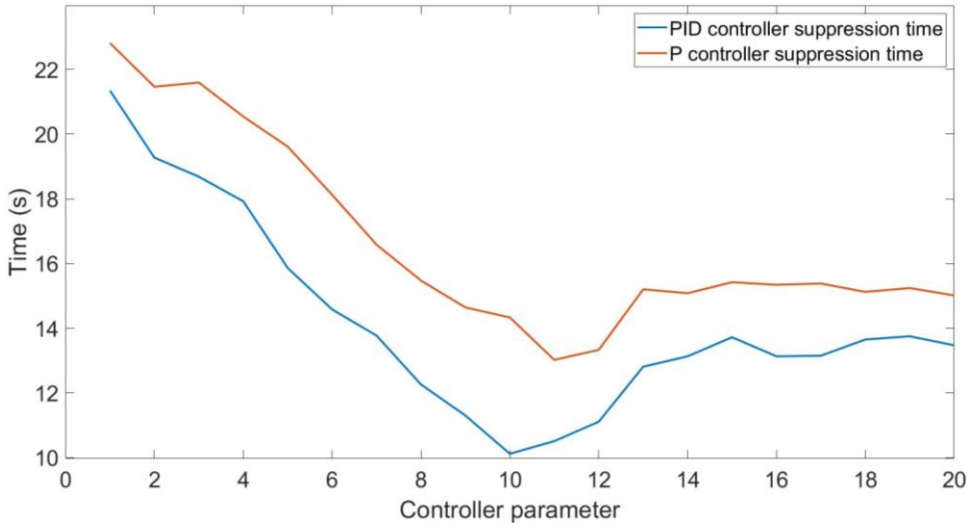

Figure 3.11 Conventional PID controller suppression time with respect to the parameters.

The tuning of the PID controller parameter was carried out using trial and error methods. Initially, the proportional parameters varied, and the other two parameters remained at zero value. It was observed that the integral parameter has no impact on the performance of the controller as it is a vibration suppression problem. The controller performance of proportional and derivative controller is shown in Figure 3.11. Based on the performance, the minimum suppression time is observed as 10 s for the case with the controller gains $K_P = 10, K_I = 0$ and $K_D = 10$. The performance of the controller was in an acceptable range of vibration amplitude reduction and achieved 88% reduction in suppression time. However, further investigation hinted that the reduction in suppression time is possible if the control actions in the above controller are inputted by accounting the delays present in the system. Other limitation in the performance of the PID controller is due to the straight PtP trajectory control input given to the robot system. This PtP trajectory restricts the PID controller to control the velocity at every sampling time point.

To overcome these problems, a new approach is proposed to control the induced vibration in NDO. The proposed controller is a second-stage controller and does not act continuously, as in the case of the PID controller. It monitors the system continuously, but the error is detected at specific points. This approach allows the controller to compute the error at selected points and estimate the controller gain. Subsequently, the displacement trajectory to be executed by the manipulator is computed from the controller gain.

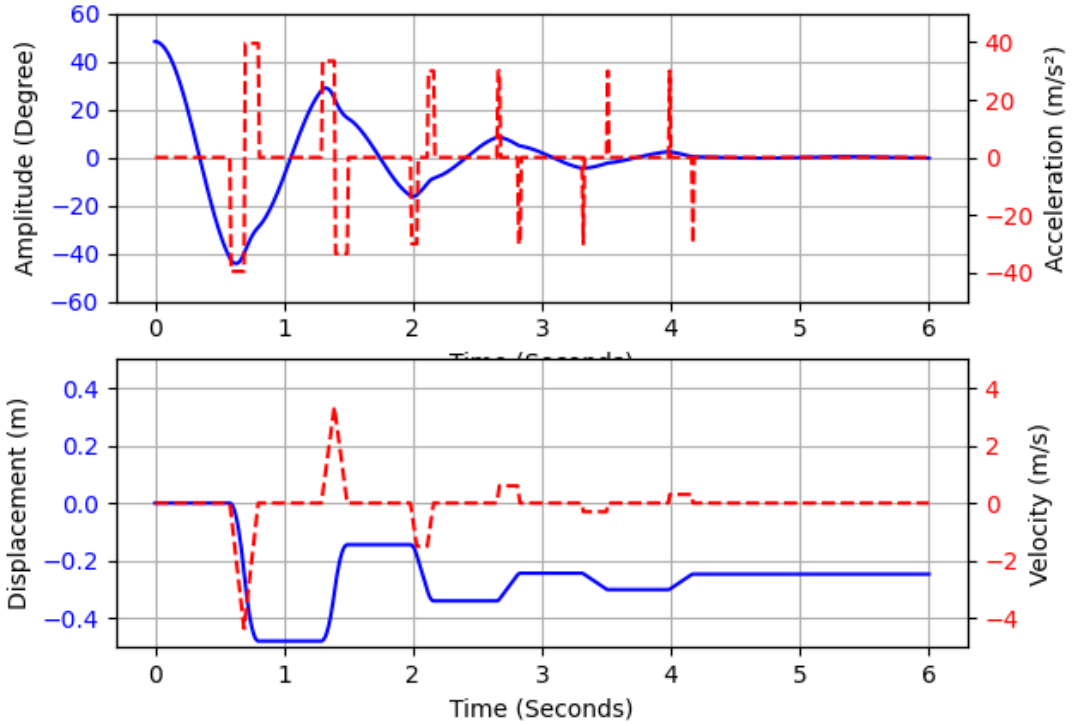

Figure 3.12 The response of selective predictive vibration amplitude error based second stage vibration controller.

In Figure 3.12, the controller simulation response is presented as the amplitude response of the NDO with the controller output: position, velocity, and acceleration profile of the base of the NDO. The model presented in equation (3.9) is used for the prediction of the maximum error as discussed in section 3.3.2 and the model parameters used during simulation are mass – 0.52 kg, length – 0.65 m and coefficient of friction – 0.0035. The controller considers the initial condition and estimates the error where it changes sign or while it will cross the equilibrium position. Although in conventional controllers, the error and control actions are always observed continuously. In this case, selection of the feedback at specified position and low update rate of the vision sensor works in favor as the angular velocity of the NDO at the equilibrium position is higher at the extreme position. Therefore, the angular difference between two consecutive time steps is higher for vision sensor feedback. This result helps reduce the sensor noise effect for high amplitude vibration. However, the sensor noise effect in controller for low amplitude vibration is less than ± 2°. This issue has been resolved by tuning the controller inactive in the said range.

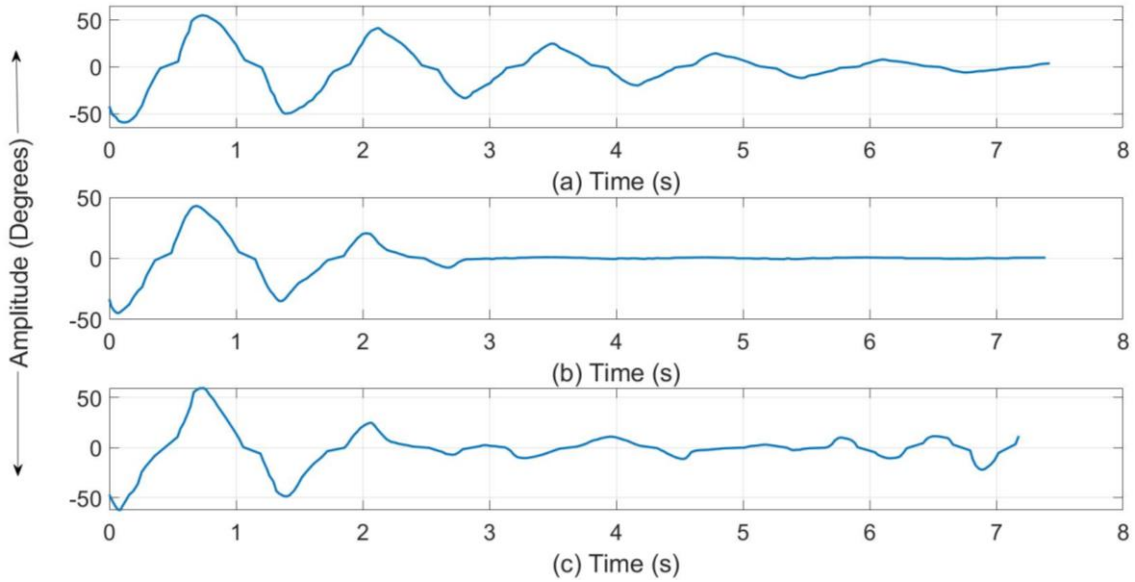

Figure 3.13 Responses with controller gain parameters K_p = (a) 0.5, (b) 1.0, (c) 1.5

The effect of K_P parameter on the performance of the controller has been shown in Figure 3.13. The image processing and the robot controller take some computation time which gets started when sensor captures the image of the object for execution of trajectory. For the designed system, the image processing time was 0.03 s, and the delay in execution of the control trajectory was 0.18 s. Initially, the controller parameter is 0.5, and the result is presented in Figure 3.13(a). The suppression time is less than 8s. After that, $K_P$values are increased step by step and experiments are performed till the gain value is 1.5. Amplitude responses with controller parameters at 1.0 and 1.5 are presented in Figure 3.13 (b) and (c), respectively. The performance of the controller has been compared using minimum amplitude suppression time and stability of the controller.

Instability in vibration suppression refers to suppression of oscillation within the acceptable limit (±2°), and a smaller error band requires higher control gain output and results in higher oscillation. In this vision-based feedback system, the visual feedback shows maximum measurement error is ±0.53°. Within the acceptable limit, the measurement error disturbs the control signal, which may cause instability in the system. Thus, the controller is deactivated in this range. It can be observed in Figure 3.13 that the minimum amplitude suppression time is 3.24 s with derivative gain K_P=1.5 but the instability is observed after the suppression. With higher control gain, the controller acts aggressively and causes instability in the NDO. It would require continuous control action,

which resulted in increased suppression time. Thus, the optimum derivative gain parameter K_P can be taken as 1.0.

3.4.3 Experimental results and discussions

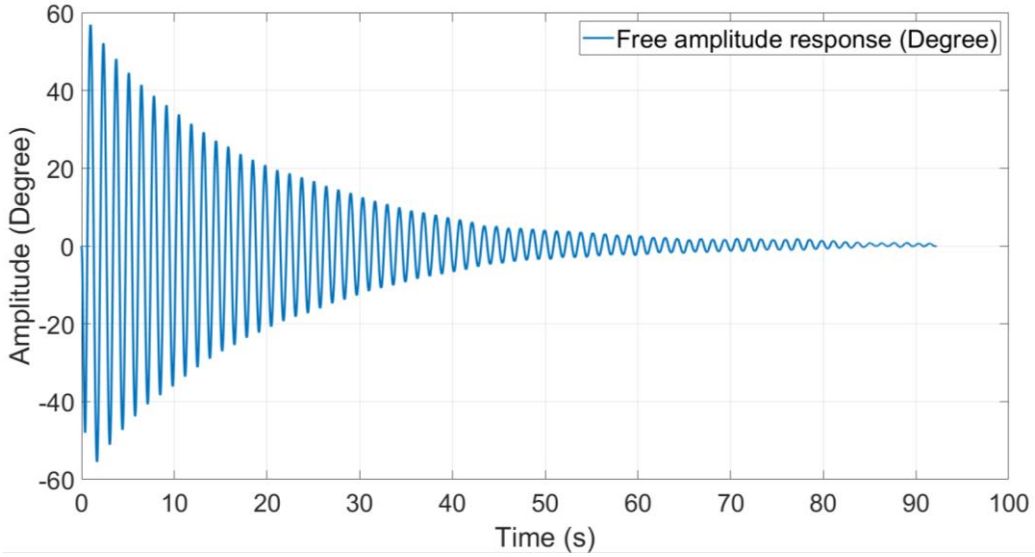

Figure 3.14 Free response of NDO with initial amplitude 56.73°

All the experiments were carried out based on the proposed controller with optimum gain parameter K_P=1.0 In this experiment, the NDO is held in the gripper at position 'A' (x = 0, y = -250, z = 800 mm) then it is moved to the hole position 'B' (x = 0, y = 0, z = 800 mm) in straight line with 2 m/s velocity. The free response of the NDO without any control is presented in Figure 3.14, with initial amplitude 56.73°. And the object reached its equilibrium position after 85 s.

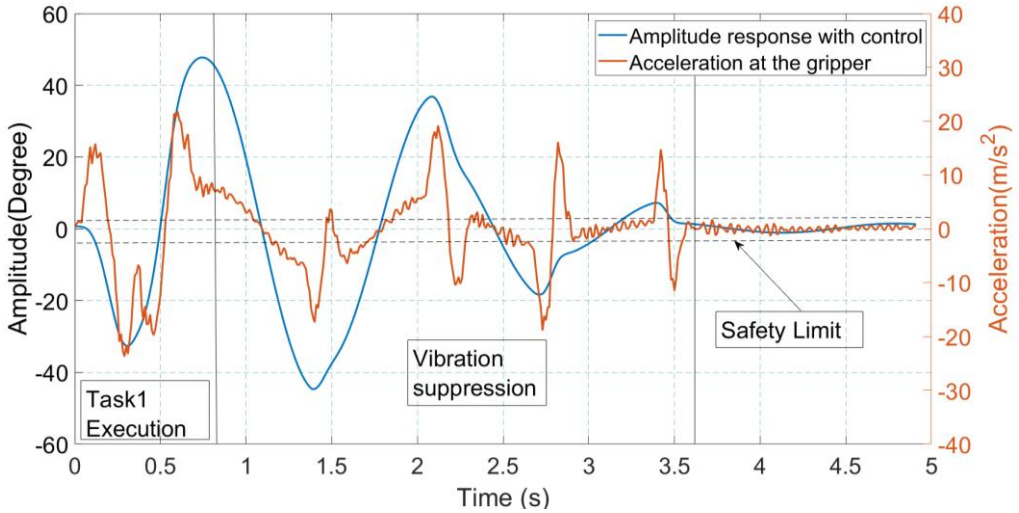

Figure 3.15 Response with optimal controller gain parameter

The vision sensor continuously monitored the amplitude of oscillation and feedback signal was sent to the controller. When oscillation amplitude is observed to be more than ±2°, the SPVAEB controller is activated to compute the predictive error using reference equilibrium position shown in Figure 3.15. The IMU sensor is used to record acceleration and angular amplitude response of the NDO with 0.01 s sampling time. Due to high-speed manipulation, the NDO is disturbed with a maximum amplitude 47.71°. Initial 1 s was the response during high-speed horizontal movement to bring the object right above the hole. It can be observed that the oscillation amplitude is suppressed before 3.8 s. Thus, the actual time used for vibration suppression is less than 2.8 s. After comparing with the vibration suppression results obtained without control and with control, the stability time is reduced to ~95%. The experiment is repeated multiple times, and the average suppression time is found to be 3.08 s with a standard deviation of 0.51 s.

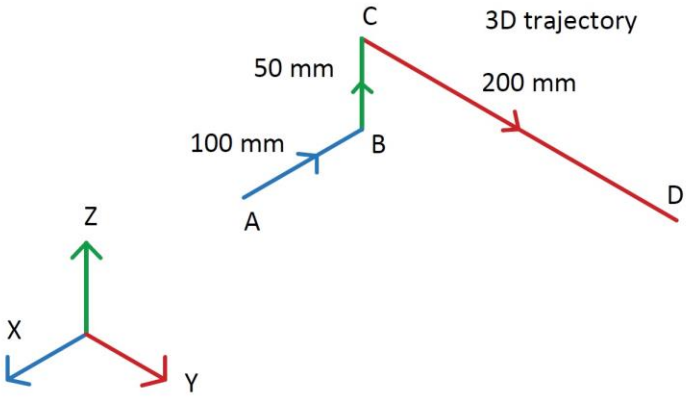

Figure 3.16 A 3D trajectory executed by the robot.

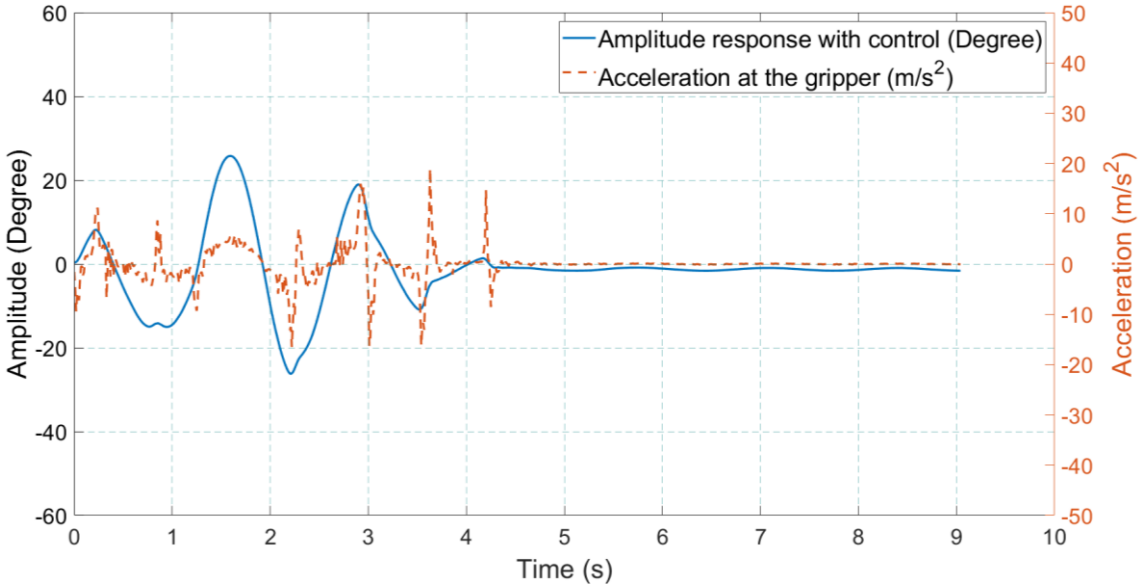

Figure 3.17 Response with 3D excitation trajectory

A 3D trajectory is also used to manipulate the NDO in the robot workspace as shown in Figure 3.16. It starts from position ‘A’ and ends at position ‘D’ via points ‘B’ and ‘C’. The displacement trajectory segments ‘AB’, ‘BC’ and ‘CD’ are 100 mm, 50 mm, and 200 mm with a velocity of 2 m/s. The amplitude response is presented in Figure 3.17.

The 2D and 3D manipulation trajectories are chosen to illustrate the efficacy of the proposed controller for vibration suppression. It can be observed that the total displacement of the 3D trajectory is more compared to the 2D trajectory displacement that brings the NDO above the hole. In addition, the travel time of the 2D and 3D trajectories are 0.75 s and 2 s, respectively. The results shown in Figure 3.15 and Figure 3.17 represent the response with execution of the 2D and 3D trajectories as well as the proposed controller responses. In case of 3D trajectory, the initial condition for the last trajectory segment “CD” is different in comparison to the 2D trajectory. Hence the vibration response of NDO will not remain same due to the motion in X as well as Z direction.

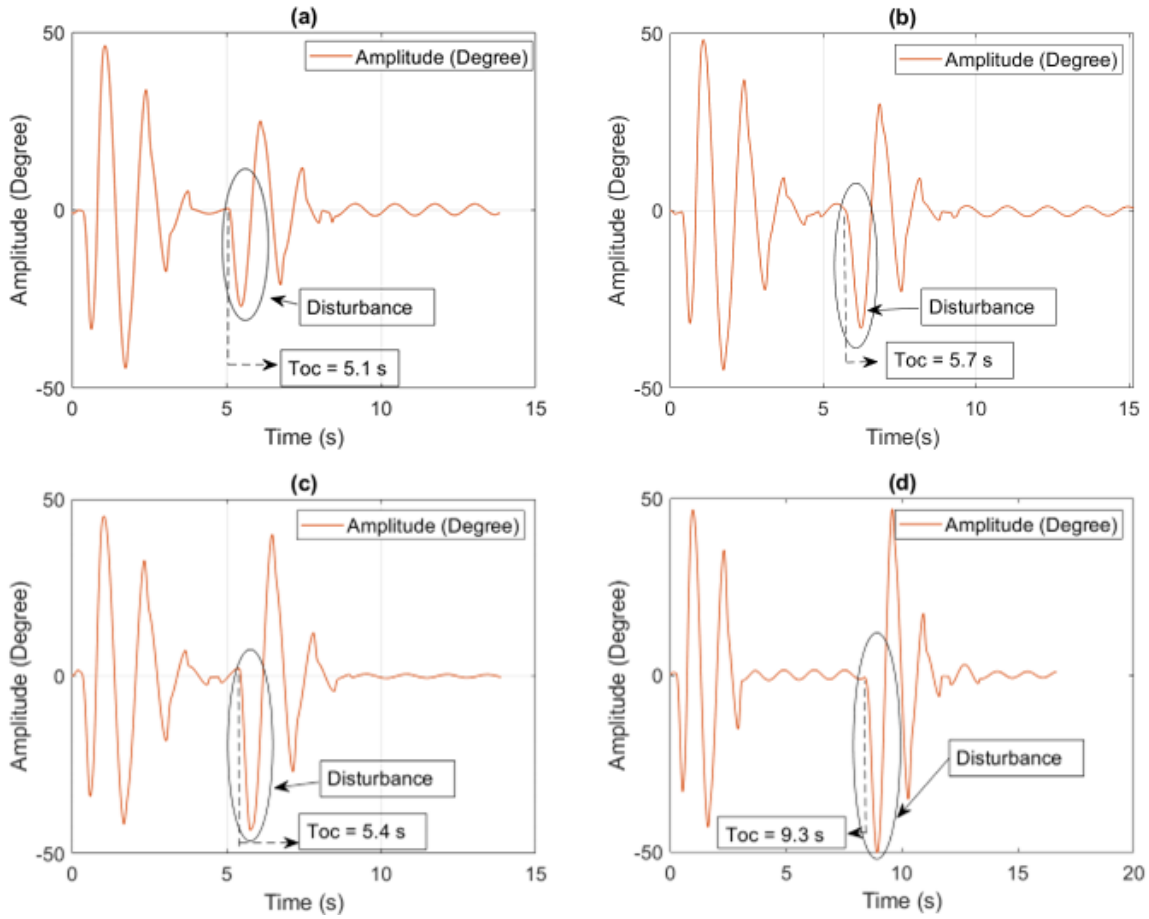

Figure 3.18 Response after providing manual disturbance to the object with amplitude (a) -27.12°, (b) -33.27°, (c) -43.25° and (d) -50.0°

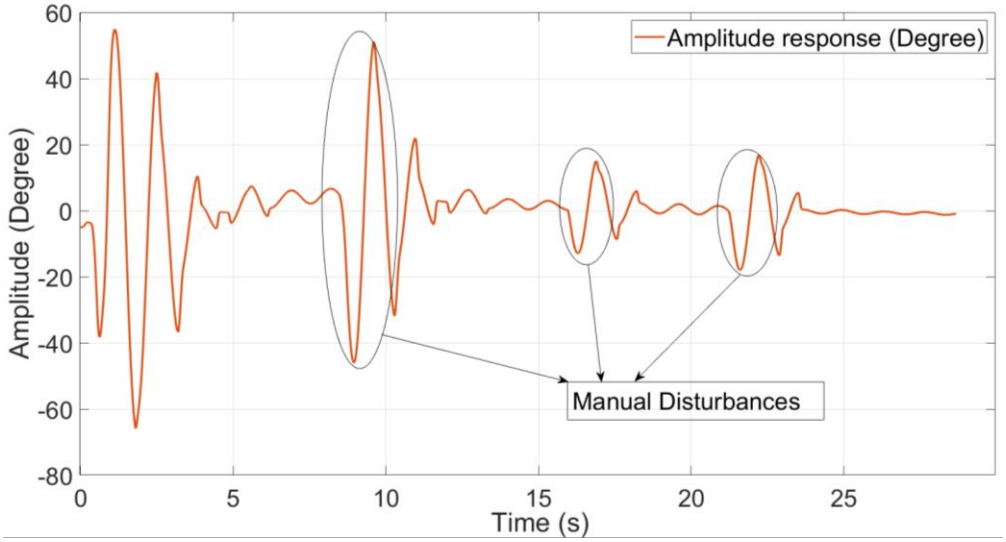

Figure 3.19 Response after providing disturbances multiple times at 8.5 s, 16 s and 21.2 s.

To test the robustness of the controller, the NDO was disturbed manually after the vibration was attenuated. The captured results are shown in Figure 3.18 with disturbance value (a) -27.12°, (b) -33.27°, (c) -43.25° and (d) -50.0° amplitude. The NDO was also disturbed multiple times in one task with -51°, -18°, and -15°. The results are presented in Figure 3.19. Based on the results, it can be concluded that the performance of the controller is robust for the above disturbance introduced intentionally.

The safety limit for control action is chosen as ±2°, so that the controller would be 'OFF' when the oscillation is below this limit. Any attempt to achieve zero error through control inputs would increase the burden on robot controller and consume more time than desired. The NDO is hinged in the gripper, making the setup very sensitive to small disturbance, even gust of airflow disturbs the NDO. Therefore, it is necessary to fix a safety limit, without which the controller may make the system unstable.

After control there may be an offset in position of the NDO from the desired position. The robot end-effector may move in both negative and positive directions. In all the cases, the input control trajectory to the manipulator is smaller in displacement compared to the previous executed trajectory. Therefore, this reduction in displacement of the trajectory results in an offset. For the proposed controller the vibration of the NDO is brought within a safety limit and this limit is user defined based on the task at hand. Otherwise, the controller will be sending input trajectory signal to the teach pendant until the vibration amplitude is very close to zero. The safety limit is chosen ±2° for this case. After the

vibration is suppressed, the manipulator is moved to bring the NDO right above the hole for assembly, with low-speed trajectory (50 mm/sec) so that the NDO will not have oscillation amplitude within the safety limit.

Table 3.1 Comparison of the performance of the SPVAEB controller with conventional PID controller

Method	**Average suppression time (s)**	**Average suppression time reduction (%)**	**Amplitude suppression (%)**
Conventional PID controller	10	88.23	95.78
SPVAEB controller	3.08	95.53	95.78

The performance of the proposed research is compared with the results of the conventional discrete PID controller, and the results are presented in Table 3.1. The performance parameters for vibration suppression task during assembly are the time to suppress vibration, percentage reduction in the suppression time, and percentage reduction in vibrational amplitude. In both the cases, the percentage reduction in suppression time is obtained taking with proposed controller to without controller performance. Similarly, the percentage suppression in the vibration amplitude is also obtained with the proposed controller to without any controller. The vibration in the NDO is suppressed to bring it within the safe limit and switch off the controller after that. It can be observed that the proposed controller performs better and takes only 3.08 s average time as compared to the 10 s obtained from the conventional PID controller. One of the limitations of this investigation is that the oscillations induced due to the robot motion in the NDO has a frequency of the order 0.76 Hz and the cases of higher and lower frequency are not considered. However, vibration suppression strategy for higher or lower frequency oscillations will remain the same.

3.5 Conclusion

This work proposes a control strategy with a vision sensor for suppression of vibration during robotic assembly of NDO in a hole. The NDO is modelled as a simple pendulum with moving support to represent the system for proof of concept, and the pendulum is considered to oscillate about a pin joint at the end-effector of the manipulator. For this case, the designed SPVAEB controller works as a second stage controller on top of the

available robot internal controller without any modification. The second stage controller suppresses ~96% vibration in less than 3 s and decreases the suppression time by ~97% in a peg-in-hole assembly task using a physics-based model of the NDO object. The controller handles the delay due to image processing and the delay in execution of any trajectory due to the robot internal controller innovatively. The present work uses a NDO that is free to oscillate about a pin joint due to the motion of the robot and uses vision sensor to suppress the vibration induced. This is not a true representation of vibration during assembly operation. However, vibration in NDO due to flexibility in robot gripper will represent a practical problem during assembly of such objects.

CHAPTER 4
VIBRATION SUPPRESSION STRATEGY FOR OBJECT WITH GRIPPER FLEXIBILITY

4.1 Introduction

In general, the robotic assembly system has three major elements: robot, gripper, and grasped object by the gripper. These elements can be designed as rigid or flexible elements. Selection of rigid and flexible element design have their advantages and limitations. If these elements are considered rigid, then there will be hardly any vibration in the system, whereas consideration of flexible elements would have high possibility to vibrate the system due to the presence of transient disturbance in industrial robots.

In chapter 3, a NDO was considered that is free to oscillate about a hinge joint. This investigation helped in identifying and understanding various issues encountered during controller design for suppression of oscillation using vision sensor. The insights gathered earlier is used for investigating a scenario where the gripper is considered as a flexible element whereas the robot and the object are rigid. Earlier, the grippers were designed for specific objects that prevented usage of these for other objects with different shapes, sizes, and weights for the task. Most recently flexible grippers or compliant grippers are being developed and some of the flexible grippers are finger-based grippers, tentacle, and universal grippers (Hughes *et al.*, 2016). Some of the flexible grippers available commercially have anthropomorphic hand and tentacle grippers (Bogue, 2016). The advantages of these flexible grippers are improved performance with less cost. However, there are certain limitations due to undesirable vibrations.

The proposed vibration suppression control methods comprise:

1. Modelling of flexible gripper-object,
2. Design of the *Predictive Vibration Amplitude Error Based* (PVAEB) second-stage controller,
3. Implementation of computer vision-based algorithm using the camera.

The gripper is considered as a flexible joint that is assumed as a torsion spring 3element. The grasped object is rigid and may have identical behaviour like a pendulum. Thus, the gripper-object system is modelled as a pendulum with a torsion spring that oscillates in a

two-dimensional vertical plane. The robot movement is limited in the horizontal direction for transient disturbance and control of the vibration.

The chapter is organized in the following ways: Section 4.2 discusses the proposed approach and section 4.3 presents the system on which the vibration suppression strategies have been implemented and the mathematical model is developed for the development of the second-stage controller. Subsequently, the steps developed for the second-stage controller and its simulation process are elaborated in section 4.4. Thereafter the experimental results of the practical implementations are discussed, and results are analyzed in section 4.5, and finally concluding remarks are presented in section 4.6.

4.2 Problem formulation

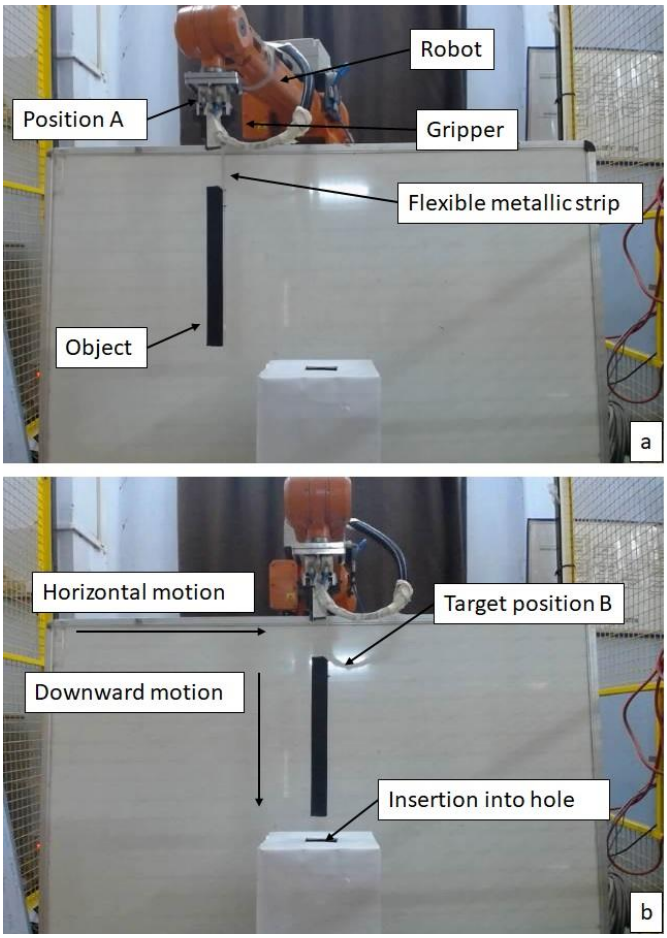

Figure 4.1 Front view of the set up for peg in hole assembly.

In robotic assembly operation, peg-in-hole is a common task performed by industrial robots. This task contains two major activities: manipulation of objects and insertion in the hole. Quite often the peg-in-hole task appears before major assembly tasks. Most of the industrial robot arm is designed to execute PtP trajectories with trapezoidal velocity

profiles. High-speed manipulation of the rigid objects grasped by flexible gripper may result in residual vibration in the object even if the object is rigid such as pipes, beams, metallic channels, etc. Current work focuses on the design of a second-stage controller to attenuate residual vibration in the object held by a flexible gripper in the 2-D vertical plane. In most cases, the internal controller of the robot is not accessible to the user except inputting the information to the Human-Robot Interface (HRI) or teach pendant, for PtP motion, trajectory, and velocity.

For the current investigation, a hollow aluminium square cross-section rigid object is connected with a flexible aluminium metallic strip to the robot end-effector. Figure 4.1 (a) presents the front view of the setup with different parts. The metallic strip was used to model the behavior of a flexible gripper that allows the object to oscillate in the vertical plane. The hollow aluminium object moves rapidly in the horizontal direction from initial position A (Figure 4.1 (a)) to target position B (Figure 4.1 (b)) to keep the end-effector right above the hole. Thereafter, it is expected to insert the said object in the hole precisely. However, acceleration during high-speed manipulation along horizontal direction results in residual vibration of the object that prevents the completion of insertion task quickly. Therefore, the necessity for a second-stage controller is felt to suppress vibration with an intent to complete the task in minimum time.

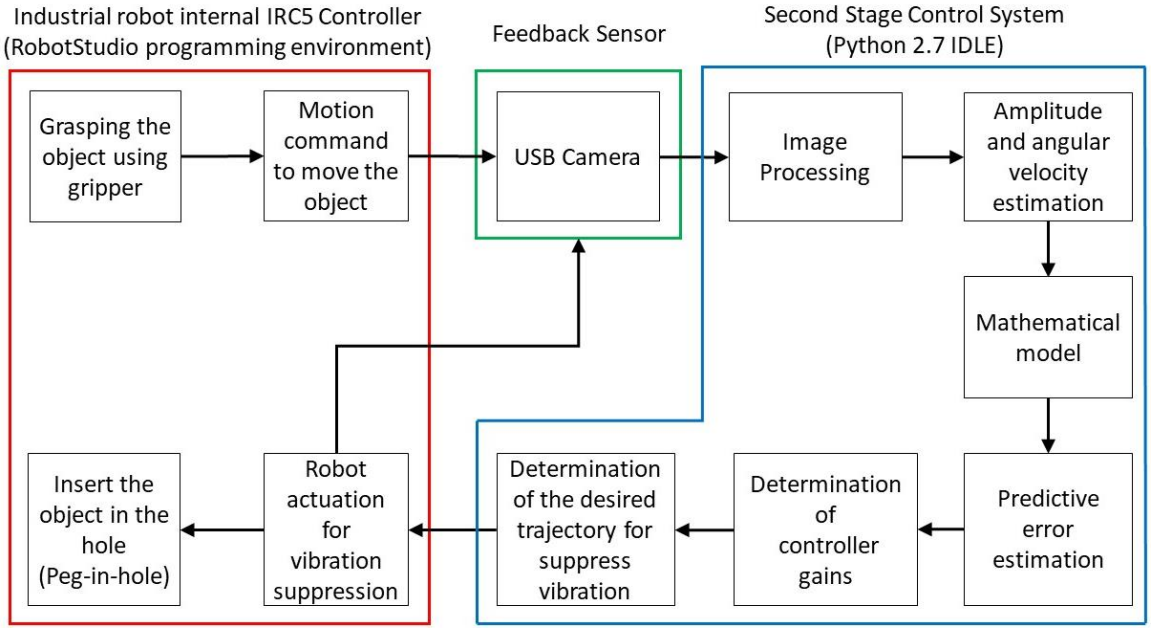

Figure 4.2 Schematic representation for vision-based residual vibration control strategy

For the problem at hand, a generic approach for the vision-based active real-time vibration control method is proposed. The schematic diagram for the proposed approach is presented in Figure 4.2. The internal controller of the industrial robot is shown on the left-hand side of the block and the proposed second-stage controller scheme is on the right-hand side. Initially, the instructions are sent to the internal controller to execute the PtP horizontal trajectory to bring the object right above the hole. This movement causes residual vibrations in the object, whose vibration is captured with the help of a vision sensor. Subsequently, the proposed second-stage controller comes into action when there is residual vibration in the object. Else the controller is not activated. The second-stage controller supplies the required control signals to the internal controller of the robot until the vibration amplitude reduces within a user-specified limit. For the design of the second-stage controller, the important steps depend on feedback received from the vision sensor, and the details of the design phases are described in the next section.

4.3 Vision-based residual vibration control method

To design the second-stage controller a computer vision-based residual vibration control method has been proposed and the important steps are (1) Estimation of residual vibration amplitude of the object using vision sensor through image processing technique, (2) Mathematical modelling of the object for simulation and control and (3) Design of Predictive Vibration Amplitude Error Based (PVAEB) second-stage controller for an industrial robot. Once the proposed second-stage controller is designed and its performance during simulation is investigated for different working conditions, the same approach can be implemented on the industrial robot to demonstrate its efficacy.

4.3.1 Estimation of residual vibration amplitude using vision sensor

The computer vision scheme used for image processing is already discussed in section 3.1 of chapter 3. The same steps for implementation are used and the result is shown in Figure 4.3.

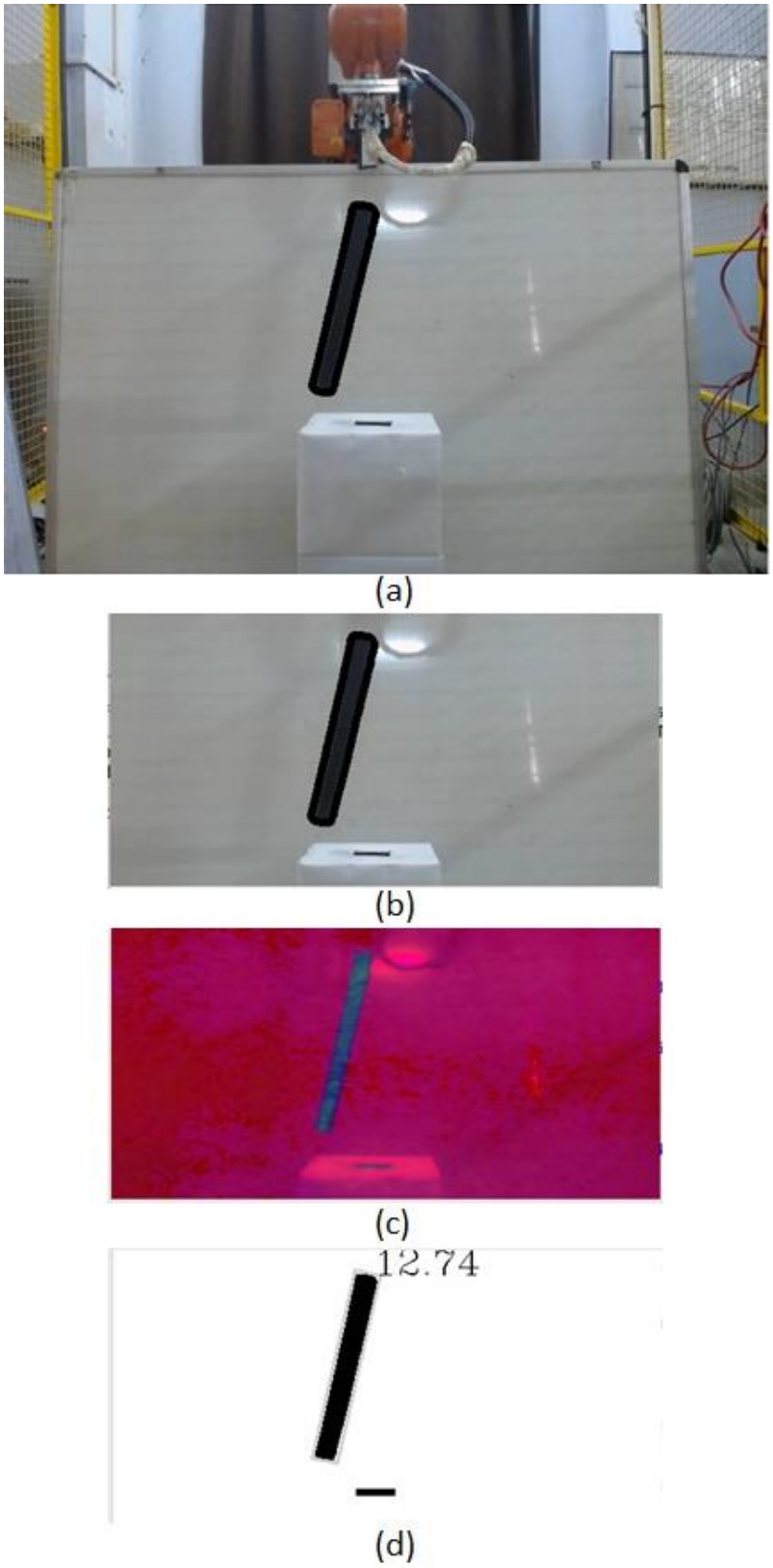

Figure 4.3 Steps for the image processing (a) Red-Blue-Green image, (b) region of interest, (c) HSV image space (d) fitting rotated rectangle on the grayscale image.

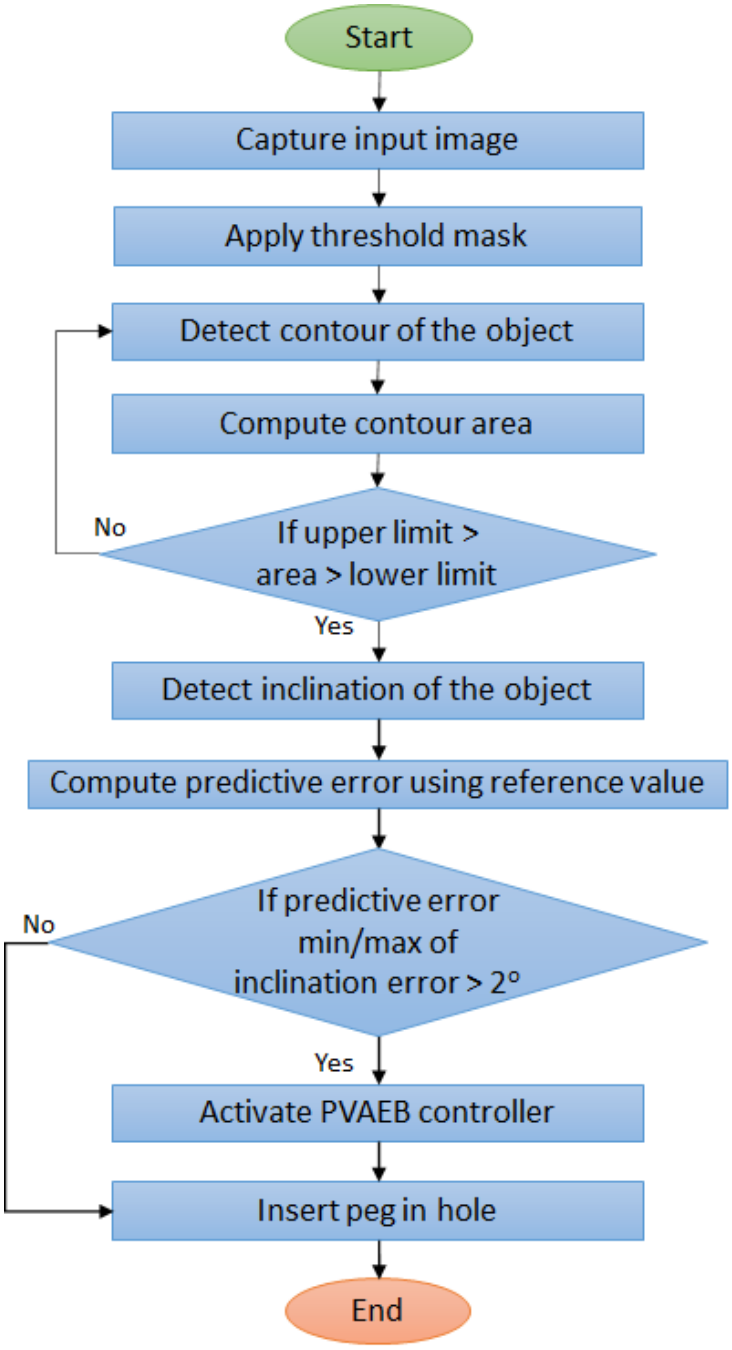

Figure 4.4 OpenCV based Algorithm1 for robotic assembly.

The image processing is carried out using OpenCV software and the steps implemented for assembly operation are presented in the form of a flowchart in Figure 4.4. The process is very much similar to what discussed in 3.1.

4.3.2 Mathematical modelling of the flexible gripper-object system

The flexible gripper object under consideration is treated as a pendulum with a torsion spring on moving support in the horizontal direction and shown in Figure 4.5.

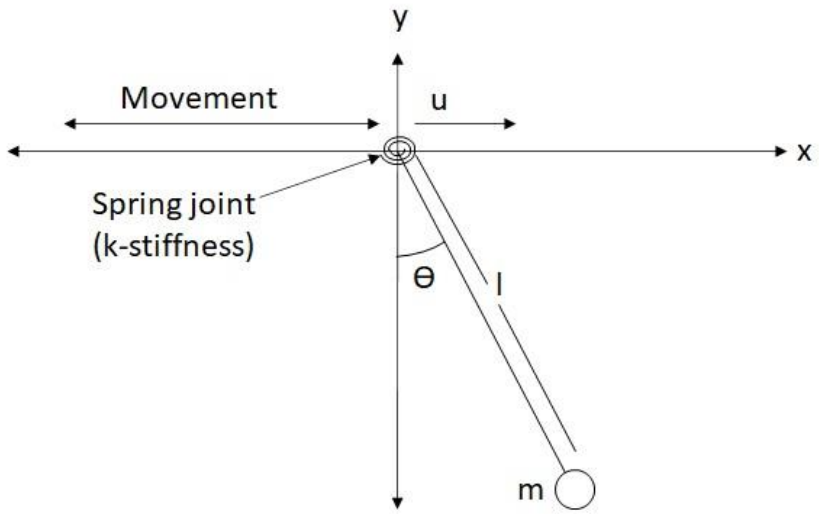

Figure 4.5 The model for oscillation of object

The spring element represents the flexible gripper, and the point mass pendulum represents the object grasped by the flexible gripper. The pendulum is attached to the moving base with a spring element that allows rotation around the joint exhibiting oscillatory motion. The free body diagram of the current system with forces acting on the pendulum due to robot acceleration (movement of end-effector is treated as a moving base) is used to develop a mathematical model. The equation of motion for the pendulum with torsion spring is derived by summing all the moments. Where the terms in the equation are defined in Table 4.1.

$$I\ddot{\theta} + IC\dot{\theta} + mgl\,sin\,\theta + k\theta + ml\mu\,cos\,\theta = 0 \qquad (4.1)$$

Table 4.1 Parameters of the NDO with torsion spring on moving support.

Symbol	Unit	Description
C	[Ns/m]	Coefficient of friction
μ	[m/s^2]	Acceleration of moving base
θ	[Rad]	Swing angle
k	[Nm/rad]	Springs torsion coefficient
m	[kg]	Mass
l	[m]	Length from joint to centre of gravity of pendulum
I	[kg.m^2]	Moment of inertia on centre of gravity of pendulum

After rearrangements, the nonlinear equation (4.1) is converted into a linear equation using the small oscillation assumption: i.e., $sin\,\theta \approx \theta$ and $cos\,\theta = 1$ when θ is small.

$$\ddot{\theta} + C\dot{\theta} + \left(\frac{mgl + k}{I}\right)\theta + \frac{ml\mu}{I} = 0 \tag{4.2}$$

$$\ddot{\theta} + C\dot{\theta} + \omega^2\theta + \frac{ml\mu}{I} = 0 \tag{4.3}$$

Where

$$\omega = \sqrt{\frac{mgl + k}{I}} \tag{4.4}$$

After solving equation (4.3) and neglecting damping and friction.

$$\omega_n = \sqrt{\frac{mgl + k}{I}} \tag{4.5}$$

Where ω_n is the natural frequency.

The EOM in state-space form using equation (4.3) is:

$$\begin{bmatrix}\dot{x}_1(t)\\ \dot{x}_2(t)\end{bmatrix} = \begin{bmatrix}0 & 1\\ -\left(\frac{mgl + k}{I}\right) & -C\end{bmatrix}\begin{bmatrix}x_1(t)\\ x_2(t)\end{bmatrix} + \begin{bmatrix}0\\ -\frac{ml}{I}\end{bmatrix}\mu(t) \tag{4.6}$$

Where

- $x_1(t)$ represents the angular position (θ) of the NDO.
- $x_2(t) = \dot{x}_1(t)$ is the angular velocity of the NDO.
- $\dot{x}_2(t) = \ddot{x}_1(t)$ is the angular acceleration of the NDO.

The objective of the experiment is to suppress the oscillatory motion by providing base motion in the horizontal x-axis direction. Therefore, an active second-stage control strategy is designed for the current work to stabilize the object by providing control movements to the three joints of the robot responsible for the movement of the end-effector position in the workspace. In this case, the orientation of the end-effector has been kept constant for the robot.

The state space form in equation (4.6) is used for numerical integration to obtain velocity and displacement which will be used in the proposed controller for the prediction of the maximum error. A Python code is written and 'odeint' library function is called for the numerical integration of the equation (4.6).

4.4 Design of second-stage controller to suppress residual vibration

To suppress the vibration, the control input trajectories should be executed when the object is at an extreme position where the amplitude is maximum and angular velocity is zero. This is a condition where the system gains maximum potential energy and zero kinetic energy. The direction of the control input trajectories is dependent on the amplitude. If the amplitude is positive, then the direction of trajectory motion is kept in the positive direction or vice-versa. This type of control system attenuates the vibration amplitude of the object measured with the help of a vision sensor, thus able to suppress the oscillation of the object being held with a flexible strip representing a torsion spring. Here the proposed second-stage controller is activated only when the robot has completed the desired PtP motion, and the object is right above the hole into which it is supposed to be inserted. This controller is so designed that the oscillation of the object is monitored continuously, and control actions are provided based on the predicted error (deflection of the object from its stable vertical down equilibrium position) that is estimated using the mathematical model (4.3)-(4.6).

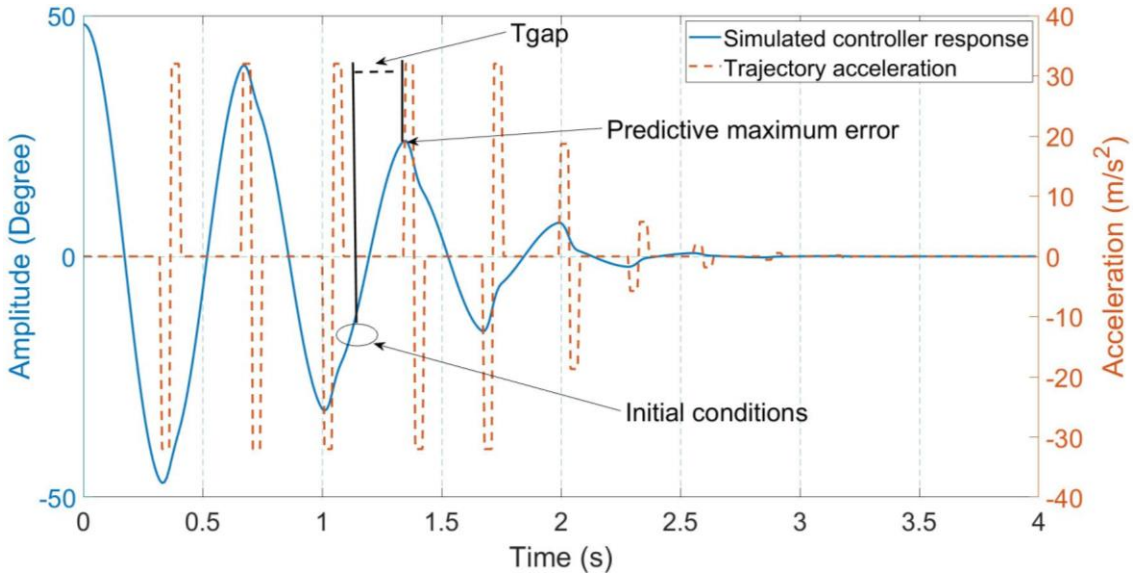

Figure 4.6 Illustrative example of predictive vibration amplitude error based second stage controller.

The control law stated in equation (3.13) of section 3.3.3 is adopted. The state space model of the NDO with gripper flexibility as provided in equation (4.6) is used to predict the maximum error. The control output is the displacement of the end-effector in the corresponding direction that suppress the vibration amplitude. The proposed control strategy is illustrated in Figure 4.6. The object has been released with initial conditions

(amplitude = 48.22° with zero angular velocity) and exhibits oscillation/response that needs to be suppressed. After which, the proposed PVAEB second-stage controller is activated. The amplitudes at two consecutive time points are used to estimate the maximum predicted error (the extreme positions of the object). Amplitude and angular velocity at this time point are implemented as initial conditions in the object mathematical model and help in the estimation of the amplitude at the next extreme position as well as the time required to reach the extreme position from the initial condition. The predicted extreme position of the object is considered as the actual error which requires a control action. Based on this predicted maximum error the controller estimates a trajectory in the x-axis direction that has a trapezoidal velocity profile as the control input to the system for attenuation of the amplitude of the vibrating system significantly. It should be noted that the SPVAEB controller in the previous chapter used the amplitudes of two consecutive time points when the amplitude changes its sign while crossing the zero-amplitude position. Whereas, in this case it is not bounded the same conditions as stated earlier.

4.4.1 Estimation of control input trajectory

Most of the industrial robots available in the market execute a PtP trajectory at the end-effector or Tool Coordinate Point (TCP) while maintaining a trapezoidal velocity profile and the time law for trajectory is known as linear interpolation with parabolic blends. Therefore, a control input trajectory has been designed based on the second-stage controller output to follow a trapezoidal velocity profile. Based on the controller output displacement in the x-axis direction, a trapezoidal velocity profile with parabolic blend is generated assuming constant acceleration which is discussed in section 3.3 of the previous chapter. In a conventional PID type dynamical vibration control system, the error monitoring, and control activities are performed simultaneously to suppress the residual vibration. In this case, the implementation of a controller for control action to attenuate vibration with limited control input is very arduous. In addition, delay caused due to image processing as well as execution of control trajectory are major challenges in the implementation of the conventional PID controller for real-time control of vibration amplitude.

4.4.2 Approach to handle system delay

The system delay is inherent in the robotic system and becomes more significant when a vision sensor is associated with the same system. Various types of delays observed in the proposed system are:

1. Robot system delay (t_{rsd}), i.e., the time consumed to execute a trajectory while instruction is sent to the internal controller of robot,
2. Hardware and software dependent delays due to vision sensor and image processing (t_{ip}),
3. Delay due to prediction of maximum error using the computational model (t_{mc}).

The proposed controller intelligently handles the delay in the robot system and the delay caused due to implementation of vision sensor. The time gap (t_{gap}) between the initial conditions and predicted extreme position shown in Figure 4.6, is treated as a delay in the execution of control action. The relation is expressed in equations (4.7)-(4.9).

$$t_{gap} = t_{ip} + t_{mc} + t_{rsd} + t_{rest} \tag{4.7}$$

$$t_{gap} = t_{sd} + t_{rest} \tag{4.8}$$

$$t_{sd} = t_{ip} + t_{mc} + t_{rsd} \tag{4.9}$$

Where t_{rest} is rest time added to the t_{gap} in real-time control. For this system, t_{ip}, t_{mc}, and t_{rsd} values are considered system delay and represented by t_{sd}. Hence, the t_{gap} is dependent on the natural frequency of the object directly and it is computed using the mathematical model discussed in (4.3). Here the t_{sd} value is defined based on whether the system has high or low natural frequency vibration. If half of the oscillation time period (T) of the object is greater than t_{sd} then the system is considered as lower frequency vibration or vice-versa as given below.

$$\begin{Bmatrix} Low\ frequency\ vibration \\ High\ frequncy\ vibration \end{Bmatrix} = \begin{Bmatrix} 1/T \leq 1/2t_{sd} \\ 1/T > 1/2t_{sd} \end{Bmatrix} \tag{4.10}$$

The rules used for intelligently handling the delay in the system is discussed below:

- **Rule (1)** – For a system with low-frequency vibration, $1/T \leq 1/2t_{sd}$, the t_{rest} value is added to execute the control input trajectory at the predicted extreme

position. In this condition, the second-stage controller acts on every predicted extreme position.

- **Rule (2)** – For a system with high-frequency vibration, $1/T > 1/2t_{sd}$, the second-stage controller cannot act on all the predicted extreme positions. Therefore, the predicted extreme position is not used, and the model predicts the next extreme position, and the control input trajectory is changed as per the control law. This is continued until the t_{gap} value becomes higher than t_{sd} value and t_{rest} is added to it.
- **Rule (3)** – If the direction of predicted extreme position, is same as the preceding extreme position, then skip the current control input trajectory. Here the directions of two consecution control input trajectory should be in opposite directions.

The above rule may come into play when the controller continues to avoid the extreme position of one side and may result in a positive or negative extreme position. This leads to the computation of the control input trajectory in one direction only. Although this input may suppress the vibration, the position of the object will be away from the target position. Post suppression of vibration, the robot must bring the object to the desired target position again, which may delay the assembly further with slow trajectory speed and may excite the object again with high trajectory speed.

Using the above rules, the system delay is handled efficiently while vibration of the object is suppressed in real-time using a low update rate vision sensor. Therefore, the present system delay is considered as an advantage and works favorably for the challenge posed.

4.4.3 Simulation of predictive error based second stage controller

The pendulum with torsion spring at the moving base system has been considered here. The natural frequency of the system depends on the physical parameters of the pendulum. The torsional stiffness in the spring impact the natural frequency of the system. The performance of the proposed system is analyzed by considering the low frequency and high-frequency vibration suppression. Simulations results demonstrate the performance of the controller proposed and interpret the working strategy.

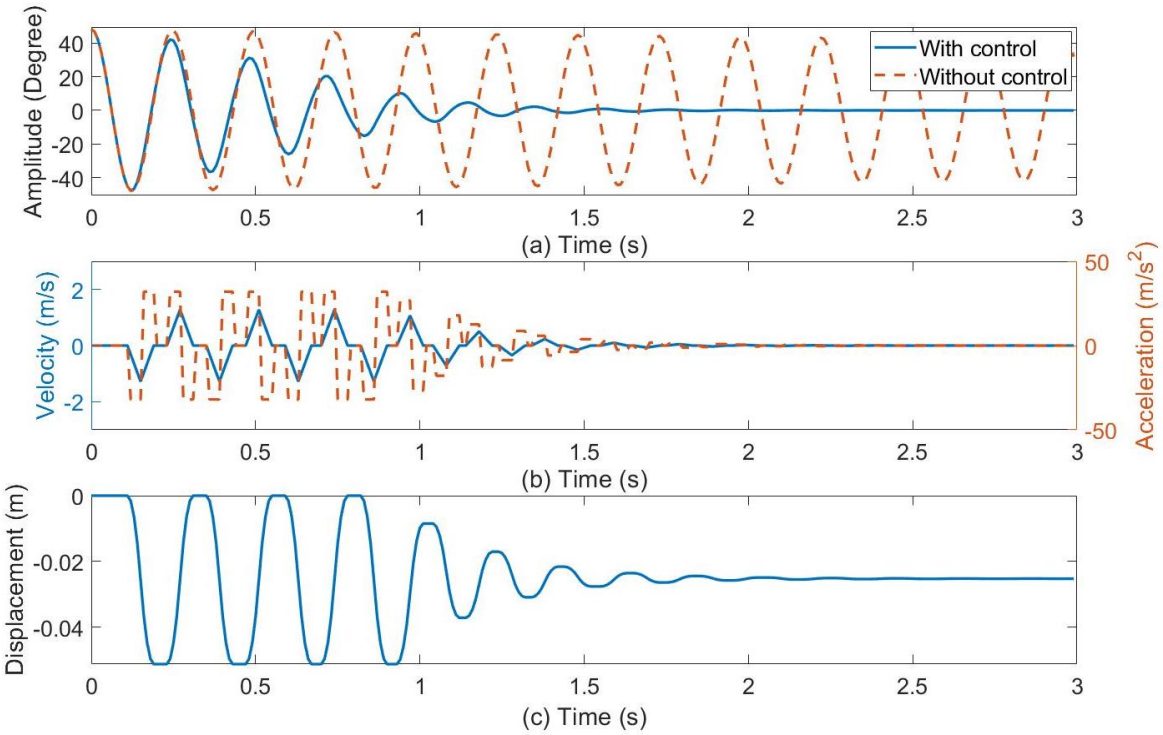

Figure 4.7 Simulated response of the system with natural frequency 4.17 Hz (a) tip response with and without control, (b) velocity and acceleration profile and (c) displacement of control trajectory

The simulated response of the system with a natural frequency of 4.17 Hz, is presented in Figure 4.7, where as the amplitude response with control and without control strategy are shown in Figure 4.7(a). Similarly the velocity and acceleration of the control input trajectories are shown in Figure 4.7(b) and the position of the robot end-effector during execution of the control input trajectories is shown in Figure 4.7(c). In this case the goal position of the end-effector is treated as zero which is to be maintained by the second stage-controller. The alternative motion for the control input prevents the end-effector position offset from the goal position within in a specified limit. Hence the offset after suppression of vibration is compensated by executing a trajectory with low speed by which the end-effector is positioned right above the goal position. In all the cases, the displacement of the trajectory is determined with reference to the desired position of the NDO and it will be dependent on the direction of the first control trajectory. If the direction of the trajectory is positive, then the subsequent control may remain on the same side as the magnitude of the displacement will be reduced gradually and vice versa.

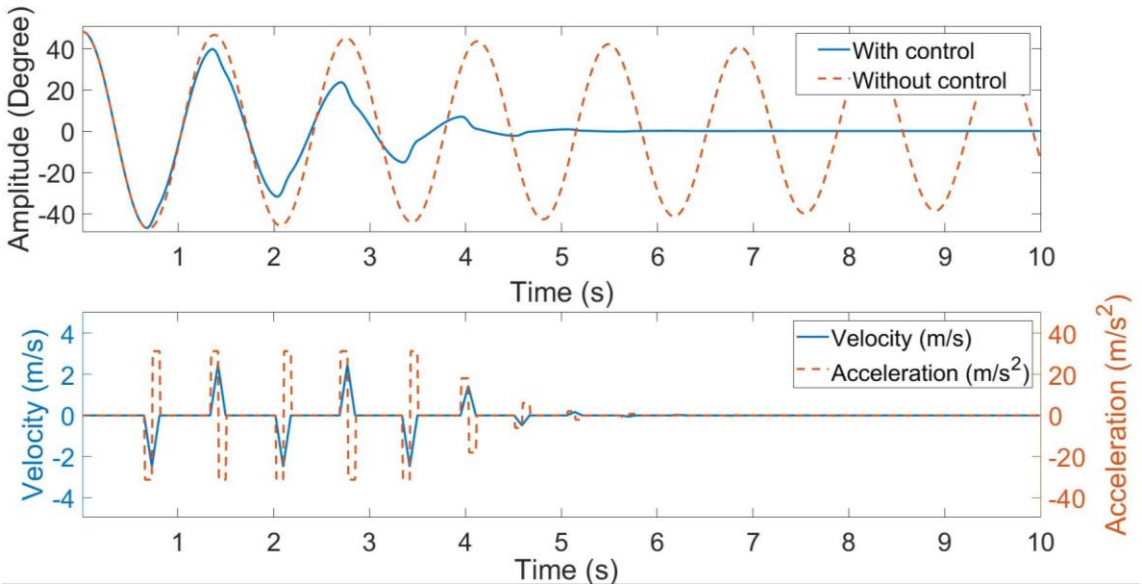

Figure 4.8 Simulated system response with natural frequency 0.75 Hz (a) tip response with and without control and (b) velocity and acceleration profile.

For the current system, t_{sd} value is 0.21 s that include image processing time, predicted error estimation time, and robot trajectory execution delay. Therefore, objects with a natural frequency greater than 2.38 Hz are considered as a system with high-frequency vibration and others as low frequency. The simulated results of vibration suppression for the low-frequency system are shown in Figure 4.8 with control and without control strategy. The system with natural frequency 0.75 Hz is considered as a low-frequency system since the delay is less than half of the time period (0.21 s < 0.665 s). In this condition, the controller can execute control action at every extreme position of the object.

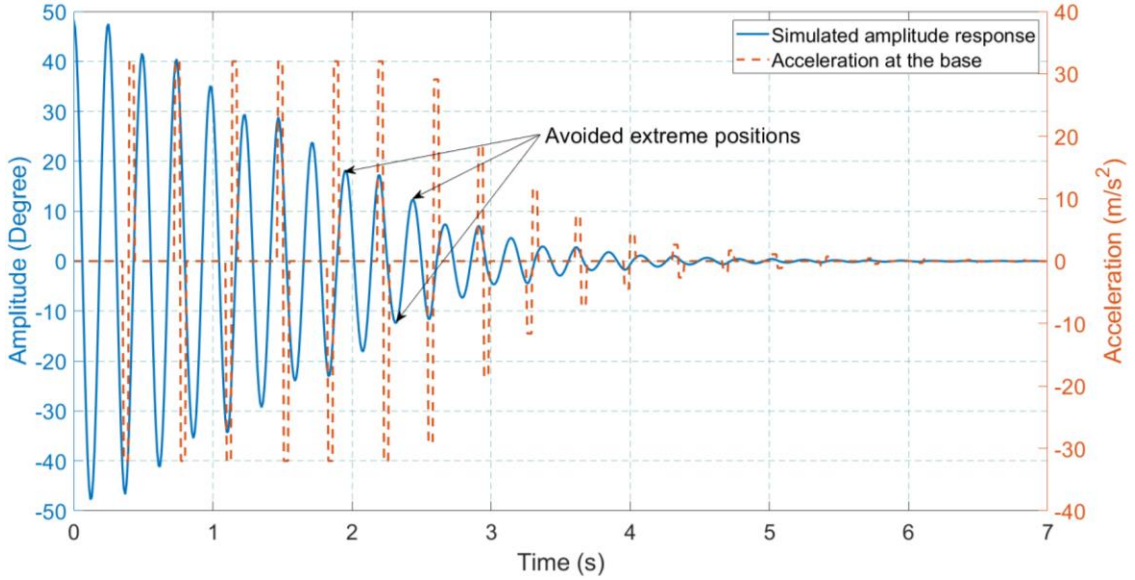

Figure 4.9 Simulated response with system delay.

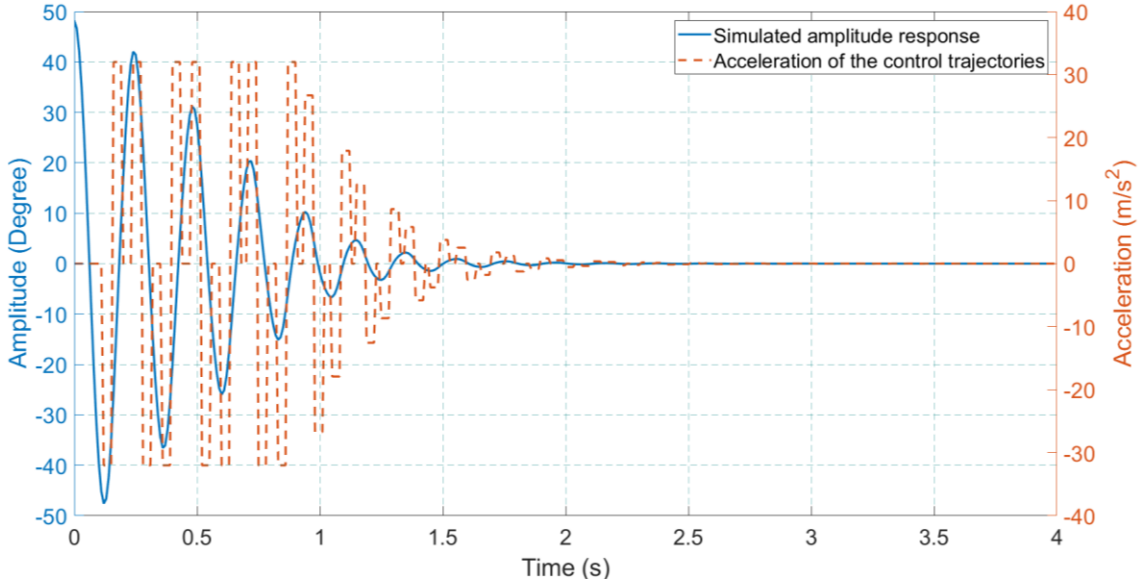

Figure 4.10 Simulated response without system delay.

For the high-frequency vibration system shown in Figure 4.9 has system delay less than half of the time period (0.21 s > 0.12 s). In this condition, the controller cannot execute the control input trajectory at every extreme position. Thus, the controller estimates the predictive maximum error continuously until the time of the predicted error is greater than the system delay. This effect has been shown in Figure 4.9 by avoiding extreme positions. If the system delay is considered negligible then for the same system, the response is shown in Figure 4.10 that took very less time to suppress the oscillation of the object.

4.5 Experimental implementation and analysis of results

The experimental setup is same as the earlier setup discussed in section 3.1 of chapter 3.

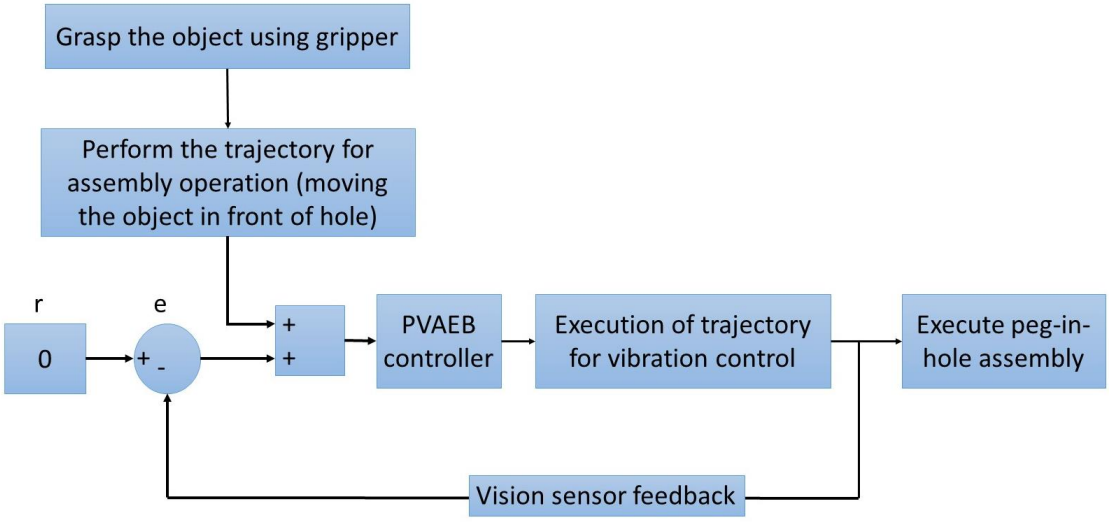

Figure 4.11 Schematic diagram of predicted error based second-stage controller design.

4.5.1 Implementation of second stage controller

The overall working principle of the proposed PVAEB second stage controller is represented in Figure 4.11. Initially, the robot performs manipulation tasks such as moving the object held by the gripper. For position control, the robots use the PtP trajectory command to move the object from an initial position 'A' to the goal position 'B' and it is executed by the robot internal controller which is supposed to perform an assembly task. The object held by the gripper oscillates due to the motion of the end-effector. This oscillation is captured using a camera and the image processing step is applied thereafter. With the help of the vision sensor and image process technique, the amplitude of oscillation is extracted. The amplitude between the two consecutive time points is used to detect the angular velocity of the object as well. The amplitude and the angular velocity are used together as the initial condition for the flexible gripper-object model to detect the predicted maximum amplitude error (the extreme position). Using all of these as input to the controller, the controller provides the output in the form of the displacement trajectory that the robot must execute.

The image processing and the robot controller consume some computation time that is initiated when the sensor captures the image of the object for the execution of the trajectory. For the designed system, the image processing time is detected as 0.03 s and

the delay in execution of the control trajectory is detected as 0.18 s. The proposed controller handles the delay intelligently discussed earlier in section 4.2. This rule-base formed works efficiently and simultaneously with the internal controller of robot, which monitors the system continuously, waits until the object reaches the maximum extreme position (maximum error) at the time of trajectory execution.

4.5.2 Real-time vibration control method

Vibration suppression requires the incremental motion of the robot end-effector. To provide the trajectory motion to the robot end-effector by the position P_d the input commands to the robot IRC5 controller becomes:

$$P = P_o + P_d \tag{4.11}$$

Where P_o is the last position of the robot end-effector. The velocity of the end-effector remains constant in all the control trajectories where the internal controller of robot is fed with the trajectory parameters in form of displacement and velocity that cannot be changed after the command is executed. The IRB 1410 robot has limited capability and has predefined velocity i.e., 10, 50, 100, 200, 500, 1000 and 2000 mm/s. For the experiment the velocity value is fixed at 1000 mm /s.

In this experiment, the robot with the object is moved from starting position 'A' to a target position 'B' horizontally in a straight-line path at high speed. The target position 'B' is right above the hole in which the object will be inserted. However, the object oscillates due to high-speed motion and the oscillation must die before the assembly process resumes. This process causes delay in the insertion of the peg in hole assembly task. If this activity is carried out without any controller, then the object would take more time and would depend on the coefficient of friction and the maximum extreme amplitude, to achieve a stable position. To reduce residual vibration, the PVAEB controller is activated, and the controller remains active until the amplitude of the object is reduced to a specified limit i.e., ±2°. This limit is treated as a safety zone, and error observed due to the use of vision sensor and linear model may affect the oscillation of the object adversely. To investigate the performance and sensitivity of the PVAEB controller, multiple experiments are performed with different initial amplitudes of the object and with the introduction of disturbance. The results of these experiments are reported in the next section to indicate the validity and robustness of the controller.

4.5.3 Experimental results and discussions

In this experiment, the robot with a flexible gripper for a peg-in-hole assembly operation at high velocity is mimicked using a rigid gripper with two connected objects. To demonstrate and test the performance of the proposed controller, the first object was a hollow square cross-section aluminium tube with a length of 322 mm, width 25.4 mm, thickness of 0.5 mm. This hollow tube is connected with an aluminium strip thickness of 1 mm, length 74 mm and width 24.5 mm, to provide flexibility similar to a flexible gripper and induce oscillation after robot motion is executed.

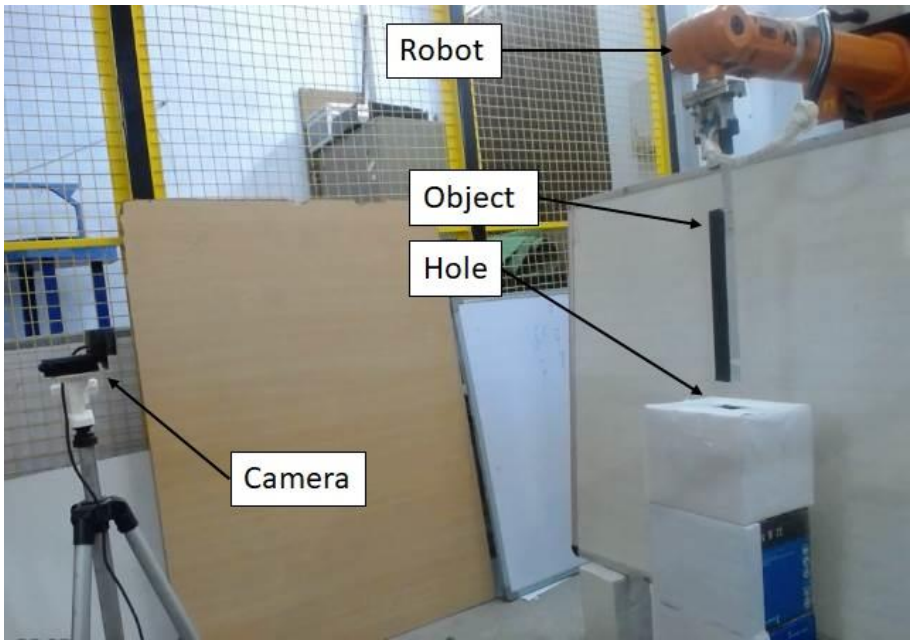

Figure 4.12 Aluminium object with flexible metal strip assembly setup.

The experimental setup of peg-in-hole assembly of aluminium object is shown in Figure 4.12. A black rubber strip is pasted on the aluminium tube to distinguish it from the white background for image processing purposes. The second experiment was conducted with a hollow PVC soft tube that has a length of 735 mm, an outer diameter of 24 mm and a thickness of 3 mm. Although the soft tube behaves similar to a deformable linear object (DLO), to satisfy the current scenario an iron pipe of length 553 mm, external diameter of 17 mm and internal diameter of 14.5 mm, is inserted. The excess 182 mm length of soft tube behaves like a flexible or soft gripper and other portions with iron pipe oscillate without any deformation. The aluminium strip with a hollow object has a high natural frequency (3 Hz) compared to the hollow PVC soft tube which has a low natural frequency (0.87 Hz).

4.5.3.1 Experimental results of Aluminium object

In this experiment, four trajectories have been used to move the object. These trajectories excite vibration in the object that is to be suppressed by the proposed controller.

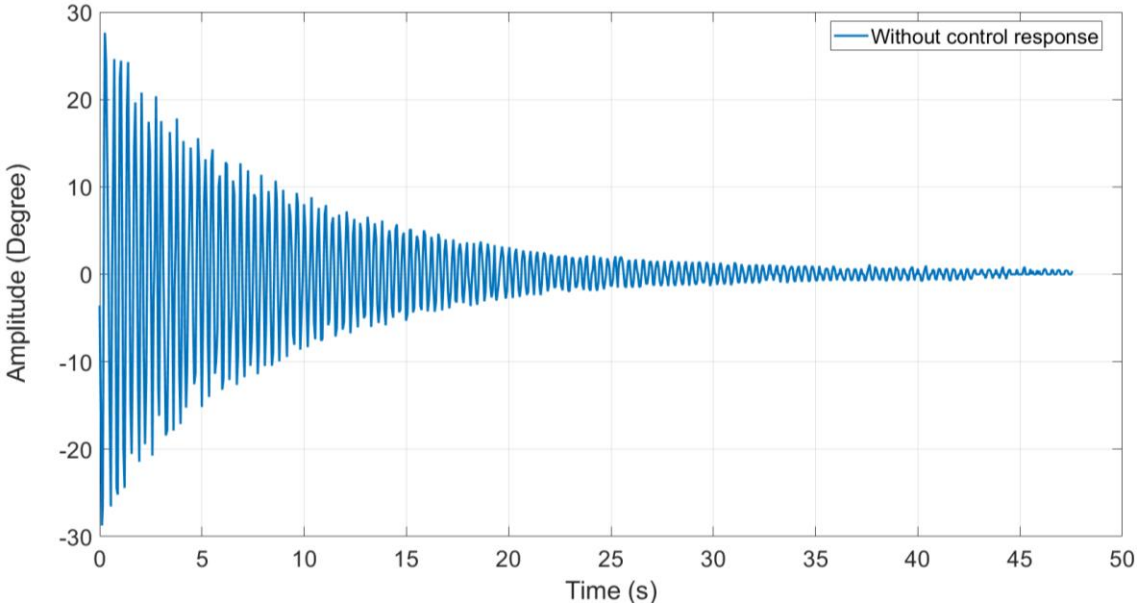

Figure 4.13 Free vibration response of the Aluminium object without any control

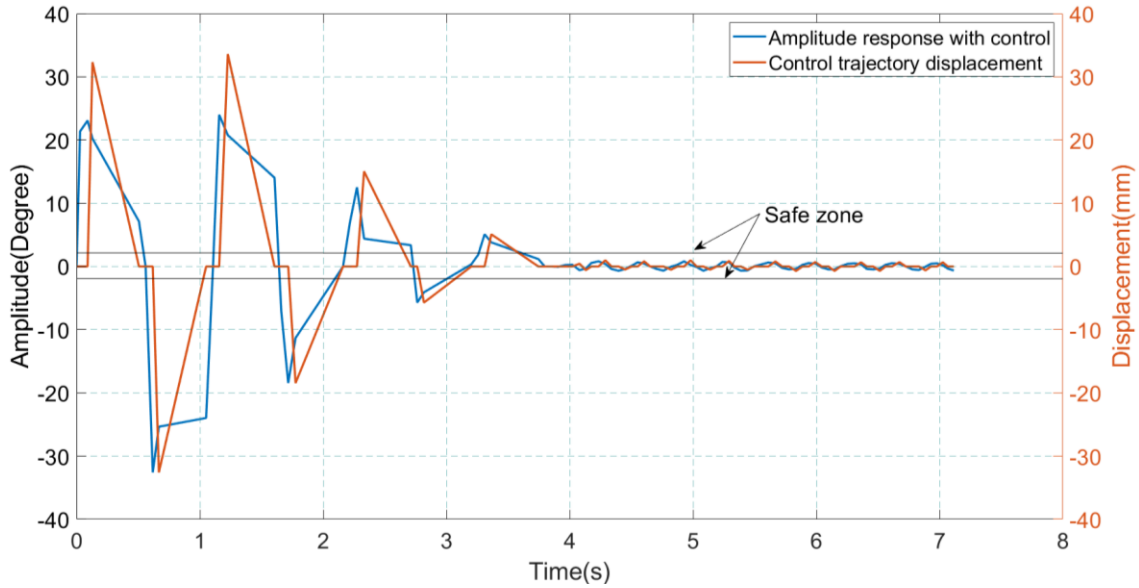

Figure 4.14 Response after controller action with ‘Trajectory1’ initialization

The ‘Trajectory1’ moves the end-effector starts from 0 mm (home) to -100 mm and returns to 0 mm at a speed of 1000 mm/s in a straight horizontal line. The high-speed motion of ‘Trajectory1” excites the object to 23.09° which is the maximum initial amplitude. The second-stage controller detects this predicted error and estimates the control input trajectory distance and direction according to the predicted error. The free

response of the object with 28.74° amplitude takes ~45 s to become stable without any control and the corresponding response is shown in Figure 4.13. The response is obtained using the image processing algorithm discussed in section 3.1.

The control response for ‘Trajectory1’ is shown in Figure 4.14. The left side ‘y-axis’ indicates the amplitude of the object with time and the right side ‘y-axis’ shows the length of control input trajectory estimated by the PVAEB second-stage controller. A safety zone ±2° is introduced for the control action, else it will be arduous to control the error value equal to zero, with the vision sensor amplitude measurement error in the range of ±0.53°. The model of the system is linearized, and the error is kept within a predictable range of amplitude thus safety limit ensures the best performance. For control action, trapezoidal velocity profile in horizontal direction is used to keep the object at an offset from the hole position after vibration suppression. This issue is fixed by providing a trajectory with a low velocity that may not disturb the object from the safety limit after vibration control.

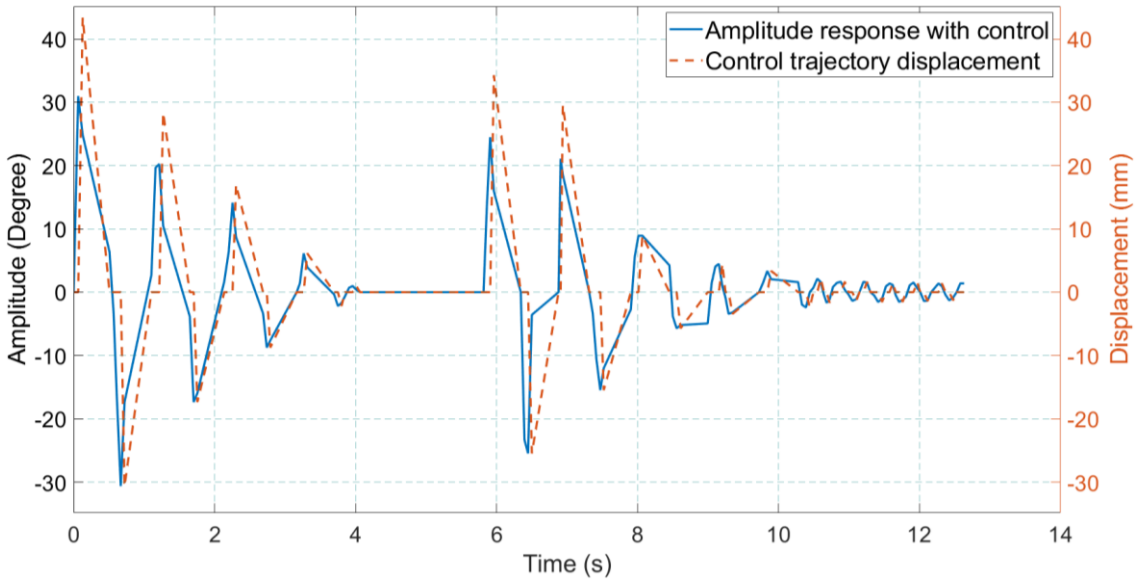

Figure 4.15 Response of the aluminium object with disturbance after stabilization

To demonstrate the robustness of the proposed controller, the object is manually disturbed by inducing vibration after the object becomes stable. It is expected that the proposed controller should suppress such induced vibration. Response from setup with such disturbance after control is shown in Figure 4.15 and Figure 4.16. The rise in amplitude observed after disturbance is 24 mm in Figure 4.15, and 25 mm and 33 mm after two consecutive in Figure 4.16. The vibration suppression of the aluminium object is achieved within 4 s. Although the suppression time is dependent on the initial maximum amplitude error of the object.

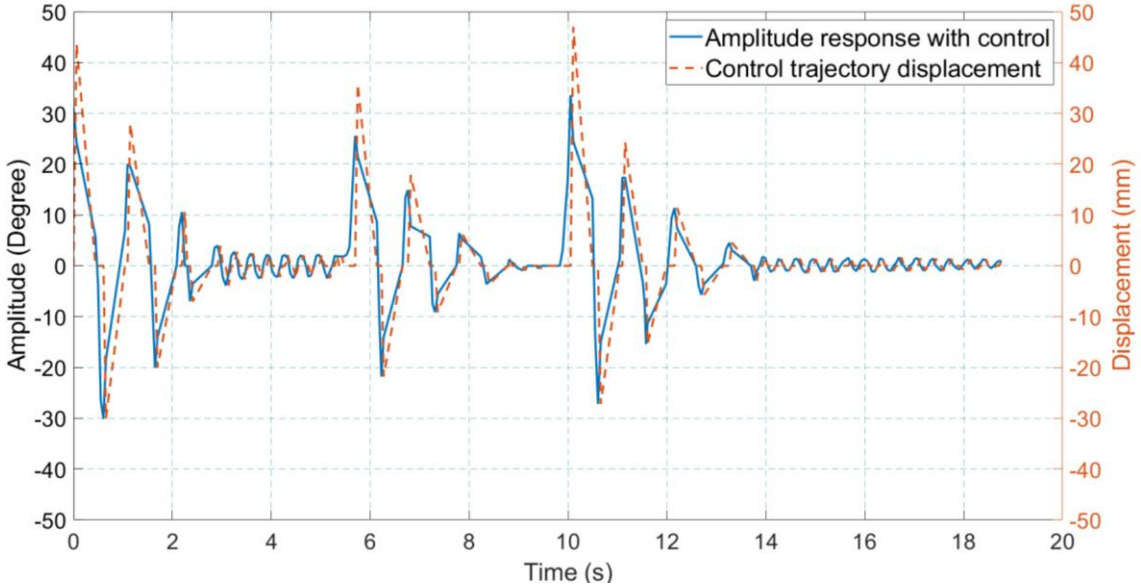

Figure 4.16 Response of the aluminium object with multiple disturbances after stabilization

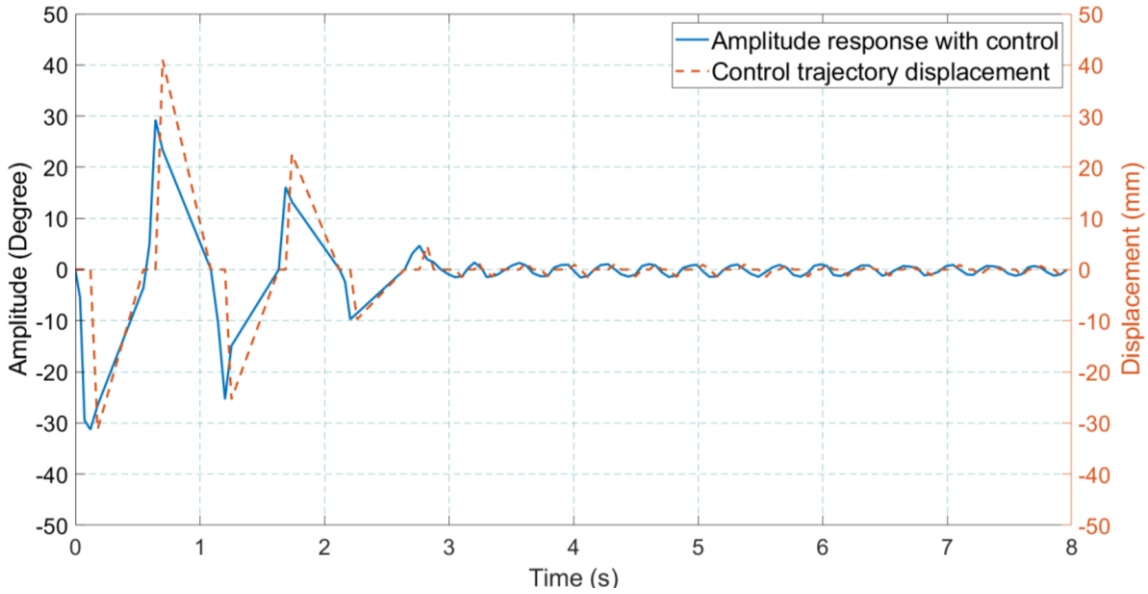

Figure 4.17 Response after controller action with ‘Trajectory2’ initialization

A ‘Trajectory2’ is chosen to move the end-effector starts from 0mm (home) to -200 mm and returns to 0 mm at a speed of 2000 mm/s in a straight horizontal line. The response of controller with excitation ‘Trajectory2’ is shown in Figure 4.17. The proposed controller suppressed the vibration within 3 s into the safe limit.

4.5.3.2 Experimental results of soft tube object

Figure 4.18 Experimental assembly setup with soft tube

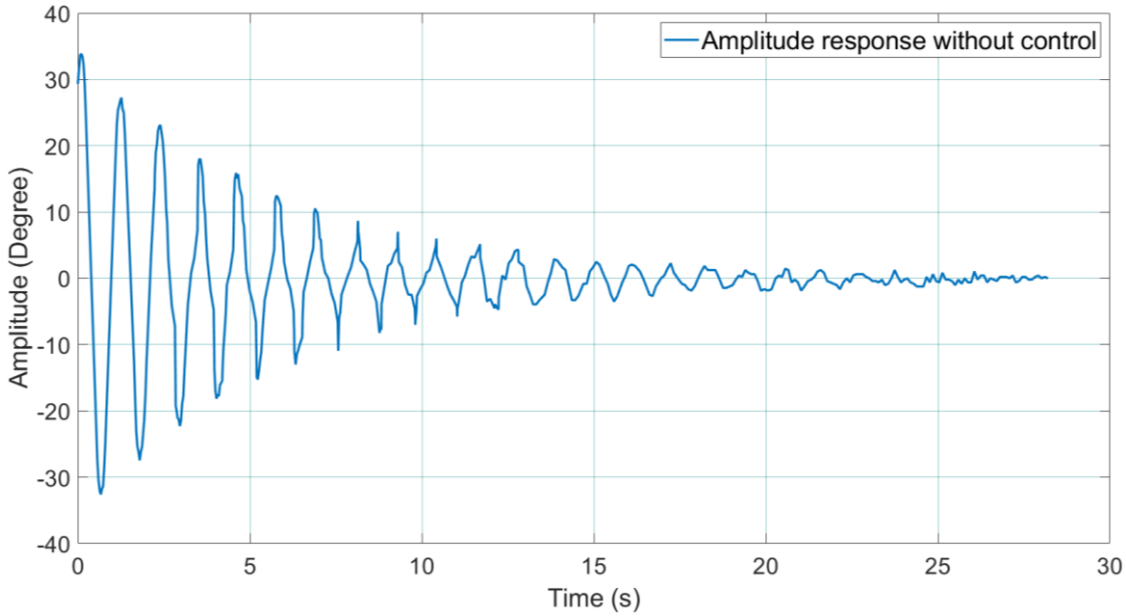

Figure 4.19 Response of the soft tube without control

The experimental setup for the soft tube object is shown in Figure 4.18. In this case, the object is moved with the initial trajectory profile that starts from -100 mm position and moves to 200 mm position, consequently, reach the target position 'B' at 0 mm with a velocity of 500 mm/s using the 'Trajectory3'. The free response of the soft object is shown in Figure 4.19, which has 31.58° amplitude and requires 28 s to suppress the oscillation without control.

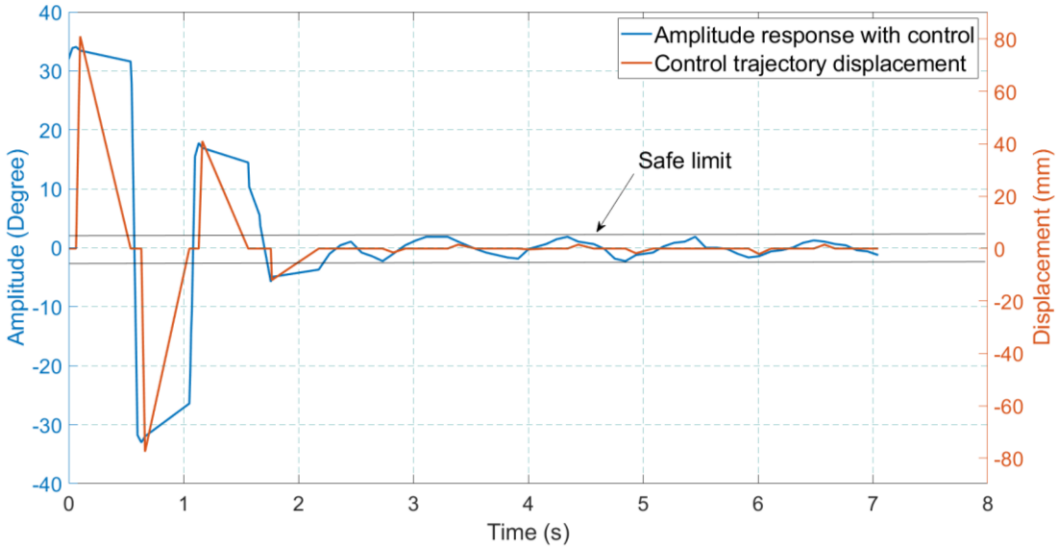

Figure 4.20 Response of the soft tube with control using initial 'Trajectory3.'

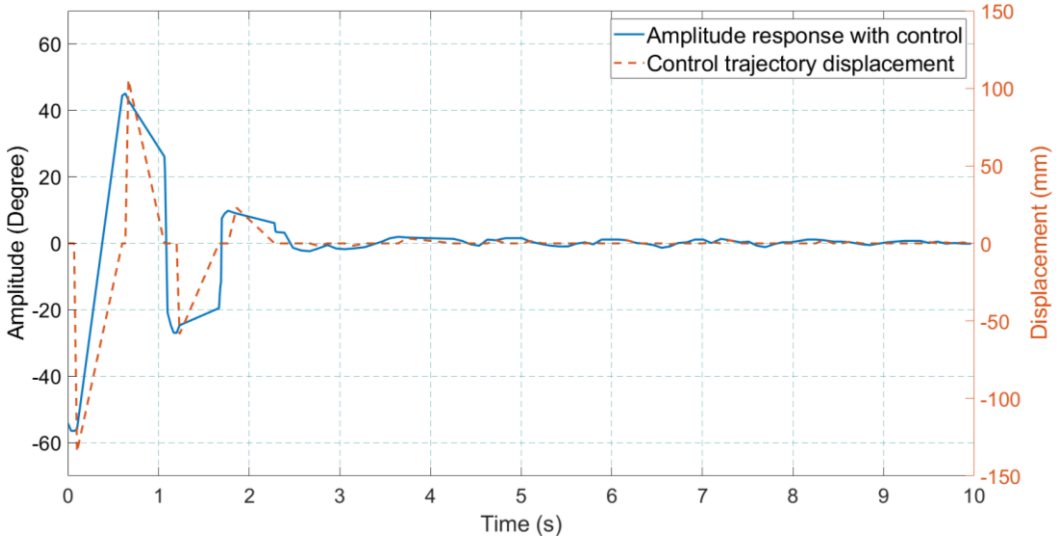

Figure 4.21 Responses of the soft tube with control using initial 'Trajectory4.'

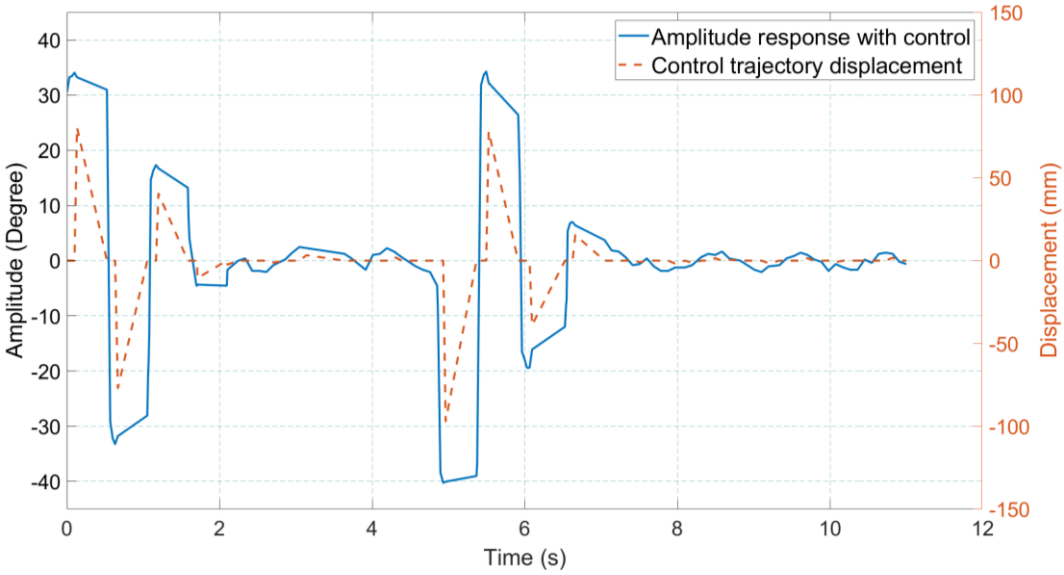

Figure 4.22 Responses of the soft tube with control in presence of manual disturbance

The controller response of the soft tube with the initial ‘Trajectory3’ is shown in Figure 4.20. Figure 4.21 presents the response of the object with a large initial amplitude -54.17° degree. This amplitude is achieved by changing the speed of the ‘Trajectory3’ to 1000 mm/s and named as ‘Trajectory4’. In both cases, the controller suppresses the vibration within 3 s. The robustness of controller performance is presented in Figure 4.22 that indicate manual disturbance after stabilization. The rise in amplitude of 40 mm is observed after disturbance. The designed controller could successfully suppress the oscillation within 3 s.

In the thesis, each experiment is conducted thrice, and a summarized representation of the repeated experiments is provided in Table 4.2. This table shows data related to the range of suppression time, average suppression time, and the reduction in average suppression time. Additionally, the range of vibration suppression time is shown in Figure 4.23.

Table 4.2 Summary of repeated experimental results.

		Vibration suppression time (s)			**Average suppression time (s)**	**Range of suppression time (s)**	**Reduction in average suppression time (%)**
Object	**Trajectory**	**Ex. 1**	**Ex. 2**	**Ex. 3**			
Al	T1	3.80	3.85	3.96	3.87	0.16	91.40
Object	T2	3.00	3.10	3.80	3.30	0.80	92.67
Soft	T3	2.20	2.24	2.50	2.31	0.30	91.74
Tube	T4	2.40	2.51	2.63	2.51	0.23	91.02

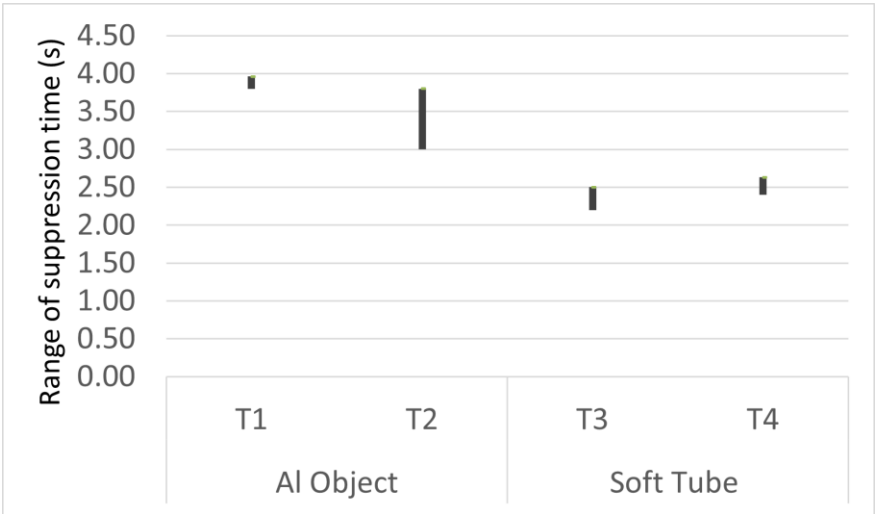

Figure 4.23 The range of suppression time of Al and soft tube object.

The results indicate that the maximum recorded range of suppression time is 0.8 s for the Al object subjected to excitation trajectory 'T2'. This outcome may be attributed to potential errors in amplitude measurement, which can impact the prediction of maximum error. Also, a small error in timing of the control trajectory execution may affect the performance is subsequent experiments.

The summary of results is also presented in Table 4.3. In this table, the best result is taken to show the best performance of the proposed control strategy.

Table 4.3 Summary of experimental results of PVAEB controller.

Object	Trajectory	Suppression time without control (s)	Suppression time with control (s)	Vibration suppression (%)	Reduction in suppression time (%)
Al	1	45	3.8	91.34	91.55
	2	45	3.0	93.21	93.33
Soft tube	3	28	2.2	94.37	92.14
	4	28	2.4	96.31	91.42

The most relevant work related to the current work is benchmarked with (Tanner and Kyriakopoulos, 2000). In this method, a data-driven robot-object model is proposed with a force sensor to suppress residual vibration of the beam to be inserted in robotic peg-in-hole assembly.

Table 4.4 Performance comparison of the proposed method.

Reference	Method	Vibration suppression	Suppression time
(Tanner and Kyriakopoulos, 2000)	Force/Torque sensor data-based robot-object model	90%	3.8 s
Proposed work	PVAEB controller	95%	3 s

4.6 Conclusion

This chapter proposed a PVAEB second-stage residual vibration suppression control strategy using a vision sensor. The vibration in the grasped object is attributed to the flexibility present in a gripper. The flexible gripper object is modelled as a pendulum with a torsion spring connected to moving support to represent the system for the proof of concept and the torsion spring represents the flexibility of the flexible gripper. For this case, the PVAEB controller collects feedback from a vision sensor and works as a second-

stage controller along with the available robot internal controller without any modification. The proposed second-stage controller do not interfere with the working of the internal controller of the robot and suppress the vibration amplitude by ~93% in less than 4 s for aluminium objects and suppress the vibration amplitude by ~95% in less than 3 s for soft tube objects. The suppression time is reduced by ~90% as compared to without control.

Above work induces oscillation in the NDO held by flexible gripper due to robot motion. However, the object to be assembled using robot may have flexibility similar to flexible beams and wires and these objects will have vibration during assembly operations. The next chapter attempts to handle this issue.

CHAPTER 5
VIBRATION SUPPRESSION STRATEGY FOR FLEXIBLE BEAMS

5.1 Introduction

In chapters 3 & 4, the horizontal motion of the robot end-effector or the object is inspired from the peg in hole assembly in general. In the case of soft tube object, the oscillation takes place when it was manipulated in vertically downward position. Therefore, horizontal motion is considered for these experimental setups. Further, the flexibility present in the gripper is considered as the cause of vibration in an NDO. In this chapter, the high level controller design is attempted to handle flexibility present in a long flexible object handled by the robot. For this case, a flexible beam is considered as a flexible object for manipulation and assembly using an industrial robot. Here vertical motion of long beams are not possible in the workspace of the ABB robot. In addition, the effect of gravity on the object will be negligible leading to very small amplitude of oscillation. The vibration induced in the flexible beam has a higher mode of vibration that dissipates within a very short time compared to the first mode of vibration. Therefore, the first-order vibration is considered as a major problem that needs quick suppression within an acceptable time. For suppression of such vibrations in the flexible beam, a control strategy is needed which should be directly applicable to an industrial robot.

The chapter is organized in the following ways: Section 5.2 describes the problem statement and discusses the proposed approach and section 5.3 presents the robot-assisted camera calibration technique, robot-vision method for flexible beam vibration measurement, the FEM based model of the flexible beam and the design of the second-stage controller. Subsequently, the simulation results, description of the experimental setup, practical implementation of the second stage controller and experimental results are elaborated in section 5.4. Finally concluding remarks regarding the work are presented in section 5.5.

5.2 Problem formulation

The current work focuses on “beam in slot” robotic assembly problem. Where the beam is considered as linear flexible beam of suitable engineering material with rectangular cross-section. This beam is grasped by the robot gripper at one end in a horizontal plane which

allows the beam to vibrate in a vertical plane due to PtP motion of the robot as shown Figure 5.1. Intuitively it can be said that the vibration will be small if the gripper grasps the long beam somewhere near the end of the beam and gradually inserts this into the slot. However, this kind of attempt would lead to vibration in the other portion of beam due to motion and would create unsafe working condition causing delays in the next operation.

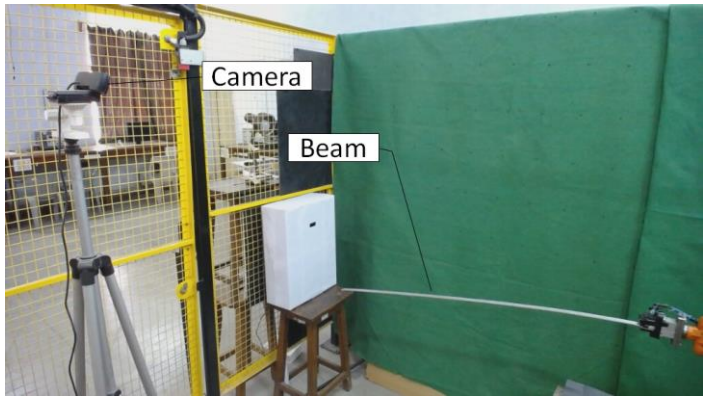

Figure 5.1 Vision based beam in slot assembly by industrial robot.

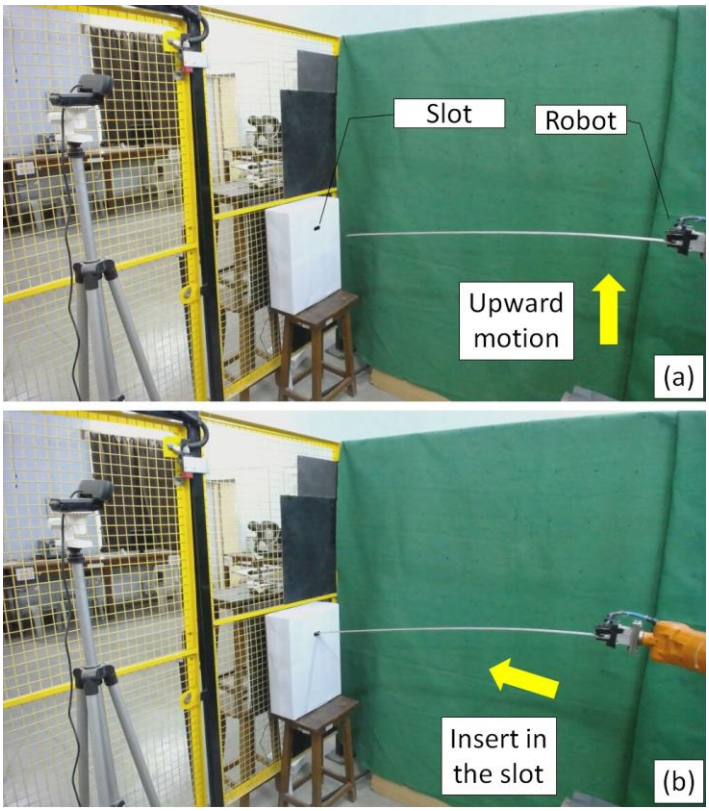

Figure 5.2 Robot movement for assembly of beam in slot (a) robot moving upward direction and (b) beam insertion in the slot.

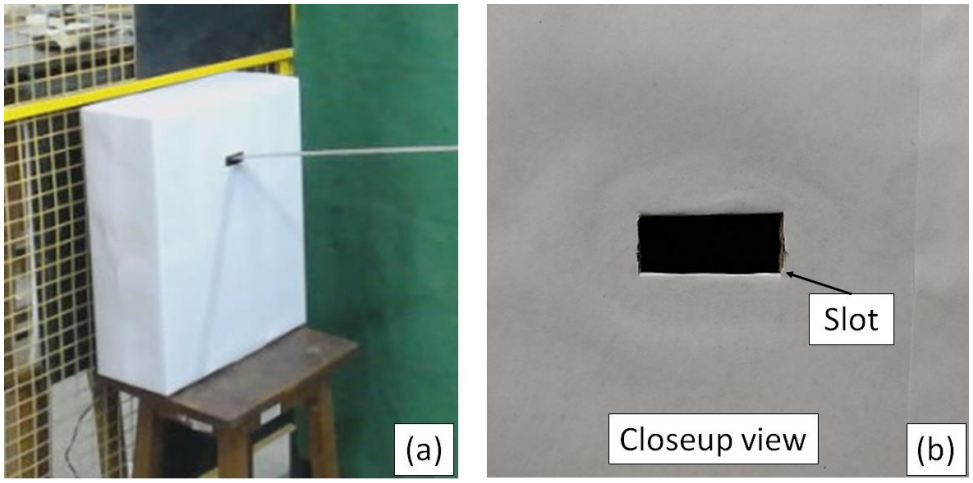

Figure 5.3 (a) Enlarged view of flexible beam in slot assembly and (b) closeup view of the slot.

For the problem at hand, the beam is moved at a high speed in the vertical upward direction as shown in Figure 5.2(a) respectively. The robot acceleration during high-speed manipulation along the vertical direction induces vibrations in the beam and the beam must be in stable position before assembly. If the tip of the beam is stable then the robot will insert the beam into the slot shown in Figure 5.2(b) and the enlarged view of the tip of the beam and slot are presented in Figure 5.3(a)-(b) respectively. Therefore, the need for design of a suitable controller arises that is capable of suppressing above vibrations with a motivation to reduce assembly time.

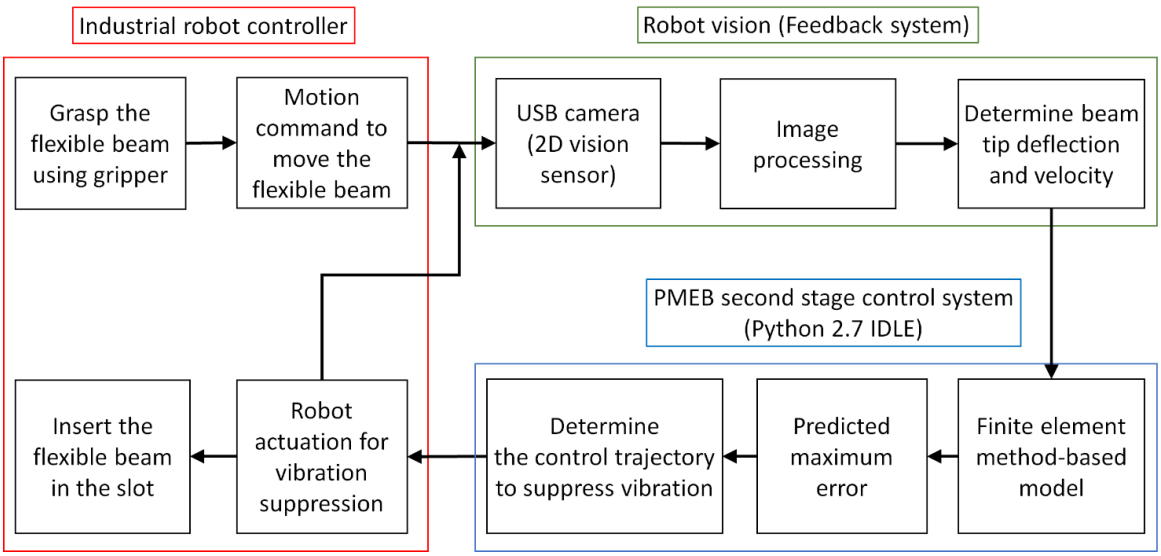

Figure 5.4 Schematic representation of robot-vision based approach for residual vibration control of a flexible beam.

The available controller in most of the commercial robots are incapable of suppressing above vibrations in the beam. Hence, a high level second stage controller has been proposed and implemented to achieve the desired aim. The proposed controller scheme is given in Figure 5.4. The controller of industrial robot is shown on the left block, the upper right block shows the robot-vision system, and the lower right block shows the computer on which the second-stage controller scheme is implemented. Initially, the industrial robot controller executes the PtP trajectory to bring the beam in front of a slot. Such motion command introduces vibrations in the flexible beam. With the help of 2D color camera, the dimension of the flexible beam, tip deflection, and velocity are obtained to use in the proposed second stage controller. Subsequently, the controller is activated if the amplitude of residual vibration exceeds the task specified limits, else this controller is not activated. The proposed second-stage controller uses the tip deflection and velocity as the current state of the beam, that are fed to the FEM model to predict the maximum error. Based on the value of maximum error and control law, the said controller sends the required control signals to the industrial robot controller until the residual vibration diminishes to a user-specified safe limit. The design details of the robot-vision system and the second stage controller are described in the next section.

5.3 Robot-vision based approach to suppress the residual vibrations

The important steps for a generic robot-vision based second stage controller to suppress the residual vibration in a flexible beam are given below.

(i) Robot-assisted camera calibration method to obtain the extrinsic parameters,
(ii) Robot-vision approach to identify the flexible beam, dimension, tip deflection and velocity,
(iii) FEM based dynamic modelling of flexible beam to predict the deflection,
(iv) Design of PMEB second stage controller.

The details of the above steps are discussed in the following subsections.

5.3.1 Robot-assisted camera calibration

Camera calibration is the most important step for the implementation of vision in any application. In the calibration process of a camera, the intrinsic parameters i.e., optical centre (u_0, v_0) , focal length (f_x, f_y) and skew coefficient (γ), and extrinsic parameters i.e., rotation and transformation matrices, are determined. Calibration in the form of

intrinsic and extrinsic parameter matrices provides the relation between 3D points in the real world to their corresponding 2D projections in pixel coordinates on the image frame. The calibration process needs predefined 3D points in a WCS and corresponding projection of the points in the image coordinate system (ICS), these points are known as perspective points.

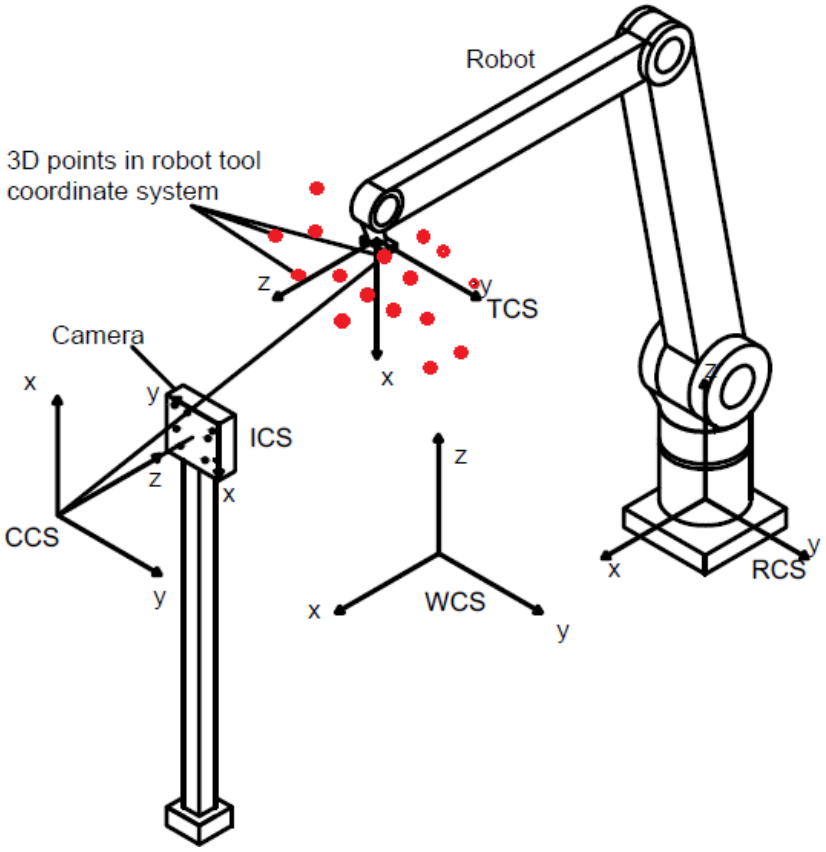

Figure 5.5 Projection of 3D points from TCS to ICS for robot-assisted camera calibration

The coordinates system to represent the robot-assisted camera calibration is shown in Figure 5.5. In this figure, the tool coordinate system (TCS) is attached to the robot gripper for the description of perspective points indicated by red circle. Likewise, the TCS is mapped to the RCS using the transformation matrix defined for the industrial robot controller. Hence both the TCS and RCS are part of the industrial robot. It should be noted that the coordinates of the perspective point are provided as feedback from the robot system. The description of RCS in WCS is described by the equation (5.1).

$$p_w = {}^{W}T_R \, p_r \tag{5.1}$$

where, p_w is the coordinates in WCS and p_r is the coordinates in RCS of perspective points. ${}^{W}T_R$ is a 4×4 homogenous transformation matrix (HTM) comprising rotation

matrix and translation vector which are already known. Therefore, the p_w is obtained using the equation (5.1) and its corresponding pixel coordinates in ICS is determined by image processing steps described below.

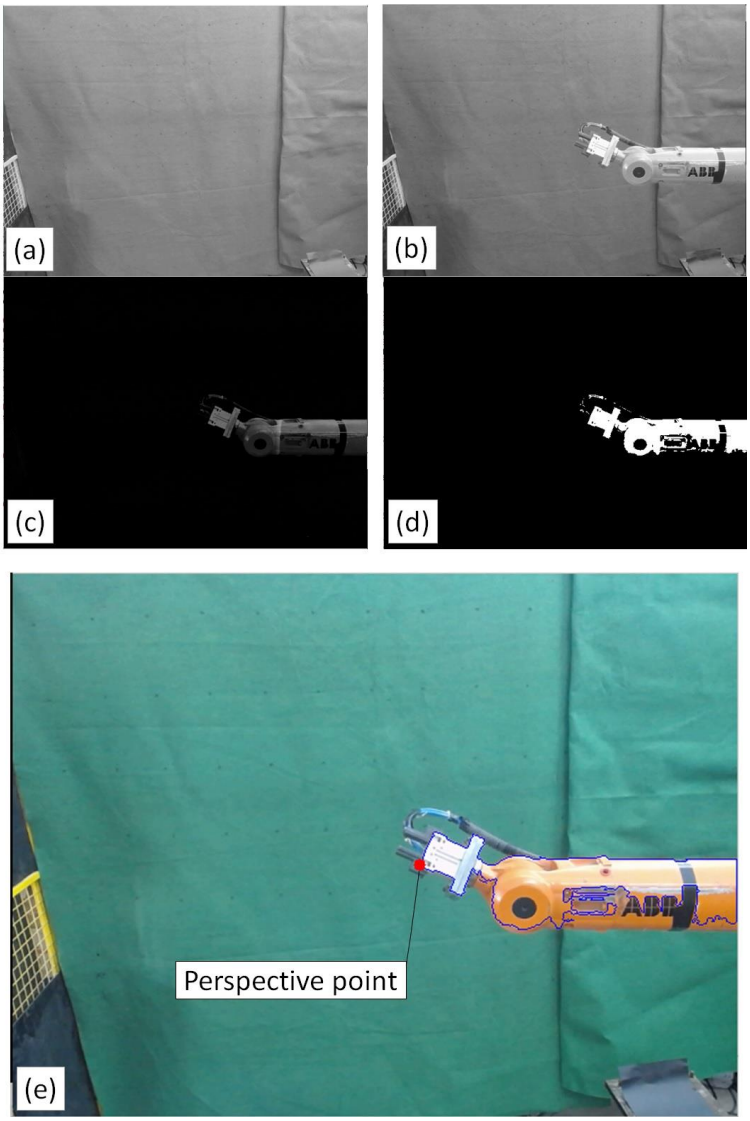

Figure 5.6 Steps for perspective point detection on the robot gripper (a) reference image without robot, (b) robot image, (c) image subtraction, (d) binary image after threshold and (e) perspective point at the left most corner of the contour on the gripper.

For the present setup, the perspective point on the robot gripper is a fixed point on the TCS as shown in Figure 5.6(e) which is the left most corner of the robot gripper part in white hue. Camera should always detect the same point because the robot provides the coordinates of this point in RCS used as perspective point p_r. The required image processing steps to detect the robot gripper part are shown in Figure 5.6 that uses image subtraction method dominantly. It is assumed that the environment is stationary which is

a requirement for background subtraction. A reference image is captured where the robot is absent in the camera frame and thereafter the robot is brought into the camera frame. These images are presented in Figure 5.6(a) and Figure 5.6(b) respectively. On these images a background subtraction operator is applied to convert non-movable objects as background. As a result, only the robot part is displayed in the camera frame as shown in Figure 5.6(c). A threshold operator is applied to the greyscale image to convert it into a binary image shown in Figure 5.6(d). Subsequently, the contours are drawn, and the maximum area of contour is selected to present the robot part only. Finally, the left-most point of the contour is selected as the p_r in ICS shown in Figure 5.6(e). It is to be noted that the orientation of the gripper is set in such a way that the corner is always in the left most position. Hence, the image coordinates of this point p_i in ICS and its corresponding coordinates p_w in the WCS are available using the above discussed approaches. The relation between point $p_i = (u, v, 1)^T$ and the corresponding point $p_w = (X_w, Y_w, Z_w, 1)^T$ is presented (Marchand *et al.*, 2016) in equation (5.2).

$$p_i = K\, \Pi\, {}^{C}T_W\, p_w \tag{5.2}$$

where

$K = \begin{bmatrix} f_x & \gamma & u_0 \\ 0 & f_y & v_0 \\ 0 & 0 & 1 \end{bmatrix}$ is the camera intrinsic parameter matrix,

$\Pi = \begin{bmatrix} 1 & 0 & 0 & 0 \\ 0 & 1 & 0 & 0 \\ 0 & 0 & 1 & 0 \end{bmatrix}$ is the projection matrix for the current perspective projection model,

${}^{C}T_W$ is a 4×4 HTM of order SE (3) to map points in WCS to CCS.

The Perspective-n-Point method (Bradski, 2000) is adopted to solve set of equations obtained from equation (5.2). For n-perspective points robot moves to different positions and these points are used for the implementation of this method. For robot-assisted camera calibration, suitable number of perspective points (p_r) in RCS are collected with the value of the corresponding pixel coordinates (p_i). The HTM ${}^{W}T_R$ is already known that map a point in RCS to WCS. The intrinsic camera parameters are constant and remain unaltered with the change in camera position. The standard checker-board method (Zhang, 2000) is used to determine the intrinsic camera parameters matrix *K*. Therefore, the only unknown matrix is ${}^{C}T_W$. The computed values (p_i and p_w) are plugged in equation (5.2) and the matrix ${}^{C}T_W$ is obtained.

It is pertinent to mention here that the extrinsic parameter obtained from checkerboard method provides information related to WCS with ICS. Where WCS is defined over the upper left most point of the checkerboard. However, the relation between this WCS and RCS is unknown, and it is not possible to find the relation between ICS and TCS. Therefore, the above discussed camera calibration method is proposed. The proposed camera calibration method eliminates any specific reference requirement such as checkerboard to obtain extrinsic parameters. In general, recalibration is required when the position of the camera or the WCS changes. Whereas the change of pose in gripper will not require recalibration and the change can be accommodated by providing the information related to translation and rotation of TCP as feedback from the robot.

5.3.2 Robot-vision approach to identify the properties of the object

The camera used for sensing is mounted outside the robot workspace whose field of view covers the complete robot-object system. To avoid any motion blur, the camera is mounted at an appropriate height to get an inclined view of the object plane. The image processing steps are implemented in Python (Van Rossum and Drake Jr, 1995) using openCV3 package (Bradski, 2000) for measurement of vibration in object. The steps followed for image processing are presented in Figure 5.7.

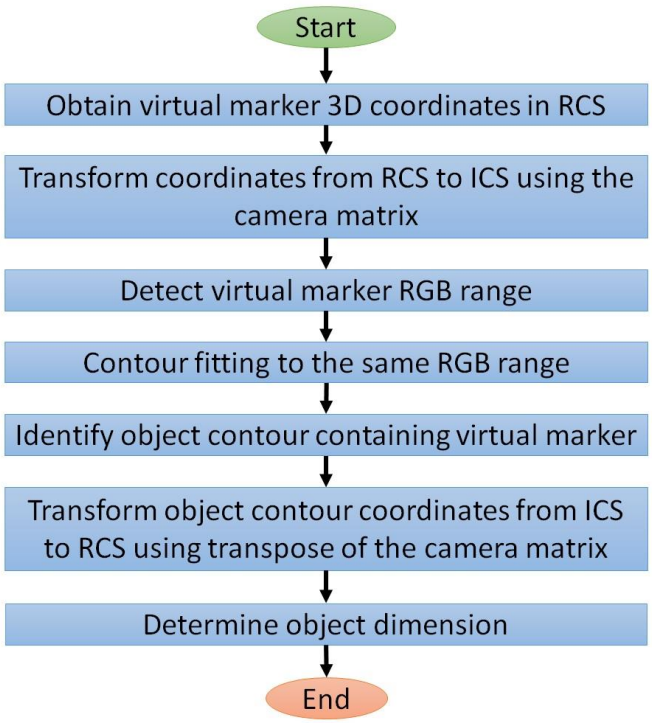

Figure 5.7 Image processing steps to identify and determine the dimension of an object.

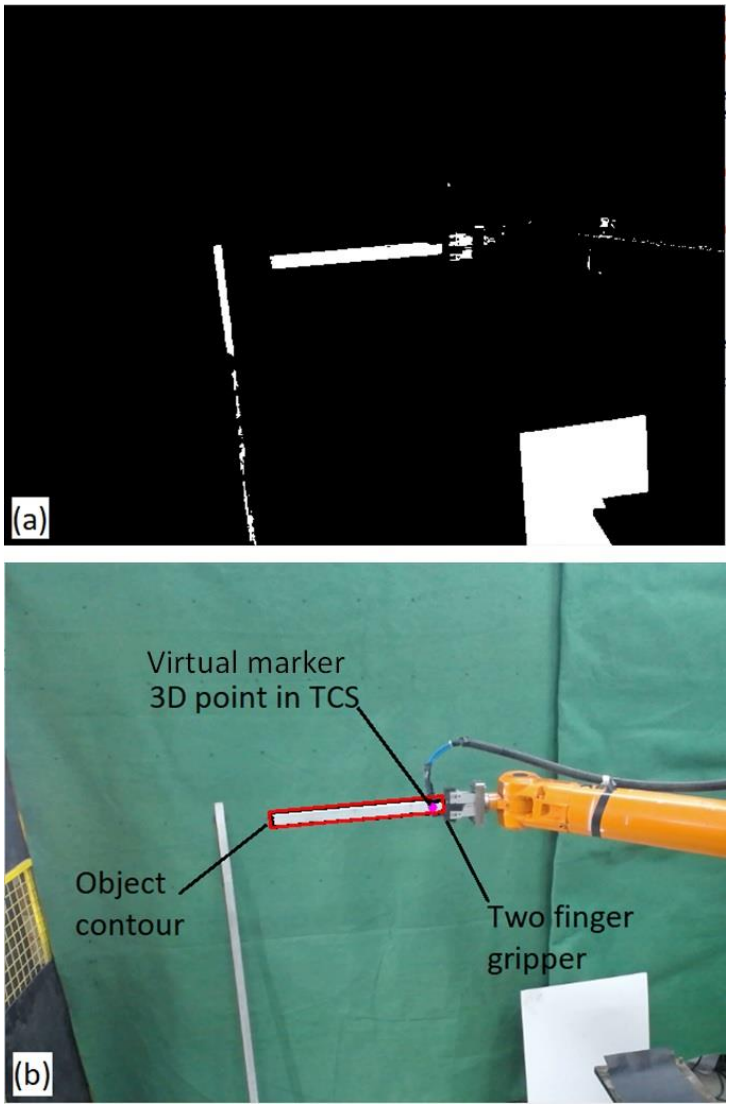

Figure 5.8 Important steps for the image processing (a) binary image after mask operator, (b) detection of the object and fitting the contour.

Initially, the camera captures a Red-Green-Blue (RGB) image of the object. In addition, a virtual marker for a 3D point in RCS is defined, which is same as the middle point of the two fingers gripper shown in Figure 5.8. The RGB value of this virtual point is same as the RGB value of the object grasped. Based on the value, RGB range can be defined by the user. A threshold mask needs to be created based on the RGB range that converts the RGB image to a binary image shown in Figure 5.8(a). For object identification, the pixel values of the determined RGB range of the object are changed to white and the remaining to the black background. There might be some other region within the RGB range that may appear too in the scene which are considered as noise. The contours are fitted on these regions using the 'findContours' operator available in openCV3.

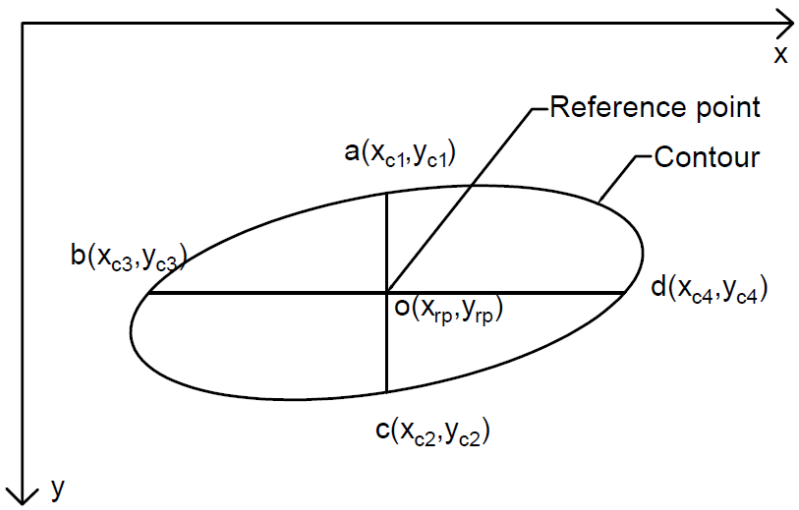

Figure 5.9 Object contour selection using reference point.

To select the contour of the object, a method is developed which eliminates the noise in the image. In this regard, a contour of the object in an image frame is shown in Figure 5.9. The reference point (x_{rp}, y_{rp}) must be located within the object contour which is the coordinates of the virtual marker. Therefore, two lines parallel to the x and y-axis of ICS, are drawn which intersects at the reference point. The coordinates of these intersecting lines lying on the contour are shown in Figure 5.9. For the reference point to be a part of the contour, two conditions must be satisfied considering the coordinates of the reference point and the intersecting points on the contour. These conditions can be stated as:

$$y_{c1} \leq y_{rp} \leq y_{c2} \tag{5.3}$$

$$x_{c3} \leq x_{rp} \leq x_{c4} \tag{5.4}$$

Hence, the reference point must satisfy above equations (5.3)-(5.4), to identify the current contour of the object. Thus, the contour of the object is drawn on the RGB image shown in Figure 5.8(b). The coordinates of this contour are transformed back to RCS and dimensions of the object are determined in SI units (mm). The above method identifies the object grasped by the gripper. In the same way, the orientation of the object can be changed for the measurement of other dimensions of the object.

The major advantages of the proposed robot-vision method to obtain the dimensions of the object are following:

(i) Eliminates the need of any physical reference to detect the object.

(ii) Accommodates the change in perspective view of the object even in deformed state by using feedback related to orientation and position of the robot end effector. Therefore, the need of any specific arrangement for the object vibration plane with respect to image plane is eliminated.

5.3.3 FEM modelling of the flexible object

The flexible object under consideration is shown in Figure 5.10. This object is treated as a cantilever beam with moving support that has a uniform cross-section. The base of the object is rigidly grasped by the gripper which is assumed as a fixed support and translation of gripper takes place in the vertical Y direction of X-Y plane. The deflection of the free end of the flexible object is observed in the same plane. To model the time evolution behaviour of the flexible object the dynamic model of the same is developed treating this as a flexible cantilever beam. Therefore Euler-Bernoulli beam theory (Rao, 2007) is applied in place of other theories i.e. Rayleigh and Timoshenko, due to negligible effect of rotary inertia and shear on the flexible beam. The flexible beam is a continuous system and the dynamic model using Euler-Bernoulli theory is discussed below.

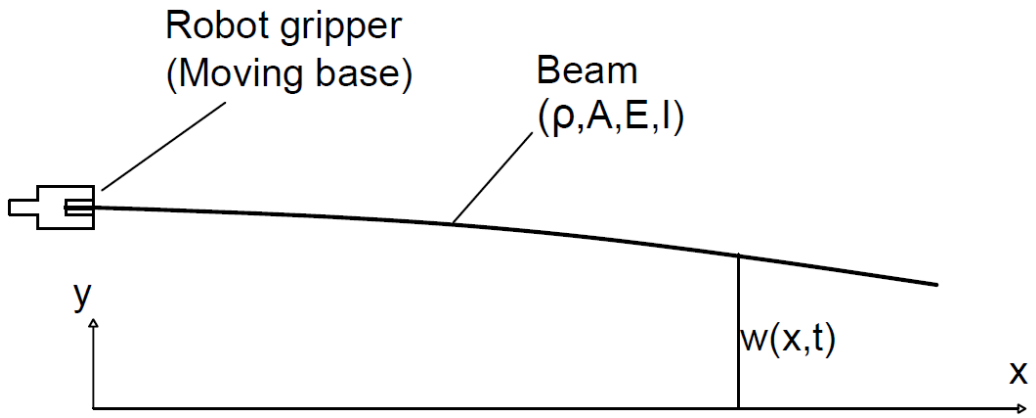

Figure 5.10 Cantilever beam with a moving base

For the continuous model of the flexible beam, *l* is the length, *b* is the width, *h* is the height of the beam, *A* is the cross-sectional area, *m* is the total mass, *I* is the moment of inertia of the beam, ρ is the density and *E* is Young's modulus. In this scenario, let $f(x,t)$ represent the force acting on the beam, and $w(x,t)$ is the deflection of the beam at time *t*. The derivation of the FEM based model is available in Appendix D and the obtained reduced-order model of the flexible is represented as

$$[m]\ddot{\vec{q}}(t) + [k]\vec{q}(t) = \{\vec{f}\} \tag{5.5}$$

$$[m] = \frac{\rho Al}{420}\begin{bmatrix} 156 & 22l & 54 & -13l \\ 22l & 4l^2 & 13l & -3l^2 \\ 54 & 13l & 156 & -22l \\ -13l & -3l^2 & -22l & 4l^2 \end{bmatrix} \tag{5.6}$$

$$[k] = \frac{EI}{l^3}\begin{bmatrix} 12 & 6l & -12 & 6l \\ 6l & 4l^2 & -6l & 2l^2 \\ -12 & -6l & 12 & -6l \\ 6l & 2l^2 & -6l & 4l^2 \end{bmatrix} \tag{5.7}$$

Where, $[m]$ and $[k]$ are mass and stiffness matrices. In real application, every beam will have some damping characteristics. Thus, viscous damping is introduced in the dynamic model of the flexible beam system shown in equation (5.8),

$$[m]\ddot{\vec{q}}(t) + [c]\dot{\vec{q}}(t) + [k]\vec{q}(t) = \{\vec{f}\} \tag{5.8}$$

where $\{\vec{f}\}$ is force vector $[F_1\ M_1\ F_2\ M_2]^T$ and $[c]$ is diagonal damping matrix obtained by implementing Rayleigh damping, which is defined by equation (5.9)

$$c = a_0[m] + a_1[k] \tag{5.9}$$

where a_0 and a_1 are the Rayleigh damping coefficients.

The nodal linear displacements are represented as ($q_1(t) = v_1$ and $q_3(t) = v_2$) and nodal angular displacement are ($q_2(t) = \theta_1$ and $q_4(t) = \theta_2$) under the application of force and moment at the node. In the practical implementation the nodal displacements $q_1(t)$ and $q_2(t)$ of the first element represent the linear and angular displacements of the base of the beam grasped by the robot gripper. Likewise, the nodal displacements $q_3(t)$ and $q_4(t)$ of the last element of the beam represent the displacements at the free end of the beam.

The robot provides motion to the base of the flexible beam. This results in force and moment applied to the first node of the first element which is responsible for vibration in the beam. These vibrations are controlled by applying the force and the moment to the base of the beam to suppress the vibration. The two controlling elements can be applied one at a time or both at the same time. In the proposed method both the elements force and moment have been tested one by one only. The controlling force (F_1) and moment (M_1) acts as the input. This force and moment are provided by executing control trajectories determined by the second stage controller discussed in subsection 3.4.

5.3.4 Design of predictive maximum error based second stage controller

A cantilever beam deflects transversely due to self-weight, while the ideal beam position is assumed to be horizontal. The static deflection observed at the tip of beam is considered as the set-point. The other deflections are caused due to vibration of the beam and comparison of the same with the static deflection is treated as an error. In this case the vibration due to the motion of the beam dies out naturally by consuming precious manufacturing time which is attributed to beam parameters that influence damping. Therefore, a control strategy is needed to reduce the suppression time drastically and make it compatible with the available internal controller of robot system.

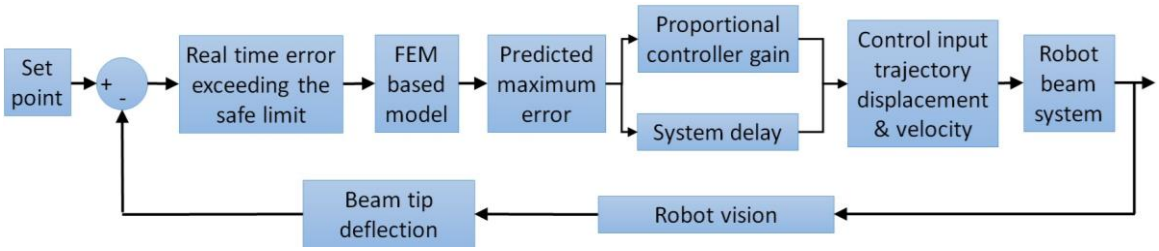

Figure 5.11 Proposed PMEB second stage controller.

In this section PMEB residual vibration suppression control strategy is presented, which is a second-stage controller for the robot beam system shown in Figure 5.11. The vibration of the tip is captured by the robot-vision system and the response in the form of tip deflection of the beam is sent as the feedback signal. This is compared with the set point to determine the real time error. If the real time error is higher than the limit set by the designer, then the controller gets activated. This strategy monitors the vibration amplitude of the beam continuously, but control actions are decided based on the maximum error. In this case the FEM based model uses the current state of the beam obtained from the robot-vision system, to compute the predicted maximum error of the vibration. For computation of the maximum error, the set point value and the extreme position of the vibration amplitude are used. The PMEB controller determines the control input trajectory based on the predicted maximum error. However, the time to complete the trajectory needs information related to the system delay, which is discussed in subsection 5.3.4.2. This information acts as input signal to the robot beam system for suppression of vibration.

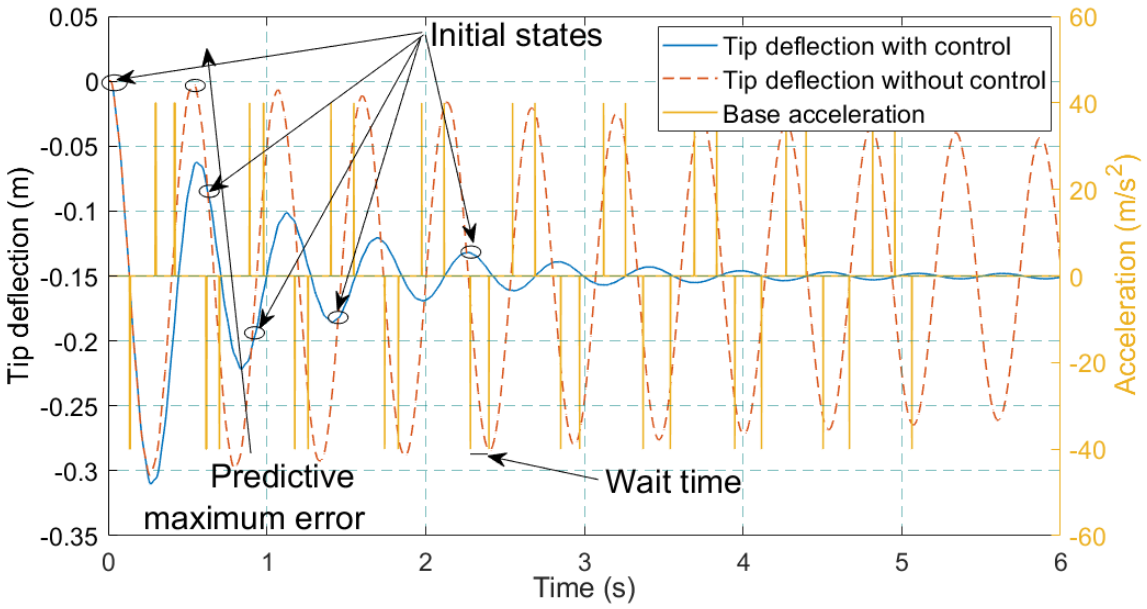

Figure 5.12 Illustrative example of PMEB second stage control strategy.

The Figure 5.12 shows the simulation response of the beam tip with control and the response without control, in addition to the base acceleration profile of the robot gripper. The response is obtained using the simulation model of the PMEB controller described in section 5.4.1. The Figure 5.12 is used to explain the working strategy of the proposed controller. Initially, the beam is assumed to be horizontal at rest with no tip deflection. When the beam is released, the tip tends to vibrate due to self-weight. The controller determines the maximum tip deflection using the FEM based model of the flexible beam considering the current state as the initial state for the model. At this stage, the controller has the information related to the forthcoming predicted maximum tip deflection which is compared with the static beam tip deflection to determine the error in deflection. The controller based on the predictive maximum error determines the displacement and velocity of the trajectory to be executed by the industrial robot controller.

Before the execution of control trajectory, various delay in the real system is handled innovatively. These delays are time for image processing, time to compute the maximum error using FEM model, and inherent delay present in the robot system. The proposed second stage control strategy has following important steps: (i) Determination of predictive maximum error using the FEM based model, (ii) Design of the input control trajectory, and (iii) Computation of delays before execution of the trajectory. These steps are described in the following subsections.

5.3.4.1 Approach to predict the maximum error

The mathematical model used for the prediction of maximum deflection of the tip is expressed in equation (5.8) and its state-space form is:

$$\begin{bmatrix} m & 0 \\ 0 & I \end{bmatrix} \begin{bmatrix} \ddot{\vec{q}} \\ \dot{\vec{q}} \end{bmatrix} + \begin{bmatrix} c & k \\ -I & 0 \end{bmatrix} \begin{bmatrix} \dot{\vec{q}} \\ \vec{q} \end{bmatrix} = \begin{bmatrix} \vec{f} \\ 0 \end{bmatrix} \tag{5.10}$$

In matrix vector form the above equation become

$$[A]\dot{\Delta} + [B]\Delta = \vec{F} \tag{5.11}$$

Where,

$$[A] = \begin{bmatrix} m & 0 \\ 0 & I \end{bmatrix}, \quad [B] = \begin{bmatrix} c & k \\ -I & 0 \end{bmatrix}, \quad \Delta = \begin{bmatrix} \dot{q} \\ q \end{bmatrix}, and \quad \dot{\Delta} = \begin{bmatrix} \ddot{q} \\ \dot{q} \end{bmatrix}$$

The equation (5.11) can be written as

$$\dot{\Delta} = [A]^{-1}.\left(\vec{F} - [B]\Delta\right) \tag{5.12}$$

Equation (5.12) represents a first-order differential system that can be discretised using following explicit numerical integration technique:

$$\Delta_{t+1} = \Delta_t + \delta t.[A]^{-1}.\left(\vec{F} - [B]\Delta_t\right) \tag{5.13}$$

The Δ_t is a column matrix that contains the velocity $(\dot{q}_t)$ and deflection (q_t) of the tip of the beam. The $\Delta(0)$ is the initial condition. At time t = 0, the velocity and deflection measured by the robot-vision system is plugged into the state space equation and the model computes the velocity and deflection for the next time step. This integration process will continue until a change in direction of the velocity is observed that in turn helps in determination of maximum deflection.

Let q_m is the predicted maximum deflection of the tip of the beam, and q_{sp} is the set point obtained from the static deflection of the tip of the beam. The difference between q_m and q_{sp} is the predicted maximum error $e(t)$ shown in equation (5.14)

$$e(t) = q_m - q_{sp} \tag{5.14}$$

This $e(t)$ is used in the control law of the PMEB controller to obtain the control trajectory which is described in the next subsection.

5.3.4.2 Approach to determine the straight motion trajectory

The proposed second stage controller is based on a well-accepted discrete PID controller. The control law, similar as discussed in the previous chapters, is the proportional controller expressed in equation (5.15)

$$u(t) = K_P e(t) \tag{5.15}$$

where K_P is the proportional control parameter, and the $u(t)$ is the control input signal. Here $u(t)$ is determined in the form of trajectory displacement and velocity explicitly and acceleration of the trajectory implicitly. The acceleration causes the force at the base of the beam which becomes the input to the FEM model of the flexible beam given in equation (5.13). The straight trajectory applies only the force to the base of the beam due to straight inline robot arm motion. To determine the input trajectory of the robot, two parameters are required, and these are displacement and velocity. These parameters are dependent on maximum error and the various types of delays present in the system. The important concept behind vibration of flexible beams is the conversion of strain energy to kinetic energy and vice versa. Therefore, the input trajectory to the robot must reduce the strain energy and in turn have less kinetic energy for vibration of the beam. This can be achieved if the robot gripper is moved in the same direction as the tip of the beam.

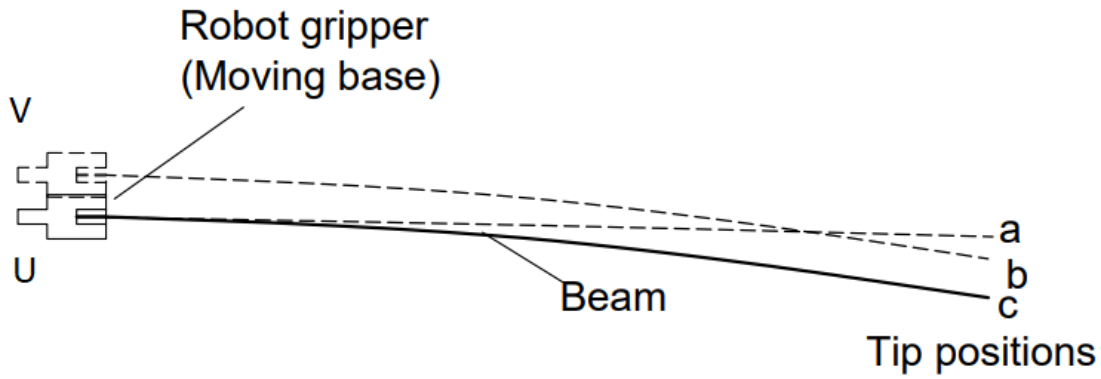

Figure 5.13 Straight motion trajectory of robot end-effector and beam tip positions

The beam shown in Figure 5.13 is in motion and let 'U' be the position at any instant with the tip shown as '*c*'. The vibration in the beam deflects the tip away which can be computed from FEM based model of the flexible beam. Assuming that the predicted extreme position of the tip of the beam is '*a*', where the beam gains the maximum strain energy. The controller determines the control input trajectory displacement based on the error that is 'UV' with a velocity to be traced by the robot gripper. Therefore, the trajectory

should be executed only when the tip of the beam is on the same side i.e., the current position of the tip with respect to the set point. In ideal conditions, the tip deflection is expected to be same as the stable tip position after execution of input trajectory. The intent behind execution of input trajectory is to reduce the tip deflection. Thus, the tip of the beam will not deflect to the predicted maximum deflection after control signal is fed and it will always be smaller than predicted.

For ideal vibration suppression, it is assumed that the reduction in tip deflection is equal to the input displacement given to the robot gripper as input. This can only be possible if the following condition in equation (5.16) is satisfied.

$$D = \frac{e(t)}{2} \tag{5.16}$$

where D is the displacement of the control trajectory.

The second parameter for the input trajectory is the velocity, which will depend on the trajectory travel time and the system delay. Here, t_{mc}.is associated with the FEM-based computational model used to prediction of maximum error. The time between the initial conditions and execution of trajectory is denoted as wait time (t_w) shown in Figure 5.12. This time duration is determined using the following equation (5.17):

$$t_w = t_{sd} + t_r \tag{5.17}$$

where t_r is rest time and t_{sd} is system delay. The expression of the t_{sd} is given in equation (4.9).

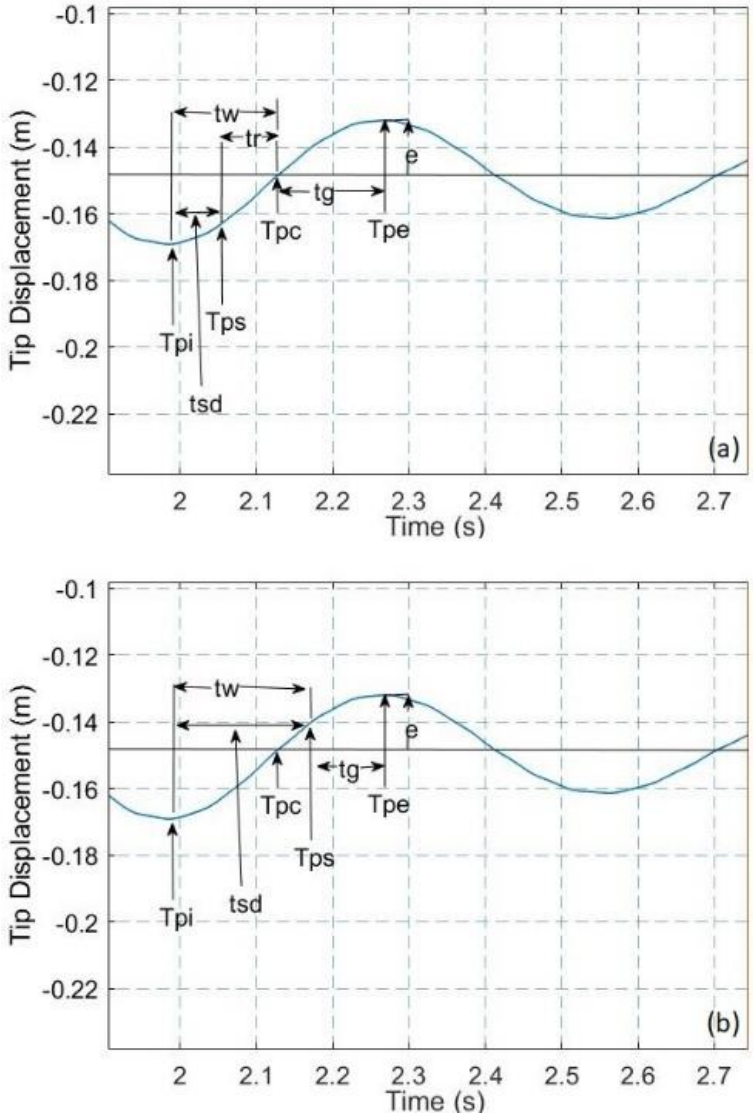

Figure 5.14 Trajectory displacement and velocity due to system delay for (a) $T_{ps} \leq T_{pc}$ and (b) $T_{ps} > T_{pc}$

Figure 5.14 explains how the system delay affect the displacement and velocity of trajectory. In the above figure,

- The T_{pi} is the time point where the controller detects the initial condition to predict the maximum error 'e'.
- The T_{pc} is the reference time point where the robot can initiate control action i.e. trajectory to suppress the vibration in response to predicted maximum error.
- The T_{ps} is the time point where the controller is ready with the computed wrist trajectory based on the predicted maximum error and
- The T_{pe} is the time point when the tip will reach the tip position without control.

The velocity of the trajectory is determined using the trajectory travel time (t_g) obtained from equations (5.18) and (5.19) for computation of velocity. The visual representation of these equations is presented in Figure 5.14, which demonstrates how the system delay affect the input trajectory parameters. Three conditions might arise during the vibration of different beams with different material properties.

$$\left.\begin{matrix} t_g = t_e - t_c \\ D = \dfrac{e}{2} \end{matrix}\right\} T_{ps} \leq T_{pc} \tag{5.18}$$

$$\left.\begin{matrix} t_g = t_e - t_{sd} \\ D = \dfrac{e - B_p}{2} \end{matrix}\right\} T_{ps} > T_{pc} \tag{5.19}$$

The equation (5.18) represents the condition where $T_{ps} \leq T_{pc}$ and D is the displacement. If the condition is $T_{ps} > T_{pc}$ the trajectory travel time (t_g) becomes shorter and the displacement (D) is presented in equation (5.19), where B_p is the current position of the tip. The third condition arise when $T_{ps} > T_{pe}$, in such a scenario the controller skips this maximum error and computes the angular displacement again for the subsequent prediction of maximum error.

5.3.4.3 Approach to determine the wrist motion trajectory.

The control law used for wrist motion trajectory is expressed as:

$$u(t) = 180 * K_P \frac{e(t)}{\pi l} \tag{5.20}$$

where $e(t)$ is the predicted maximum error, which is converted into angular error (degrees) using the arc-length relationship. Based on the value of $u(t)$ the angular displacement and velocity of the trajectory will be determined taking into account of system delay.

The wrist motion of robot is specified in terms of roll, pitch, and yaw angles. In this case, the wrist trajectory is in the vertical plane and therefore control action is specified using pitch motion. There are two design parameters of pitch motion i.e., angular displacement and velocity. The important concept behind the vibration of flexible beam is the conversion of strain energy to kinetic energy and vice versa. Therefore, the controlled

wrist trajectory should be so designed that the robot must reduce the strain energy and have less kinetic energy available for vibration of the beam. This process can be achieved by rotating the base of the beam in the same direction as the tip of beam, which will reduce tip deflection.

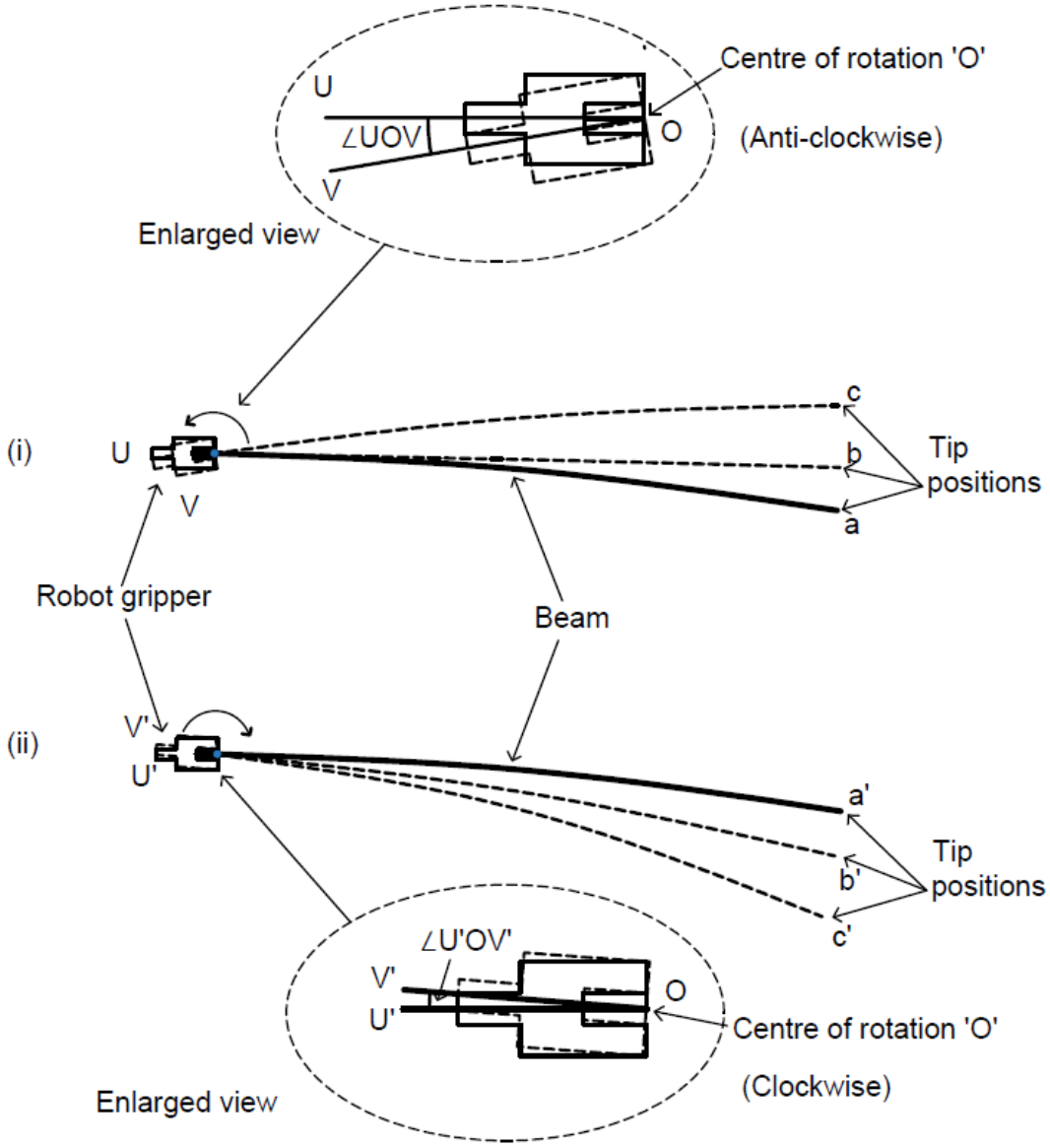

Figure 5.15 Robot angular control actions and beam tip positions

In Figure 5.15(i), the beam is grasped by the robot gripper at initial position ‘U’ and the deflected tip position of beam is at ‘a’ indicate the stable position. The vibration in the beam deflects the tip away from the stable position that is computed from the obtained model of the beam using system identification approach. Assuming that the predicted

extreme position of the beam is ‘c’, where the beam gains the maximum strain energy. The controller estimates the wrist trajectory i.e., angular displacement in degrees based on the error $\angle UOV$ with angular velocity to be used by the robot gripper. The trajectory should be executed only when the tip of the beam is on the same side as compared to the stable position to reduce the gain in strain energy and rotate the base of the beam. Ideally, the tip deflection should be same as the stable tip position at the end of the trajectory execution. In this case, the amplitude of the beam vibration reduces from the start of the trajectory execution. Consequently, the tip of the beam will not deflect to the predicted maximum error after control signal is communicated and it will always be smaller than the predicted value that is the position ‘b’. This is the case when beam tip direction is upward and wrist trajectory rotates the robot gripper about the center of rotation ‘O’ in anticlockwise direction. Similarly, the wrist motion in clockwise direction will deflect the tip in the downward direction and the control action is illustrated in Figure 5.15(ii).

It is expected that the input angular displacement signal should not be greater than the current angular error created by the beam tip, otherwise it will lead to increased tip amplitude which is undesirable. Therefore, it is assumed that the reduced tip amplitude is equal to the pitch angle of the robot gripper for vibration suppression. This can be ensured if the following condition specified in equation (5.21) is satisfied where $\theta_T(t)$ is pitch angle and $\theta_e\,(t)$ is the maximum angular error.

$$\theta_T(t) = \frac{\theta_e\,(t)}{2} \tag{5.21}$$

$$\theta_e\,(t) = 180 * \frac{e(t)}{\pi l} \tag{5.22}$$

The angular velocity parameter is decided based on the delays, similarly, as explained in section 5.3.4.2. The parameters used in equations (5.18) and (5.19) are changed accordingly. The angular velocity of the trajectory is determined using the trajectory travel time t_g obtained from equations (5.23) and. (5.24). The explanation presented in Figure 5.14, which demonstrates how the system delay is also applicable for the computation of angular displacement and angular velocity of wrist trajectory.

$$\left.\begin{aligned} t_g &= t_e - t_c \\ \theta_T &= \frac{\theta_e}{2} \end{aligned}\right\} T_{ps} \leq T_{pc} \tag{5.23}$$

$$\left.\begin{aligned} t_g &= t_e - t_{sd} \\ \theta_T &= \frac{\theta_e - \theta_{cp}}{2} \end{aligned}\right\} T_{ps} > T_{pc} \tag{5.24}$$

Where θ_{cp} is the current angular position of the tip. In this case, the angular displacement of the control trajectory is the pitch motion. These angles can be expressed in terms of quaternions which is a convenient mathematical notation to represent spatial orientation and rotation in 3D space. Therefore, the Euler angle is converted into the quaternions using Euler-quaternion relationship given in (Henderson, 1977). The above steps help the controller to handle the delay innovatively that uses low update rate camera for the robot vision system. Hence, it can be concluded that the present controller can handle the delays favourably for the assembly of flexible beam using robot.

5.4 Simulation and experimental implementation of second stage controller

In this section the simulation performance of the proposed PMEB second stage controller, and experimental implementation has been presented. The simulation and experiments have been carried out on two flexible beams with different lengths.

5.4.1 Simulation of PMEB second stage controller

Table 5.1 Parameters of flexible beams

Properties (Unit)	**Symbol**	**Beam1**	**Beam2**	**Beam3**
Material	-	Al	Al	SS
Length (m)	l	1.24	1.53	0.60
Height (m)	h	0.003	0.003	0.001
Width (m)	b	0.025	0.025	0.025
Density (kg.m^{-3})	ρ	2700	2700	8000
Moment of inertia (m^4)	I	5.625x10^{-11}	5.625x10^{-11}	20.83x10^{-11}
Young modulus (GPa)	E	69	69	195

To test the efficacy of the proposed controller beams made of Aluminium (Al) and Stainless Steel (SS) are considered and the parameters are listed in Table 5.1. These parameters are used for simulation of flexible beams using FEM based model and experimentation. The state space model of the flexible beam obtained using FEM method as provided in equation (5.13) is used to predict the maximum error.

Natural frequencies of the flexible beam with their mode shape vibration are provided in Table 5.2. These natural frequency values are obtained using the equation (5.25),

$$det\left[[k] - \omega^2[m]\right] = 0 \tag{5.25}$$

Table 5.2 Mode of flexible beam vibration and corresponding natural frequencies

	Natural frequency		
Mode of vibration	**Beam1**	**Beam2**	**Beam3**
1	1.59	1.04	2.21
2	9.98	6.55	13.88
3	27.96	18.36	38.88
4	54.83	36.02	76.25

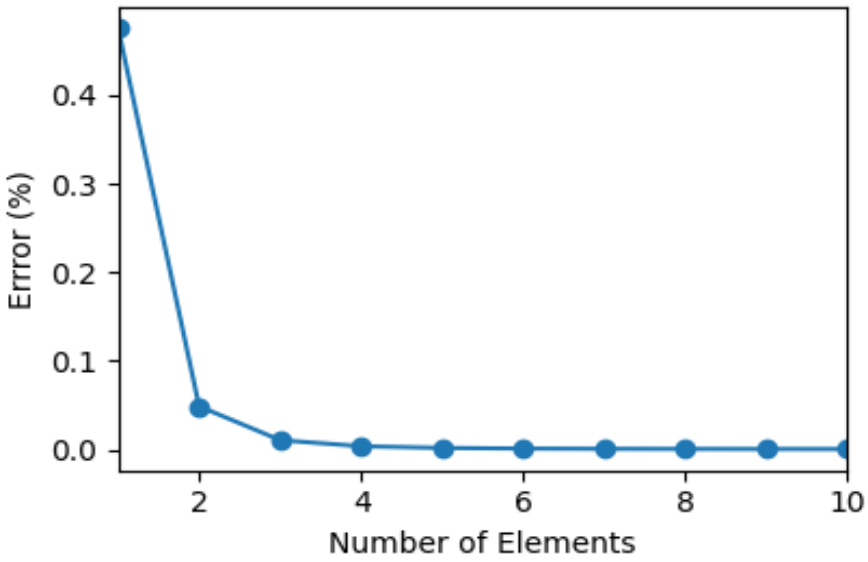

Figure 5.16 Percentage error against the number of elements of the flexible beam

The exact frequency of the cantilever beam system is obtained using $\left(\omega_n = (\beta_n l)^2 \sqrt{\frac{EI}{\rho A l^4}}\right)$ (Romaszko *et al.*, 2015) where $\beta_1 l = 1.875$ corresponding to first mode. The percentage error between the first mode frequency obtained from equation (5.25) and the exact first mode frequency against the number of elements is shown in Figure 5.16.

The proposed PMEB second stage controller was simulated to analyse the behaviour of the flexible beam. To perform simulation, Python IDLE program is used and the parameters available in Table 5.1 are used to imitate the behaviour of beam considered in the actual experiments. The Rayleigh damping coefficients discussed in equation (5.9)

were determined by comparing the free vibration response of the actual flexible beam with free vibration response using simulation. The damping coefficients are found to be a_0 = 0.08 and a_1 = 0.0002 for Beam1 and Beam2 whereas a_0 = 0.15 and a_1 = 0.0003 for Beam3 which are subsequently used in simulations as well as experiments.

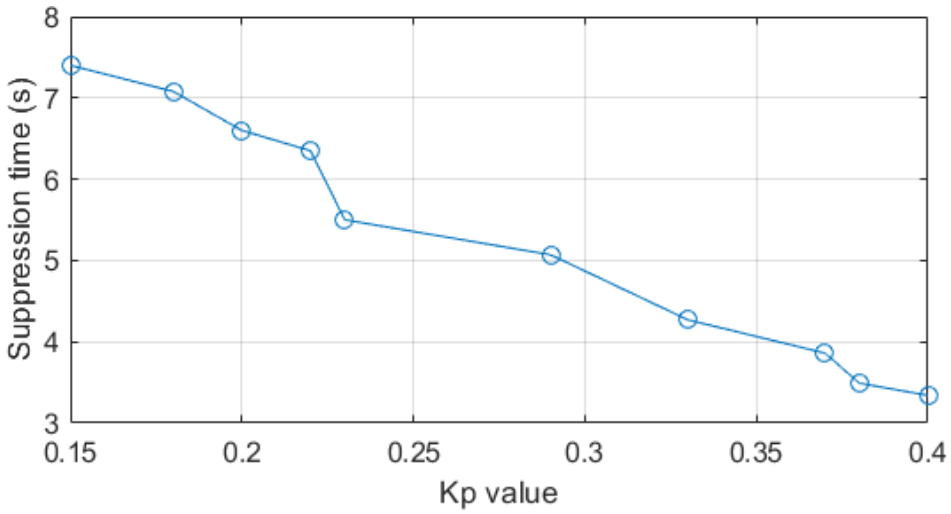

Figure 5.17 Comparison of vibration suppression time against K_p value

Based on the tuning of the control parameter gain, the controller behaviour can be categorized as slow, moderate and aggressive. The control structure of the proposed controller is a predictive type where a trajectory is determined depending on maximum error and this trajectory cannot be altered during vibration suppression. Thus, the controller gain K_p provides the relation between error with the trajectory displacement, based on the equation (5.18). This equation provides a limit on the gain value for the problem at hand. Therefore the simulated performance of the designed controller is tested by varying the K_p values. The simulated suppression time against different values of K_p are presented in Figure 5.17.

It can be observed that the suppression time decreases as the K_p value is increased gradually from 0.15 to 0.4. For K_p value greater than 0.4, the velocity profile fails to satisfy the constraint on acceleration obtained from LSPB. Some results with various K_p values are presented in Appendix **B**. It is well accepted in robotics community that the acceleration for any articulated industrial robot is limited to 5g (Kaneko *et al.*, 2003). Therefore, for a valid trapezoidal velocity profile based trajectory, constraints on the choice of acceleration during blend must be satisfied for a practical solution. Hence, the K_p value is selected as 0.4.

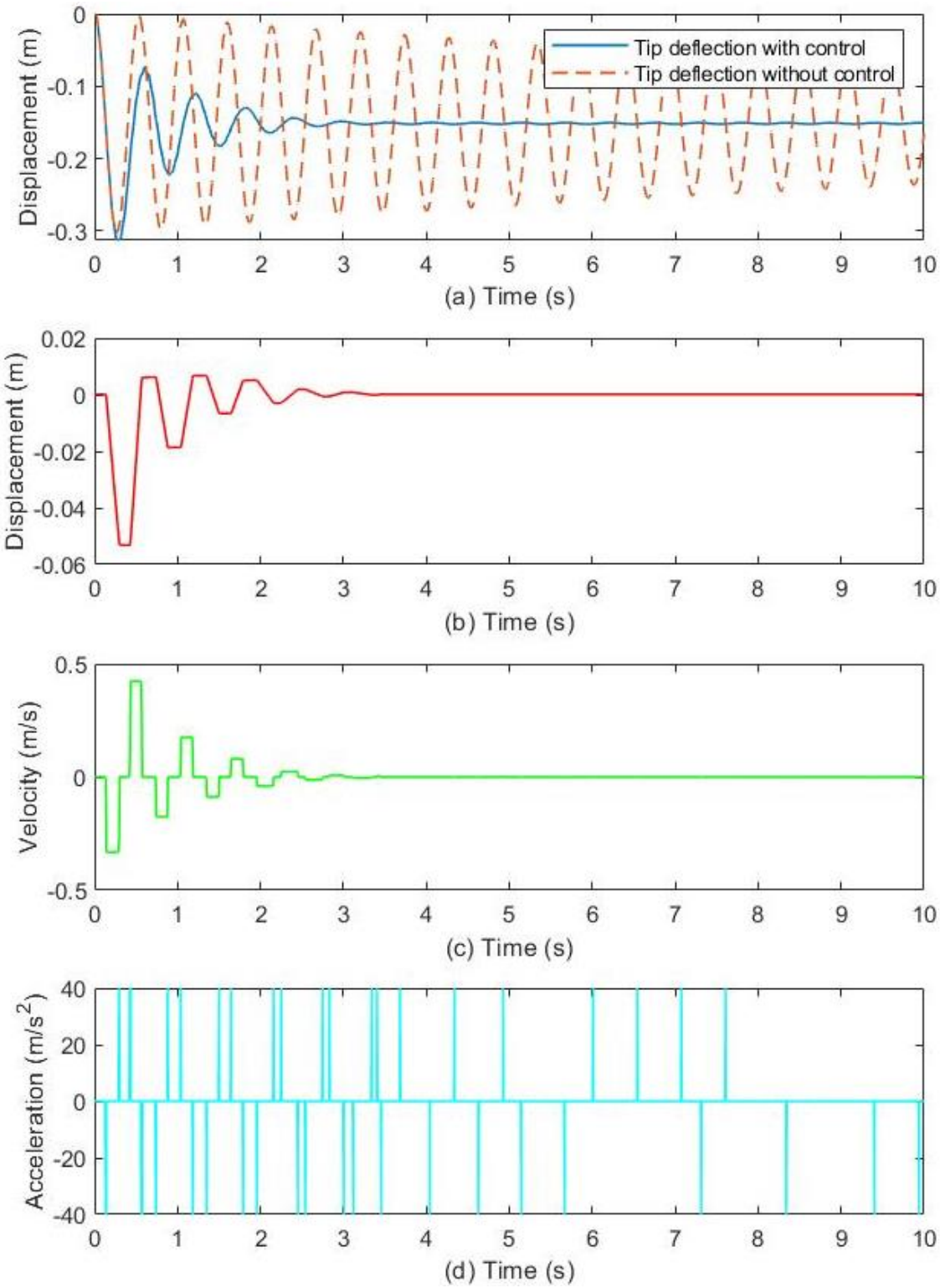

Figure 5.18 Simulated response of Beam1 (a) beam tip response with and without control, (b) displacement, (c) velocity, and (d) acceleration of the control trajectory at the base of the beam.

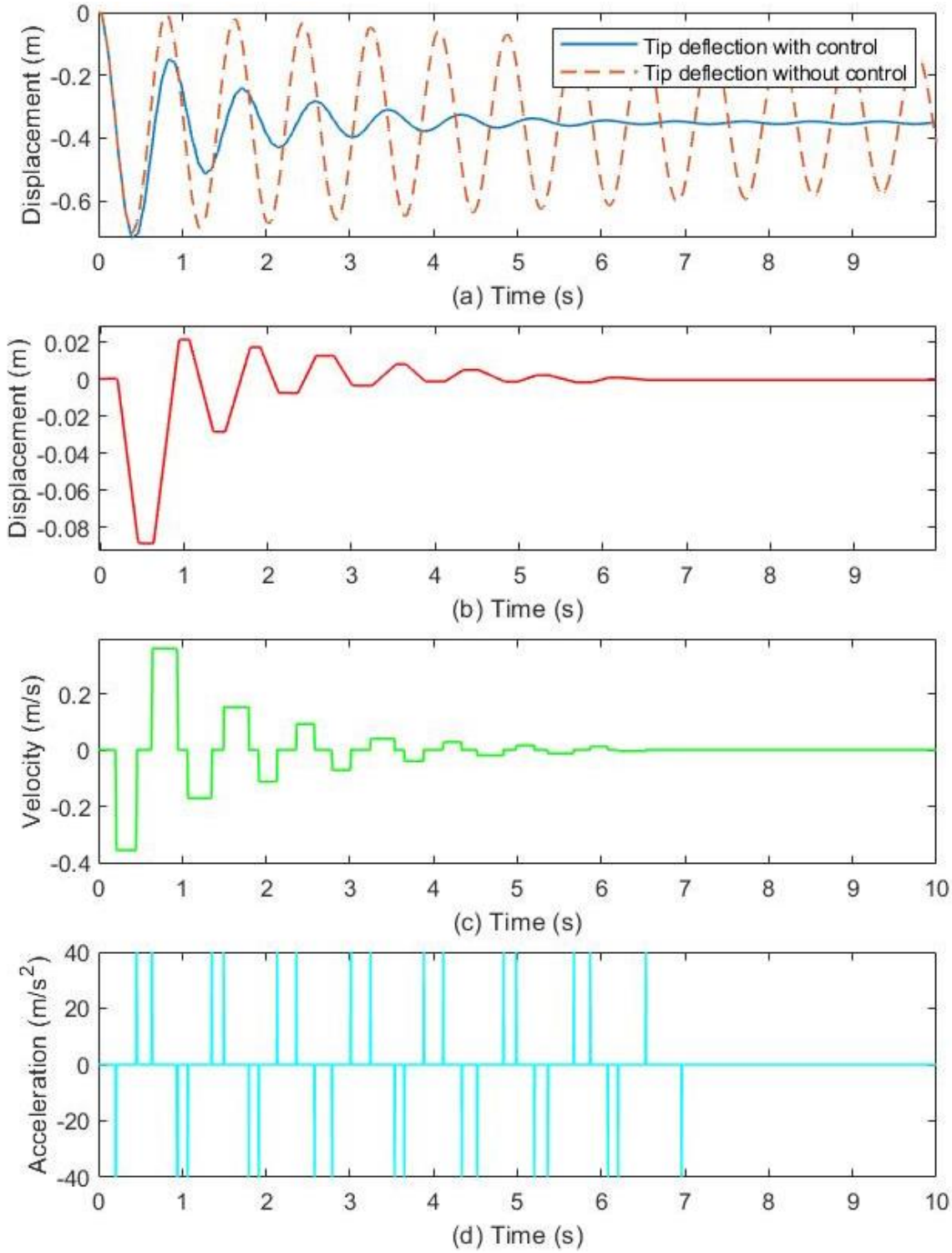

Figure 5.19 Simulated response of Beam2 (a) beam tip deflection with and without control, (b) displacement, (c) velocity, and (d) acceleration of the control trajectory at the base of the beam.

The simulation of Beam1 is shown in Figure 5.18. It is assumed that the beam is straight and horizontal with zero tip deflection and zero velocity initially. Such vibration in the

beam is possible if it is released suddenly from the straight horizontal position. In this case, the vibration in beam can be attributed to self weight. The tip response of Beam1 is shown with control and without control to compare the time required to suppress vibration. Along with these the trajectory profile of displacement, velocity and acceleration given to base of Beam1 is displayed. The movement given to the base of the beam is the control input trajectory that has to be executed by the robot gripper and these motions take place in the vertical plane. It can be observed that the tip vibration of Beam1 is suppressed within 3 s as compared to 55 s for without control scenario and the suppression time is reduced by 94.55%. It can be noticed that the base displacement of Beam1 has a zig-zag profile which indicates that the base returns to the desired position with a negligible offset. It is important to observe in Figure 5.18 that the controller is kept 'ON' for a very small error which forces the controller to compute the displacement and velocity of the trajectory even though the error is too small to observe. Thus the controller can be kept 'OFF' by specifying a user defined error limit. Such as in the simulation response of Beam2 is presented in the Figure 5.19 with the controller got kept 'OFF' after reaching the error limit. This error limit can be treated as safe limit. For effective functioning of this control system, the system delay value should be as small as possible.

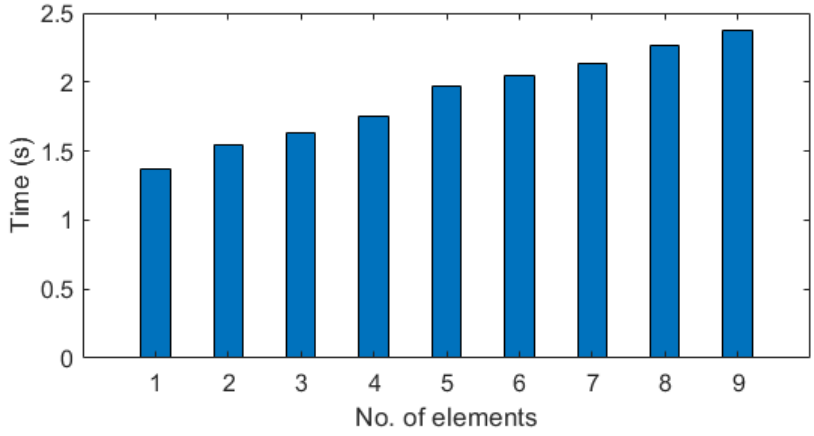

Figure 5.20 The processing time using FEM based model against the no. of elements.

In order to quantify the delay caused by the FEM based model processing time, against number of beam elements are simulated and the results are shown in Figure 5.20. In this figure, the time step value is selected as 0.0001 s for the dynamic analysis of the FEM model. However, increase in time step value i.e. 0.0002 s, generate high computational error with the increase in number of beam elements. In this case computational error of the order 0.5% is observed for the single beam element case and consumed 0.67 s to complete

the model processing time. Thus, the time step 0.0002 s is chosen for the dynamic analysis of robot vision flexible beam system.

5.4.2 Experimental setup details for implementation

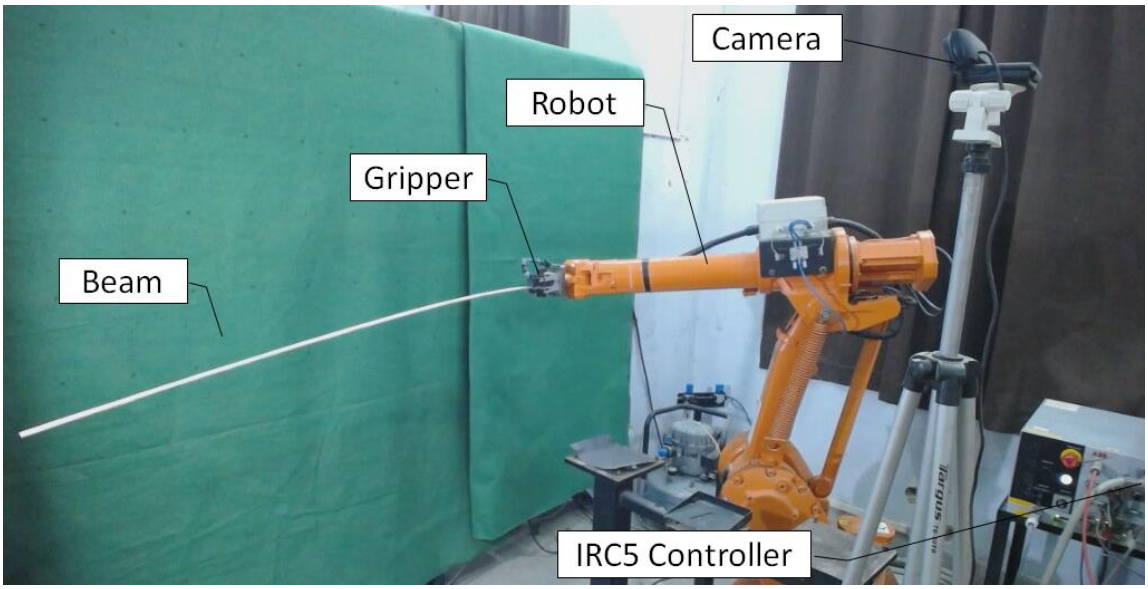

Figure 5.21 Experimental setup with camera, industrial robot, controller, gripper, and beam.

The details of experimental setup are same as in the previous chapter. However, for the beams, robot scenario is changed as shown in Figure 5.21, which consists of an industrial robot, industrial robot controller, color camera, a flexible metallic beam, a gripper, and a computer system.

5.4.3 Experimental implementation of second stage controller

To improve visibility of the tip, the sensor is mounted at some reasonable inclination to cover the width of the beam. This configuration enables the vision sensor to track the beam tip effectively. The inclination of the vision sensor cannot measure the exact dimension of the beam, therefore position and orientation of the beam in the 3D space are updated using the robot vision system. Therefore, a need for robot camera calibration arises and the important steps used are described in section 5.3.1.

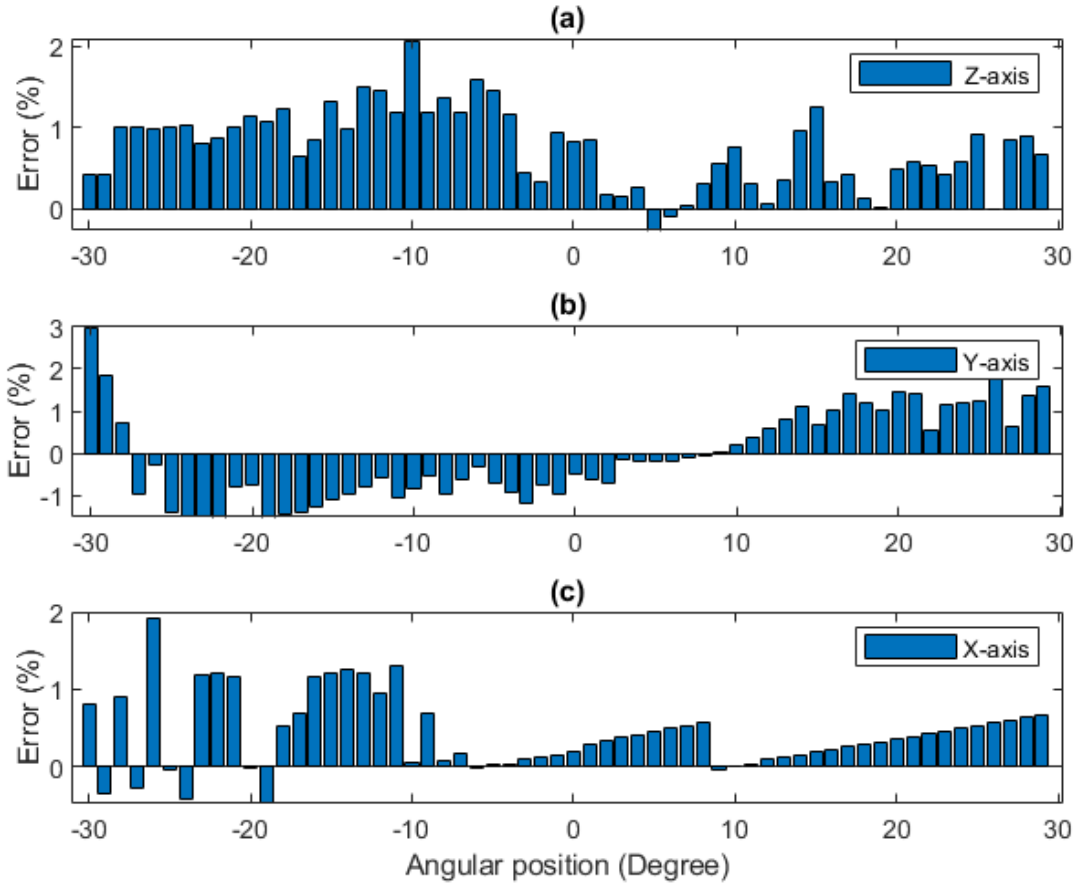

Figure 5.22 Percentage error in object dimension measurement against angular position of an object about (a) z-axis, (b) y-axis and (c) x-axis of WCS

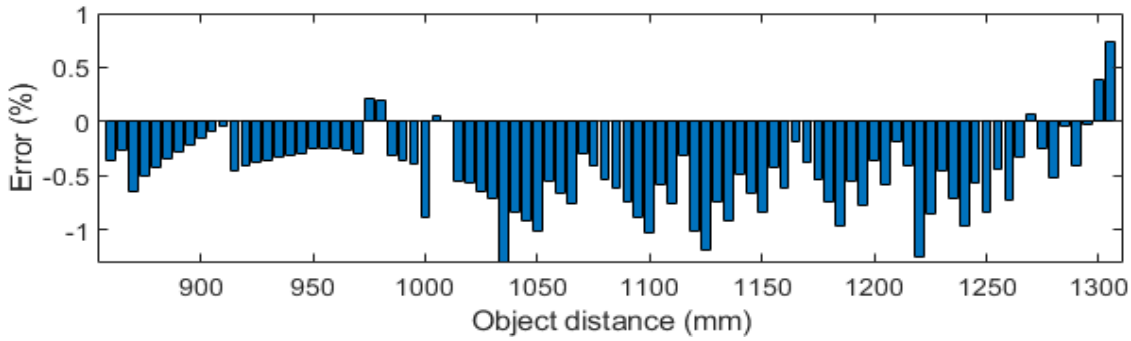

Figure 5.23 Percentage error in object dimension measurement against object position along the z-axis of WCS

In the present robot system, the coordinates of RCS in WCS are [1000, 1200, -640] in mm, with same orientation. Camera is calibrated with this configuration. The intrinsic and extrinsic camera parameter with standard error is presented in Table C.5.1 of Appendix **C**. The mean reprojection error is 0.3845 pixel. A hollow aluminium square tube with length 396 mm is selected to analyse the accuracy of the proposed robot-vision system for

measurement of object dimension in 3D space. The percentage error in measurement of the tube, at different angular positions expressed with respect to the x, y, and z-axis of the WCS are shown in Figure 5.22. Whereas the percentage error at different positions of the tube along the z-axis are shown in Figure 5.23. It can be observed that the maximum error percentage in measurement is within the acceptable range, i.e., 3%. The sources of error for these measurements can be attributed to errors in the determination of the camera matrix and the visible rear corner as well as the edges of the tube which become part of the image when the orientation of the object is changed.

Measurement of vibrations of the object i.e., flexible beam requires some more steps along with image processing. In this case, the extreme left point on the object contour is considered as the tip of the beam as shown in Figure 5.24 and the right most point of the contour is the base of the beam. These contour points of the object are valid if the beam is held horizontal. The image coordinates of the extreme left, and right, are converted to the WCS. Thus, the tip position in the WCS is compared with the base of the beam to compute the deflection.

To operate the second stage controller, the dimensions of the beam, the material properties, and user defined safety limit are necessary. The dimensions (l, b, h) and the material properties of the beam i.e., E and ρ are fed to the controller before the assembly operation. The overall behaviour of the proposed controller is shown in Figure 5.12. As per computed control signal, the robot gripper is moved in the vertical plane during the experiments. The excitation at the base of the beam will be impulse type as the trajectory chosen has a trapezoidal velocity profile.

5.4.4 Experimental results with straight motion trajectory

To validate the efficacy of the proposed controller, experiments are conducted. In the experiment, the robot was commanded to perform manipulation tasks at high speed, which induced vibration in the beam. In particular, the gripper of the robot moved the base of the beam from position ‘A’ to position ‘B’ and returned to ‘A’. This is a PtP excitation trajectory. The detail of the trajectories used for these experiments are provided in Table 5.3 which have different velocities.

The trajectory for this motion was considered as an excitation trajectory and treated as the impulse excitation to the base of the gripper. The response observed during excitation

trajectory was forced vibration, but after execution of the trajectory the beam showed free vibration response as no force was acting at the base. Therefore, the conditions to excite vibration in the beam during simulation and experiments were different. In the present experiment, the ABB made robot is capable of moving with predefined velocities, without any control over acceleration. Based on the simulation results, the velocity of the control input trajectories is observed to be around 200 mm/s. Therefore, the velocity of control input trajectories was chosen as 200 mm/s. The high velocity values were not chosen in this case because high acceleration would result in a higher mode of vibration in the beam. Similarly, the low velocity values were not chosen as it increases the vibration suppression time which is undesirable for the experiments.

Table 5.3 Details of excitation trajectories used in control by straight motion.

Trajectory	**Displacement (mm)**	**Velocity (mm/s)**
'Trajectory1'	50	300
'Trajectory2'	100	300
'Trajectory3'	50	500
'Trajectory4'	100	500

5.4.4.1 Results of Beam1

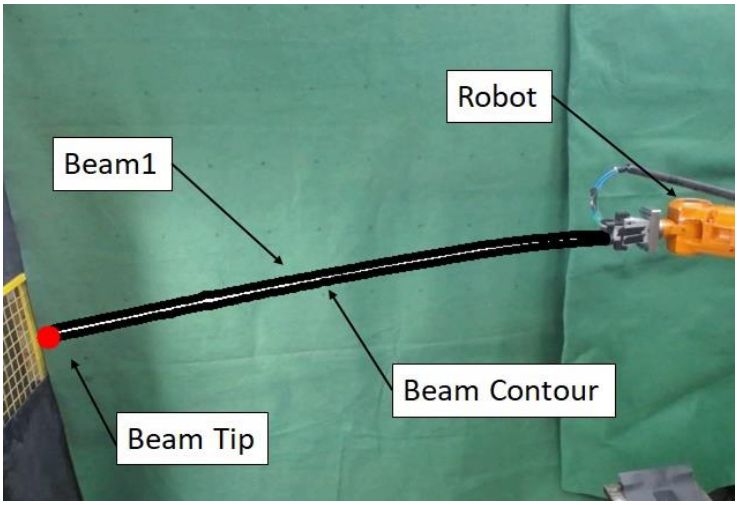

Figure 5.24 Identification of beam from captured image of Beam1 in experimental setup

The experimental setup for Beam1 is shown in Figure 5.24. Using the robot-vision system and image processing approach the Beam1 is detected from the captured image. The red circle shown in Figure 5.24, indicates the tip of the beam which is tracked throughout the experiment and the tip deflection is measured with respect to the base of the beam. The

length of Beam1 is 1280 mm out of which 40 mm of the length is grasped by the robot using a two-finger gripper. Therefore, the effective length of Beam1 is 1240 mm.

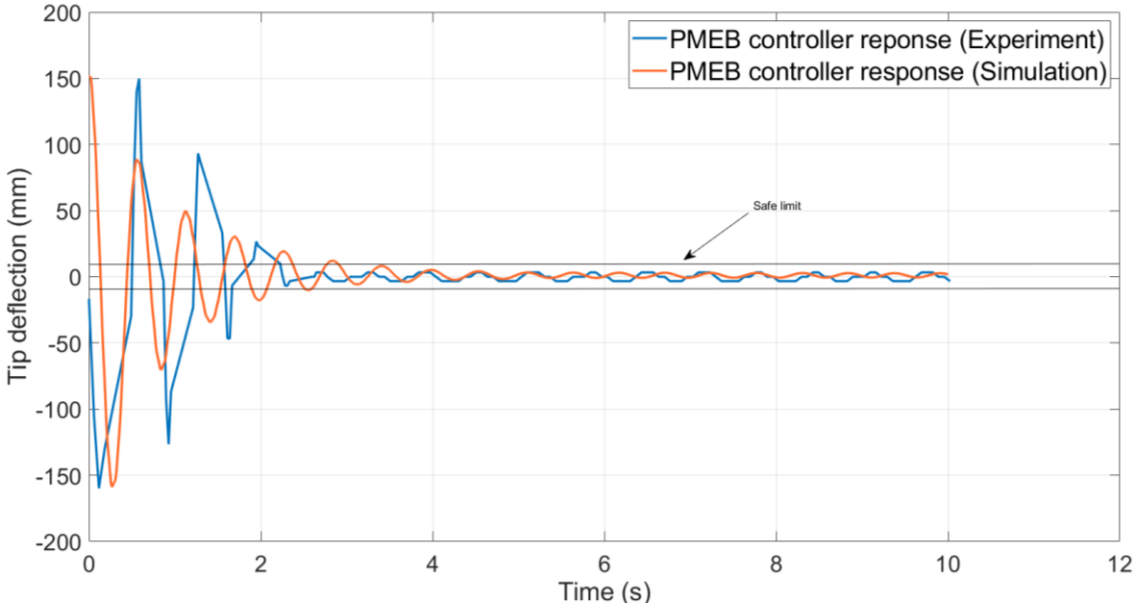

Figure 5.25 Experimental versus simulation result of the deflected beam

To compare the performance of the PMEB controller, the vibration responses from simulation and the experiments are presented in Figure 5.25. In this case, the free vibration response of Beam1 with horizontal position and zero initial velocity is simulated, whereas for the experiments Beam1 executed some trajectory to induce vibration. It was observed that the simulated response and experimental response are in good agreement.

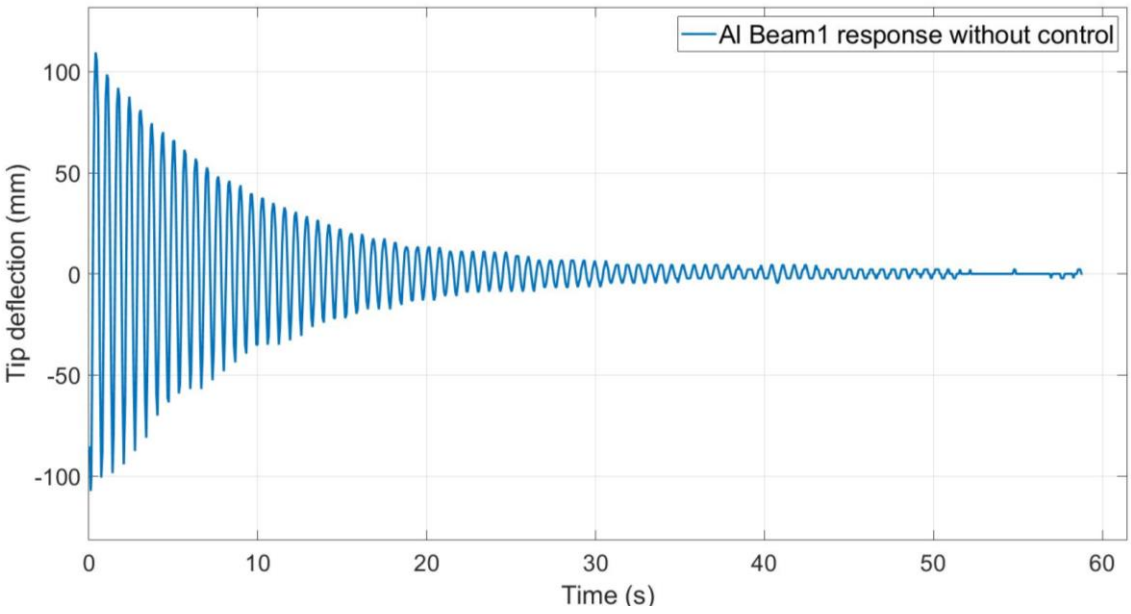

Figure 5.26 Free response of the Beam1

After providing the necessary motion ‘Trajectory1’, the free response of the Beam1 without any controller actions is presented in Figure 5.26. The initial tip amplitude is observed to be 109.5 mm and took more than 53 s to dampen the amplitude of the Beam1 within 3 mm range.

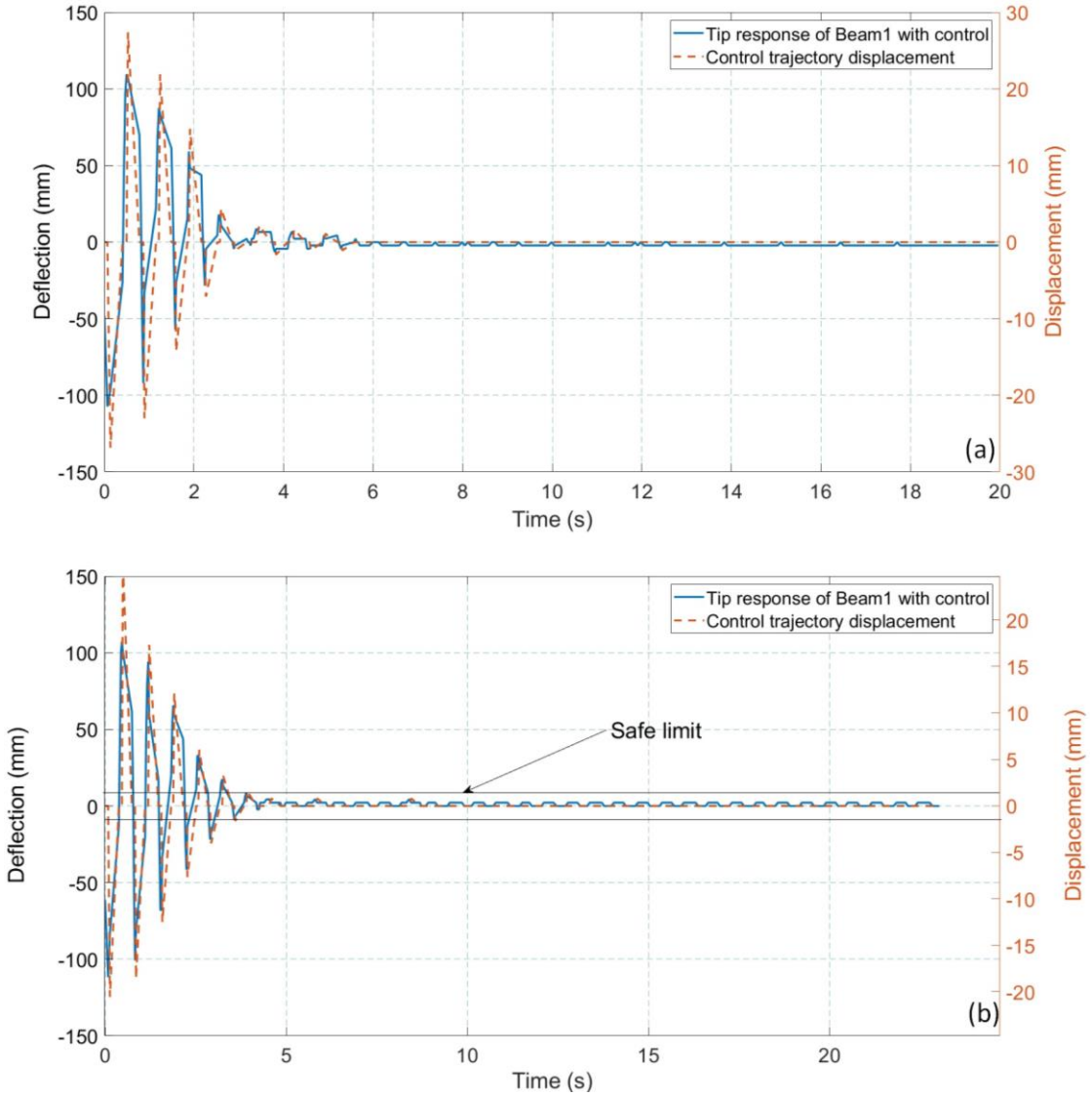

Figure 5.27 Response of Beam1 after robot arm control actions excited by (a) ‘Trajectory1’ and (b) ‘Trajectory2.’

For the control experiment, the robot is commanded to use ‘Trajectory1’ for manipulation before the assembly task, and the first response of Beam1 with control is presented in Figure 5.27 (a). With the excitation ‘Trajectory2’, the controller response is shown in Figure 5.27 (b) and the video of the controller response is recorded which can be seen using the link[1]. In these figures, the control input trajectory displacement and tip

[1] https://youtu.be/ryxYtJxDwBM - (Robot-vision based vibration suppression of Al Beam1)

deflection of beam are shown to demonstrate the performance of the second stage controller. The controller suppresses residual vibration in 3.9 s and the beam vibration is within the safe limit ±10 mm. For the assembly tasks, the Beam1 is inserted in a slot of size 50 mm × 20 mm. When the maximum tip deflection is suppressed to this limit, the controller is deactivated, and the beam is inserted into the slot[2]. The percentage reduction in suppression time with controller action is ~95%, and in the same time period the vibration amplitude is reduced by ~96%.

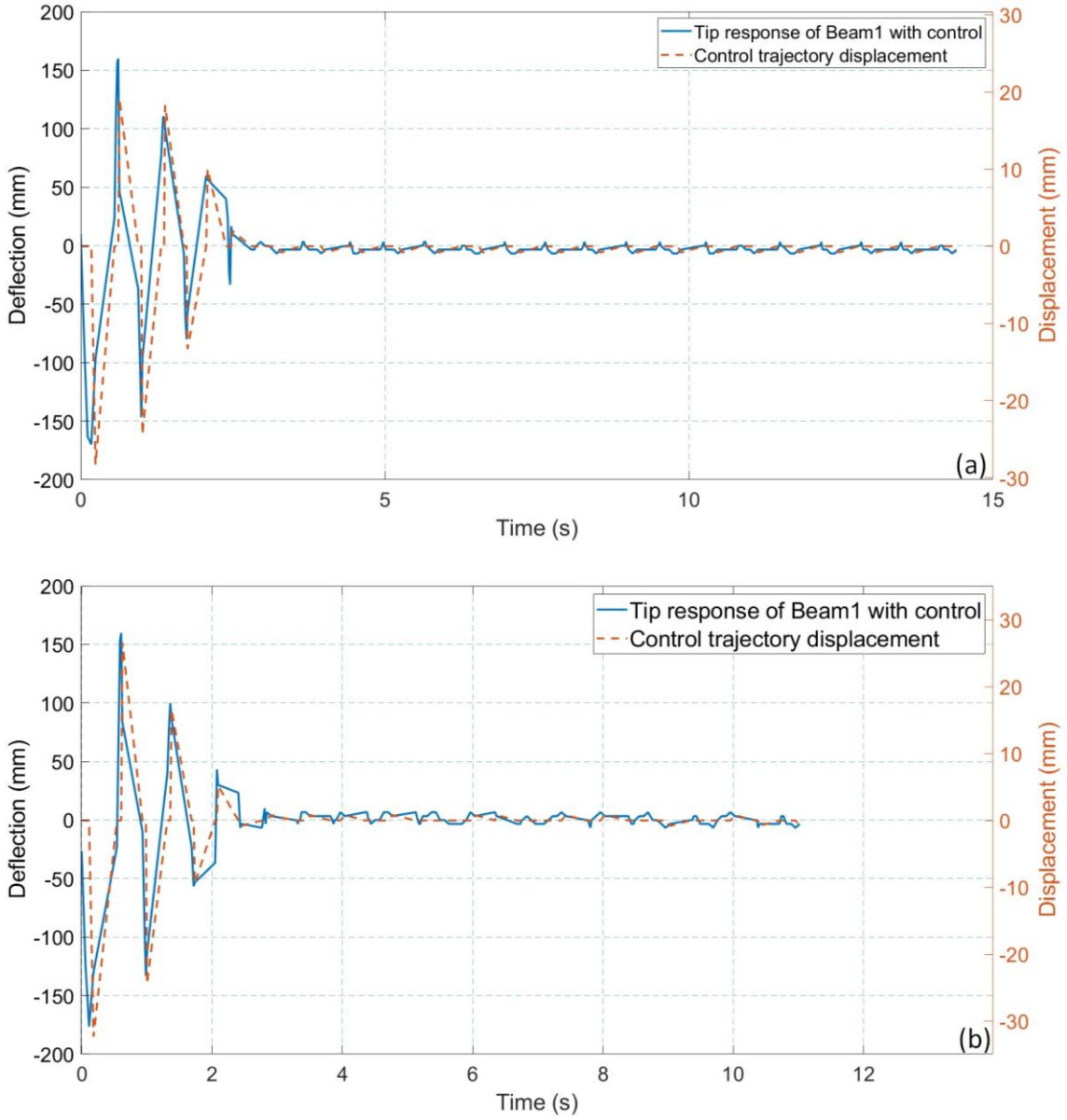

Figure 5.28 Response of Beam1 after robot arm control actions excited by (a) 'Trajectory3' and (b) 'Trajectory4.'

[2] https://youtu.be/-If3Ewkj8v8 – (Assembly of Beam1 into a slot)

The controller responses with excitation trajectories ‘Trajectory3’ is shown in Figure 5.28 (a). The increase in velocity of trajectories increases the tip deflection and is found to be 169.80 mm compared to the deflection caused by trajectories with reduced velocities. However, the controller could complete the suppress the vibration in less than 3 s. The increased initial tip deflection results in increased time for free vibration response and requires 61 s to dampen the vibration, without control. Whereas the implementation of controller reduced the tip deflection by ~97% and suppression time by ~96%. Similarly, the ‘Trajectory4’ deflected the beam tip by 159.7 mm and the time required to dampen the vibration is 60 s without any control. However, the reduction in tip deflection is achieved by more than 97% and suppression time reduced by more than 95%. These experiments have been performed multiple times and the average suppression time is observed to be 4.2 s with a standard deviation of 0.162 s to reduce the vibration amplitude to ~10 mm.

5.4.4.2 Results of Beam2

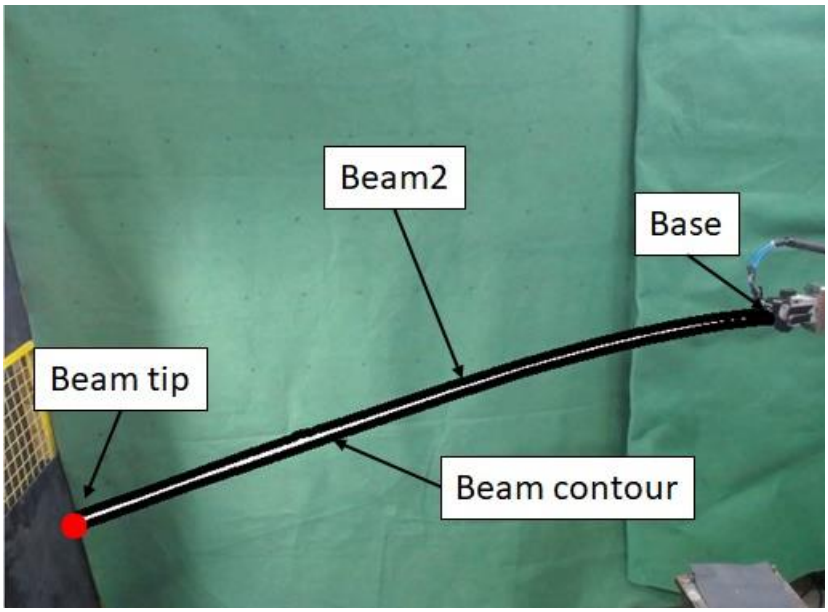

Figure 5.29 Identification of beam from captured image of Beam2 in experimental setup

In this experiment, the flexible beam of 1570 mm length is used of which 40 mm length is grasped by the robot gripper as shown in Figure 5.29. Therefore 1530 mm becomes the effective length of the Beam2. It can be observed that the camera captured the complete length of the long beam with a very small part of the robot gripper being visible in the scene. However, the captured image did not impact the controller performance, adversely. In this case controller input to the robot, in turn moved the robot arm to suppress the

vibration of the beam. The robot arm motion in essence caused movement of end-effector in straight line trajectory.

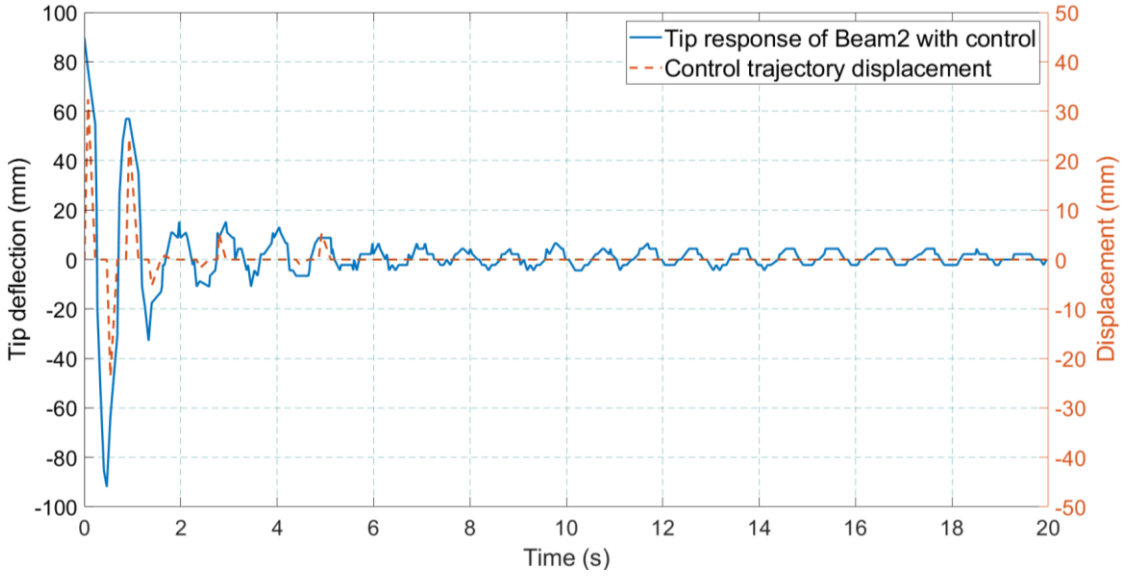

Figure 5.30 Response of Beam2 after robot arm control actions excited by 'Trajectory1.'

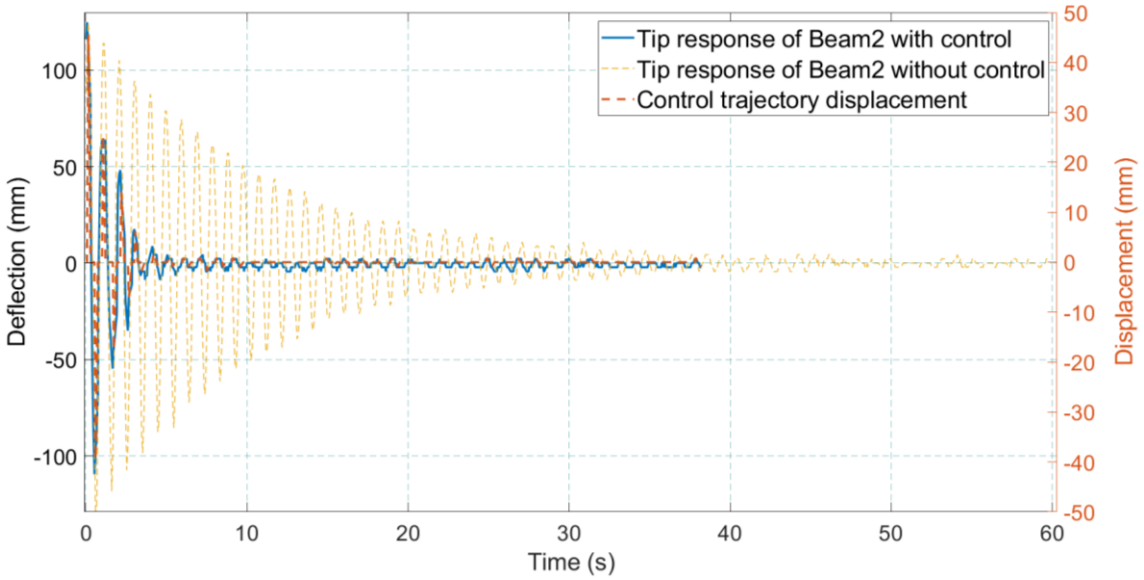

Figure 5.31 Response of Beam2 without control and with robot arm control actions excited by 'Trajectory2.'

The beam is manipulated with the use of 'Trajectory1', and the initial tip deflection is observed 92 mm. The response of Beam2 is presented in Figure 5.30. The controller suppressed the vibration in 4 s. With the excitation input as 'Trajectory2', the corresponding response of the beam is shown in Figure 5.31[3] with and without controller implemented. The initial tip deflection is observed as 124.4 mm and the vibration

[3] https://youtu.be/AE9IP7RSo4M - (Robot-vision based vibration suppression of Beam2)

amplitude of the tip is suppressed in ~55 s without application of control strategy. The proposed controller suppressed the tip vibration within 3.7 s so that the beam deflection is within ±10 mm of the safe limit. It can be observed that the proposed control strategy drastically reduced the tip deflection and suppression time to bring the beam within the safe limit.

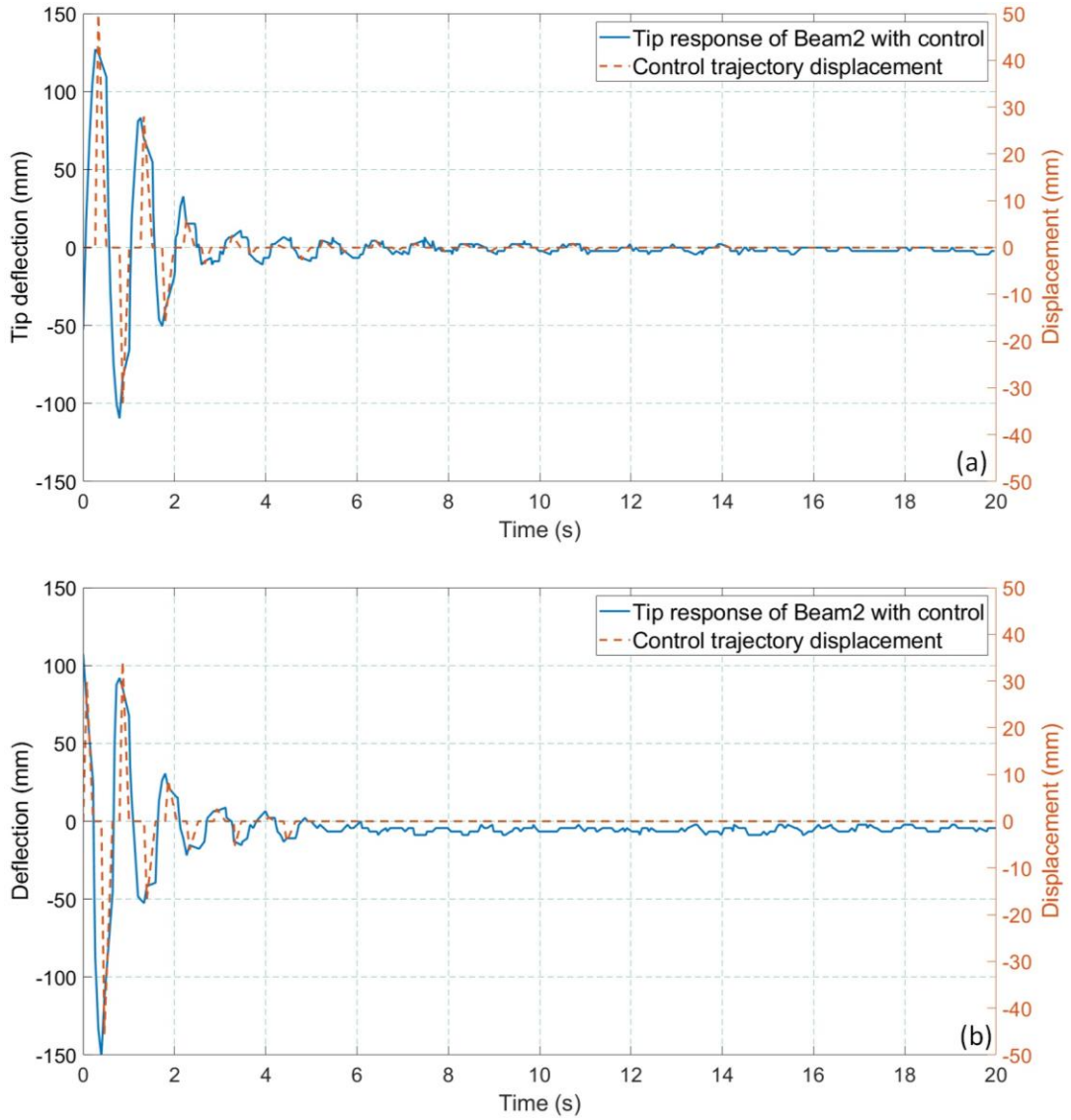

Figure 5.32 Response of Beam2 after robot arm control actions excited by (a) 'Trajectory3' and (b) 'Trajectory4.'

The controller response with excitation 'Trajectory3' is shown in Figure 5.32 (a). The high speed of 'Trajectory3' deflected the beam tip by 131.33 mm. The proposed controller suppressed vibration in 3 s. The 'Trajectory4' deflected the beam to 149.87 mm that also increases the suppression time with and without control. Without controller it took 57 s and with controller 4s for suppression. Though there is an offset in the tip deflection

response, it remains in the safe limit. This offset may occur due to error in the measurement. In experiments of Beam 2, the minimum and maximum vibration suppression time are 3.7 s and 4.7s respectively. The maximum and maximum reduction in vibration amplitude is of the order 93% and 95% and reduction in suppression time is of the order 92% and 94%.

5.4.4.3 Results of Beam3

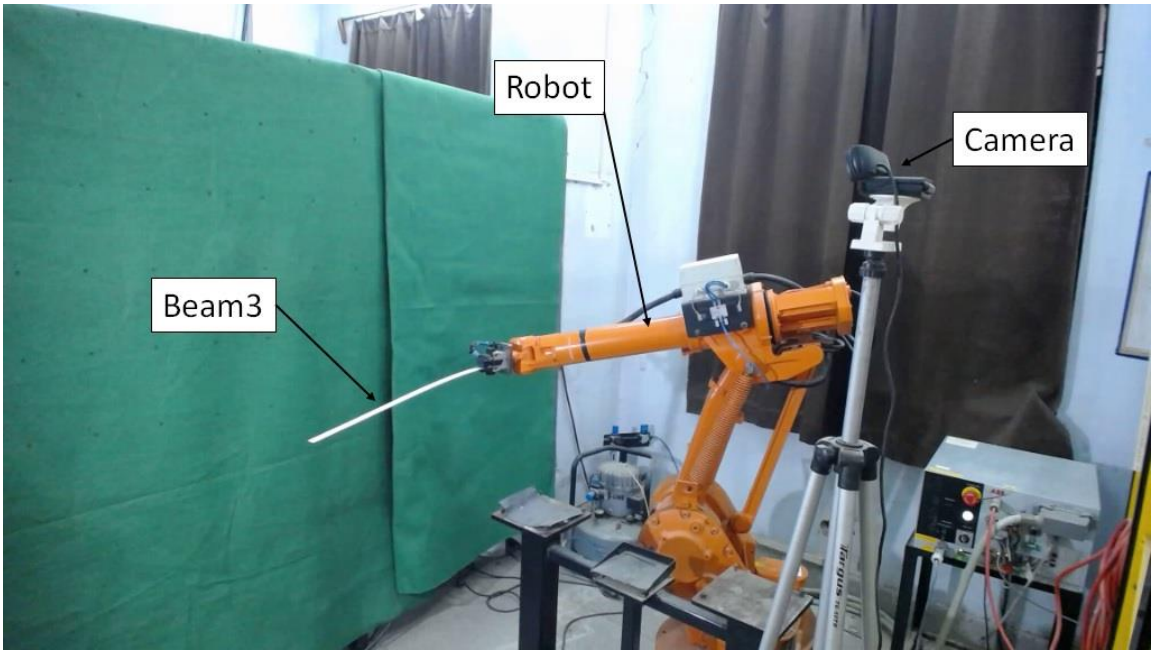

Figure 5.33 Experimental setup of Beam3

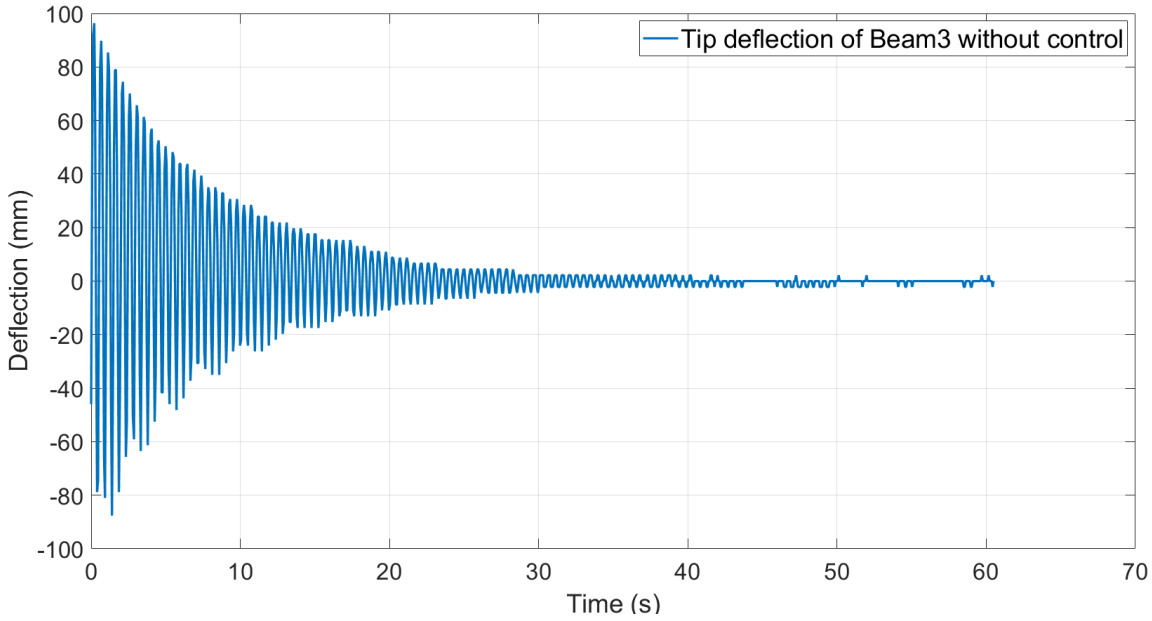

Figure 5.34 Free response of the Beam3

The experimental setup is shown in Figure 5.33, displaying the beam in the gripper, the camera, robot, and its internal controller. The parameters of the beam used in the experiment are presented in Table 5.1. The free response is presented in Figure 5.34, which is excited by the 'Trajectory1'. The vibration of the flexible beam is suppressed without any control in 34 s due to its own structural damping.

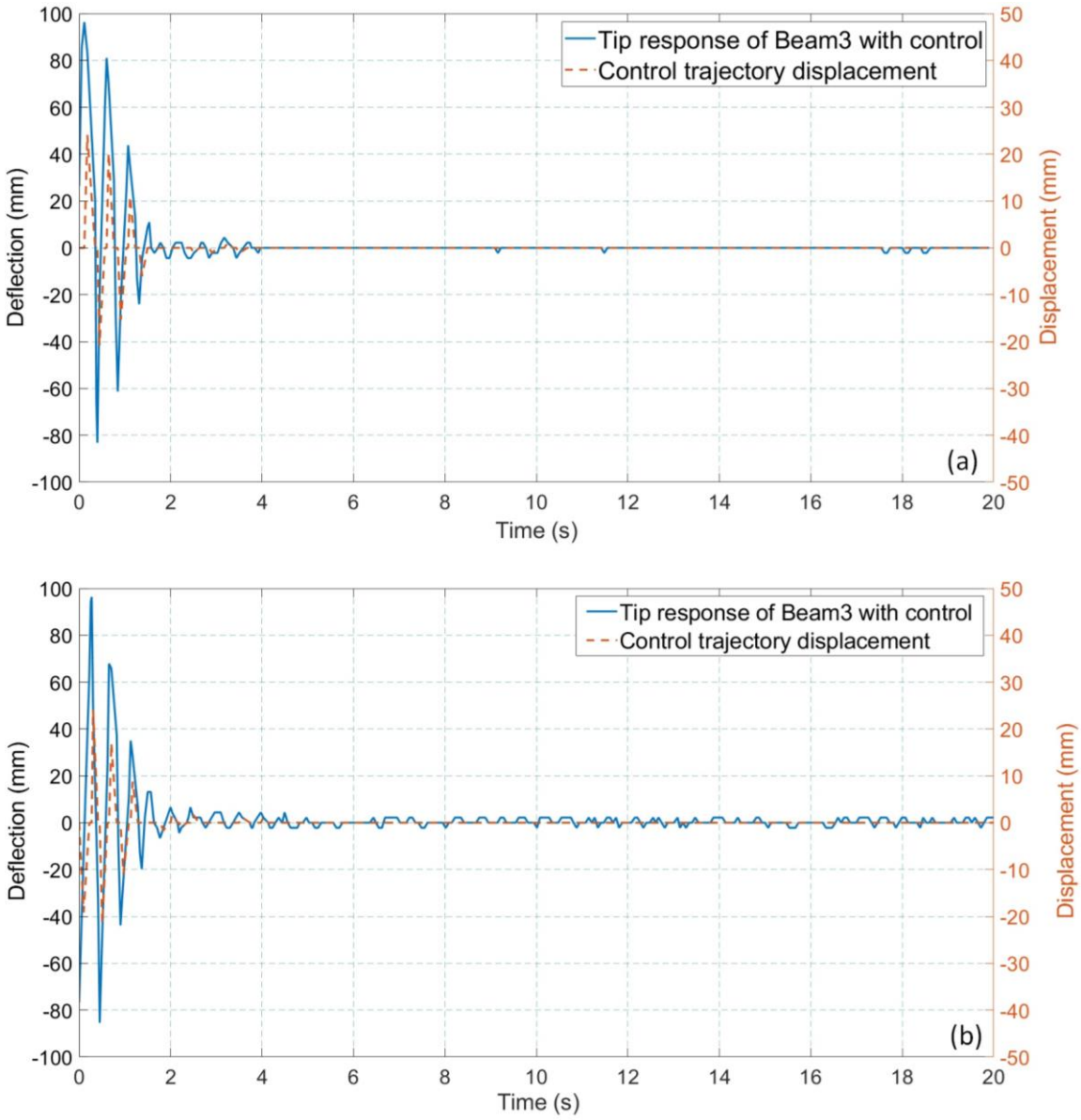

Figure 5.35 Responses of Beam3 after robot arm control actions excited by (a) 'Trajectory1' and (b) 'Trajectory2.'

The controller responses of the Beam3 with 'Trajectory1' and 'Trajectory2 are presented in Figure 5.35. In this case, both beams deflected with an initial maximum amplitude of 96 mm. The effect of different displacement with same velocity did not create much difference in the performances. The Beam3 used here has a high natural frequency

of 2.21 Hz compared to Beam1 and Beam2. However, its high frequency behavior does not affect the controller performance. The vibration is suppressed in 2 s with the proposed control strategy within the safe limit.

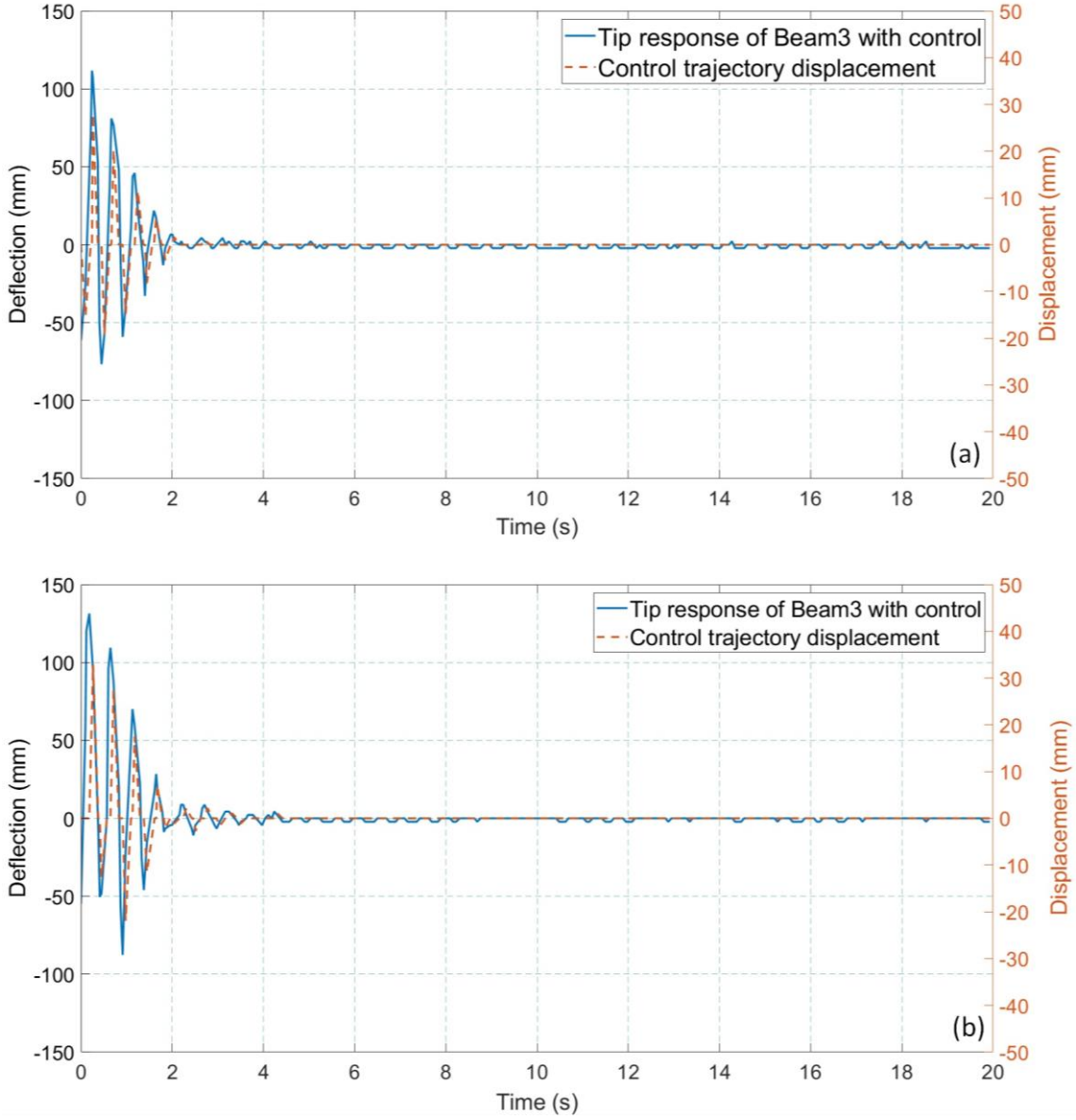

Figure 5.36 Response of Beam3 after robot arm control actions excited by (a) 'Trajectory3' and (b) 'Trajectory4.'

The controller responses with excitation 'Trajectory3' and 'Trajectory4' are presented in Figure 5.36. The proposed controller was successful in suppressing the vibrations in all the experiments. The experiments were repeated three times and summary of these results are provided in Table 5.4. The range of suppression time in repeated experiments results of all trajectories using straight line motion is shown in Figure 5.37.

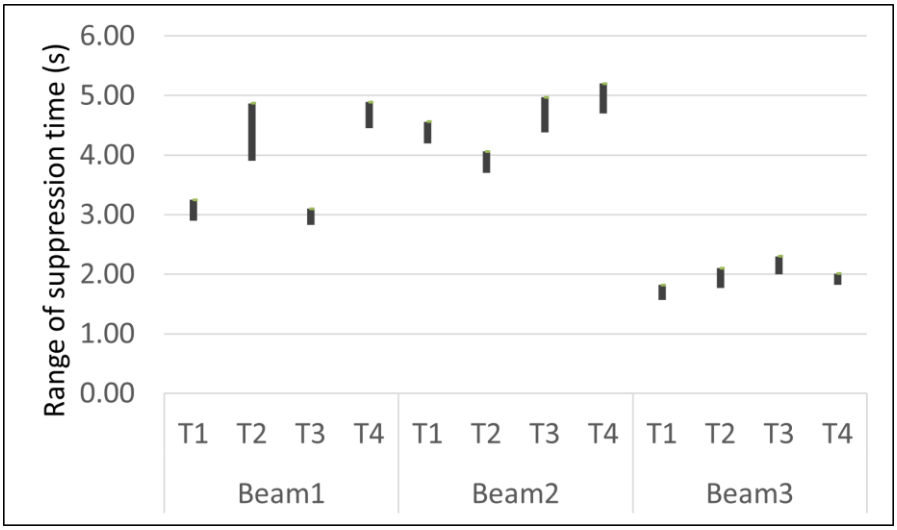

Figure 5.37 The range of suppression time in repeated experiments results of all trajectories using straight line motion.

Table 5.4 Summary of repeated experimental results of PMEB controller for straight line motion.

Object	Trajectory	Vibration suppression time (s) Ex. 1	Ex. 2	Ex. 3	Average suppression time (s)	Range of suppression time (s)	Reduction in average suppression time (%)
Beam1	1	2.90	2.99	3.25	3.05	0.35	94.25
	2	3.90	4.46	4.87	4.41	0.97	91.68
	3	2.83	2.89	3.10	2.94	0.27	95.18
	4	4.45	4.57	4.89	4.64	0.44	92.27
Beam2	1	4.20	4.47	4.56	4.41	0.36	91.68
	2	3.70	3.84	4.06	3.87	0.36	92.97
	3	4.38	4.63	4.97	4.66	0.59	91.53
	4	4.70	4.90	5.20	4.93	0.50	91.35
Beam3	1	1.57	1.80	1.82	1.73	0.25	94.91
	2	1.77	2.00	2.10	1.96	0.33	94.25
	3	2.00	2.20	2.30	2.17	0.30	94.30
	4	1.82	1.88	2.01	1.90	0.19	95.24

It has been observed that Beam1 and Beam2 exhibit a higher range for suppression times in comparison to Beam3. This disparity arises from the inherent characteristics of these beams. Specifically, the aluminum beams (Beam1 and Beam2) are lengthier and more susceptible to instability when contrasted with the stainless steel (SS) beam. It is worth noting that in some instances, the motion of robot may create a second mode of vibration in the beams, potentially leading to inaccuracies in tip deflection measurements.

The summary of the experimental results is specified in Table 5.5. In this table the suppression time with control and without control, as well as percentage reduction in suppression time and amplitude are provided. The best result is taken to demonstrate the performance of the proposed method. It can be summarized that the proposed controller has effectively suppressed the vibrations in flexible beams of different dimensions that used different trajectories for manipulation. The percentages reduction in amplitude varies between 92 to 98% and percentage reduction in suppression time vary between 91 to 93%.

Table 5.5 Summary of experimental results of PMEB controller for straight line motion.

Beam	**Trajectory**	**Initial deflection (mm)**	**Suppression time without control (s)**	**Suppression time with control (s)**	**Vibration suppression (%)**	**Reduction in suppression time (%)**
Beam1	1	109.50	53	2.90	92.00	94.53
	2	109.80	53	3.90	96.45	92.64
	3	169.80	61	2.83	97.00	95.36
	4	159.70	60	4.45	97.22	92.58
Beam2	1	92.00	53	4.20	92.85	92.08
	2	124.80	55	3.70	94.80	93.27
	3	127.00	55	4.38	94.82	92.04
	4	140.10	57	4.70	92.85	91.75
Beam3	1	96.22	34	1.57	97.72	95.38
	2	96.36	34	1.77	93.18	94.79
	3	111.70	38	2.00	98.00	94.74
	4	136.40	40	1.82	93.57	95.45

5.4.4.4 Experimental result with manual disturbance

The robustness of the proposed controller is tested for large amplitude and manual disturbance after vibration suppression. The response of the tip of Beam1 with 'Trajectory2' is presented in Figure 5.38. Here the initial tip deflection is 159.7 mm, and the vibration is suppressed within 5 s. Post vibration suppression of Beam1, the beam is manually disturbed twice in succession, to induce disturbance for performance evaluation of the controller. The response shown in Figure 5.38 justifies and validates the robust performance of the controller in presence of disturbance.

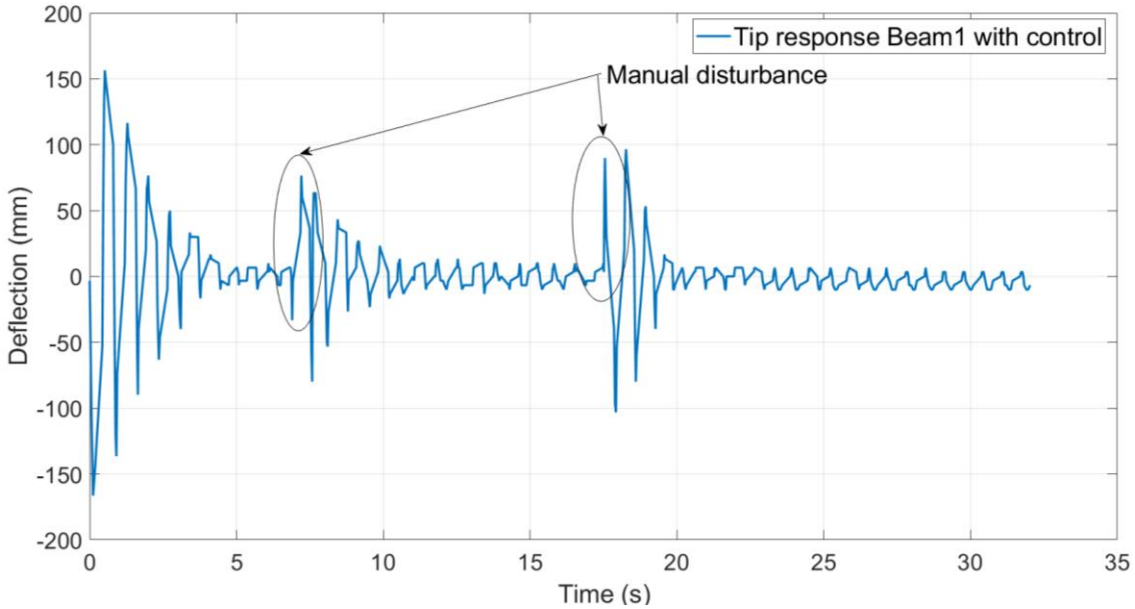

Figure 5.38 Response of Beam1 with 'Trajectory2'and manual disturbance after vibration suppression

5.4.5 Experimental results with wrist motion trajectory

In the experiment, the excitation trajectory nature is same as in the earlier experiments. The detail of the trajectories is presented in Table 5.6. The excitation trajectories used in the earlier experiments do not affect the deflection of beam tip. Thus, in present experiments the displacement remains constant while velocities are changed from 200 mm/s to 500 mm/s.

Table 5.6 Details of excitation trajectories used in control by wrist motion.

Trajectory	Displacement (mm)	Velocity (mm/s)
'Trajectory1'	150	200
'Trajectory2'	150	300
'Trajectory3'	150	400
'Trajectory4'	150	500

In these experiments the wrist motion trajectories are used to suppress the vibration of beams. The anti-motion provided to the robot wrist changed the orientation of the beam held by the end-effector. The angular motion available in wrist require to apply the torque at the base of the beams in place of force. The experiments are performed on the same three beams discussed in Section 5.4.4. The performance of these beams is recorded in

video format and for the respective links, the results are presented in the figures shown below.

5.4.5.1 Results of Beam1

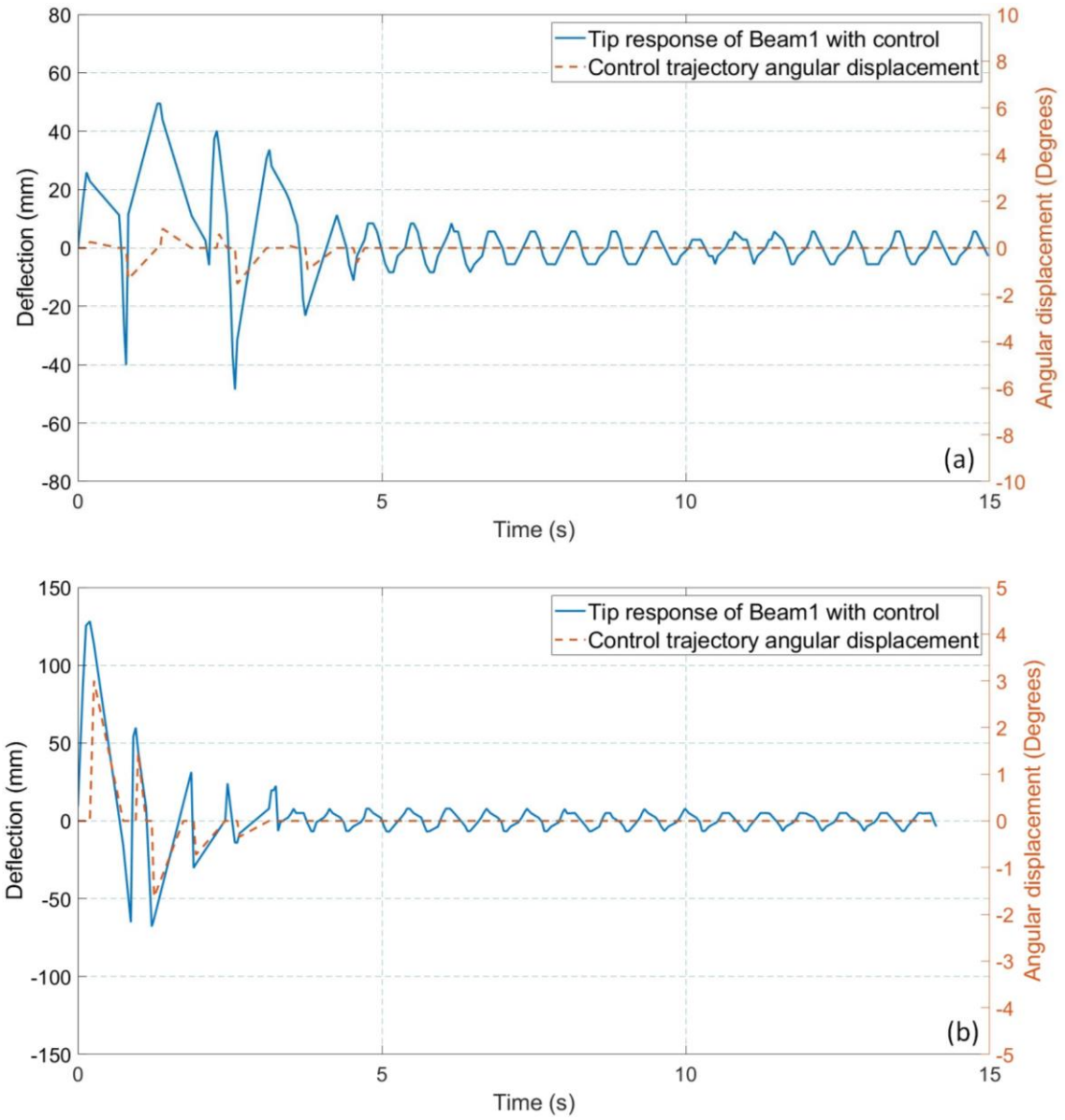

Figure 5.39 Response of Beam1 with robot wrist control actions excited by (a) 'Trajectory1' and (b) 'Trajectory2.'

The experimental setup is the same as in the earlier experiments. The beam is moved with excitation 'Trajectory1' and the results in shown in Figure 5.39 (a). The excitation 'Trajectory2' is executed and the response of Beam1 is presented in Figure 5.39 (b)[4]. The

[4] https://youtu.be/vwzEObdJRo0 (Robot-vision based vibration suppression using wrist motion of Beam2)

initial amplitude of tip deflection is 129.24 mm, which is suppressed within 4.35 s to bring within ±10 mm safe limit.

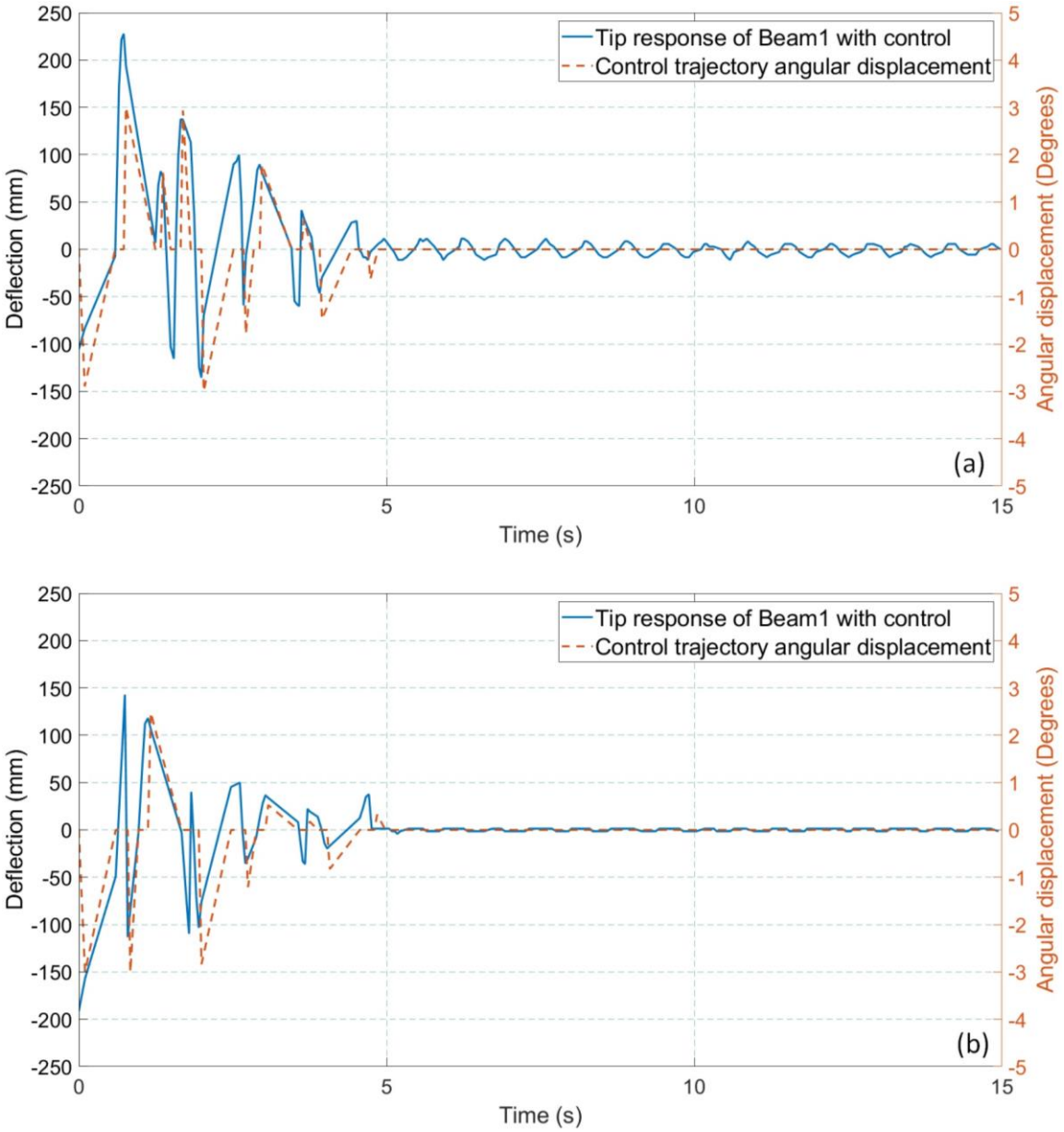

Figure 5.40 Response of Beam1 with robot wrist control actions excited by (a) 'Trajectory3' and (b) 'Trajectory4.'

The controller responses with excitation 'Trajectory3' and 'Trajectory4' are shown in Figure 5.40. The increase in velocity of 'Trajectory3' and 'Trajectory4' increased the tip deflection up to 152.9 mm and 191.43 mm respectively. The increase in initial deflection resulted in increased time of free response from 58 s to 61 s. This vibration amplitude is suppressed to ~ 96 % in 4.58 s and took 4.8 s to bring the amplitude within the safe limit

and reduced suppression time by ~ 96 %. It can be observed that in all the experimental results the proposed controller effectively suppressed vibration in less than 5s and vibration amplitude is within the safe limit.

5.4.5.2 Results of Beam2

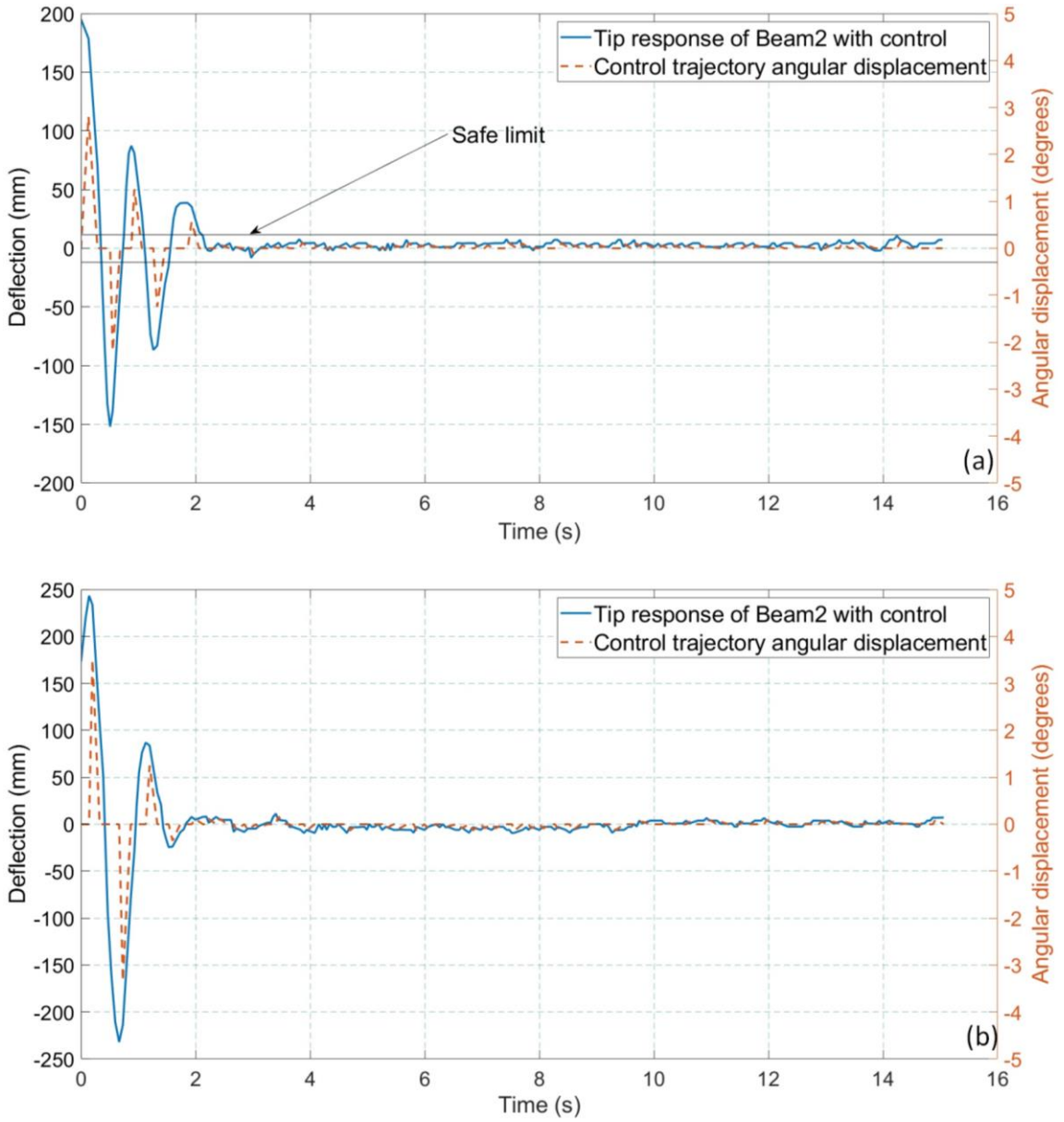

Figure 5.41 Response of Beam2 with robot wrist control actions excited by (a) 'Trajectory1' and (b) 'Trajectory2.'

In the experiment, the robot is commanded with the excitation 'Trajectory1' for the assembly operation. This kind of trajectory induces vibration in the beam which needs to be suppressed in less time. The response of Beam2 with control signal is presented in

Figure 5.41 (a)[5], where it shows the control trajectory as angular displacement and corresponding response of the tip. The maximum tip deflection is 195.1 mm, and the controller suppresses the vibration in 2.22 s to bring the amplitude within the safe limit of ±10 mm. The response with excitation 'Trajectory2' is presented in Figure 5.41 (b). The beam is deflected by 243.40 mm and suppressed within 2 s.

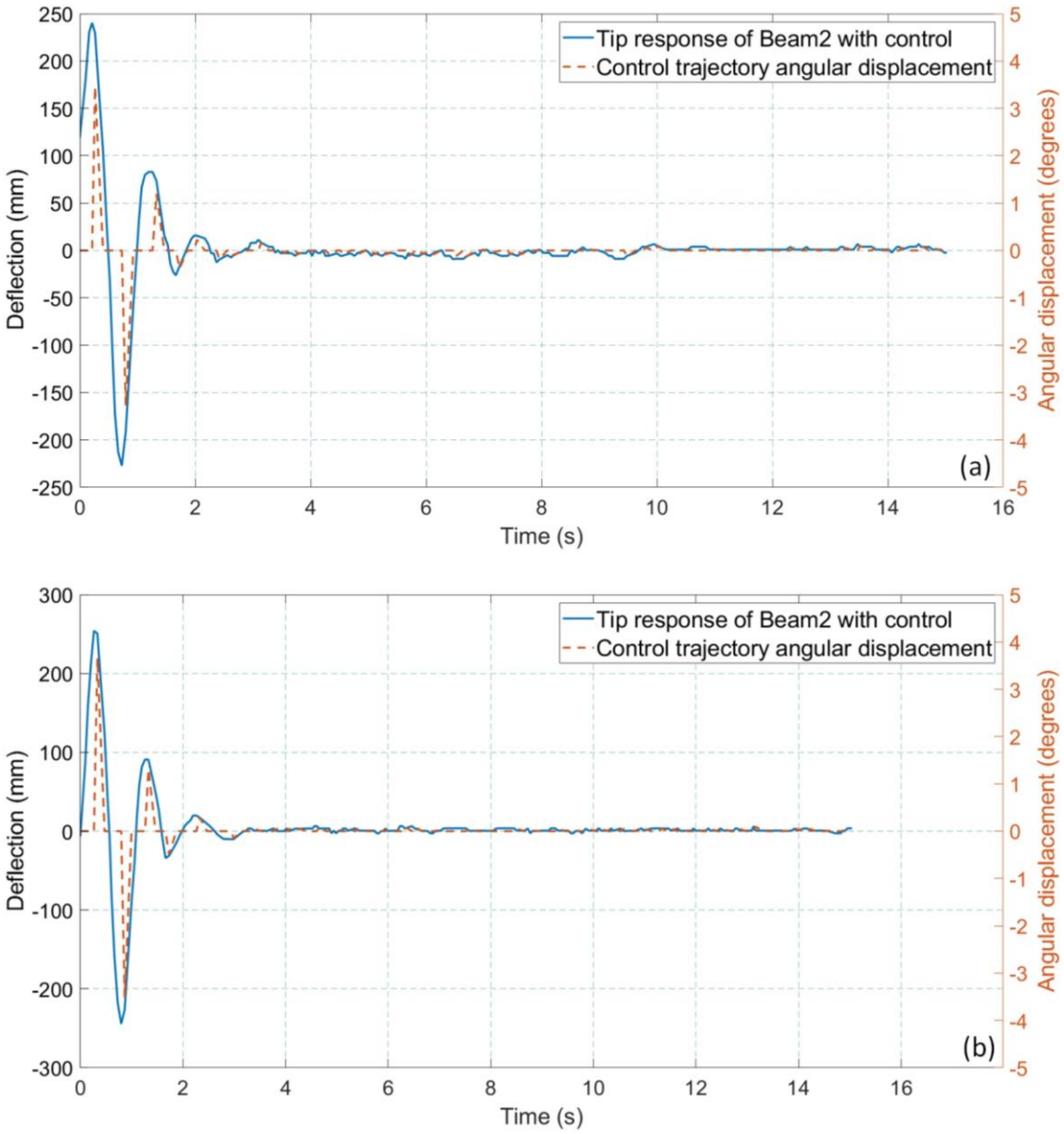

Figure 5.42 Response of Beam2 with robot wrist control actions excited by 'Trajectory3' and 'Trajectory4.'

The controller responses with excitation trajectories 'Trajectory3' and 'Trajectory4' are shown in Figure 5.42. The experiments are performed multiple times with other

[5] https://youtu.be/jQUo5jnYGCM (Robot-vision based vibration suppression using wrist motion of Beam1)

trajectories and the average suppression time is observed to be 2.68 s to bring the amplitude within the safe limit. The controller reduced the suppression time up to 97.37 %.

5.4.5.3 Results of Beam3

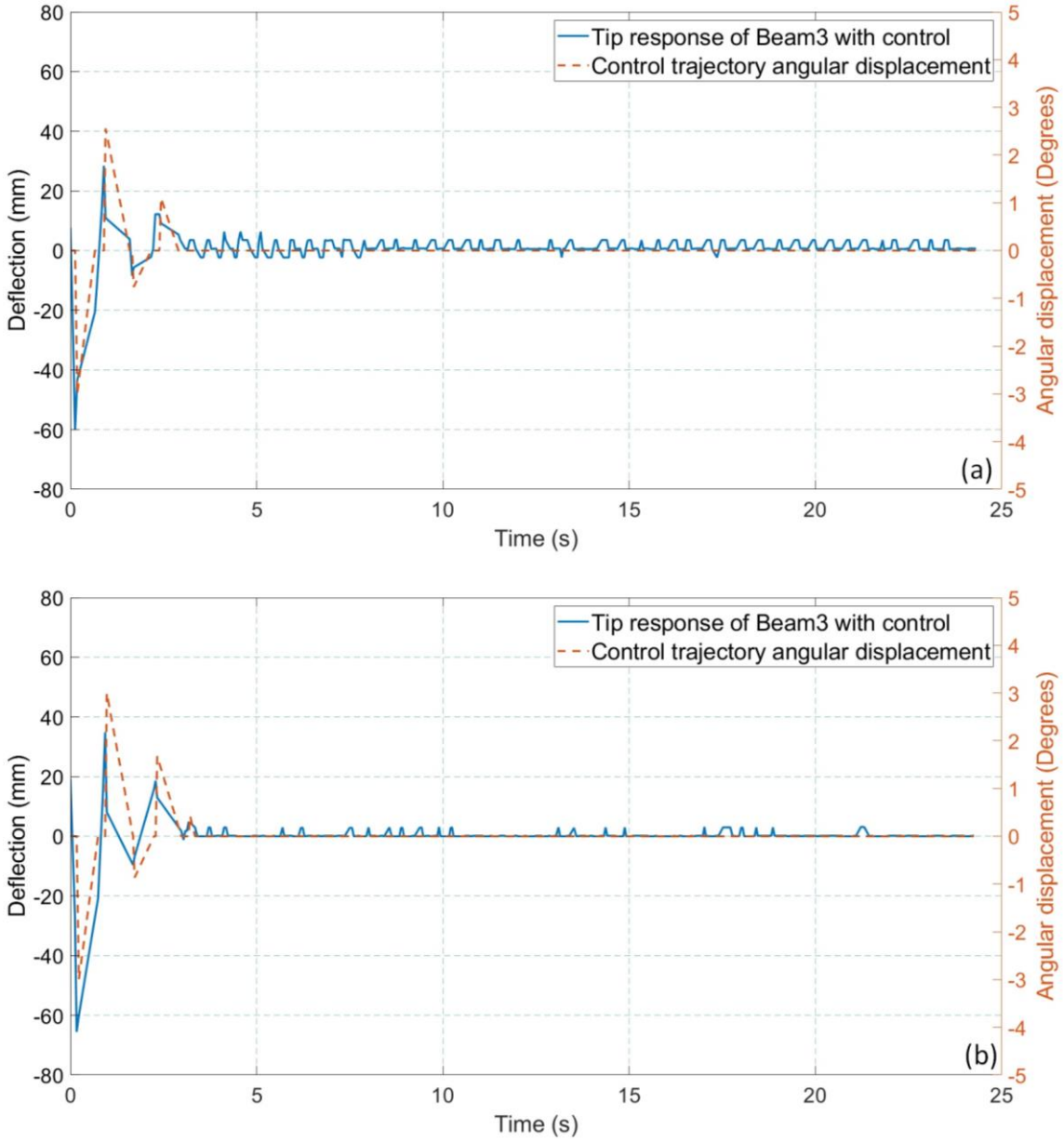

Figure 5.43 Response of Beam3 with robot wrist control actions excited by (a) 'Trajectory1' and (b) 'Trajectory2.'

The response of the Beam3 with excitation 'Trajectory1' is presented in Figure 5.43 (a). In this case, the beam vibrated with an initial maximum deflection of 60 mm and the vibration is suppressed in 3 s with the proposed control strategy whereas took 34 s to be within the safe limit for without control scenario. Figure 5.43 (b) presents the controller response excited by 'Trajectory2'.

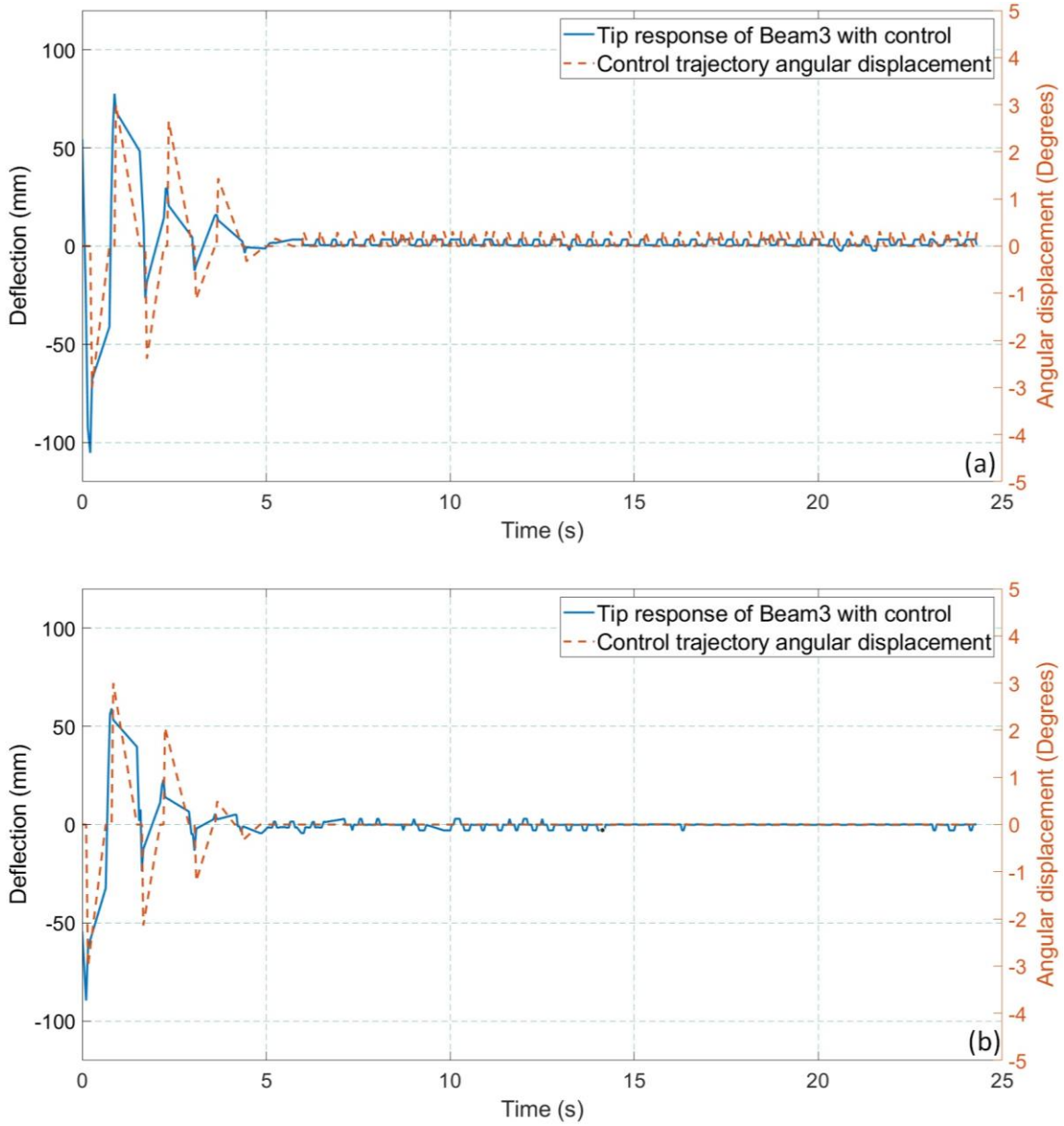

Figure 5.44 Response of Beam3 with robot wrist control actions excited by (a) 'Trajectory3' and (b) 'Trajectory4.'

The controller responses with excitation trajectories 'Trajectory3' and 'Trajectory4' are show in Figure 5.44 (a) and (b)[6] respectively. The initial trajectory displacement is found to be 105.3 mm (Figure 5.44 (b)) which is higher compared to the deflection produced by 'Trajectory1'. Thus, the time taken to suppress the vibration is 4.4 s. The experiments were replicated thrice, and a concise summary of the repeated experimental outcomes is detailed in Table 5.7. The range of suppression time across all trajectories is graphically depicted in Figure 5.45.

[6] https://youtu.be/Z2w3X0Yfx5Q (Robot-vision based vibration suppression using wrist motion of Beam3)

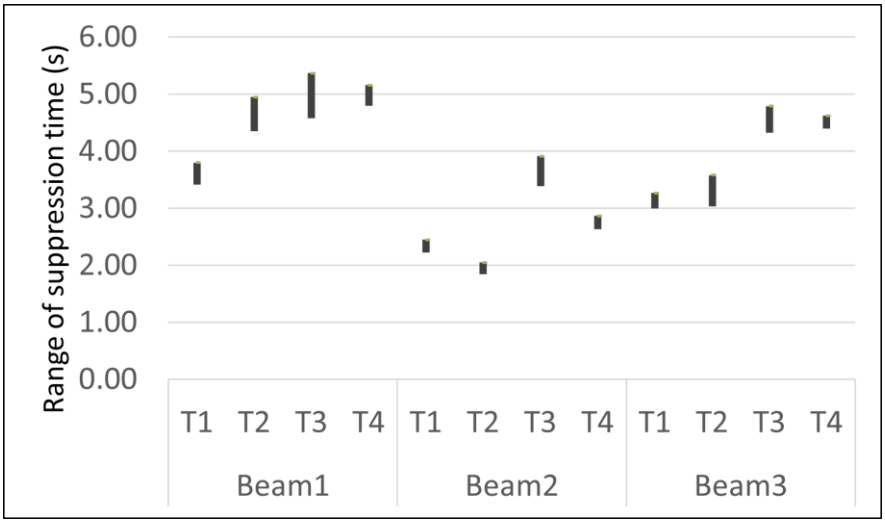

Figure 5.45 The range of suppression time in repeated experiments results of all trajectories using wrist motion.

Table 5.7 Summary of repeated experimental results of PMEB controller by wrist motion.

Object	Trajectory	Vibration suppression time (s)			Average suppression time (s)	Range of suppression time (s)	Reduction in average suppression time (%)
		Ex. 1	Ex. 2	Ex. 3			
Beam1	1	3.41	3.60	3.80	3.60	0.39	91.99
	2	4.35	4.70	4.95	4.67	0.60	91.52
	3	4.58	5.01	5.37	4.99	0.79	91.40
	4	4.80	4.95	5.16	4.97	0.36	91.85
Beam2	1	2.22	2.30	2.45	2.32	0.23	96.43
	2	1.84	2.00	2.05	1.96	0.21	97.20
	3	3.39	3.57	3.91	3.62	0.52	94.82
	4	2.63	2.81	2.87	2.77	0.24	96.10
Beam3	1	3.00	3.21	3.27	3.16	0.27	90.71
	2	3.03	3.22	3.58	3.28	0.55	90.64
	3	4.32	4.51	4.79	4.54	0.47	88.05
	4	4.40	4.53	4.62	4.52	0.22	88.71

It can be observed that the range of suppression time for the wrist motion trajectories is small. In some case ranges are high and may be attributed to error in prediction or error in timing the control trajectory through delays. The summary of the results in shown in Table 5.8. In this table, the suppression time of the beams with control and without control, to bring within the safe limit for the slot and percentage reduction are provided. In every experiment, the safe limit is chosen as ±10 mm.

Table 5.8 Summary of experimental results of PMEB controller by wrist motion

Beam	Trajectory	Initial deflection (mm)	Suppression time without control (s)	Suppression time with control (s)	Vibration suppression (%)	Reduction in suppression time (%)
Beam1	1	49.46	45	3.41	79.78	92.42
	2	129.24	55	4.35	92.26	92.09
	3	152.90	58	4.58	93.46	92.10
	4	191.43	61	4.80	94.30	92.13
Beam2	1	195.10	65	2.22	94.87	96.58
	2	243.40	70	1.84	95.89	97.37
	3	240.30	70	3.39	95.84	95.16
	4	254.10	71	2.63	96.06	96.30
Beam3	1	60.09	34	3.00	94.16	91.18
	2	65.57	35	3.03	95.42	91.34
	3	89.50	38	4.32	95.86	88.63
	4	105.30	40	4.4	96.47	89.00

5.4.6 Comparison of the controller performance and discussions

The important differences between the proposed PMEB controller and the conventional PID controller are the computational method to predict the maximum error using robot vision and the approach proposed to handle different types of delays present in the system. In most industrial robots, the delays are included while implementing the control strategy in the internal controller. However, for the proposed high-level controller, both robot internal controller and second stage controller must work coherently so that the control input would suppress vibration effectively. Thus, implementation of only PID control scheme in high level controller for vibration suppression will not be effective. Secondly, while executing the robot control action, the second stage controller is put on hold for a short period of time until the control action is completed. In such a case, the delay becomes critical and must be handled carefully.

Above statements are justified through evaluation of vibration suppression performance of an error based discrete PID type controller with PMEB controller. In this case, the discrete PD controller is implemented for different gain values using trial and error method to obtain minimum time to suppress the vibration in flexible beam. The above problem being a vibration suppression problem, position control is not essential. Thus, integral controller is not included in the conventional PID controller. In this PD controller, neither

the method to predict maximum error nor various delays during implementation are included. Additionally, the conventional controller is error based therefore the prediction of maximum error using FEM model becomes redundant. The controller response of Beam1 and Beam2 are presented in Figure 5.46 (a) and (b), using a discrete PD controller with proportional and derivative gains 0.1 and 0.01 respectively. The experiments are repeated thrice using these gain parameters, and the average suppression time of the controller for the Beam1 and Beam2 are 8.1 s and 13 s respectively where the safe limits are ±10 mm. The discrete PD controller requires almost 200% time compared to the proposed PMEB controller.

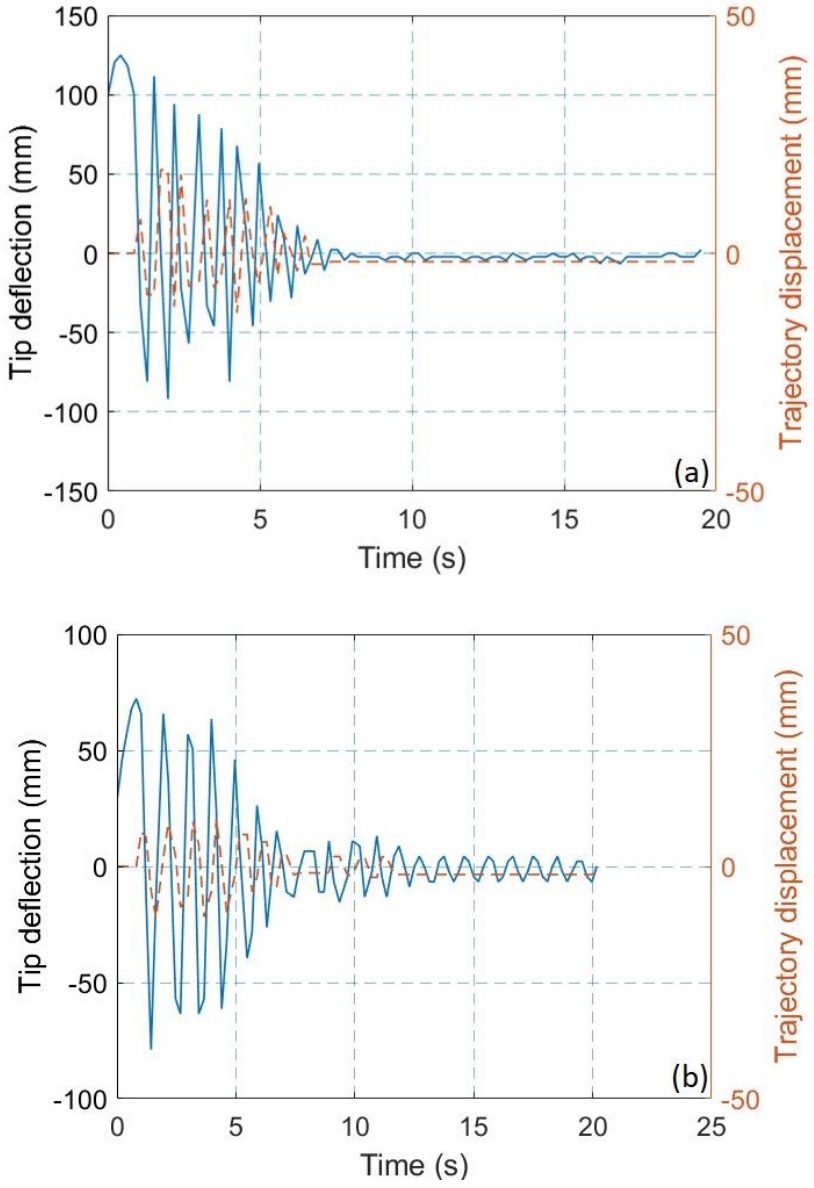

Figure 5.46 Vibration suppression response of (a) Beam1 and (b) Beam2 with PD controller

It is important to mention that the gains of PD controller need to be optimized based on changes in beam parameters as these cause change in dynamical behavior.

The factors that may affect the results of the experiments are inaccuracies in computation of Rayleigh damping coefficients (a_0, a_1), inaccurate model parameters and initial conditions (tip deflection and velocity). The robot-vision system used for the experimentation is a low-cost 30 fps webcam, however due to the delays in vision systems and delays in image processing, the performance of the webcam is reduced to 18 fps in real-time. Frequency aliasing is a common limitation for sensors with low update rate, especially in vibration control problems. Therefore, the current robot-vision can be applied to a flexible beam system with the first mode of vibration frequency up to 9 Hz. Both the beams have low natural frequencies i.e., 1.6 Hz and 1.05 Hz respectively at first mode. Therefore, vision sensors with a higher frame rate are necessary for higher frequency vibration systems.

To compare and prove the improved performance of the proposed controller with work present in literature is taken. The most recent work, which is similar to the present work, was carried out by (Kapsalas *et al.*, 2018). They achieved a reduction in vibration by 97% in 3.1 s, where the performance parameter was the acceleration response of the tip of the beam with control to without control. This approach is useful for vibration suppression but exact suppression of vibration amplitude in the range of millimeters is not discussed here. Furthermore, in the case of lightweight objects, the force/torque sensor may provide noisy feedback which is a major limitation for the implementation of such tasks. Similarly, another vision based vibration suppression of a deformable linear object (DLO) was presented by (Huang *et al.*, 2014). Where the developed PID controller reduced the vibration amplitude by 96% and the suppression time by 75% of DLO, grasped by a two degree of freedom robot. The controller performance is good; however, implementation of this method requires modification to the internal controller of the robot which in turn increases the cost. The type of control trajectories was straight in line motion, whereas the angular motion for vibration suppression were not used earlier.

It can be observed that the reduction in vibration amplitude is ~97% in an average time of 4.2 s for the current work. In this case, the suppression time is greater as the dimensions of the beams are different from the dimensions used in the literature. The present work demonstrates an explicit reduction in vibration amplitude using camera sensor as

compared to implicit acceleration reduction in literature where force sensor was used. Moreover, the proposed robot vision based method determines the tip position of the flexible beam and the dimension of beam required for assembly tasks. In addition, the proposed camera calibration method can be reused to obtain the extrinsic parameters if the position of the camera is changed to an unknown position or disturbed. The comparative results are presented in Table 5.9 to highlight the contributions of the proposed research.

Table 5.9 Comparison of performance of the proposed method with other methods

References	**Method**	**Amplitude suppression (%)**	**Suppression time reduction (%)**
(Yue and Henrich, 2006)	DLO vibration reduction using Fuzzy controller with force/torque sensor	97%	92%
(Huang *et al.*, 2014)	DLO vibration reduction using PID with vision sensor	96%	75%
(Kapsalas *et al.*, 2018)	Al beam vibration reduction using I-type controller with force/torque sensor	97%	83.09%
Proposed work	Robot-vision based PMEB controller	97%	92.56%

The limitations of the present work are use of the first mode of beam vibration for vibration suppression and natural frequency greater than 9 Hz require high speed camera. The robot-vision system is capable of measuring the in-plane vibration of beam and out of plane vibration cannot be detected by the present robot vision system.

5.5 Conclusion

Robotic assembly of a flexible beam in slot is a challenging task where the vibration in flexible beam due to PtP motion of the robot induces vibration. In this chapter, robot-vision based second stage controller to suppress the vibration of the flexible beam is proposed. In which a robot-assisted camera calibration method, robot-vision method with a virtual marker to identify the object in workspace, and PMEB second-stage controller are proposed. For feedback, a commercially available 2D camera is utilized to measure the

vibrations of the beam in the 3D task space. The flexible beam is modelled using the FEM and its dimensional parameters are updated in FEM with the help of the robot-vision system in real-time to predict the maximum deflection. The proposed controller used the straight motion trajectories and wrist motion trajectories to suppress the vibration. The important findings from the experiments are the vibration amplitude is suppressed to ~97% in an average of 4.2 s and the suppression time is reduced by an average of ~93% in comparison with control to without control scenarios using straight motion trajectories. Using the angular control trajectories, the controller is capable of suppressing the vibration amplitude by ~96% in 2 s and reduce the suppression time by ~97% as compared with control to without control scenario. The above said controller performance is also compared with a classical error based discrete PD controller and the vibration suppression methods available in literature. The FEM model used in the proposed controller requires a change in input values with the change in handled object. In addition, the FEM requires increased computational time to make accurate prediction of the vibration amplitude. Therefore, an approach should be proposed so that the vision-based controller will not require such a computational model. For which, a system identification-based controller is needed so that the controller will be independent of object parameters.

CHAPTER 6
SYSTEM IDENTIFICATION METHOD FOR ROBUST ACTIVE VIBRATION SUPPRESSION OF FLEXIBLE BEAMS

In chapter 5, a FEM based model of flexible beam is used to predict the error in tip deflection of flexible beam. The flexible beam model was assumed as a cantilever beam with moving base. The boundary conditions in FEM based model changes with the change of beam setup that does not make it a general method to apply for the proposed strategy. The computation involved in FEM model increase load on the PC and increase in delay, which is not desirable. Additionally, the accuracy of prediction is based on accuracy of the assumed model and its parameters value. It is difficult to measure all the parameters values using the proposed robot vision method. Some of the parameters such as Rayleigh damping coefficient and modulus of elasticity cannot be determined using obtained dimensions from robot vision. Therefore, the method cannot be directly used in the assembly task without prior knowledge of material properties. However, if the robot is working with known and same material properties of all the flexible objects, the proposed strategies can be applied to the robot system. In most robot assembly operations, the material properties vary and time consuming to obtain the exact values, therefore a system identification method can be used to predict the response of the flexible object.

In this chapter, a data-based approach is used for system identification of the flexible object. System identification method eliminates pre-requirement of all the parameters and optimizes assumed model of the response of flexible object that is obtained using the robot vision method. The system identification process takes places online while the robot is manipulating the flexible object in the assembly operation.

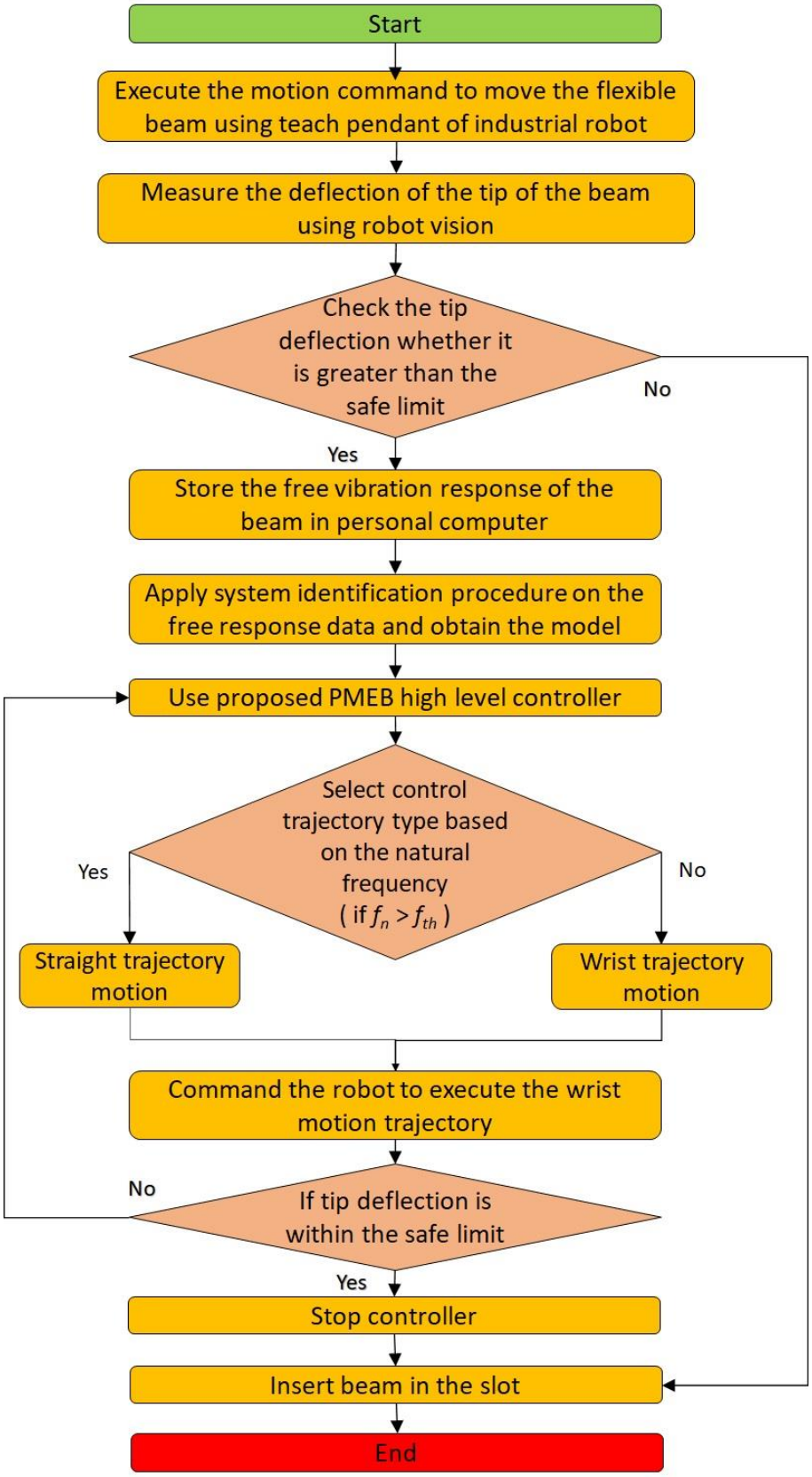

Figure 6.1 Flowchart of the robot vision method based system identification and vibration suppression.

The flowchart of the proposed approach is presented in Figure 6.1. A flexible beam held by the gripper of a robot is commanded through the teach pendant to insert into a slot. This task is performed by the robot internal controller, which controls the movement of industrial robots. However due to high-speed manipulation, the flexible beam vibrates after executing such motion commands. This vibration in the flexible beam consumes a good amount of productive time to become motionless before actual assembly. Whereas the actual purpose of this command is to place the motionless flexible beam, right in front of the slot for an assembly. Therefore, the robot vision-based feedback system, discussed in chapter 5, is used to determine the dimensions of the flexible beam held by the robot gripper and its tip deflection at that instant. If the maximum tip deflection is higher than the specified safety limit, then the information related to the real time tip deflection is stored in PC connected to the robot vision system for system identification. As the robot remains static while the tip deflection is recorded, the same is considered as free response of the flexible beam. The free response data is used for system identification and the parameters of vibration response of the flexible beam are optimized using a nonlinear optimization method. The optimized model is used in the proposed controller to send control signals to the robot internal controller for vibration suppression of the flexible beam. The controller communicates with the robot internal controller through socket programming developed in Python IDLE and sends commands to it for execution of the control action by the robot. The PMEB controller is used to suppress vibration using both straight and wrist motion at the end-effector of the robot. The performance of the controller is analyzed based on the natural frequency of the beam that helps the robot to select the type of control trajectory for better control. These inputs will reduce the vibration of the flexible beam and attempts to bring the vibration amplitude within the safe limit required for assembly operation. The optimization steps are discussed in the next section.

6.1 Data-based system parameter identification

In the present system, the optimized vibration response model of the robot beam system can be used to compute predicted tip deflection. For computation of error, tip deflection of the beam in static position is compared with the current tip deflection. If the error is computed based on the maximum predicted tip deflection, then the computed value is considered as maximum predicted error. Although the use of a dynamic model to predict error yields a positive result and works best when the physical and dynamic parameters of the beam are known, however the industrial set up throws challenges with regard to

unknown beam dimensions and material properties. Therefore, it would be advantageous if the data driven system identification based model is used to predict the vibrational behavior of the flexible beam.

The PMEB controller suppresses tip vibration of the flexible beam, caused by manipulation of the robot. The vision sensor provides feedback on the deflection of the beam and whether the values are within the user-specified safe limit. If it exceeds the safe limit, the feedback system records free response of the beam tip while end-effector of the robot is motionless. This free response data is used to determine the relationship between the deflection of the beam tip with respect to time. For the current problem, the first mode of free vibration of the beam is considered where the system response can be modelled as a response of damper-spring-mass system. In this case the spring is assumed to have linear behavior with constant stiffness. As a result, equation (6.1) can be used to express the first mode of damped vibration.

$$x = Xexp^{-\zeta\omega_n t}\cos(\omega_d t - \alpha) \tag{6.1}$$

Where x - amplitude of the vibration, X - maximum amplitude, ζ - coefficient of damping, ω_n - natural frequency, ω_d - damped frequency, t – time and α - the phase angle. The stored data is fitted with equation (6.1) and the parameters are optimized using the generalized reduced gradient (GRG) algorithm (Lasdon *et al.*, 1978) available in nonlinear solver of Microsoft Office Excel.

6.2 Design of data-driven model based PMEB controller

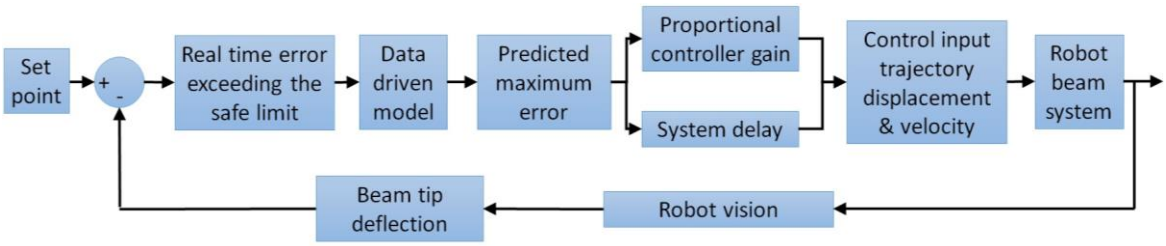

Figure 6.2 Design of data-driven model-based PMEB controller

The PMEB controller is used for the vibration suppression of flexible beams, as discussed in the previous chapter. It uses this relationship, as given in equation (6.1), to predict the maximum error once the above parameters are known for a robot-beam system. The block diagram of the proposed controller is shown in Figure 6.2. The FEM model is replaced by

the data driven model for predicting the maximum error. The overall strategy is the same as given in chapter 5.

Because the equation (6.1) does not include the tip velocity, prediction of the maximum error is only possible if the maximum tip deflection is available. In the current system, the phase angle cannot be detected. As a result, the extreme tip deflection is used to predict the next maximum tip deflection. This process of taking maximum amplitude is advantageous for cameras with a low frame rate and hence reduces the cost of controller. In addition, the high-speed tip vibration creates a motion blur effect, which will cause increased measurement error. In contrast, near the extreme position of the beam, the speed is less or zero at the maximum position, and the object appears stationary. As a result, the accuracy in determining the tip deflection is high at extreme positions.

The controller continuously monitors the error and detects the maximum deflection of the tip. The detected maximum amplitude is fed into equation (6.1), which determines the next maximum deflection. Taking the maximum predicted error, the controller determines the control trajectory that can be executed once. The control trajectory is executed after taking into account of various system delays.

The control trajectory is executed after taking into account various delays present in the system. The delays related to the current system are specified in equation (4.9). In chapter 5, the FEM model is used for the prediction of maximum deflection of the flexible beam tip. The computational time for this model was approximately 0.67 s. However, the model chosen through system identification will have reduced computation load compared to the FEM model.

The next section describes the assessment of the system identification method.

6.3 Assessment of data-based model optimization

As discussed above, the free vibration response data of the beam tip is used to optimize the model. The full free response provides the best fit to the model. Figure 6.3 (a) shows the experimental data obtained by the robot vision for the entire period of free response. The same data is used to optimize the model presented in equation (6.1)using the GRG nonlinear method. Figure 6.3 (b) presents the predicted response obtained using the optimized model. However, optimizing the model using the vibration response data of

full-time span consumes much time which temporarily halts the operation and is undesirable. It would be beneficial if the time span of the vibration response is reduced within an acceptable error. This can be accomplished by optimizing the assumed model using the free response of the beam tip of different time spans.

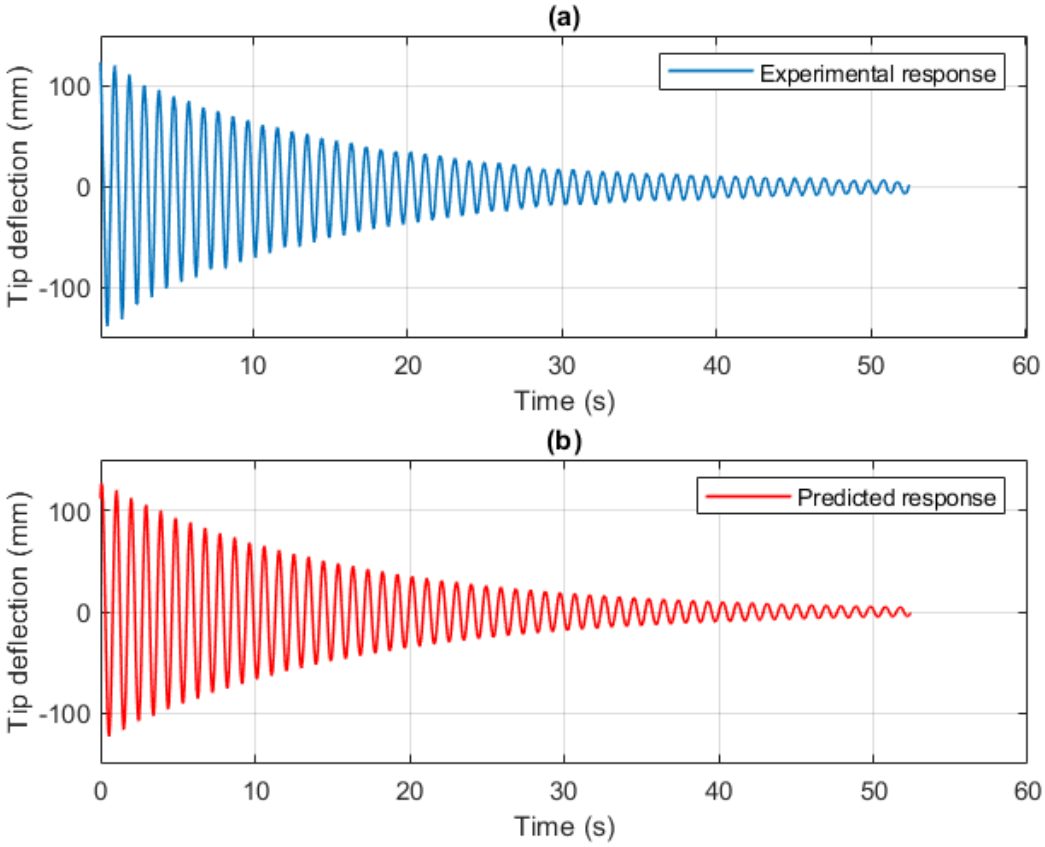

Figure 6.3 Free response of the tip of the beam (a) experimental response and (b) predicted response

Table 6.1 Model optimization analysis of Beam1

Time span (s)	ζ	Frequency (Hz)	SSE (mm)	Error in frequency
0-50	0.01	1.525	35116	0
0-30	0.01	1.524	35141	-0.001
0-20	0.01	1.525	35233	-0.000
0-10	0.01	1.525	35771	-0.000
0-5	0.01	1.528	44425	0.003
0-3	0.01	1.526	44503	0.001
0-2	0.01	1.527	45694	0.002
0-1	0.00	1.528	16830784	0.003

Table 6.2 Model optimization analysis of Beam2

Time span (s)	ζ	Frequency (Hz)	SSE (mm)	Error in frequency
0-80	0.01	1.0458	8438	0
0-40	0.01	1.0456	8552	-0.0002
0-20	0.01	1.0453	9043	-0.0005
0-10	0.01	1.0450	10136	-0.0008
0-5	0.01	1.0450	10809	-0.0008
0-3	0.01	1.0454	8857	-0.0004
0-2	0.01	1.0454	33774	-0.0004
0-1	0.00	1.0293	2302992	-0.165

Table 6.3 Model optimization analysis of Beam3

Time span (s)	ζ	Frequency (Hz)	SSE (mm)	Error in frequency
0-45	0.01	2.092	29817	0.000
0-30	0.01	2.092	29819	0.000
0-20	0.01	2.091	30088	-0.001
0-10	0.01	2.085	35979	-0.006
0-5	0.01	2.078	51831	-0.013
0-3	0.01	2.075	60963	-0.016
0-2	0.01	2.092	29817	0.000
0-1	0.00	2.095	47161	0.003

The Table 6.1, Table 6.2, and Table 6.3 show the analysis of the model parameter and its performance while taking different time span data of the free response of Beam1, Beam2 and Beam3. It includes damping coefficient 'ζ', natural frequency 'f', sum of squared errors (SSE) and error in frequency. The SSE is the squared sum of errors in the measured and predicted response. Error in the frequency is obtained by finding the difference between the natural frequency of the beam and the frequency available in the optimized model. Tables 6.1 to 6.3 provide the results of the optimization process conducted for different time span of the free vibration response. The GRG solver used the full time span for the free response which provides the best result. This result is compared with the result of shorter responses up to 1s. The obtained result shows that there is no significant deviation in SSE till the span of 3s. However, there is sudden increase observed for the shorter time span of 2s and 1s. Thus, based on the obtained model parameters, it can be concluded that approximately 3s of data of beam tip free vibration is sufficient to obtain the model parameter within acceptable error limit.

Table 6.4 Trial solution for GRG optimization.

Trial	Maximum amplitude (X – mm)	Coefficient of damping (ζ)	Natural frequency – (f - Hz)	Phase angle (α - rad)
1	116	0.1	0.159	0
2	50	0.5	0.318	1
3	10	0.8	0.477	0.5
4	10	0.9	0.637	-0.5
5	150	0.3	0.796	0.01

Table 6.5 Optimization results using the trial solution.

Trial No.	Maximum amplitude (X – mm)	Coefficient of damping (ζ)	Natural frequency (f - Hz)	Phase angle (α - rad)	Sum of squared error (SSE – mm)
1	128.48	0.01	1.045	-0.51	8438.03
2	128.48	0.01	1.045	-0.51	8438.03
3	128.48	0.01	1.045	-0.51	8438.03
4	128.48	0.01	1.045	-0.51	8438.03
5	128.49	0.01	1.045	-0.51	8438.03

The optimization of model is carried out using the GRG nonlinear method by applying random initial trial solution to it. The trial solutions are shown in the Table 6.4 and the optimization result is presented in Table 6.5. It can be observed that the convergence takes place with global optimum solution as solver reaches the same solution with different initial trial solutions.

Table 6.6 Modal parameters of the beams after optimization

Beams	ζ	Frequency (Hz)
Beam1	0.01	2.092
Beam2	0.01	1.525
Beam3	0.01	1.045

The model parameters obtained for all the beams after optimization are presented in Table 6.6. The assembly experiments are carried out using vision systems using the above parameters. The experimental implementation and results are presented in the next subsections.

6.4 Experimental implementation

The experimental setup is same as in the previous chapter 5. The same three beams are used, and the description is given in Table 5.1. The PMEB controller used the data-driven model for the prediction of maximum error. It reduced the t_{mc} drastically from 0.67 s to 0.005 s and leads to an overall reduction in t_{sd}. The reduction in overall system delay

lowers the possibility of skipping the upcoming maximum error in vibration suppression of flexible beams with high frequency. This results in the overall performance improvement of the proposed controller.

6.5 Experimental results

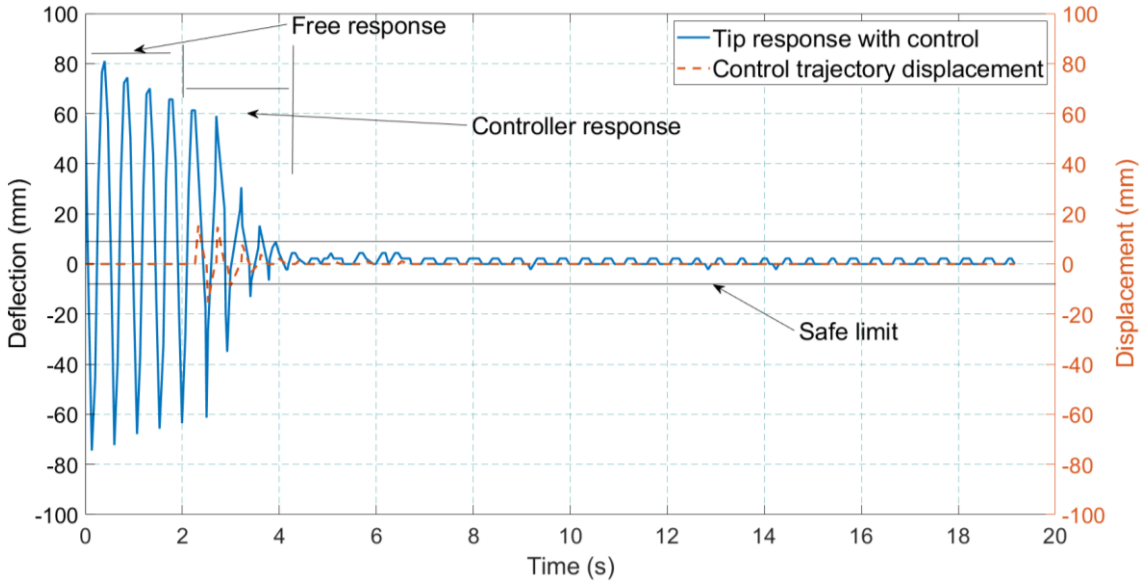

Figure 6.4 The Beam3 tip free and controller response

The working of the proposed method can be demonstrated with a response as shown in Figure 6.4. It is a response of Beam3 that depicts displacement of the straight trajectory and corresponding tip response to the control signal. The initial free response is used for system identification and after obtaining the model the controller activated and suppresses vibration. For all experiments, the velocity of the control trajectory is fixed at 200 mm/s. The maximum tip deflection is 81.03 mm, and the straight motion trajectory is used for vibration suppression. The controller suppresses the vibration in less than 2 s in the safe limit of 10 mm. The controller is turned OFF when the deflection reaches the user-defined safe limit. The other experiments using the straight and wrist trajectories are presented in the next section.

6.5.1 Experimental results with arm motion trajectories

The experiments conducted using the arm motion trajectories provides motion the end-effector of the robot in a straight line. The details of excitation trajectories that is used in these experiments are provided in Table 6.7. These excitation trajectory causes vibration in the beam with different maximum deflection, which must be suppressed in a short time.

Table 6.7 Details of excitation trajectories used in control by straight trajectory.

Trajectory	Displacement (mm)	Velocity (mm/s)
'Trajectory1'	50	200
'Trajectory2'	100	200
'Trajectory3'	50	400
'Trajectory4'	100	400

6.5.1.1 Results of Beam1

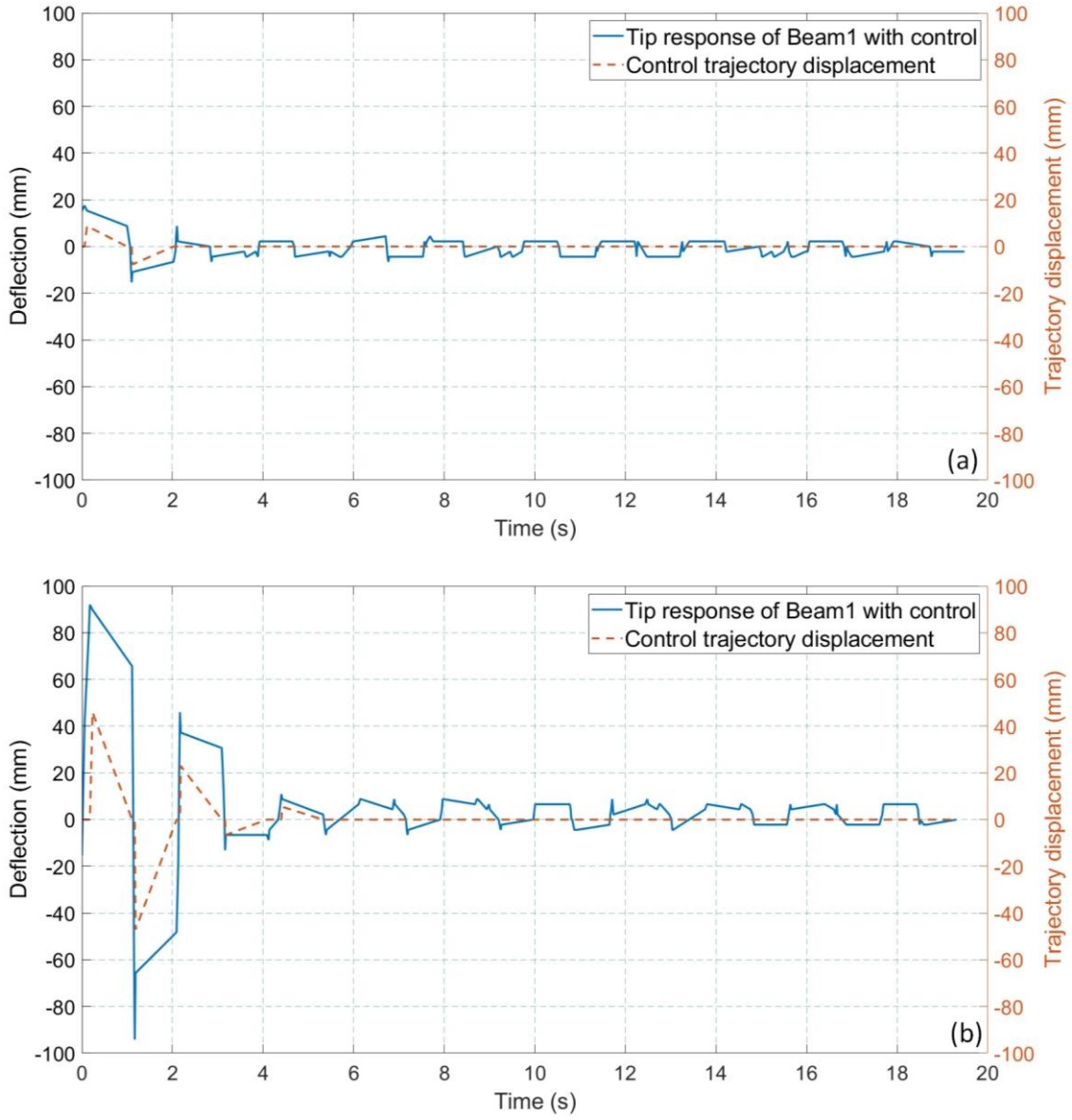

Figure 6.5 Controller response of Beam1 with arm motion and excited by (a) 'Trajectory1' and (b) 'Trajectory2'

The experimental results of Beam1 with excitation 'Trajectory1' and 'Trajectory2' are presented in Figure 6.5. The 'Trajectory1' did not deflect the beam tip significantly may

be due to low speed. However, ‘Trajectory2’ deflected the beam tip by 91.98 mm which takes 50 s to reduce tip deflection without any control. With control it took 5.39 s to suppress the vibration and reduced the vibration suppression time by 90%. The safe limit is 10mm that is adopted for all the experiments.

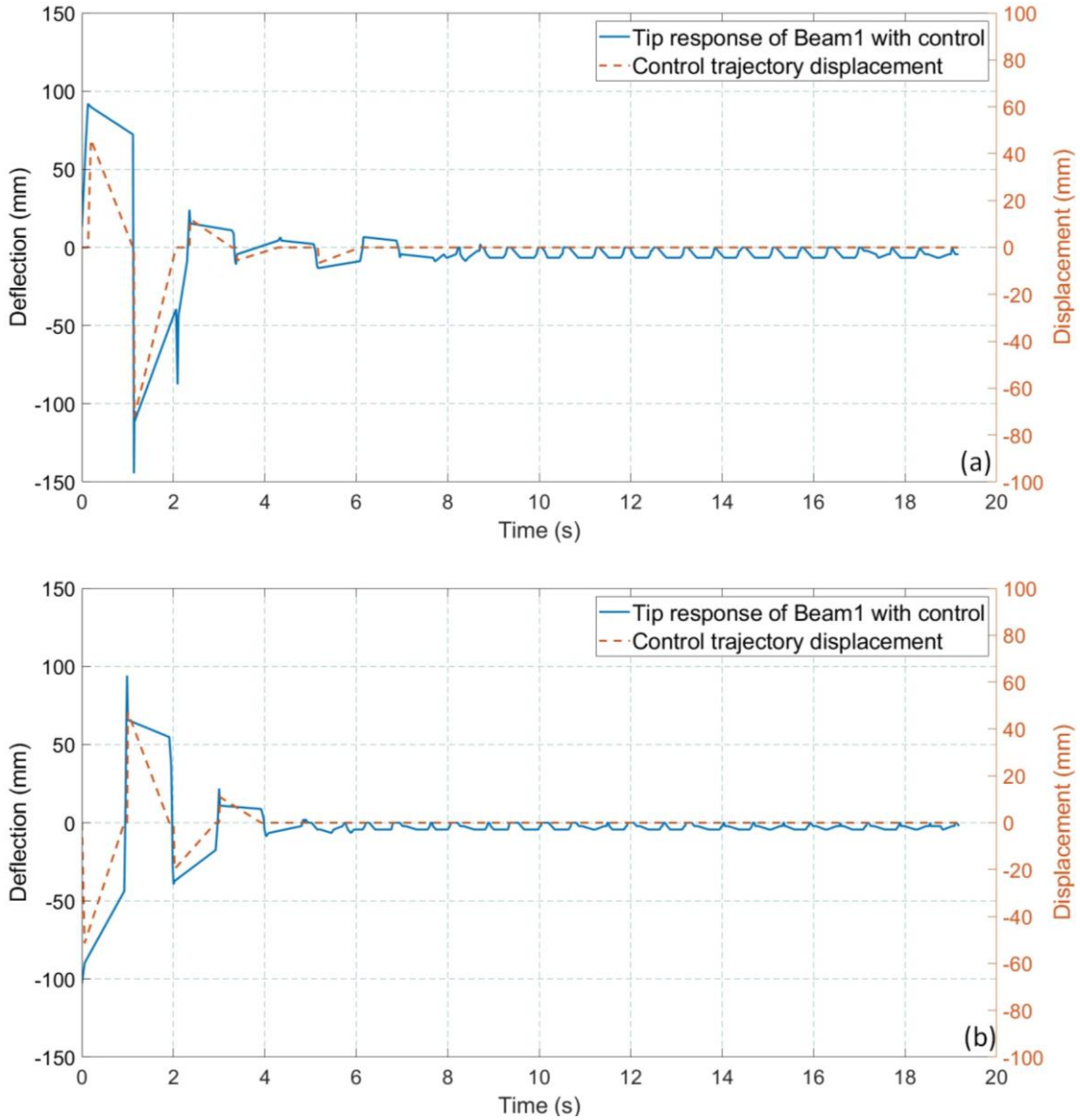

Figure 6.6 Controller response of Beam1 with arm motion and excited by (a) ‘Trajectory3’and ‘Trajectory4’

The results with excitation ‘Trajectory3’ and ‘Trajectory4’ are presented in Figure 6.6. The initial maximum deflection of 102.9 mm is observed with the excitation ‘Trajectory4’. The maximum vibration suppression is achieved up to 95.62% while comparing to the initial maximum deflection and deflection after vibration suppression. The maximum reduction in vibration suppression time is 93.63%, which is achieved in response with

excitation ‘Trajectory1’. Most of the vibration is suppressed in less than 5 s regardless of the initial deflection except for response with ‘Trajectory3’. In this experiment, the vibration is suppressed within 4 s. However, due to measurement error in deflection it exceeded the safe limit that has taken some more time to suppress.

6.5.1.2 Results of Beam2

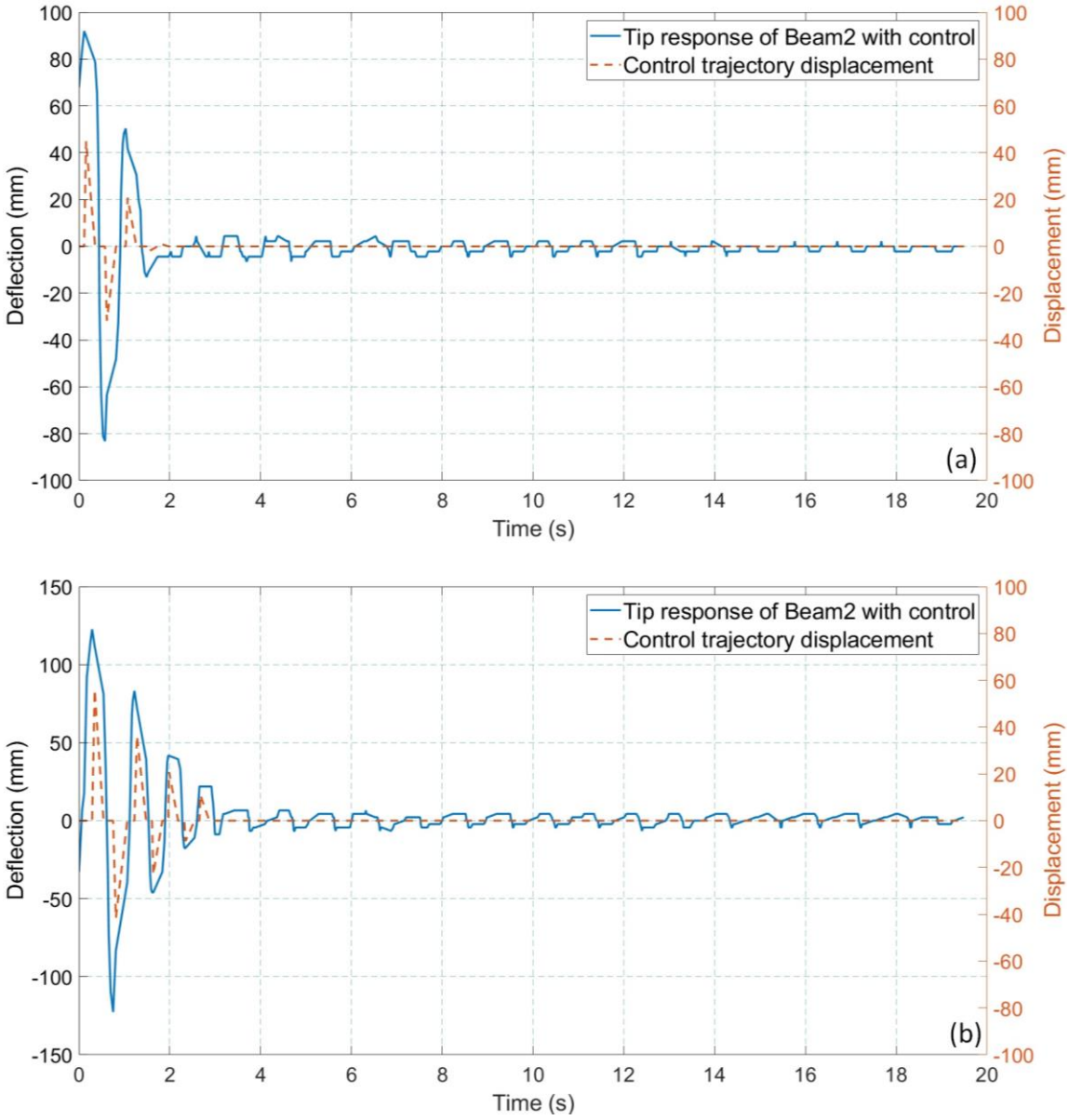

Figure 6.7 Controller response of Beam2 with arm motion and excited by (a) ‘Trajectory1’ and (b) ‘Trajectory2’

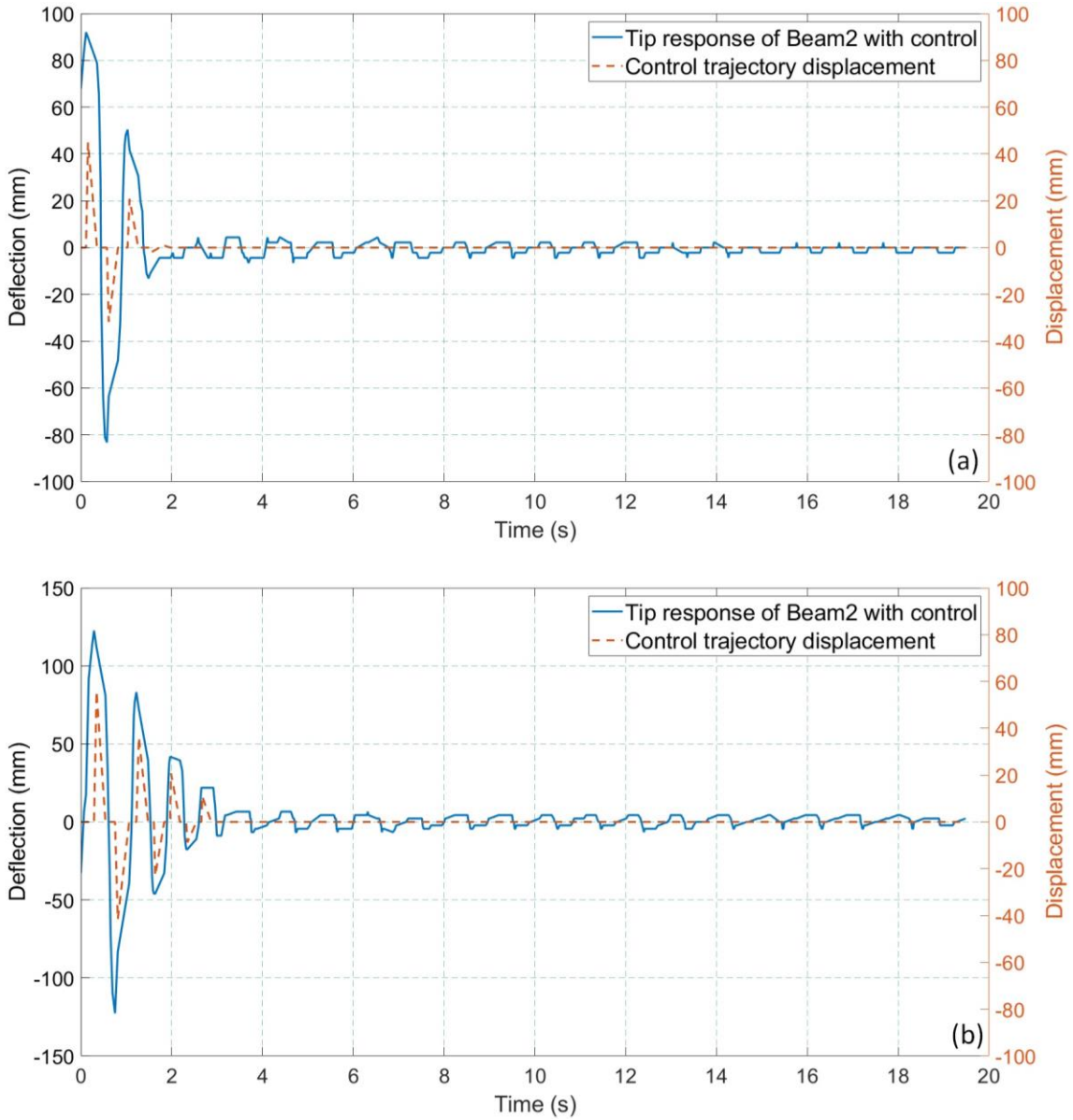

Figure 6.8 Controller response of Beam2 with arm motion and excited by (a) 'Trajectory3' and (b) 'Trajectory4'

The experimental results of Beam2 with the same excitation trajectories are presented in Figure 6.7, and Figure 6.8. The minimum and maximum deflections are 92 mm and 177.4 mm respectively where up to 96.3% vibration amplitude is suppressed. The minimum and maximum suppression time taken to suppress vibration in the safe limit are 1.78 s and 3.42 s. The reduction in suppression time is achieved by 96.64%.

6.5.1.3 Results of Beam3

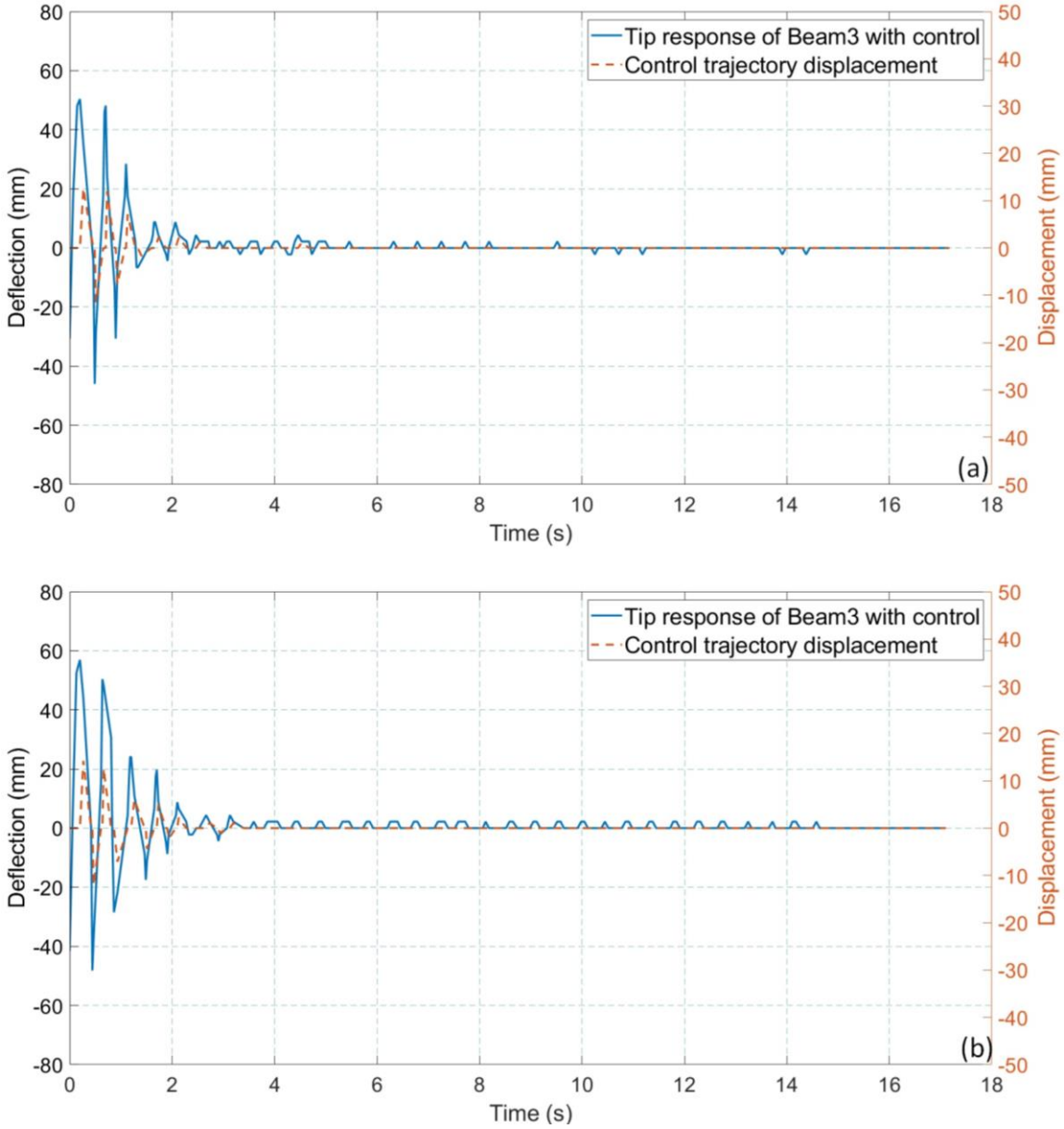

Figure 6.9 Controller response of Beam3 with arm motion and excited by (a) 'Trajectory1' and (b) 'Trajectory2'

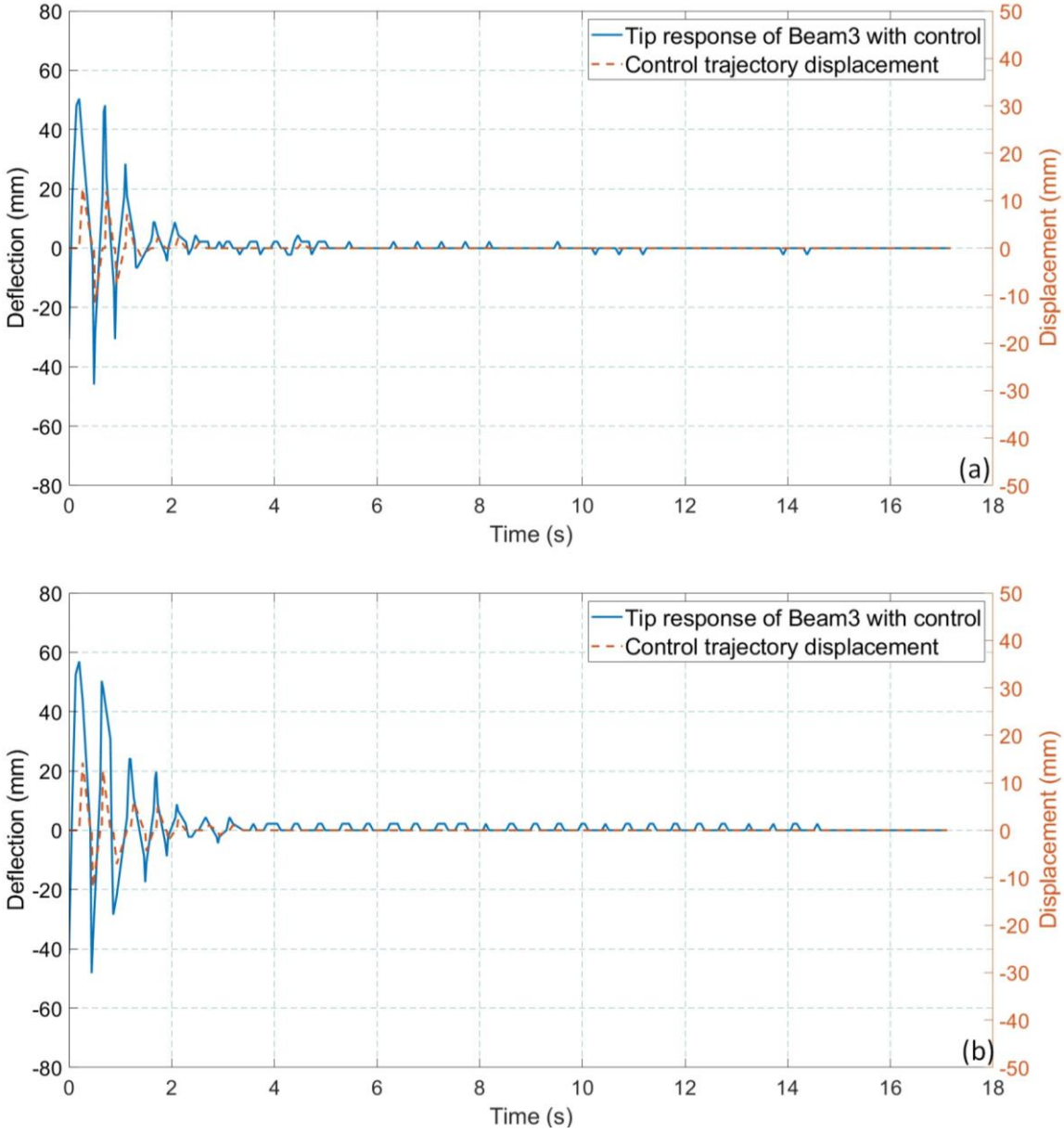

Figure 6.10 Controller response of Beam3 with arm motion and excited by (a) 'Trajectory3' and 'Trajectory4'

The experimental results of Beam3 are presented in Figure 6.9, and Figure 6.10. The minimum and maximum suppression time achieved are 1.73 s and 3.12 s whereas maximum reduction in vibration suppression time is 94.45%. The maximum reduction in vibration amplitude is 96.42%. Each experiment with one trajectory is repeated three times and the summary of the repeated experimental results are provided in Table 6.8. The range of suppression time is shown in Figure 6.11 and the summary of the results is presented in Table 6.9.

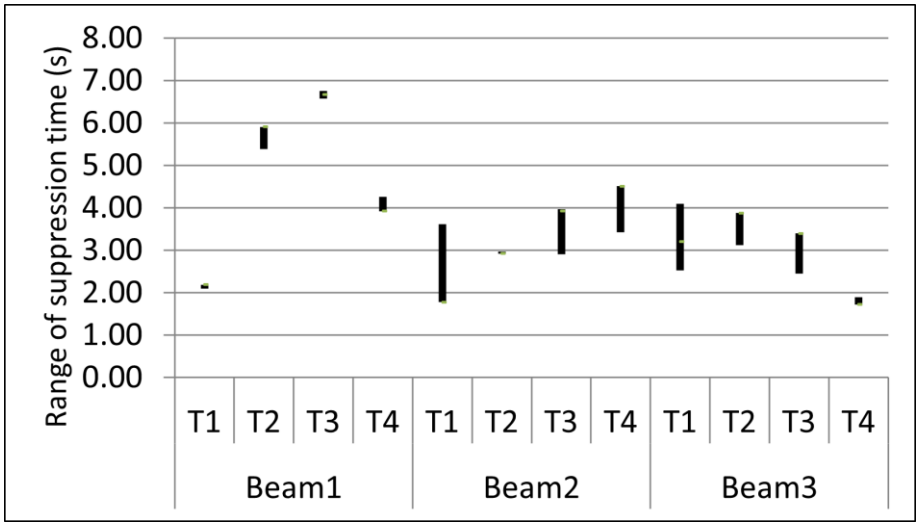

Figure 6.11 The range of suppression time of repeated experiments for all trajectories.

Table 6.8 Summary of repeated results of second stage controller for straight line motion trajectories.

Object	Trajectory	Vibration suppression time (s)			Average suppression time (s)	Range of suppression time (s)	Reduction in average suppression time (%)
		Ex. 1	Ex. 2	Ex. 3			
Beam1	1	2.10	2.17	2.19	2.15	0.09	93.47
	2	5.57	5.39	5.91	5.62	0.52	88.75
	3	6.75	6.57	6.67	6.66	0.18	86.67
	4	4.11	4.26	3.92	4.10	0.34	92.12
Beam2	1	2.53	3.62	1.78	2.64	1.84	95.01
	2	2.97	2.95	2.92	2.95	0.05	94.64
	3	2.91	3.97	3.93	3.60	1.06	93.45
	4	3.42	4.13	4.51	4.02	1.09	93.07
Beam3	1	2.53	4.10	3.21	3.28	1.57	88.29
	2	3.80	3.12	3.88	3.60	0.76	88.00
	3	2.45	3.40	3.39	3.08	0.95	90.06
	4	1.90	1.82	1.72	1.81	0.18	94.15

It has been observed that range of suppression time is higher for Beam2 and Beam3. This may be due error in the determination of model parameters that affect the prediction of the maximum error.

Table 6.9 Summary of results of second stage controller for straight line motion trajectories.

Beam	Trajectory	Initial deflection (mm)	Suppression time without control (s)	Suppression time with control (s)	Vibration amplitude suppression (%)	Reduction in suppression time (%)
Beam1	1	17.92	33	2.10	51.13	93.64
	2	91.98	50	5.39	89.12	89.22
	3	91.98	50	6.57	93.29	86.86
	4	102.90	52	3.92	95.62	92.46
Beam2	1	92.00	53	1.78	95.23	96.64
	2	122.60	55	2.92	92.85	94.69
	3	124.80	55	2.91	93.00	94.71
	4	177.40	58	3.42	96.30	94.10
Beam3	1	50.37	28	2.53	95.00	90.96
	2	56.94	30	3.12	96.15	89.60
	3	59.13	31	2.45	96.30	92.10
	4	61.32	31	1.72	96.42	94.45

6.5.2 Experimental results with wrist motion trajectories

In these experiments, the angular control trajectories are provided by the PMEB controller to suppress vibration of beams. The details of the excitation trajectories are provided in the Table 6.10.

Table 6.10 Details of trajectories used for exciting vibration in beams.

Trajectory	Displacement (mm)	Velocity (mm/s)
‘Trajectory1’	50	250
‘Trajectory2’	100	250
‘Trajectory3’	50	400
‘Trajectory4’	100	400

6.5.2.1 Results of Beam1

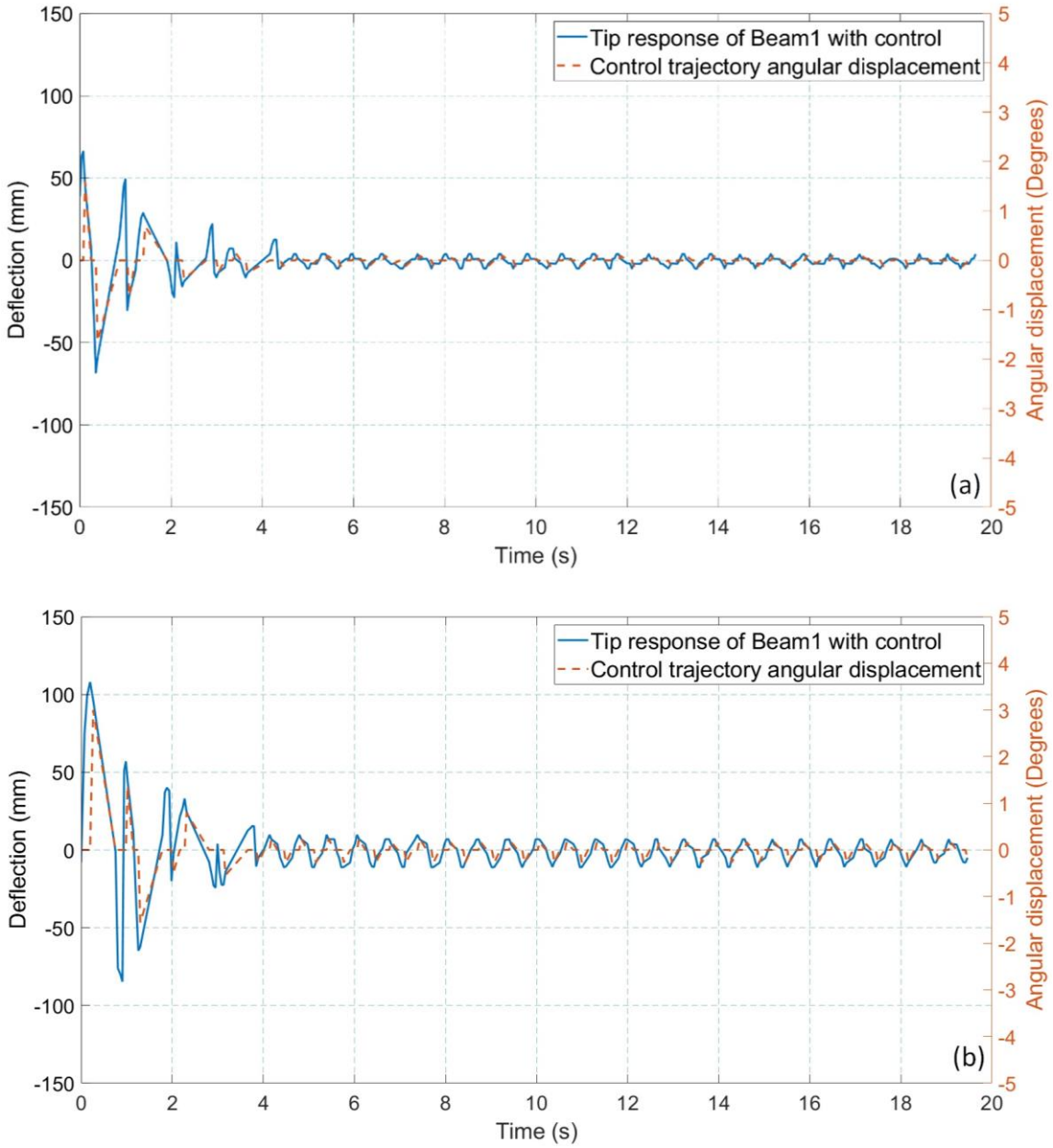

Figure 6.12 Controller response of Beam1 with wrist motion and excited by (a) 'Trajectory1' and (b) 'Trajectory2'

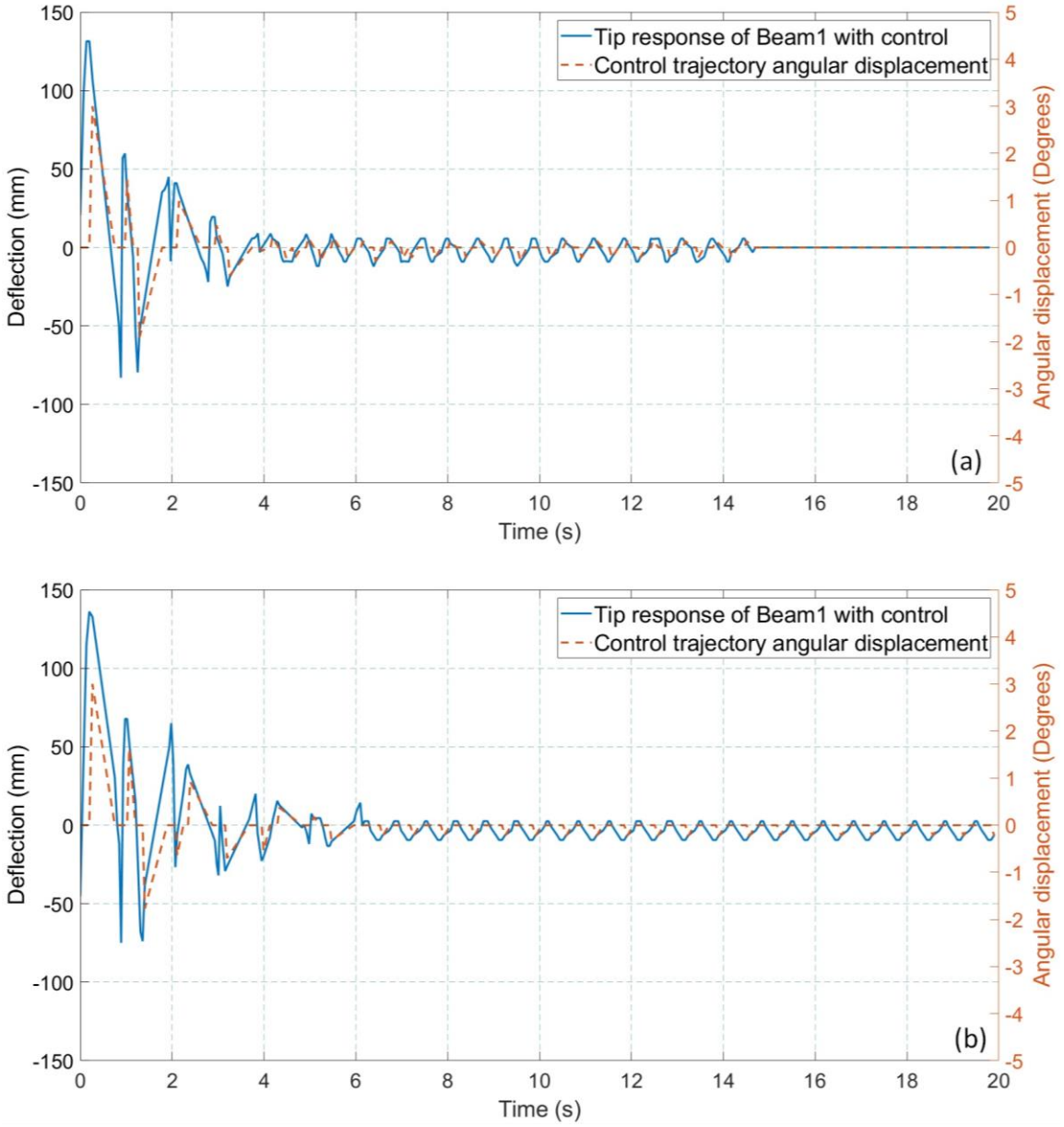

Figure 6.13 Controller response of Beam1 with wrist motion and excited by (a) 'Trajectory3' and (b) 'Trajectory4'

The results of Beam1 excited with the above trajectories are presented in Figure 6.12 and Figure 6.13. The minimum and maximum deflection of beam are observed to be 66.11 mm and 136 mm that takes about 45 s to 54 s in complete vibration suppression without control. The suppression time is achieved from 4.3 s to 6.18 s. The maximum suppression of amplitude is achieved by 95.58% and reduction in suppression time is 92.62%.

6.5.2.2 Results of Beam2

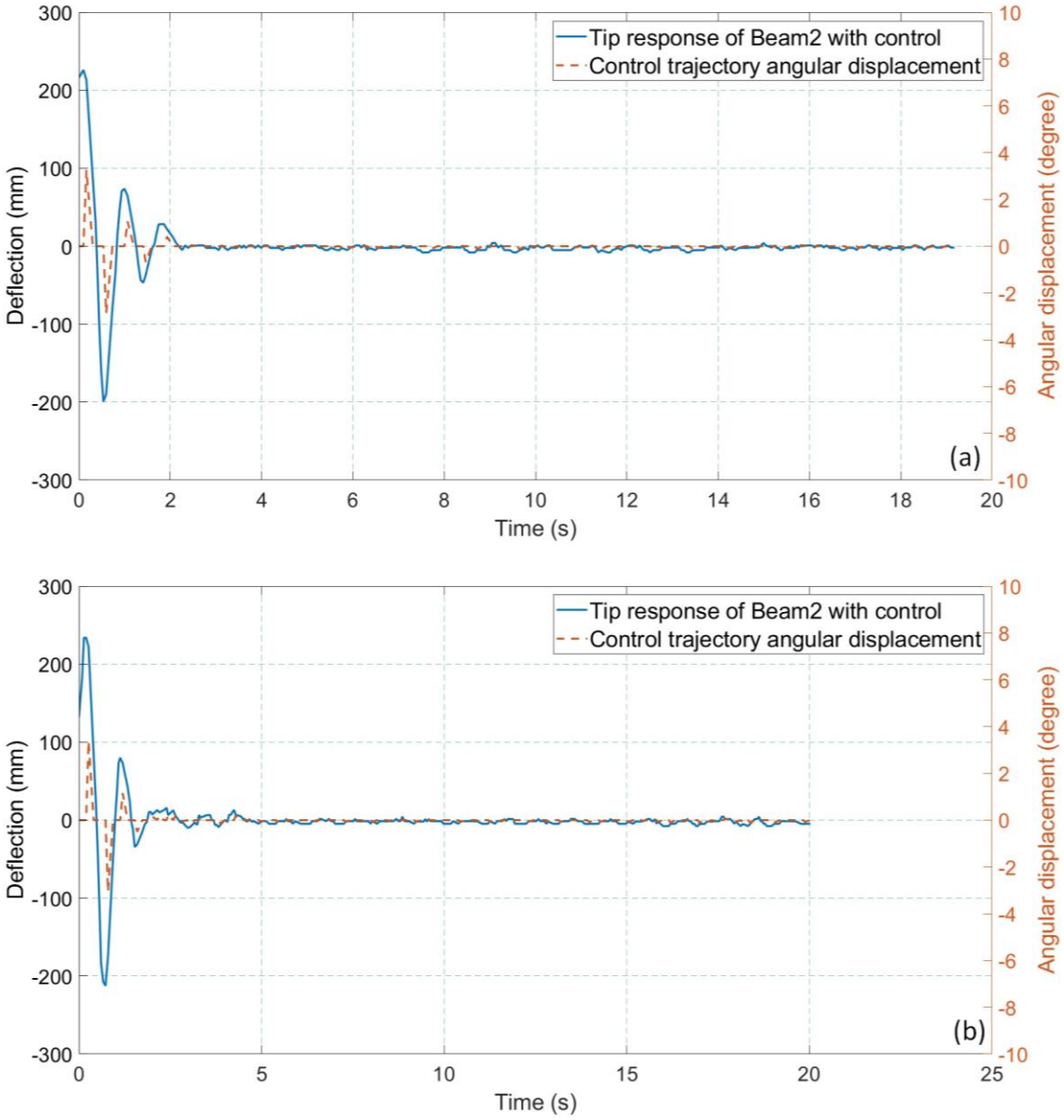

Figure 6.14 Controller response of Beam2 with wrist motion and excited by (a) 'Trajectory1' and (b) 'Trajectory2'

The 'Trajectory1' deflected the Beam2 tip by 226.1 mm and the observed suppression time is 60 s as shown in Figure 6.14 (a). The vision suppression is achieved in 2.26 s. The controller suppressed the vibration amplitude by 98% and reduced the suppression time by more than 96%. The Figure 6.14 (b) presents the results with 'Trajectory2' that achieved ~96% vibration suppression in 2.8 s.

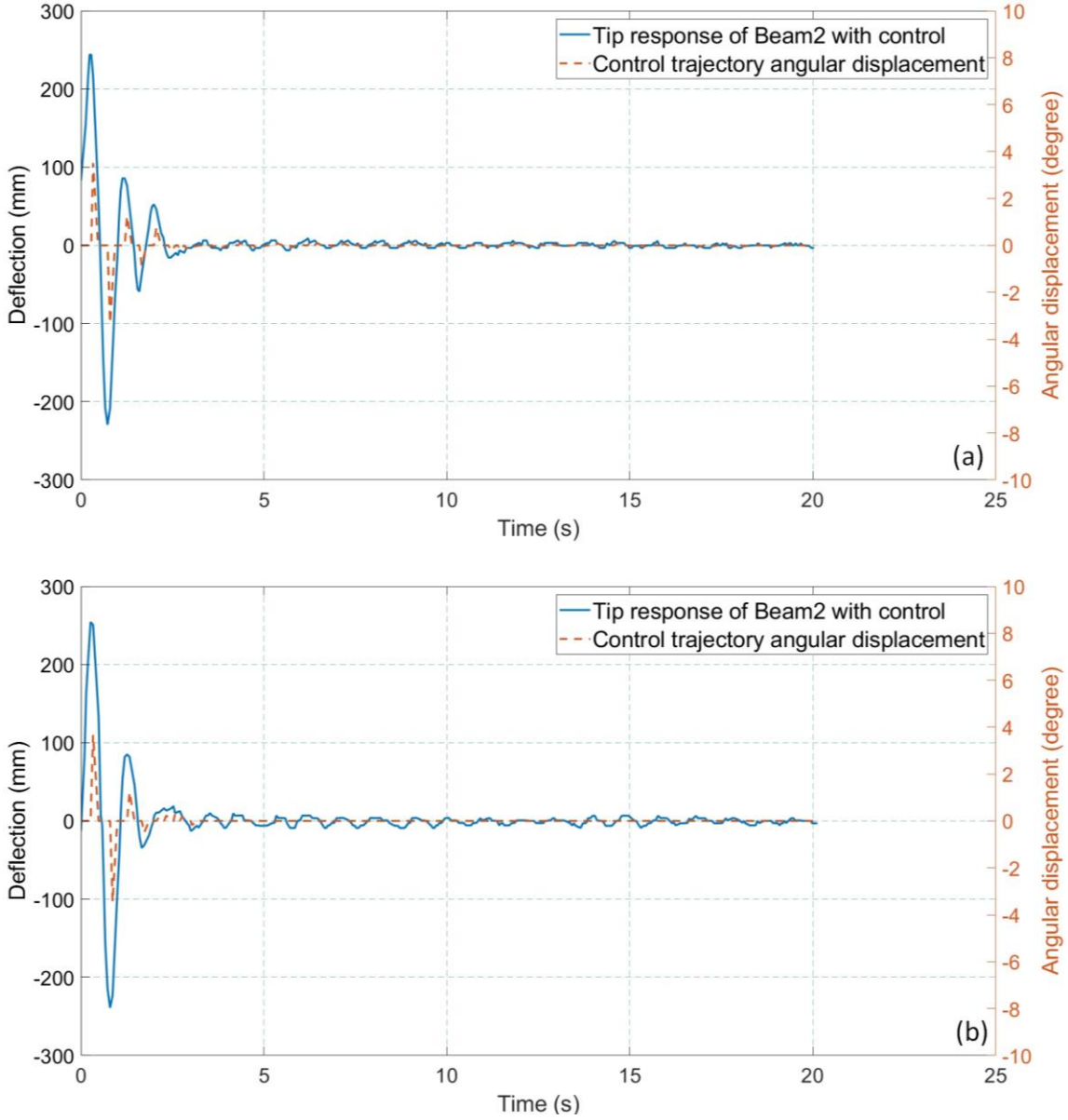

Figure 6.15 Controller response of Beam2 with wrist motion and excited by ‘Trajectory3’ and (b) ‘Trajectory4’

The results of Beam2 are presented in Figure 6.15 with excitation ‘Trajecotry3’ and ‘Trajectory4’. The overall maximum suppression of amplitude is achieved by 98% and reduction in suppression time is 96.23% using the wrist motion trajectories in the controller.

6.5.2.3 Results of Beam3

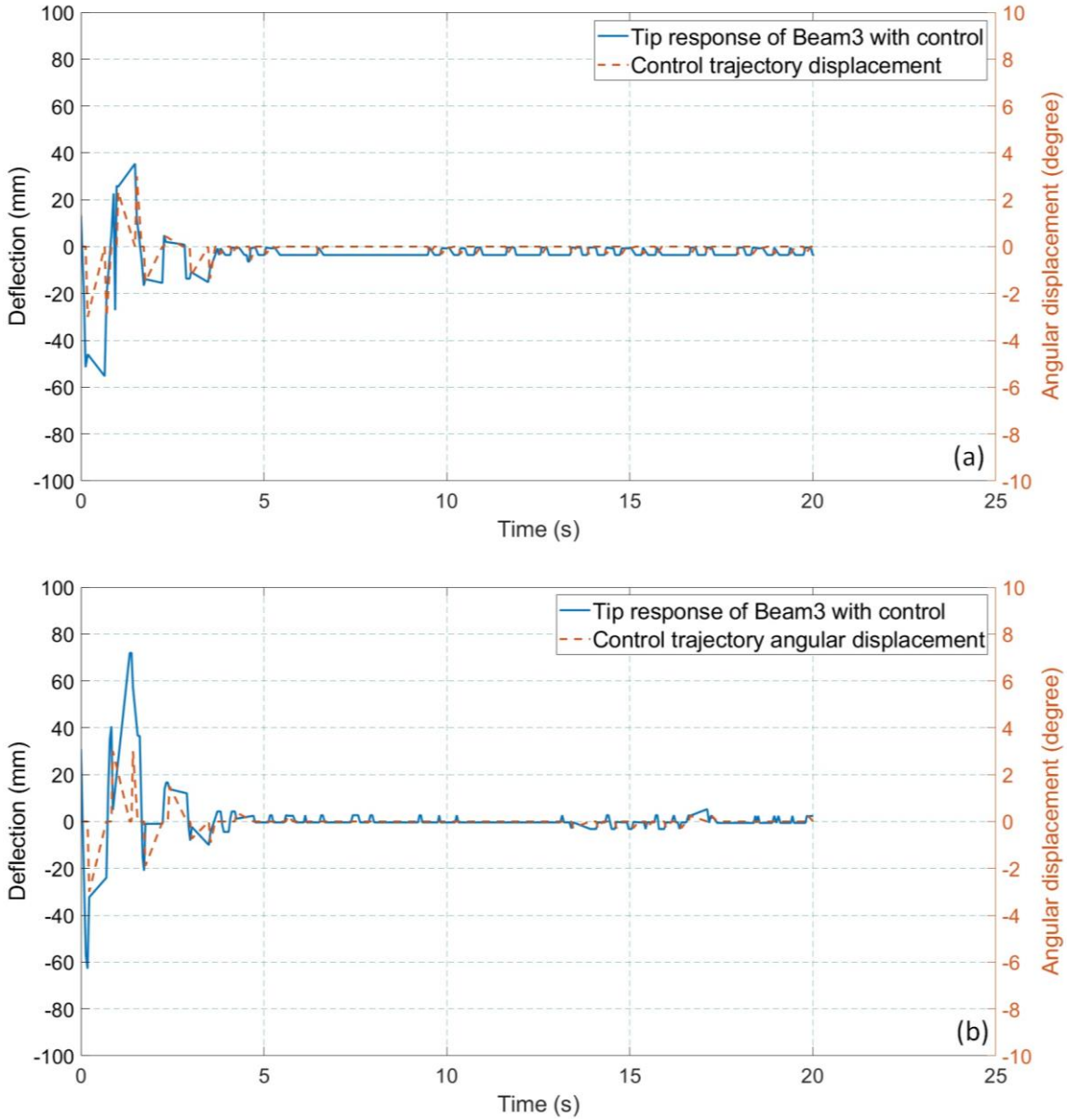

Figure 6.16 Controller response of Beam3 with wrist motion and excited by (a) 'Trajectory1' and (b) 'Trajectory2'

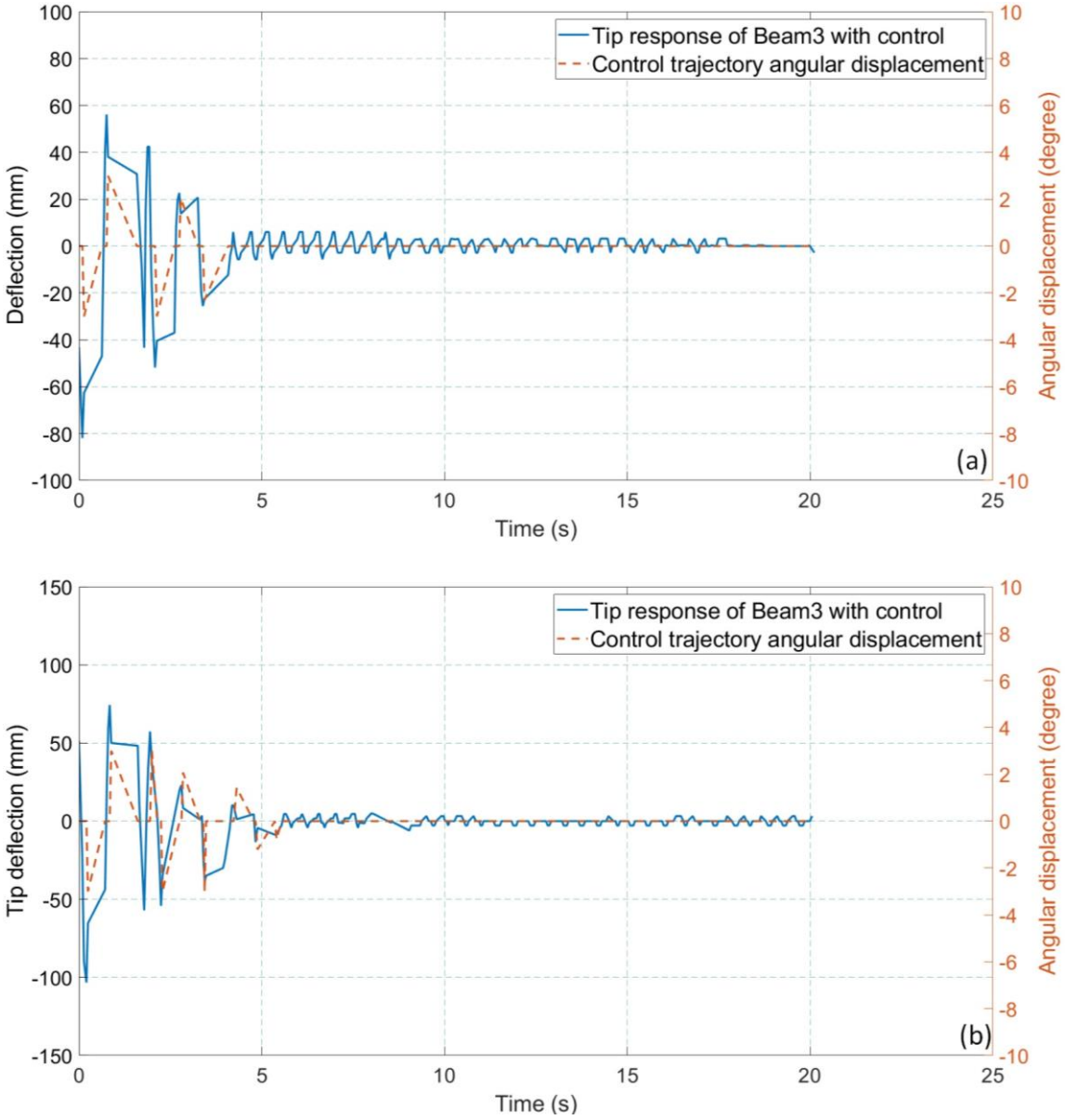

Figure 6.17 Controller response of Beam3 with wrist motion and excited by 'Trajectory3' and (b) 'Trajectory4'

The results of Beam3 are presented in Figure 6.16 and Figure 6.17. The maximum suppression of amplitude is achieved by 96.50% and reduction in suppression time is 88.34%.

The experiments were repeated three times, and the performance is shown in tables above for straight and wrist motion trajectories. The performance of PMEB controller with wrist trajectories is better than the straight trajectories as it takes less suppression time and reduces deflection to the set point closely. However, Beam3 performance is slower as taking more time to suppress vibration than response obtained with the straight trajectories.

The high frequency of the beam compared to other low-frequency beams could cause such controller behavior. Here, providing wrist motion to the beam changes the orientation of the set point as well as the position of the beam without vibration. As a result, due to the high frequency, the error in tip deflection also increases. Though, these issues can be handled by setting a threshold frequency (f_{th}) that can be used to decide whether the controller provides straight or wrist motion trajectories. The threshold frequency is chosen as 2 Hz based on the performance. If the natural frequency (f_n) is less than the threshold, the controller provides wrist motion to the robot end-effector else straight motion trajectory can be used. Another point of view in selecting the type of control motion is energy consumption by the robot during actuation. The angular motion of the wrist does not affect the position of the robot end-effector. All actuator motion is reduced because the angular motion is limited to 3 degrees. Whereas the straight trajectory motion requires the robot actuator to travel further, it consumes more energy. The summary of the repeated results is provided in Table 6.11. The range of suppression time is provided in Figure 6.18 and the summary of results is shown in Table 6.12.

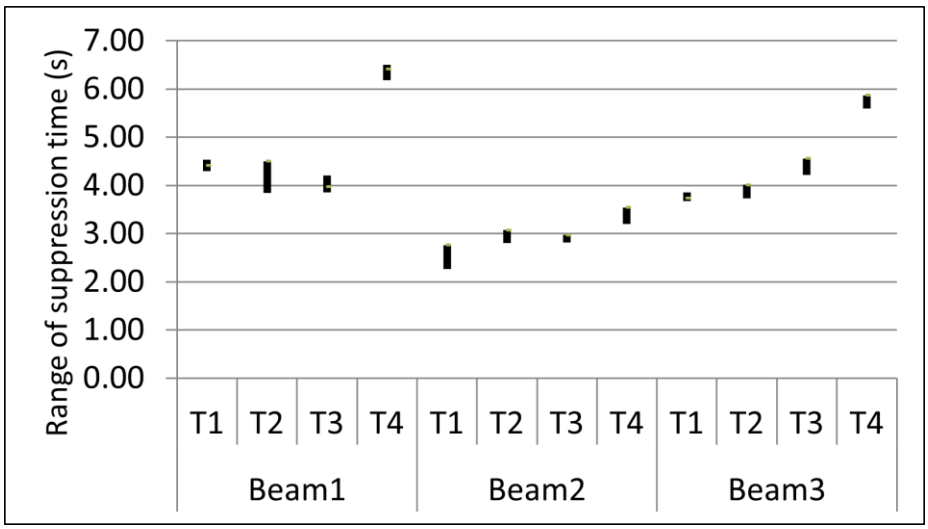

Figure 6.18 The range of suppression time of repeated experiments for all trajectories using wrist motion.

Table 6.11 Summary of repeated results of second stage controller for wrist motion trajectories.

Object	Trajectory	Vibration suppression time (s)			Average suppression time (s)	Range of suppression time (s)	Reduction in suppression time (%)
		Ex. 1	Ex. 2	Ex. 3			
Beam1	1	4.30	4.53	4.41	4.41	0.23	90.19
	2	3.84	4.01	4.50	4.12	0.66	92.08
	3	3.86	4.20	3.97	4.01	0.34	92.43
	4	6.18	6.50	6.41	6.36	0.32	88.22
Beam2	1	2.26	2.53	2.76	2.52	0.50	95.81
	2	2.80	2.95	3.07	2.94	0.27	95.10
	3	2.82	2.85	2.97	2.88	0.15	95.28
	4	3.20	3.31	3.54	3.35	0.34	94.51
Beam3	1	3.67	3.85	3.74	3.75	0.18	87.49
	2	3.73	3.90	4.01	3.88	0.28	87.88
	3	4.22	4.48	4.56	4.42	0.34	87.00
	4	5.60	5.70	5.87	5.72	0.27	84.10

Table 6.12 Summary of results of second stage controller for wrist motion trajectories.

Beam	Trajectory	Initial deflection (mm)	Suppression time without control (s)	Suppression time with control (s)	Vibration suppression (%)	Reduction in suppression time (%)
Beam1	1	66.11	45	4.3	92.59	90.44
	2	108.00	52	3.84	90.74	92.62
	3	131.40	53	3.86	93.53	92.72
	4	136.00	54	6.18	95.58	88.56
Beam2	1	226.1	60	2.26	97.83	96.23
	2	233.90	60	2.80	95.72	95.33
	3	243.83	61	2.82	97.40	95.38
	4	254.30	61	3.2	98.00	94.75
Beam3	1	51.46	30	3.67	96.50	87.77
	2	62.83	32	3.73	93.30	88.34
	3	81.92	34	4.22	92.67	87.59
	4	103.4	36	5.6	95.55	84.44

Table 6.13 Comparison of performance of the proposed method with other methods

References	**Method**	**Amplitude suppression (%)**	**Suppression time reduction (%)**
(Yue and Henrich, 2006)	DLO vibration reduction using Fuzzy controller with force/torque sensor	97.00%	92.00%
(Huang *et al.*, 2014)	DLO vibration reduction using PID with vision sensor	96.00%	75.00%
(Kapsalas *et al.*, 2018)	Al beam vibration reduction using I-type controller with force/torque sensor	97.00%	83.09%
Proposed work	Data based PMEB controller	98.00%	96.23%

6.6 Conclusion

A system identification approach is presented using the robot vision approach for the active vibration suppression regardless of material and dimension of beams. The system identification method used a GRG nonlinear solver to optimize the assumed model of the response of a flexible beam using tip deflection data of the beam obtained using the robot vision. The optimized model of beams is used in PMEB controller with both straight and wrist motion trajectories to suppress vibration. The performance of the controller is analyzed by comparing straight and wrist trajectories results. Based on the performance of controller, natural frequency based selection of control trajectory is suggested for best performance. The result obtained justifies the implementation of system identification method in the PMEB control.

CHAPTER 7
CONCLUSIONS AND FUTURE PROSPECTIVES

The thesis encapsulates the development of vision-based control strategies for vibration suppression due to flexibility observed in the object, wrist of a robot system and orientation of an object during assembly operation. To achieve the end result of the identified objectives the chapters are presented in succession. In which the respective chapters discuss the development of vision based controller for an industrial robot (i) To suppress residual vibration of the non-deformable object (NDO) for peg in hole assembly scenario (ii) To suppress the residual vibration of the NDO with wrist/gripper flexibility, for peg in hole assembly scenario (iii) To suppress the residual vibration in horizontal beams for beam and slot assembly scenario using arm and wrist motion (iv) To suppress the residual vibration in horizontal beams for beam in slot assembly scenario using arm and wrist motion with less computational burden on controller.

Every chapter has concluded the work achieved without consolidating the aims and objectives of the thesis. This chapter provides a summary of the important contributions of the thesis. The contributions of the research in robot vision and vibration suppression of flexible objects in a robotic assembly are addressed in section 7.1. The limitations and the outlines of future work are presented in sections 7.2 and 7.3, respectively.

7.1 Contributions

In summary, this thesis reviewed existing literature on robotic assembly and identified research gaps related to vibration suppression methodologies. The challenges in robotic assembly include object flexibility, delays, limited access to the robotic system, camera calibration, and vision systems.

The thesis proposed several vibration suppression strategies to address these gaps using vision-based active high-level control strategies. In chapter 3, a control strategy using a vision sensor was proposed to suppress vibration during the robotic assembly of a non-deformable object. Chapter 4 explored the impact of flexible gripper objects on vibration and proposed a PVAEB controller. Chapter 5 proposed a robot-vision based controller for suppressing the vibration of a flexible beam. Chapter 6 developed a methodology for system identification of flexible objects to enhance the performance of PMEB controller.

The proposed strategies were developed using a variety of approaches, including modeling flexibility due to flexible gripper, FEM-based modeling of flexible beams, robot-assisted camera calibration, and virtual marker based object identification. Here the developed control systems could handle various materials and dimensions of flexible objects and were updated using the robot-vision method. In these approaches, the vibration of the flexible beam was reduced by providing control input in the form of straight and wrist motion trajectories. The important contributions of each chapter and improvements in the proposed work are presented in Table 7.1.

Table 7.1 Comparison and improvement in proposed work.

	Chapter 3	**Chapter 4**	**Chapter 5**		**Chapter 6**	
Object type	NDO	NDO with a flexible gripper	Flexible beams		Flexible beams	
Object position	Vertical	Vertical	Horizontal		Horizontal	
Object modeling method	Physics-based model	Physics-based model	FEM-based Model		Data-driven model	
Camera calibration	Checkerboard method	Checkerboard method	Robot-assisted		Robot-assisted	
Vision feedback	Amplitude	Amplitude	Tip deflection		Tip deflection	
Proposed controller	SPVAEB	PVAEB	PMEB		PMEB	
Types of control motion	Arm motion	Arm motion	Arm motion	Wrist motion	Arm motion	Wrist motion
Maximum reduction vibration amplitude	96%	95%	98%	97%	97%	98%
Maximum reduction in suppression time	98%	90%	96%	98%	97%	97%

Table 7.1 shows the types of objects, object positions, and modeling methods in the respective chapters. The proposed control strategies include camera calibration methods and vision-based feedback. Finally, the performance of the proposed controllers using arm and wrist motion is presented. Overall, the thesis has made significant contributions to the field of vision-based active high-level vibration suppression strategies for industrial robots in the presence of flexibility and delays.

The key accomplishments can be summarized as follows:

- A camera calibration method is proposed to measure the extrinsic parameters of the vision sensor without needing a physical reference or marker from the robotic system. It eliminates the need to place the camera sensor at a known position in the robot workspace.
- A low-cost camera robot vision method is developed that can be used for multiple purposes, such as identifying the object grasped by the robot gripper, measuring the dimensions of identified objects, analyzing the vibration behavior of flexible objects, and providing feedback for assembly.
- A prediction-based vibration suppression methodologies have been proposed for both deformable and non-deformable objects and successfully implemented on an NDO that behaves like a simple pendulum. The method uses a simple camera as feedback and a vision-based SPVAEB second-stage controller to suppress vibrations.
- In developing a vision-based controller, a FEM-based beam model is used to suppress vibrations in flexible beams. The parameters of the model are updated using robot vision feedback, and the controller is designed to minimize the maximum error in vibration using straight and wrist motion trajectories.
- A vision-based system identification method is proposed to identify the vibration behavior of flexible objects, which can predict the maximum error in vibration and determine the straight and wrist motion trajectories that suppress the vibration.
- The proposed methods handled the inherent delays due to the robot system, the vision system, and model processing intelligently so that the controlled inputs are timed properly. The performance of the controller is compared with other methods available in the literature and validated through experiments on an industrial robot without modifying its internal controller.
- An approach for wrist motion is proposed that reduces the vibration in beams and consumes reduced energy compared to control using arm motion of robot. The angular motion of the wrist does not affect the position of the robot end-effector. All actuator motion is reduced because the angular motion is limited to only one joint axis. In contrast, the straight-line trajectory motion requires the robot actuator to actuate all the arm joints, which requires more energy.

The following subsection describes some of the limitations of the present thesis and discusses the future scope.

7.2 Limitations of the proposed research

- The current vision sensor is unsuitable for measuring high frequencies of more than 9 Hz vibration due to the Nyquist condition and reduced frame rate caused by the image processing algorithm. Moreover, the low shutter speed of camera results in blurry images of the object in motion, leading to inaccurate vibration estimation at high speeds. A high-speed camera with a fast shutter speed and a high-end computer processor is required to overcome these limitations.
- The ability of the proposed vision system to identify objects is limited to their color only. Objects with multiple colors or complex patterns can be challenging to identify. Moreover, the RGB values of background may overlap with the RGB range of objects, leading to incorrect beam dimension measurements by the robot vision. In the present monocular camera the dimensional measurement error is 3% and use of stereo camera will have improved accuracy.
- For the effective modeling of flexible beam using FEM model, the Rayleigh damping coefficients should be identified based on the material properties and shape before implementation of the vibration suppression strategies.
- The proposed vibration suppression methodologies used the first mode of vibration of flexible objects only. This method will be applicable for 2D or in-plane vibration of flexible beams. A stereo vision system would be necessary to handle three-dimensional vibrating systems. Therefore, flexible system with higher modes of vibration would be challenging to suppress its vibration by the proposed methodologies.
- During assembly of beam in slot the safety limit was ±10 mm. Therefore, robotic assembly with smaller safety limit will require longer time and the flexible beam may become unstable during vibration suppression process.
- Designing trajectories for vibration-free translation of objects is a crucial aspect of vibration control. However, commercially available industrial robots have hardware limitations that restrict acceleration variation during a PtP motion with a trapezoidal velocity profile, which makes it impractical to achieve vibration-free translation.

7.3 Future Perspectives

For the research work covered in this thesis, there are several potential areas of further research regarding the vision for vibration analysis and suppression in robotic assembly. Some perspectives are:

- In future work, a 3D vision sensor can be used to measure the out-of-plane vibration of flexible objects such as wires, round beams, and sheets, which was not addressed in the present study.
- The strategy for handling flexible objects should be designed to allow the robot to grasp the beam at any position rather than only at one end.
- High-capacity hardware can be used to speed up the image processing during robot assembly using vision system. Even the accuracy of vibration response prediction will improve and will be able to handle vibration frequency more than 9Hz.
- In the future, suitable image processing methods need to be developed to detect and control the higher mode vibrations.
- An AI-based system identification method for the controller may be explored for complex 3D flexible objects to suppress the vibration and evaluate the effectiveness of the controller.

APPENDICIES

Appendix A: Technical details of ABB 1410

The specification of ABB 1410 industrial robot:

Robot type	-	ABB 1410
Structure	-	Articulated
Handling capacity	-	5 kg
Reach	-	1.44 m
Robot weight	-	225 kg
Repeatability	-	0.05 mm
Robot controller	-	IRC5 controller

Robot workspace side view-

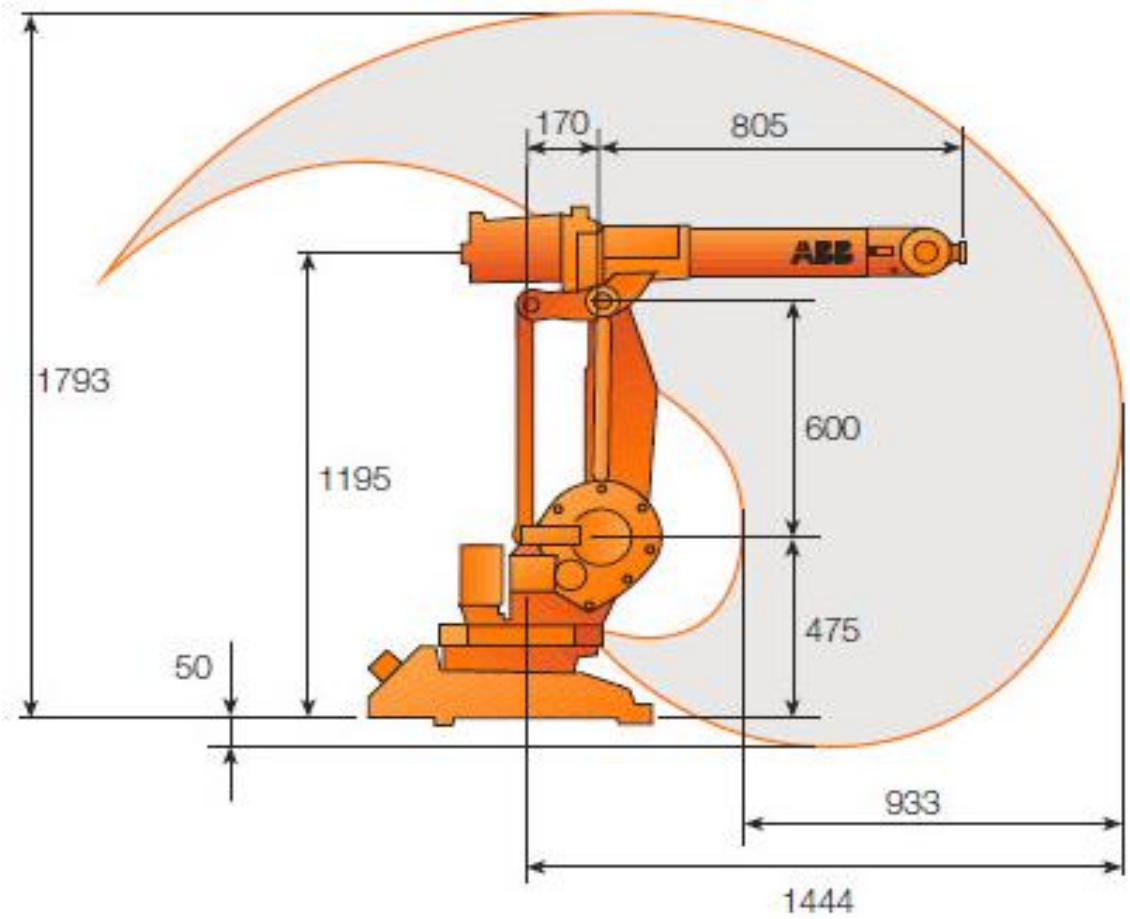

Figure A.3.1 ABB 1410 robot workspace side view.

Robot motion

Axis	Type of motion	Range of movement
1	Rotation motion	+170 to -170
2	Arm motion	+70 to -70
3	Arm motion	+70 to -65
4	Rotation motion	+150 to -150
5	Bend motion	+115 to -115
6	Turn motion	+300 to -300

Velocity (1-phase power supply)

Axis 1	Axis 2	Axis 3	Axis 4	Axis 5	Axis 6
105/s	105/s	105/s	280/s	280/s	280/s

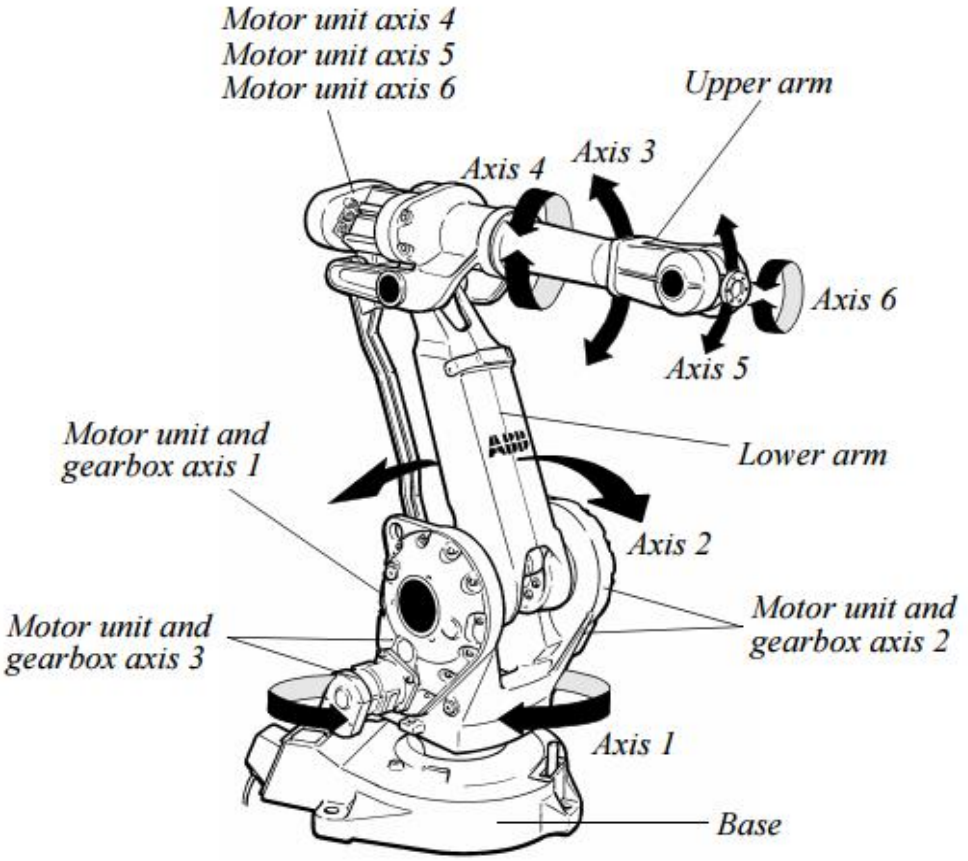

Figure A.3.2 Robot structure with joint rotation direction and motor unit.

Appendix B: PMEB simulation responses

The stability of the proposed controller cannot be tested with the available techniques such as the root-locus technique. Therefore, stability is tested by observing the controller performance with various controller parameters. Some simulation results are presented that describe the performance of the controller with different K_p values in Figure B.5.1. The suppression time decreases while gradually increasing the K_p value from 0.1 to 0.4. Further increment in *Kp* requires high acceleration to achieve a valid trapezoidal velocity profile which is practically impossible to obtain. Two results with K_p = 0.5 and 1 are presented in Figure B.5.2 and B.5.3 to describe such limitations. Increasing the controller parameter turns the controller aggressive which ultimately requires control input trajectory of high displacement within a very short travel time. This condition raises the requirement of an unrealistic hike in acceleration. Therefore, the controller is stable in region $0 < Kp \leq 0.4$ and unstable above 0.4.

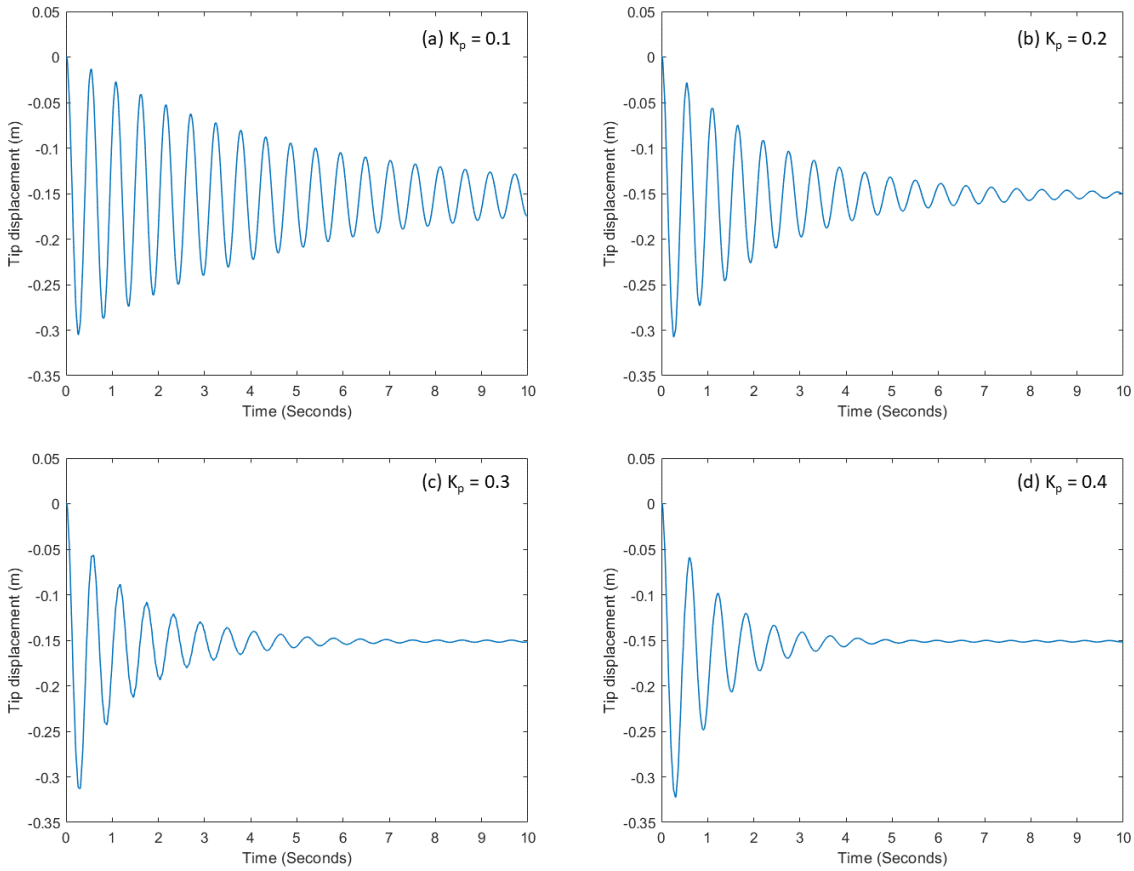

Figure B.5.1 Simulation response with K_p = 0.1, 0.2, 0.3 and 0.4

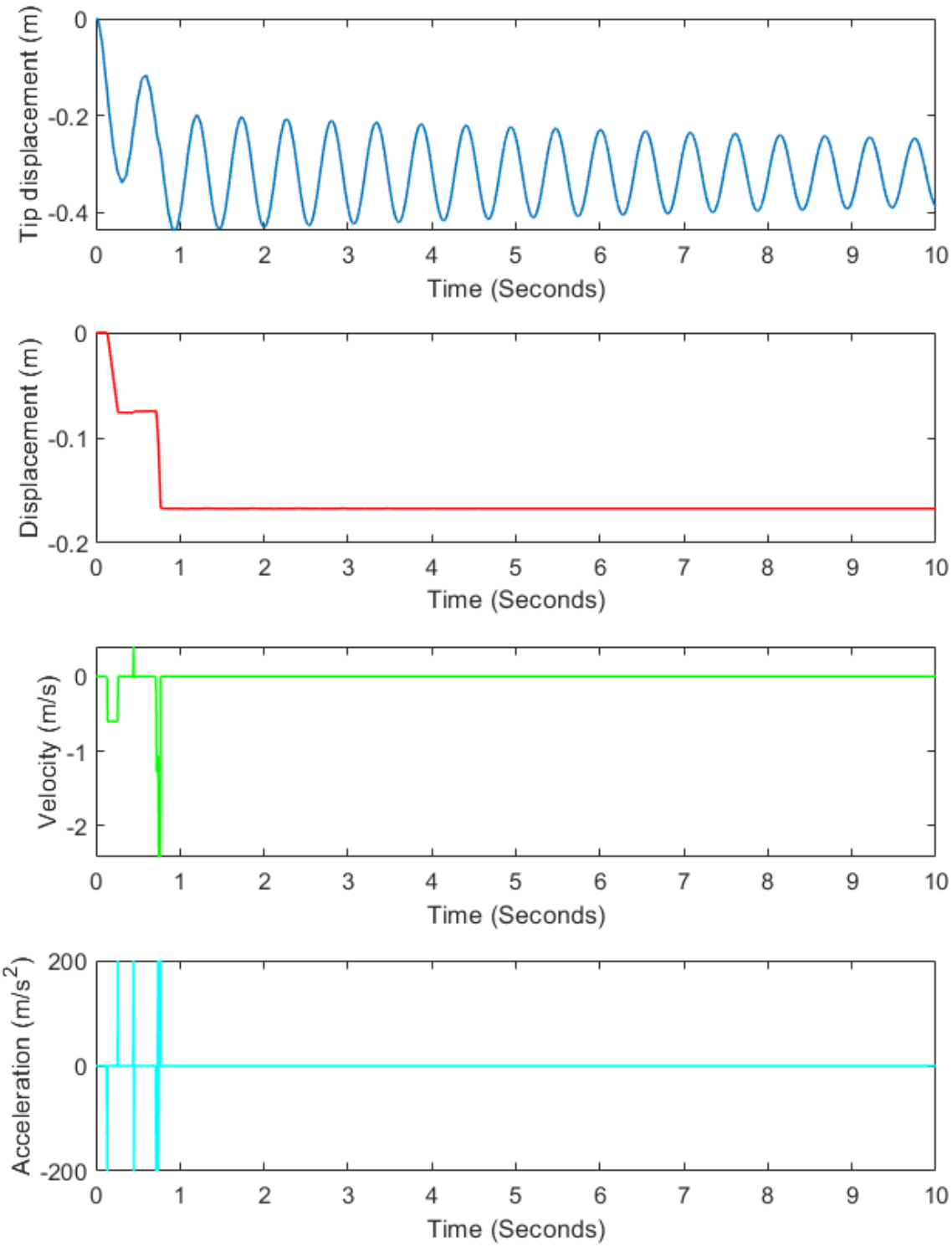

Figure B.5.2 Simulation response with K_p = 0.5

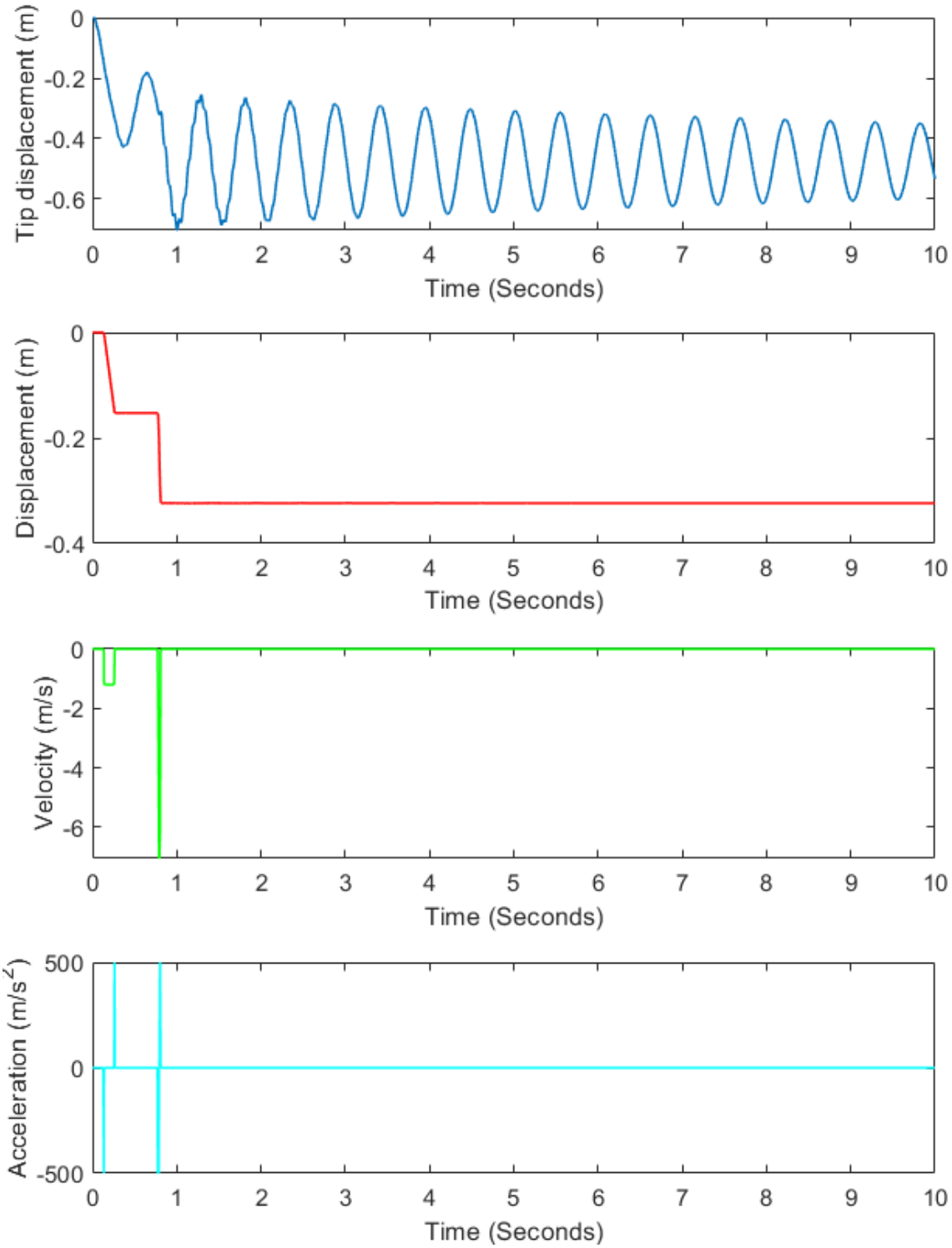

Figure B.5.3 Simulation response with $K_p = 1$

Appendix C: Camera calibration using checkerboard.

Table C.5.1 presents the intrinsic and extrinsic parameter of the camera used in the current system. The intrinsic camera parameters are obtained using the MATLAB camera calibration application. The checkerboard image is presented in Figure C.5.1. The extrinsic parameter is obtained using the proposed camera calibration approach discussed in section 5.3.1. These extrinsic parameters show the position of the vibration plane of the flexible beam in which the experiments have been conducted.

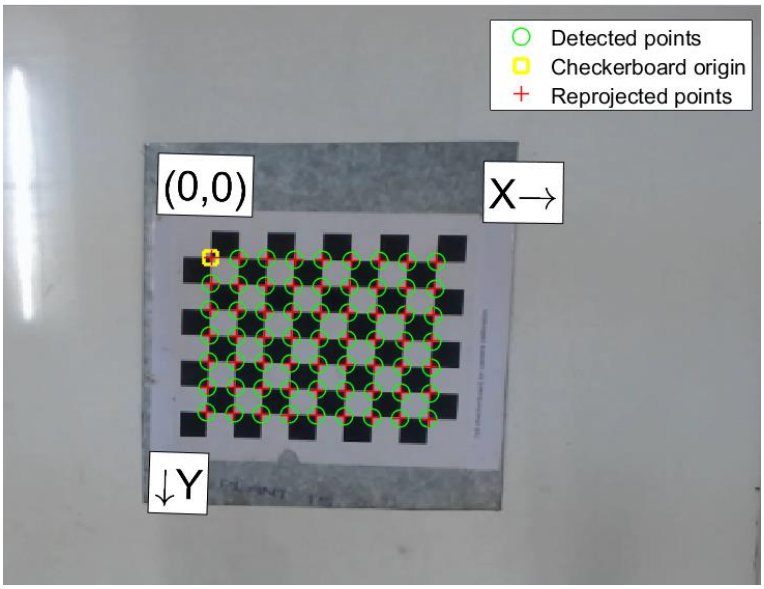

Figure C.5.1 Checkerboard used in camera calibration for intrinsic parameters.

Table C.5.1: Intrinsic and extrinsic parameters of the camera

Intrinsic camera parameters		
Focal length (pixels)	505.0664 ± 0.5486	503.3715 ± 0.6160
Principal point (pixels)	313.1068 ± 0.1953	238.8168 ± 0.3371
Radial distortion	0.0849 ± 0.0020	-0.1901 ± 0.0039
Extrinsic camera parameters		
Rotation vector ($[x_\theta\ y_\theta\ z_\theta]$) (rad)		
0.3069 ± 0.0045	-0.0211 ± 0.0044	-0.0578 ± 0.0009
Translation vector ($[x\ y\ z]$) (mm)		
171.2569 ± 0.5847	-54.6520 ± 0.8867	1303.8831 ± 2.4071

Appendix D: FEM based mathematical modelling of flexible beam.

The equation of motion model is derived using Hamilton's principle (Rao, 2007):

$$\int_{t_1}^{t_1} (\delta K_e + \delta W - \delta P_e) dt = 0 \tag{D.1}$$

Where K_e is the kinetic energy, P_e is the total potential energy generated by the bending moment of the beam, and W is the work done by the external force $f(x,t)$, and corresponding expressions are represented in equations (D.2) – (D.4).

$$T = \frac{1}{2}\rho A \int_0^l \dot{w}^2 \, dx \tag{D.2}$$

$$P = EI \int_0^l w_{,xx}^2 dx \tag{D.3}$$

$$W = \int_0^l f(x,t) w dx \tag{D.4}$$

Substituting the above equations in equation (D.1), and after application of the process of variation and simplification, the equations of motion are derived as follows (Rao, 2007)

$$\rho A \frac{d^2 w}{dt^2} + EI \frac{d^4 w}{dx^4} = f(x,t) \tag{D.5}$$

Following boundary conditions are applied to the dynamic model of flexible beam.

$$w(0,t) = 0, \frac{dw(0,t)}{dx} = 0 \tag{D.6}$$

$$\frac{d^2 w(l,t)}{dx^2} = 0, \frac{d^3 w(l,t)}{dx^3} = 0 \tag{D.7}$$

The continuous models are computationally expensive and have very limited application in vibration control problems. Whereas the discretized model approximates the solution in simple mathematical form within the acceptable error range. Thus, the discretized model of above continuous model is used. In this case, the finite element method (FEM) is chosen to discretize the model.

The flexible beam is considered as an assemblage of 1D elements since the height and width are small compared to the length of the beam. The approximation of the dynamic model equations (D.5)-(D.7) is determined by implementing the Galerkin method to

develop the discrete system model. The transverse displacement $w(x,t)$ of the flexible beam is represented by:

$$w(x,t) = \vec{\phi}^{t}(x)\vec{q}(t) \tag{D.8}$$

where $\vec{q}(t)$ is the nodal displacement vector, and $\vec{\phi}(x)$ is the shape function vector.

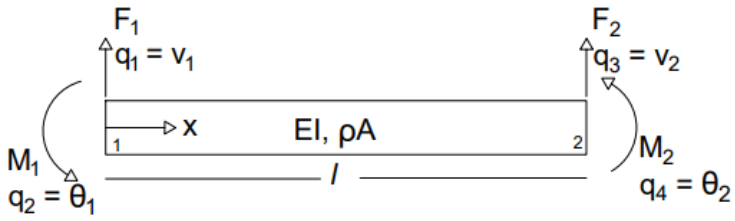

Figure D.1 Free body diagram of beam element

A typical Euler-Bernoulli beam element can be represented by four degrees of freedom shown in Figure D.1. Therefore, the nodal displacement vector must have four nodal displacement elements $[q_1(t), q_2(t), q_3(t), \text{and } q_4(t)]$ and four shape function $[\phi_1(x), \phi_2(x), \phi_3(x), \text{and} \phi_4(x)]$. The $q_1(t)$, $q_3(t)$ are transverse displacements and the $q_2(t)$, $q_4(t)$ are angular displacements. The transverse displacement field within the element is assumed to be a cubic equation (Rao, 2018) in *x*.

$$w(x,t) = a_0 + a_1 x + a_2 x^2 + a_3 x^3 \tag{D.9}$$

The above equation must satisfy the following boundary conditions.

$$\left.\begin{aligned} w(0,t) &= q_1, \quad w_{,x}(0,t) = q_2 \\ w(l,t) &= q_3, \quad w_{,x}(l,t) = q_4 \end{aligned}\right\} \tag{D.10}$$

Therefore, the shape functions are represented by

$$\phi_1(x) = 1 - 3\left(\frac{x}{l}\right)^2 + 2\left(\frac{x}{l}\right)^3 \tag{D.11}$$

$$\phi_2(x) = x - 2l\left(\frac{x}{l}\right)^2 + l\left(\frac{x}{l}\right)^3 \tag{D.12}$$

$$\phi_3(x) = 3\left(\frac{x}{l}\right)^2 - 2\left(\frac{x}{l}\right)^3 \tag{D.13}$$

$$\phi_4(x) = -l\left(\frac{x}{l}\right)^2 + l\left(\frac{x}{l}\right)^3 \tag{D.14}$$

The equation (D.8) is substituted into equations (D.2), (D.3), and (D.4), the kinetic energy, potential energy (bending strain energy) and external work done are represented as

$$T = \frac{1}{2}\dot{\vec{q}}^t.\rho A\int_0^l \vec{\phi}\vec{\phi}^t\,dx.\dot{\vec{q}} = \frac{1}{2}\dot{\vec{q}}^t.[m].\dot{\vec{q}} \tag{D.15}$$

$$P = \frac{1}{2}\vec{q}^t.EI\int_0^l \vec{\phi}_{,xx}\vec{\phi}_{,xx}^t\,dx.\vec{q} = \frac{1}{2}\vec{q}^t.[k].\vec{q} \tag{D.16}$$

$$\delta W = \delta\vec{q}^t\int_0^l \phi(x)f(x,t)dx = \delta\vec{q}^t.\vec{f}(t) \tag{D.17}$$

$$[m] = \rho A\int_0^l \vec{\phi}\vec{\phi}^t\,dx \tag{D.18}$$

$$[k] = EI\int_0^l \vec{\phi}_{,xx}\vec{\phi}_{,xx}^t\,dx \tag{D.19}$$

$$\vec{f}(t) = \int_0^l \vec{\phi}(x)f(x,t)dx \tag{D.20}$$

Thus, equations (D.18)-(D.19) represent the mass and stiffness of the system.

REFERENCES

Ahmad, R. and Plapper, P. (2016), "Safe and Automated Assembly Process using Vision Assisted Robot Manipulator", *Procedia CIRP*, Vol. 41, pp. 771–776.

Alici, G., Kapucu, S. and Bayseç, S. (1999), "Swing-free transportation of suspended objects with robot manipulators", *Robotica*, Vol. 17 No. 5, pp. 513–521.

August, W., Ren, J., Notheis, S., Haase, T., Hein, B. and Wörn, H. (2010), "3D pendulum swinging control by an industrial robot manipulator", *Joint 41st International Symposium on Robotics and 6th German Conference on Robotics 2010, ISR/ROBOTIK 2010*, Vol. 2, pp. 1310–1316.

Barosz, P., Gołda, G. and Kampa, A. (2020), "Efficiency analysis of manufacturing line with industrial robots and human operators", *Applied Sciences (Switzerland)*, Vol. 10 No. 8, available at:https://doi.org/10.3390/APP10082862.

Bhowmick, S., Nagarajaiah, S. and Lai, Z. (2020), "Measurement of full-field displacement time history of a vibrating continuous edge from video", *Mechanical Systems and Signal Processing*, Elsevier Ltd, Vol. 144, p. 106847.

Bhuyan, M.K. (2019), *Computer Vision and Image Processing Fundamentals and Applications*, 1st ed., CRC Press.

Bogue, R. (2016), "Flexible and soft robotic grippers: the key to new markets?", *Industrial Robot: An International Journal*, Vol. 43 No. 3.

Boschetti, G., Caracciolo, R., Richiedei, D. and Trevisani, A. (2014), "A Non-Time Based Controller for Load Swing Damping and Path-Tracking in Robotic Cranes", *Journal of Intelligent and Robotic Systems: Theory and Applications*, Vol. 76 No. 2, pp. 201–217.

Bradski, G. (2000), "The OpenCV Library", *Dr. Dobb's Journal of Software Tools*.

Cao, C., Do, V., Lee, B. and Lee, B. (2019), "Applying 3D Vision Sensing to an Industrial Robot for Vehicle Assembly under Noisy Environment", *23rd International Conference on Mechatronics Technology (ICMT)*, IEEE, pp. 1–5.

Chang, W.-C. and Wu, C.-H. (2012), "Hand-Eye Coordination for Robotic Assembly Tasks", *International Journal of Automation and Smart Technology*, Vol. 2 No. 4, pp. 301–308.

Chang, W.C. (2018), "Robotic assembly of smartphone back shells with eye-in-hand visual servoing", *Robotics and Computer-Integrated Manufacturing*, Elsevier Ltd, Vol. 50 No. August 2016, pp. 102–113.

Chang, Y.C. and Shaw, J. (2007), "Low-frequency vibration control of a pan/tilt platform with vision feedback", *Journal of Sound and Vibration*, Vol. 302 No. 4–5, pp. 716–727.

Chen, M.Z. and Zheng, Y.F. (1995), "Vibration-Free Handling of Deformable Beams by Robot End-Effectors", *Journal of Robotic Systems*, Vol. 12 No. 5, pp. 331–347.

Chen, S.J., Hein, B. and Wörn, H. (2007), "Swing attenuation of suspended objects transported by robot manipulator using acceleration compensation", *IEEE International Conference on Intelligent Robots and Systems*, pp. 2919–2924.

Chen, W., Li, X., Teo, S.J., Lin, W. and Low, K.H. (2015), "A flexible fixtureless assembly of T-joint frame structures", *2015 IEEE/RSJ International Conference on Intelligent*

Robots and Systems, Hamburg, Germany, pp. 2360–2365.

Cienfuegos, A.S., Saha, B.N., Romero-Hdz, J. and Ortega, D. (2016), "Efficient Integration of Template Matching, Calibration and Triangulation for Automating Peg Hole Insertion Task Using Two Cameras", *International Journal of Computer Science and Engineering*, Vol. 3 No. 11, pp. 61–70.

Çil, Z.A., Mete, S., Özceylan, E. and Ağpak, K. (2017), "A beam search approach for solving type II robotic parallel assembly line balancing problem", *Applied Soft Computing*, Vol. 61, pp. 129–138.

Cui, H., Sun, R., Fang, Z. and Lou, H. (2020), "A novel flexible two-step method for eye-to-hand calibration for robot assembly system", *Measureme and Control*, pp. 1–10.

Deniz, C. and Cakir, M. (2018), "A solution to the hand-eye calibration in the manner of the absolute orientation problem", *Industrial Robot*, Vol. 45 No. 1, pp. 64–77.

Dharmara, K. and Monfared, R.P. (2018), "Robotic assembly of threaded fasteners in a non-structured environment", *The International Journal of Advanced Manufacturing Technology*, The International Journal of Advanced Manufacturing Technology, pp. 1–15.

Di, P., Huang, J., Chen, F., Sasaki, H. and Fukuda, T. (2009), "Hybrid Vision-Force Guided Fault Tolerant Robotic Assembly for Electric Connectors", *2009 International Symposium on Micro-NanoMechatronics and Human Science, Nagoya*, pp. 86–91.

Ding, F., Huang, J., Matsuno, T. and Fukuda, T. (2011), "Skill-based vibration suppression in manipulation of deformable linear objects", *2011 Int. Symp. on Micro-NanoMechatronics and Human Science, Symp. on "COE for Education and Research of Micro-Nano Mechatronics", Symposium on "Hyper Bio Assembler for 3D Cellular System Innovation"*, pp. 421–426.

Ding, F., Huang, J., Wang, Y., Fukuda, T. and Matsuno, T. (2012), "Adaptive sliding mode control for manipulating deformable linear object with input saturation", *2012 IEEE International Conference on Mechatronics and Automation, ICMA 2012*, pp. 1862–1867.

Ding, F., Huang, J., Wang, Y., Matsuno, T. and Fukuda, T. (2014), "Vibration damping in manipulation of deformable linear objects using sliding mode control", *Advanced Robotics*, Vol. 28 No. 3, pp. 157–172.

Ding, F., Huang, J., Yao, W. and He, S. (2019), "Anti-swing Control in Manipulation of a Deformable Linear Object using Dynamic Surface Control", *ICARM 2018 - 2018 3rd International Conference on Advanced Robotics and Mechatronics*, IEEE, pp. 503–508.

Ding, F., Li, Q., Jiang, C., Han, X., Liu, J., Du, H. and Lei, F. (2021), "Event-triggered control for nonlinear leaf spring hydraulic actuator suspension system with valve predictive management", *Information Sciences*, Elsevier Inc., Vol. 551, pp. 184–204.

Ding, J., Wang, C. and Lu, C. (2019), "Transferable Trial-Minimizing Progressive Peg-in-hole Model", *IEEE/RSJ International Conference on Intelligent Robots and Systems (IROS)*, IEEE, Macau, pp. 5862–5868.

Enebuse, I., Foo, M., Ibrahim, B.S.K.K., Ahmed, H., Supmak, F. and Eyobu, O.S. (2021), "A comparative review of hand-eye calibration techniques for vision guided robots", *IEEE Access*, IEEE, Vol. 9, pp. 113143–113155.

Fang, S., Huang, X., Chen, H. and Xi, N. (2016), “Dual-arm robot assembly system for 3C product based on vision guidance”, *Proceedigns of The2016 IEEE International Conference on Robotics and Biomimetics, ROBIO, Qingdao, China*, pp. 807–812.

Feng, K., Zhang, X., Li, H. and Huang, Y. (2017), “A Dual-Camera Assisted Method of the SCARA Robot for Online Assembly of Cellphone Batteries”, *An Internation Conference on Intelligent Robotics and Applications*, Vol. 1, Springer, Cham, pp. 576–587.

Fleischer, J., Lanza, G., Dosch, S., Elser, J. and Pangboonyanon, W. (2014), “Fixtureless alignment of joining partners within the assembly of aluminum space frame structures”, *Procedia CIRP*, Vol. 18, pp. 221–225.

Gao, M., Li, X., Yang, Y., He, Z. and Huang, J. (2017), “An automatic assembling system for sealing rings based on machine vision”, *Journal of Sensors*, Vol. 2017, available at:https://doi.org/10.1109/ISIE.2017.8001281.

Ge, J., Chi, Z. and Li, Q. (2014), “Small Part Assembly with Dual Arm robot and Smart Camera”, *ISR/Robotik 2014; 41st International Symposium on Robotics*, pp. 286–291.

Gilli, M., Lumia, R. and Pastorelli, S. (2014), “Precision robotic assembly using attractive regions”, *Internation Journal of Recent Andvaces in Mechanical Engineering*, Vol. 3 No. 3, pp. 109–128.

González, A., Fang, Z., Socarras, Y., Serrat, J., Vázquez, D., Xu, J. and López, A.M. (2016), “Pedestrian detection at day/night time with visible and FIR cameras: A comparison”, *Sensors (Switzerland)*, Vol. 16 No. 6, pp. 1–11.

Ha, J.E. (2013), “An image processing algorithm for the automatic manipulation of tie rod”, *International Journal of Control, Automation and Systems*, Vol. 11 No. 5, pp. 984–990.

Hayat, A.A., Chaudhary, S., Boby, R.A., Udai, A.D., Dutta Roy, S., Saha, S.K. and Chaudhury, S. (2022), *Vision Based Identification and Force Control of Industrial Robots*, Vol. 404, Springer Singapore, Singapore, available at:https://doi.org/10.1007/978-981-16-6990-3.

Helfrick, M.N., Niezrecki, C., Avitabile, P. and Schmidt, T. (2011), “3D digital image correlation methods for full-field vibration measurement”, *Mechanical Systems and Signal Processing*, Elsevier, Vol. 25 No. 3, pp. 917–927.

Henderson, D. (1977), “Euler Angles, Quaternions, and Transformation Matrices”, *NASA JSC Report*, p. 42.

Henrich, D., Ogasawara, T. and Woern, H. (1999), “Manipulating deformable linear objects - contact states and point contacts”, *Proceedings of the IEEE International Symposium on Assembly and Task Planning*, No. April, pp. 198–204.

Ho, C., Chen, Y. and Li, P. (2018), “Machine vision based in-process light-emitting diode chip mounting system”, *MEASUREMENT AND CONTROL*, pp. 1–11.

Hu, K., Cao, Q. and Zhang, H. (2016), “A compliant robotic assembly system based on multiple sensors”, *2016 IEEE International Workshop on Advanced Robotics and Its Social Impacts (ARSO) Shanghai*, IEEE, Shanghai, pp. 73–78.

Huang, J., Di, P., Fukuda, T. and Matsuno, T. (2008), “Dynamic Modeling and Simulation of Manipulating Deformable Linear Objects”, *Proceedings of 2008 IEEE International Conference on Mechatronics and Automation*, IEEE, pp. 858–863.

Huang, J., Ding, F., Wang, H. and Wang, Y. (2014), "Vibration Suppression of Deformable Linear Object Based on Vision Feedback", *Applied Methods and Techniques for Mechatronic Systems. Lecture Notes in Control and Information Sciences*, Vol. 452, available at:https://doi.org/10.1007/978-3-642-36385-6.

Huang, Y., Zhang, X., Chen, X. and Ota, J. (2017), "Vision-guided peg-in-hole assembly by Baxter robot", *Advances in Mechanical Engineering*, Vol. 9 No. 12, pp. 1–9.

Hughes, J., Culha, U., Giardina, F., Guenther, F., Rosendo, A. and Iida, F. (2016), "Soft manipulators and grippers: A review", *Frontiers Robotics AI*, Vol. 3 No. NOV, pp. 1–12.

Jain, R.K., Datta, S., Majumder, S. and Dutta, A. (2011), "Two IPMC fingers based micro gripper for handling", *International Journal of Advanced Robotic Systems*, Vol. 8 No. 1, pp. 1–9.

Jain, R.K., Majumder, S. and Dutta, A. (2013), "SCARA based peg-in-hole assembly using compliant IPMC micro gripper", *Robotics and Autonomous Systems*, Elsevier B.V., Vol. 61 No. 3, pp. 297–311.

Jain, R.K., Majumder, S., Ghosh, B. and Saha, S. (2015), "Design and manufacturing of mobile micro manipulation system with a compliant piezoelectric actuator based micro gripper", *Journal of Manufacturing Systems*, The Society of Manufacturing Engineers, Vol. 35, pp. 76–91.

Jain, R.K., Majumder, S., Ghosh, B. and Saha, S. (2017), "Analysis of multiple robotic assemblies by cooperation of multimobile micromanipulation systems (M 4 S)", *Int J Adv Manuf Technol*, The International Journal of Advanced Manufacturing Technology, Vol. 91, pp. 3033–3050.

Jain, R.K., Saha, S. and Ghosh, B. (2018), "A Piezoelectric Actuator Based Compact Micro-manipulation System for Robotic Assembly", *In Precision Product-Process Design and Optimization: Select Papers from AIMTDR*, pp. 73–97.

Jain, R.K., Saha, S. and Majumder, S. (2013), "Development of piezoelectric actuator based compliant micro gripper for robotic peg-in-hole assembly", *2013 IEEE International Conference on Robotics and Biomimetics, ROBIO 2013*, IEEE, pp. 1562–1567.

Jain, S. and Khorrami, F. (1995), "Positioning of Unknown Flexible Payloads for Robotic Arms Using a Wrist-Mounted Force/Torque Sensor", *IEEE Transactions on Control Systems Technology*, Vol. 3 No. 2, pp. 189–201.

Ji, Y. (2010), "A computer vision-based approach for structural displacement measurement", in Tomizuka, M. (Ed.), *Sensors and Smart Structures Technologies for Civil, Mechanical, and Aerospace Systems 2010*, Vol. 7647, pp. 76473H1-11.

Ji, Y. and Chang, C.C. (2006), "Identification of structural dynamic behavior for continuous system based on videogrammetric technique", *Smart Structures and Materials 2006: Smart Structures and Integrated Systems*, Vol. 6173 No. 2006, pp. 61731I-1–12.

Ji, Y.F. and Chang, C.C. (2008), "Nontarget Image-Based Technique for Small Cable Vibration Measurement", *Journal of Bridge Engineering*, Vol. 13 No. 1, pp. 34–42.

Jiang, J., Huang, Z., Bi, Z., Ma, X. and Yu, G. (2020), "State-of-the-Art control strategies for robotic PiH assembly", *Robotics and Computer-Integrated Manufacturing*, Elsevier Ltd, Vol. 65 No. April 2019, p. 101894.

Jiang, T., Cui, H. and Cheng, X. (2020), "A calibration strategy for vision-guided robot assembly system of large cabin", *Measurement*, Elsevier Ltd, Vol. 163, p. 107991.

Jiang, T., Cui, H., Cheng, X. and Tian, W. (2021), "A Measurement Method for Robot Peg-in-Hole Prealignment Based on Combined Two-Level Visual Sensors", *IEEE Transactions on Instrumentation and Measurement*, Vol. 70.

Jiang, X., Koo, K., Kikuchi, K., Konno, A. and Uchiyama, M. (2012), "Robotized Assembly of a Wire Harness in a Car Production Line", *Advanced Robotics*, Vol. 25 No. 3–4, pp. 473–489.

Jiang, Z. and Kohno, M. (2002), "Robotic Manipulation of Flexible Objects Based on Vibration Control Using Force Sensors", *In IEEE International Conference on Systems, Man and Cybernetics*, pp. 1–6.

Kaneko, M., Takenaka, R. and Ishikawa, M. (2003), "The Capturing Robot with Super High Acceleration", *Experimental Robotics VIII*, Vol. 5 No. 2, pp. 362–371.

Kapsalas, C.N., Sakellariou, J.S., Koustoumpardis, P.N. and Aspragathos, N.A. (2018), "An ARX-based method for the vibration control of flexible beams manipulated by industrial robots", *Robotics and Computer-Integrated Manufacturing*, Elsevier Ltd, Vol. 52 No. July 2017, pp. 76–91.

Kim, J.Y., Cho, H.S. and Kim, S. (1998), "A visual sensing system for measuring parts deformation and misalignments in flexible parts assembly", *Optics and Lasers in Engineering*, Vol. 30, pp. 379–401.

Kobari, Y., Nammoto, T., Kinugawa, J. and Kosuge, K. (2013), "Vision based compliant motion control for part assembly", *IEEE International Conference on Intelligent Robots and Systems*, pp. 293–298.

Korta, J., Kohut, P. and Uhl, T. (2014), "OpenCV based vision system for industrial robot-based assembly station : calibration and testing", *Pomiary Automatyka Kontrola*, Vol. 60 No. 1, pp. 35–38.

Lasdon, L.S., Waren, A.D., Jain, A. and Ratner, M. (1978), "Design and Testing of a Generalized Reduced Gradient Code for Nonlinear Programming", *ACM Transactions on Mathematical Software (TOMS)*, Vol. 4 No. 1, pp. 34–50.

Lazar, C., Paneseu, D., Laezko, A. and Braeseu, C. (2003), "Vision-Based Integrated System for Robotic Assembly", *IFAC Proceedings Volumes*, Vol. 36 No. 23, pp. 113–118.

Le, D.T., Andulkar, M., Zou, W., Stadter, J.P. and Berger, U. (2016), "Self adaptive system for flexible robot assembly operation", *2016 IEEE 21st International Conference on Emerging Technologies and Factory Automation (ETFA), Berlin*, IEEE, Berlin, Heidelberg, pp. 1–5.

Liu, C., Song, L., Chen, K. and Xu, J. (2019), "Image-based visual servoing using a set for multiple pin-in-hole assembly", *Assembly Automation*, No. October, available at:https://doi.org/10.1108/AA-08-2018-110.

Liu, H., Zhu, W., Dong, H. and Ke, Y. (2019), "An adaptive ball-head positioning visual servoing method for aircraft digital assembly", *Assembly Automation*, Vol. 39 No. 2, pp. 287–296.

Liu, H., Zhu, W., Dong, H. and Ke, Y. (2020), "Hybrid Visual Servoing for Rivet-in-hole Insertion Based on Super-twisting Sliding Mode Control", *International Journal of Control, Automation and Systems*, Vol. 18 No. 51675479, pp. 2145–2156.

Liu, J., Wu, J. and Li, X. (2019), "Robust and accurate hand–eye calibration method based on Schur matric decomposition", *Sensors (Switzerland)*, Vol. 19 No. 20, available at:https://doi.org/10.3390/s19204490.

Liu, S., Li, Y., Member, S. and Xing, D. (2020), "Sensing and Control for Simultaneous Precision Peg-in-Hole Assembly of Multiple Objects", *IEEE TRANSACTIONS ON AUTOMATION SCIENCE AND ENGINEERING*, IEEE, Vol. 17 No. 1, pp. 310–324.

Liu, S., Xing, D., Li, Y., Zhang, J. and Xu, D. (2019), "Robust Insertion Control for Precision Assembly With Passive Compliance Combining Vision and Force Information", *IEEE/ASME TRANSACTIONS ON MECHATRONICS*, Vol. 24 No. 5, pp. 1974–1985.

Liu, S., Xu, D., Zhang, D. and Zhang, Z. (2016), "High precision automatic assembly based on microscopic vision and force information", *IEEE Transactions on Automation Science and Engineering*, Vol. 13 No. 1, pp. 382–393.

Ma, G., Lou, Y., Li, Z., Gao, M., Yang, Y., Liu, Y., He, Z., *et al.* (2016), "A machine vision based sealing rings automatic grabbing and putting system", *2016 IEEE 14th International Conference on Industrial Informatics (INDIN), Poitiers*, pp. 202–206.

Ma, Y., Du, K., Zhou, D. and Zhang, J. (2019), "Automatic precision robot assembly system with microscopic vision and force sensor", *International Journal of Advanced Robotic Systems*, pp. 1–15.

Ma, Y., Liu, X., Zhang, J., Xu, D., Zhang, D. and Wu, W. (2020), "Robotic grasping and alignment for small size components assembly based on visual servoing", *International Journal of Advanced Manufacturing Technology*, Vol. 106 No. 11–12, pp. 4827–4843.

Malis, E. (2002), "Survey of vision-based robot control", *Ensieta*, p. 16.

Marchand, E., Uchiyama, H. and Spindler, F. (2016), "Pose Estimation for Augmented Reality : A Hands-On Survey", *IEEE Transactions on Visualization and Computer Graphics, Institute of Electri- Cal and Electronics Engineers*, Vol. 22 No. 12, pp. 2633–2651.

Mishra, A., Sainul, I.A., Bhuyan, S., Deb, S., Sen, D. and Deb, A.K. (2018), "Development of a Flexible Assembly System Using Industrial Robot with Machine Vision Guidance and Dexterous Multi-finger Gripper", *Precision Product-Process Design and Optimization. Lecture Notes on Multidisciplinary Industrial Engineering. Springer, Singapore.*, pp. 31–71.

Mittal, R. and Nagrath, I. (2015), *Robotics and Control, McGraw Hill Education*, McGraw Hill, New Delhi.

Mu, N., Wang, K., Xie, Z. and Ren, P. (2017), "Calibration of a flexible measurement system based on industrial articulated robot and structured light sensor", *Optical Engineering*, Vol. 56 No. 5, p. 054103.

Nagarajan, P., Perumaal, S.S. and Yogameena, B. (2017), "Vision based pose estimation of multiple peg-in-hole for robotic assembly", *In International Conference on Computer Vision, Graphics, and Image Processing*, Springer, Cham, pp. 50–62.

Nagrath, I. and Gopal, M. (2021), *Control Systems Engineering*, New Age International Publishers.

Nammoto, T., Kosuge, K. and Hashimoto, K. (2013), "Model - based compliant motion control scheme for assembly tasks using vision and force information", *2013 IEEE*

International Conference on Automation Science and Engineering (CASE), Madison, WI, pp. 948–953.

Natsagdorj, S., Chiang, J.Y., Su, C.H., Lin, C.C. and Chen, C.Y. (2015), "Vision-based assembly and inspection system for golf club heads", *Robotics and Computer-Integrated Manufacturing*, Elsevier, Vol. 32, pp. 83–92.

Nerakae, P., Uangpairoj, P. and Chamniprasart, K. (2016), "Using Machine Vision for Flexible Automatic Assembly System", *Procedia Computer Science*, Vol. 96, pp. 428–435.

Noe, D. (1999), "Sensing and acting in intelligent assembly systems", *Annual Reviews in Control*, Vol. 23, pp. 171–176.

Nottensteiner, K., Bodenmüller, T., Kaßecker, M., Roa, M.A., Stemmer, A., Stouraitis, T., Seidel, D., *et al.* (2016), "A Complete Automated Chain for Flexible Assembly using Recognition , Planning and Sensor-Based Execution", *ISR 2016: 47st International Symposium on Robotics*, pp. 1–8.

Ogun, P.S., Usman, Z., Dharmaraj, K. and Jackson, M.R. (2015), "3D vision assisted flexible robotic assembly of machine components", *Eighth International Conference on Machine Vision (ICMV 2015)*, Vol. 9875, p. 98751O.

Pai, P.F., Feng, D. and Duan, Y. (2013), "High-fidelity camera-based method for noncontact vibration testing of structures", *Collection of Technical Papers - AIAA/ASME/ASCE/AHS/ASC Structures, Structural Dynamics and Materials Conference*, pp. 1–23.

Pankow, M., Justusson, B. and Waas, A.M. (2010), "Three-dimensional digital image correlation technique using single high-speed camera for measuring large out-of-plane displacements at high framing rates", *Applied Optics*.

Pires, J.N. and Azar, A.S. (2018), "Advances in robotics for additive/hybrid manufacturing: robot control, speech interface and path planning", *Industrial Robot*, Vol. 45 No. 3, pp. 311–327.

Pitchandi, N. and Subramanian, S.P. (2017), "Genetic Algorithm Based Camera Calibration for Vision Assisted Robotic Assembly System", *IET Computer Vision*, Vol. 11 No. 1, pp. 50–59.

Pitipong, S., Pornjit, P. and Watcharin, P. (2010), "An automated four-DOF robot screw fastening using visual servo", *2010 IEEE/SICE International Symposium on System Integration*, IEEE, pp. 379–383.

Prabhu, V.A., Song, B., Thrower, J., Tiwari, A. and Webb, P. (2016), "Digitisation of a moving assembly operation using multiple depth imaging sensors", *International Journal of Advanced Manufacturing Technology*, Vol. 85 No. 1–4, pp. 163–184.

Prabhu, V.A., Tiwari, A., Hutabarat, W., Thrower, J. and Turner, C. (2014), "Dynamic alignment control using depth imagery for automated wheel assembly", *Procedia CIRP*, Vol. 25, Elsevier B.V., pp. 161–168.

Qin, Z., Wang, P., Sun, J., Lu, J. and Qiao, H. (2016), "Precise Robotic Assembly for Large-Scale Objects Based on Automatic Guidance and Alignment", *IEEE Transactions on Instrumentation and Measurement*, IEEE, Vol. 65 No. 6, pp. 1398–1411.

Qiu, Z.C., Zhang, X.T., Zhang, X.M. and Han, J. Da. (2016), "A vision-based vibration sensing and active control for a piezoelectric flexible cantilever plate", *JVC/Journal*

of Vibration and Control, Vol. 22 No. 5, pp. 1320–1337.

Quan, C., Tay, C.J., Sun, W. and He, X. (2008), "Determination of three-dimensional displacement using two-dimensional digital image correlation", *Applied Optics*, Vol. 47 No. 4, pp. 583–593.

Rao, S.S. (2007), *Vibration of Continuous Systems*, *Vibration of Continuous Systems*, John Wiley & Sons, Hoboken, available at:https://doi.org/10.1002/9780470117866.

Rao, S.S. (2018), *The Finite Element Method in Engineering*, Sixth., Katey Birtcher, Cambridge.

Réthoré, J., Morestin, F., Lafarge, L. and Valverde, P. (2014), "3D displacement measurements using a single camera", *Optics and Lasers in Engineering*, Elsevier, Vol. 57, pp. 20–27.

Ri, S. (2020), "Accurate and fast out-of-plane displacement measurement of flat objects using single-camera based on the sampling moiré method", *Measurement Science and Technology*, Vol. 32 No. 3, pp. 1–6.

Romaszko, M., Sapiński, B. and Sioma, A. (2015), "Forced vibrations analysis of a cantilever beam using the vision method", *Journal of Theoretical and Applied Mechanics*, Vol. 53 No. 1, pp. 243–254.

Van Rossum, G. and Drake Jr, F.L. (1995), "Python reference manual", *Centrum Voor Wiskunde En Informatica Amsterdam*.

Ruth, D.J.S. (2019), "Robotic Assemblies Based on IPMC Actuators", *Ionic Polymer Metal Composites for Sensors and Actuators. Engineering Materials*, Springer, pp. 183–194.

Saha, S.K. (2008), *Introduction to Robotics*, McGraw Hill.

Sato, J., Ichikawa, Y., Yamada, T., Ito, K., Yamamoto, H., Fujihara, M., Kawaguchi, S., *et al.* (2020), "Development of an intelligent power module inserter", *IEEJ Journal of Industry Applications*, Vol. 9 No. 2, pp. 140–148.

Schmitt, R. and Cai, Y. (2014), "Single camera-based synchronisation within a concept of robotic assembly in motion", *Assembly Automation*, Vol. 34 No. 2, pp. 160–168.

Schoettler, G., Nair, A., Luo, J., Bahl, S., Ojea, J.A., Solowjow, E. and Levine, S. (2019), "Deep reinforcement learning for industrial insertion tasks with visual inputs and natural rewards", *ArXiv*, pp. 1–10.

Schoettler, G., Nair, A., Ojea, J.A., Levine, S. and Solowjow, E. (2020), "Meta-reinforcement learning for robotic industrial insertion tasks", *ArXiv*.

Shao, C., Ye, X., Qian, J., Zhang, Z. and Zhu, D. (2020), "Robotic precision assembly system for microstructures", *Proceedings of the Institution of Mechanical Engineers. Part I: Journal of Systems and Control Engineering*, Vol. 234 No. 8, pp. 948–958.

Shen, F., Qin, F., Zhang, Z., Xu, D., Member, S., Zhang, J. and Wu, W. (2021), "Automated Pose Measurement Method Based on Multivision and Sensor Collaboration for Slice Microdevice", *IEEE Transactions on Industrial Electronics*, Vol. 68 No. 1, pp. 488–498.

Shi, J., Hamner, B., Simmons, R. and Singh, S. (2012), "Mobile Robotic Assembly on a Moving Vehicle", *Proceedings of the ASME/ISCIE 2012 International Symposium on Flexible Automation*, Missouri, pp. 1–7.

Shoureshi, R., Momot, M., Mitchell, O.R. and Feddema, J. (1989), "Vision-Based

Intelligent Control for Automated Assembly", *Journal of Intelligent and Robotic Systems*, Vol. 2 No. 2–3, pp. 153–170.

Smith, R., Starr, G., Lumia, R. and Wood, J. (2004), "Preshaped Trajectories for Residual Vibration Suppression in Payloads Suspended from Multiple Robot Manipulators", *Proceedings of the 2004 IEEE International Conference on Robotics and Automation*, IEEE, New Mexico, pp. 1599–1603.

Song, H., Kim, Y., Lee, D. and Song, J. (2017), "Electric connector assembly based on vision and impedance control using cable connector-feeding system", *Journal of Mechanical Science and Technology*, Vol. 31 No. 12, pp. 5997–6003.

Song, R., Li, F., Fu, T. and Zhao, J. (2020), "A robotic automatic assembly system based on vision", *Applied Sciences (Switzerland)*, Vol. 10 No. 3, available at:https://doi.org/10.3390/app10031157.

Song, R., Li, F., Quan, W., Yang, X. and Zhao, J. (2021), "Skill learning for robotic assembly based on visual perspectives and force sensing", *Robotics and Autonomous Systems*, Elsevier B.V., Vol. 135, p. 103651.

Starr, G.P. (1985), "Swing-free transport of suspended objects with a path-controlled robot manipulator", *Journal of Dynamic Systems, Measurement and Control, Transactions of the ASME*, Vol. 107 No. 1, pp. 97–100.

Tanner, H.G. and Kyriakopoulos, K.J. (2000), "A Manipulated Deformable Object as an Underactuated Mechanical System", *Advanced Manufacturing*, Springer, London, pp. 175–196.

Visioli, A. (2006), "Practical PID control", *Basics of PID Control*, pp. 1–18.

Visvalingam, M. and Whyatt, J.D. (1990), "The Douglas-Peucker algorithm for line simplification: re-evaluation through visualization", *Computer Graphics Forum*, Vol. 9, Oxford, UK, Blackwell Publishing Ltd., pp. 213–225.

Wan, A., Xu, J., Chen, H., Zhang, S. and Chen, K. (2017), "Optimal Path Planning and Control of Assembly Robots for Hard-Measuring Easy-Deformation Assemblies", *IEEE/ASME Transactions on Mechatronics*, Vol. 22 No. 4, pp. 1600–1609.

Wang, L., Chen, Y., Li, H., Kemao, Q., Gu, Y. and Zhai, C. (2020), "Out-of-plane motion and non-perpendicular alignment compensation for 2D-DIC based on cross-shaped structured light", *Optics and Lasers in Engineering*, Elsevier Ltd, Vol. 134 No. April, p. 106148.

Wang, P., Qin, Z., Xiong, Z., Lu, J., Xu, D., Yuan, X. and Liu, C. (2015), "Robotic assembly system guided by multiple vision and laser sensors for large scale components", *2015 IEEE International Conference on Robotics and Biomimetics, IEEE-ROBIO 2015*, pp. 1735–1740.

Wang, Y., Wang, P., Liu, C., Hao, G., Xiong, Z., Quan, X., Yuan, X., *et al.* (2018), "Contact Force/Torque Prediction and Analysis Model for large length-diameter ratio peg-in-hole assembly", *Proceedings of the 2018 IEEE International Conference on Robotics and Biomimetics*, IEEE, Malausia, pp. 5–10.

Weng, C.-Y. and Chen, I.-M. (2017), "The Task-level Evaluation Model for a Flexible Assembly Task with an Industrial Dual-arm Robot", *2017 IEEE 8th International Conference on CIS & RAM, Ningbo*, IEEE, Ningbo, pp. 356–360.

Whitney, D.E. (1982), "Quasi-static assembly of compliantly supported rigid parts", *Journal of Dynamic Systems, Measurement and Control, Transactions of the ASME*,

Vol. 104 No. 1, pp. 65–77.

Xing, D., Liu, F., Qin, F. and Xu, D. (2016), "Coordinated Insertion Control for Inclined Precision Assembly", *IEEE Transactions on Industrial Electronics*, Vol. 63 No. 5, pp. 2990–2999.

Xing, D., Xu, D., Liu, F., Lim, H. and Zhang, Z. (2016), "Precision Assembly Among Multiple Thin Objects With Various Fit Types", *IEEE/ASME Transactions on Mechatronics*, Vol. 21 No. 1, pp. 364–378.

Xu, J., Hou, Z., Liu, Z. and Qiao, H. (2019), "Compare Contact Model-based Control and Contact Model-free Learning: A Survey of Robotic Peg-in-hole Assembly Strategies", No. March, pp. 1–15.

Xu, L. Da, Wang, C., Bi, Z. and Yu, J. (2012), "AutoAssem: An automated assembly planning system for complex products", *IEEE Transactions on Industrial Informatics*, IEEE, Vol. 8 No. 3, pp. 669–678.

Yang, H., Kim, M.S. and Lee, D. (2020), "Distributed Rotor-Based Vibration Suppression for Flexible Object Transport and Manipulation", *Proceedings - IEEE International Conference on Robotics and Automation*, pp. 1230–1236.

Yang, R., Jiang, C., Miao, Y., Ma, J., Zhang, X., Yang, T. and Sun, N. (2019), "A Flexible Rope Crane Experiment System", *Applications of Modelling and Simulation*, Vol. 3 No. 1, pp. 11–17.

Yang, Z., Liu, W., Li, H. and Li, Z. (2018), "A coaxial vision assembly algorithm for un-centripetal holes on large-scale stereo workpiece using multiple-DOF robot", *IST 2018 - IEEE International Conference on Imaging Systems and Techniques, Proceedings*, IEEE, pp. 9–14.

Yu, B., Liu, W., Zhang, Y., Ma, D., Yue, Y. and Zhang, J. (2022), "Relative instability compensation method for hand–eye collaborative system in large-scale components measurement", *Measurement: Journal of the International Measurement Confederation*, Elsevier Ltd, Vol. 194 No. March, p. 111082.

Yue, S. and Henrich, D. (2001), "Manipulating deformable linear objects: Attachable adjustment-motions for vibration reduction", *Journal of Robotic Systems*, Vol. 18 No. 7, pp. 375–389.

Yue, S. and Henrich, D. (2005), "Manipulating deformable linear objects: Sensor-based skills of adjustment motions for vibration reduction", *Journal of Robotic Systems*, Vol. 22 No. 2, pp. 67–85.

Yue, S. and Henrich, D. (2006), "Manipulating Deformable Linear Objects : Fuzzy-Based Active Vibration Damping Skill", *Journal of Intelligent Robotic Systems*, Vol. 46 No. 1, pp. 201–219.

Yumbla, F., Abeyabas, M., Luong, T., Yi, J. and Moon, H. (2020), "Preliminary Connector Recognition System Based on Image Processing for Wire Harness Assembly Tasks", *2020 20th International Conference on Control, Automation and Systems (ICCAS 2020)*, Busan, Korea, pp. 1146–1150.

Zhang, C., Pu, J. and Niu, X. (2019), "An Autonomous Robotic Alignment Strategy Based on Visual Gudiance", *IOP Conference Series: Materials Science and Engineering*, Vol. 612 No. 3, available at:https://doi.org/10.1088/1757-899X/612/3/032123.

Zhang, G., Li, C., Zhang, X., Liu, G., Liu, Y., Zhao, J. and Xu, S. (2019), "An adaptable robotic system for assembling irregular earphone parts on factory automation", *IEEE*

International Conference on Robotics and Biomimetics, ROBIO 2019, pp. 52–58.

Zhang, J., Wu, W., Shen, F. and Deng, Y. (2015), "Interference Fit Assembly of Micro-parts Based on Microscopic Vision and Force", *Key Engineering Materials,* Vol. 645–646, pp. 1016–1023.

Zhang, Y.J., Liu, L., Huang, N., Radwin, R. and Li, J. (2021), "From Manual Operation to Collaborative Robot Assembly: An Integrated Model of Productivity and Ergonomic Performance", *IEEE Robotics and Automation Letters*, Vol. 6 No. 2, pp. 895–902.

Zhang, Z. (2000), "A flexible new technique for camera calibration", *IEEE Transactions on Pattern Analysis and Machine Intelligence,* Vol. 22 No. 11, pp. 1330–1334.

Zhang, Z., Zhang, L. and Yang, G.Z. (2017), "A computationally efficient method for hand–eye calibration", *International Journal of Computer Assisted Radiology and Surgery*, Springer International Publishing, Vol. 12 No. 10, pp. 1775–1787.

Zhao, Y., Gao, F., Zhao, Y. and Chen, Z. (2020), "Peg-in-Hole Assembly Based on Six-Legged Robots with Visual Detecting and Force Sensing", *Sensors*, Vol. 20 No. 10, pp. 1–22.

Zheng, D., Zhang, Y., He, Z., Shen, H. and Shi, J. (2013), "Study of assembly automation for strain gauge based on machine vision", *Proceedings - 2013 5th International Conference on Intelligent Human-Machine Systems and Cybernetics, IHMSC, Hangzhou*, IEEE, pp. 401–405.

Zhu, W., Liu, H. and Ke, Y. (2020), "Sensor-Based Control Using an Image Point and Distance Features for Rivet-in-Hole Insertion", *IEEE Transactions on Industrial Electronics*, IEEE, Vol. 67 No. 6, pp. 4692–4699.

Zurn, M., Wnuk, M., Hinze, C., Lechler, A., Verl, A. and Xu, W. (2021), "Kinematic Trajectory following Control for Constrained Deformable Linear Objects", *IEEE International Conference on Automation Science and Engineering*, Vol. 2021-Augus, pp. 1701–1707.

LIST OF PUBLICATIONS

A. International Journal Publications

1. Jalendra, C., Rout, B.K. and Marathe, A. (2022), "**Vision sensor based residual vibration suppression strategy of non-deformable object for robot-assisted assembly operation with gripper flexibility**", Industrial Robot, Vol. 49 No. 5, pp. 851-864. https://doi.org/10.1108/IR-09-2021-0197
2. Jalendra, C., Rout, B.K. and Marathe, A. (2022), "**Robot-vision based control strategy to suppress residual vibration of a flexible beam for assembly**", Industrial Robot. https://doi.org/10.1108/IR-07-2022-0169
3. Jalendra, C., Rout, B.K. and Marathe, A. (2023), "**Vision based control strategy to suppress residual vibration of flexible beams for robotic assembly using wrist motion**", Journal of Mechanical Engineering Sciences. (Accepted)

B. Peer reviewed Conference Publications

1. Jalendra, C., and Rout, B.K. (2020), "**Vibration Suppression of Non-Deformable Metal Strip for Robot Assisted Assembly Operation**", 2020 International Conference on Emerging Trends in Communication, Control and Computing (ICONC3), IEEE, Lakshmangarh, pp. 1–6.
2. Jalendra, C., Rout, B.K. and Marathe, A.M. (2021), "**Residual Vibration Suppression of Non-deformable Object for Robot-Assisted Assembly Operation Using Vision Sensor**", Intelligent Learning for Computer Vision. CIS 2020. Lecture Notes on Data Engineering and Communications Technologies, Springer Singapore, pp. 539–551.
3. Jalendra, C. and Rout, B.K. (2023), "**Vibration Suppression of Flexible Beams for Robotic Assembly Using Vision and Wrist Motion**" In Proceedings of the 2023 6th International Conference on Advanced in Robotics, Ropar, pp. 1-5.

C. Patent

1. Jalendra, C., and Rout, B.K., "**Robust active vibration suppression of a flexible object using robot vision in a robot-assisted assembly operation**"
   (IN Application – 202311041395)

BIOGRAPHIES

Candidate

Mr. Chetan Jalendra has a bachelor's in technology (B.Tech.) in Mechanical Engineering from Shridhar University in Pilani, Rajasthan, India. He is currently pursuing a Ph.D. at the Pilani campus of the Birla Institute of Technology and Science (BITS) in Rajasthan, India, and was awarded Junior and Senior Research Fellowships (JRF and SRF) by the Council for Scientific and Industrial Research (CSIR), New Delhi. His current research interest is on use of computer vision to understand nonlinear mechanical vibration of flexible objects and pursued research on vibration suppression of flexible objects in robot assembly operations augmented with computer vision. He has already published three peer-reviewed research papers in Q2 International Journals and three peer-reviewed international conferences. He has submitted a few other works for PATENT and conferences.

Supervisor

Prof. B K Rout is working as a Professor in the Department of mechanical engineering as well as Coordinator of the Centre for Robotics and Intelligent Systems (CRIS) of Birla Institute of Technology & Science (BITS) Pilani, (Rajasthan) India. He has worked as Associate Dean in Academic Registration & Counselling Division (ARCD), and Head of Department (HOD) in Mechanical Engineering. He has more than twenty-five years of experience in Industry and Academia. He has published several papers in various national and international journals and conferences. He has worked on a number of Govt funded sponsored research and development projects. His current research interest is in rehabilitation robotics, industrial robotics, and statistical techniques to model, synthesize and optimize complex dynamic systems, statistical methods for system design, parameters design, and tolerance design of mechanical equipment. He has been guiding research students in mobile robotics, robust design of manipulators, topologically optimized compliant structure, and mechanism areas. He was selected as IUSSTF Research Fellow in 2012 to conduct research at Rehabilitation Institute of Chicago, Affiliated to Feinberg School of Medicine, North Western University Chicago, Illinois (USA). He is a fellow of professional bodies like the Institution of Engineering (IE) Indian Institute of Industrial

Engineers (IIIE) and a member of Indian society for theoretical and applied mechanics (ISTAM).

Co-Supervisor

Dr. Amol Marathe has more than ten years of experience in academia and four years of experience in research and industry. He received his Ph. D. from IISc, Bangalore, a master's degree from Pune University, and a bachelor's degree from Shivaji University. After his Ph.D., he worked as a researcher and research & development engineer at JNCASR, Honeywell (Bangalore), and CRL (Pune), respectively. He joined BITS, Pilani, as Assistant Professor in 2012. He is currently interested in the development of perturbation methods and non-smooth dynamical systems. He has been involved in teaching Advanced Mathematical Methods, Nonlinear Systems and CAD.